**University of Liverpool**

**Department of Chemistry**


# Contact and Medium Effects on Molecular Electronics

## Volume 1

Thesis submitted in accordance with the requirements of the University of Liverpool for the degree of Doctor of Philosophy

By

Samantha Catarelli

# Abstract

The initial aim of this project was to form a single-pot molecular spintronics technique. To achieve such a goal an understanding of the effect of measurement environment, and the of the metal-molecule contact are important. While the gold-thiol system has been well studied, little work has been done on the ferromagnetic contacts needed for molecular spintronics. It was therefore necessary to measure not only different metals but also different molecular anchors to work towards the best possible combination. A broadening of the understanding of the effect of the metal contact was initially performed by using PM-IRRAS to investigate molecular monolayers formed on Ni through potential assisted assembly. Co was also investigated as a possible metal for molecular spintronics. As a means of achieving a single-pot molecular spintronics setup deposition of Co from ionic liquids was investigated, although this was unsuccessful. Although a single-pot molecular spintronic system was ruled out for the time being, when used in tandem with an ionic liquid environment, Co allowed for successful single molecule conductance measurements. Furthermore these measurements showed similar conductance values to the analogous Au systems.

The potential of the ionic liquid environment in molecular electronics was investigated in depth. Through the use of single molecule conductance measurements and electrochemical measurements ionic liquids were seen to be an exciting opportunity for molecular electronics. Ionic liquids extend the abilities of molecular electronics compared to more traditional environments. Furthermore the characteristics of ionic liquids can be exploited to allow desirable molecular traits to be witnessed. For example when viologen containing molecules were previously investigated in aqueous electrolytes an off-on switching was seen, whereas in ionic

liquids analogous molecules showed off-on-off switching, likely as a result of the ionic liquid locking the ring conformation.

This project has shown that when performing molecular electronics measurements both the environment and the metal-molecule contact are important. These findings are important to note because it means that when forming a molecular electronic system the entire junction should be carefully considered, rather than just the molecular backbone. Through careful choice of the entire molecular electronic junction a system rivaling those of traditional electronics may be formed.

## Acknowledgements

I would like to thank my supervisor Professor Richard Nichols for his help and guidance, without which this thesis would not have been possible.

I also owe my gratitude to Professor Simon Higgins, and the rest of the Nichols-Higgins research groups, particularly Professor Donald Bethell. The guidance provided from all has always been well received, and incredibly useful in achieving the experimental goals set out.

The molecular spintronics work could not have been performed without the aid of Professor Walther Schwarzacher and his group at the University of Bristol. I am grateful to Drs. Douglas Szumski, and James Sadler for their guidance on the aqueous Ni and Co platings performed here, and their willingness to answer all of my questions.

Without Professor Paul Low's group the EC-STM measurements would not have been possible. I am thankful to Dr. Josef Gluyas for providing TMS-V-TMS and its characterisation, Santiago Marquez-Gonzalez for providing and characterizing the Ru containing compounds, and Dr Ross Davidson for providing the OPE molecules.

I would also like to thank Professor Harry Anderson whose group provided the porphyrin molecules used in this work.

I am grateful to Dr Alexandre Lawrenson, who always answered my Spartan® questions, Dr. Carly Brooke for synthesizing the 6V6 used throughout, and who along with Sarah Chappell always helped with anything I needed in the synthesis lab. All three were always willing to provide a few minutes of distraction when needed.

I must thank my parents, my brother and his wife, who were willing to listen about experiments going right and wrong, even when they did not know what I was on about.

# Contents

# Abbreviations

| | |
|---|---|
| 11-MUA | 11-Mercaptoundecanoic acid |
| 6-MHA | 6-Mercaptohexanoic acid |
| 6pTTF6 | 6-Pyrrolo-tetrathiafulvalene |
| 6V6 | 6-[1'-(6-Mercapto-hexyl)-[4,4']bipyridinium]-hexane-1-thiol |
| 6V6H | 1-Hexyl-1'-(6-mercaptohexyl)-[4,4'-bipyridine]-1,1'-diium |
| 8-MOA | 8-Mercaptooctanoic acid |
| AC | Alternating current |
| BDET | Benzenediethenylenethiol |
| BDMT | Benzenedimethane dithiol |
| $BMIM^+$ | 1-Butyl-3methylimidazolium |
| BMIM-OTf | 1-Butyl-3-methylimidazolium triflate |
| $BMIM\text{-}PF_6$ | 1-Butyl-3-methylimidazolium hexafluorophosphate |
| BMIM-TFSA | 1-Butyl-3-methylimidazolium bis(trifluorosulfonyl) amide |
| $BMP^+$ | 1-Butyl-1-methylpyrrolidinium |
| BPC | N-(n-butyl)pyridinium chloride |
| CE | Counter electrode |
| CMOS | Complementary metal-oxide-semiconductor |
| CPE | Constant phase element |
| CV | Cyclic voltammetry |
| DCM | Dichloromethane |
| DC | Direct current |
| DMSO | Dimethyl sulfoxide |
| DOS | Density of states |
| DPV | Differential pulse voltammetry |
| DRAM | Dynamic random access memory |
| EC-STM | Electrochemical-scanning tunnelling microscopy |
| EIS | Electrochemical impedance spectroscopy |
| EMIM | 1-Ethyl-3-methylimidazolium |
| FRA | Frequency response analyser |
| FWHM | Full width half maximum |
| GMR | Giant magnetoresistance |
| HER | Hydrogen evolution reaction |
| HOMO | Highest occupied molecular orbital |
| HT | Hexanethiol |
| IR | Infrared |
| LIA | Lock-in-amplifier |
| LUMO | Lowest unoccupied molecular orbital |
| ML | Monolayer |
| MR | Magnetoresistance |
| OCP | Open circuit potential |
| ODT | Octanedithiol |

| | |
|---|---|
| OFN | Oxygen free nitrogen |
| OHP | Outer Helmholtz plane |
| OPD | Overpotential deposition |
| OPE | Oligo(phenylene ethynylene) |
| OT | Octanethiol |
| PEM | Photoelastic modulator |
| PFPE | Perfluoropolyether |
| PM-IRRAS | Polarization modulation-infrared reflection absorption spectroscopy |
| PNA | Peptide nucleic acid |
| PZC | Point of zero charge |
| QRE | Quasi-reference electrode |
| RAM | Random access memory |
| RbDS | $Rb^+$ dodecyl sulphate |
| RE | Reference electrode |
| SAM | Self-assembled monolayer |
| SCE | Saturated calomel electrode |
| SDS | Sodium dodecyl sulphate |
| STM | Scanning tunnelling microscope |
| STM-BJ | Scanning tunnelling microscopy-break junction |
| STS | Scanning tunnelling spectroscopy |
| TFBM | [4-(trifluoromethyl)phenyl]methanethiol |
| THF | Tetrahydrafuran |
| TMR | Tunnelling magnetoresistance |
| TMS | Trimethylsilane |
| TMS-V-TMS | 1,1'-Bis(4-((trimethylsilyl)ethynyl)benzyl)-[4,4'-bipyridine]-1,1'-diium |
| UHV | Ultra high vacuum |
| UPD | Underpotential deposition |
| V | Viologen |
| WE | Working electrode |
| XPS | X-ray photoelectron spectroscopy |
| XRD | X-ray diffraction |

## Symbols

| | |
|---|---|
| $A$ | Electrode area |
| $a$ | "Hydrodynamic radius" of the redox species |
| $a$ | nF/RT |
| $\beta$ | Attenuation factor |
| $c^*$ | Bulk concentration (mol $cm^{-3}$) |
| $D$ | Diffusion coefficient |
| $d$ | Distance |
| $e$ | Elementary charge |

| | |
|---|---|
| $E^{\circ}$ | Formal Potential |
| $E_P$ | Peak potential |
| $F$ | Faraday's constant |
| $G$ | Conductance |
| $G_0$ | Quantum of conductance |
| $h$ | Planck's constant |
| $\hbar$ | h/2π |
| $I$ | Current |
| $I_0$ | Setpoint current |
| $I_P$ | Peak current |
| $k$ | Rate constant of electron transfer |
| $k$ | Boltzman constant |
| $L$ | Length |
| $m$ | Mass |
| $m^*$ | Effective mass |
| $n$ | Number of electrons |
| $O$ | Oxidised species |
| Ø | Effective barrier height in eV |
| $q$ | Charge of an electron |
| $R$ | Gas Constant |
| $R$ | Reflectivity of light |
| $R$ | Reduced species |
| $R_{CT}$ | Charge transfer resistance |
| $R_\Omega$ | Solution resistance |
| $s$ | Distance |
| $s_0$ | Setpoint distance |
| $T$ | Absolute temperature |
| $T$ | Probability of tunnelling |
| $v$ | Scan rate |
| $V_{bias}$ | Bias voltage |
| $Z'$ | Resistance |
| $Z''$ | Reactance |
| $\alpha$ | Transfer coefficient |
| $\beta$ | Attenuation factor |
| $\gamma$ | Modelling parameter in Kuznetsov-Ulstrup model related to the effect of bias on the effective electrode potential at the redox centre |
| $\Delta E_P$ | Peak separation |
| $\epsilon$ | Energy |
| $\eta$ | Solution dynamic viscosity |
| $\eta$ | Overpotential |
| $\kappa$ | Electronic transmission coefficient |
| $\lambda$ | Reorganization energy |

| | |
|---|---|
| $\xi$ | Modelling parameter in Kuznetsov-Ulstrup model related to effective electrode potential at the redox centre |
| $\rho$ | Density of states |
| $\varphi$ | Barrier height |
| $\phi$ | Angle of incidence |
| $\Psi$ | Charge transfer parameter |
| $\Psi$ | Wavefunction |
| $\omega$ | Nuclear vibration frequency |

# Chapter 1:

# Introduction

# Introduction

Computational devices are ever present in daily life. The consumer desire for smaller, faster devices has dictated the pace of innovation in this field, with corporate competition ensuring consumer demands are met. The integrated circuits essential in computational devices have revolutionized the world. This revolution was correctly anticipated in 1965 by Gordon Moore, who foresaw the access of the masses to both home and portable computers.[8] Moore also predicted that the number of transistors per devices would double every 18 to 24 months.[8] This is known as Moore's Law, which has been largely adhered to. This is particularly evident in the growth in the number of transistors on an Intel® microprocessor from 2300 in 1971, to $1.4 \times 10^9$ in 2012.[10] Unfortunately it is estimated the limits of Moore's Law may be reached as early as 2018.[11]

Current electronic devices are prepared using top-down techniques, where nanoscale devices are machined from large starting materials. The top-down nature of these electronics is considered a possible downfall, as the technology available to machine them becomes limited. Fabrication cost also limits the current scaling down of devices, with an exponential increase in the cost of constructing new manufacturing plants accompanying the exponential increase in the number of transistors.[12] More fundamental, however, is the fact that as the devices become smaller, device defects have a larger impact on the resulting device.[12] To continue to meet consumer demands, therefore, the microprocessor industry must adapt to the limitations of current technology. An appealing option to overcome these limitations is to incorporate bottom-up techniques, which may eventually allow the creation of high density devices at little relative cost. Molecular electronics is amongst the bottom-up technologies of interest in a role for future electronics. The ultimate limit of current

devices is the 0.3 nm distance between the atoms of a Si crystal.[11, 13] At these dimensions the devices are controlled by quantum rather than classical physics, making molecules well suited for these dimensions.

The current trend in computational device miniaturisation will continue through innovation. Limits to device size have been threatened since Moore's Law was published.[13] The predicted limitation has, however, always been surpassed with technological and materials innovations. The most recent International Technology Roadmap for Semiconductors predicts that between 2020 and 2025 the 10 nm and less realm will be reached.[14] While a smooth transition to this size is predicted, it is also predicted that the geometric limit will likely be met in this time. Furthermore the ITRS suggests that rather than solely aiming to adhere to Moore's Law the microchip industry should aim to add other functionalities to their devices.[14] Research in molecular electronics may in future provide the innovation necessary to feed the demand for smaller, faster and more novel devices. Innovation and research in the field of molecular electronics holds promise for the wider electronics industry.

## Molecular Electronics

Molecular electronics may in the future help to satisfy the demand for smaller and faster computational devices. It is predicted semiconductor technologies will be viable for at least the next decade, although innovation may become prohibitively expensive.[15] In anticipation of the future limitations of semiconductor devices alternative technologies are being vigorously investigated, including bottom-up technologies like molecular electronics. Molecular electronics aims to form key electronic components from molecules, including switches, diodes, and transistors.[16, 17] While the foundations for molecular electronics were laid in the early 1970s[1] interest

in these technologies did not take off until the late 1990s to early 2000s. Interest in molecular electronics can be broken into three time periods: 1) Investigations performed around the time of Aviram and Ratner's landmark molecular diode paper.[1] 2) Investigations performed prior to the establishment of single molecule measurement techniques. 3) Investigations performed after Haiss[18] and Tao[19] established methods to measure the conductance of single molecules in 2003.

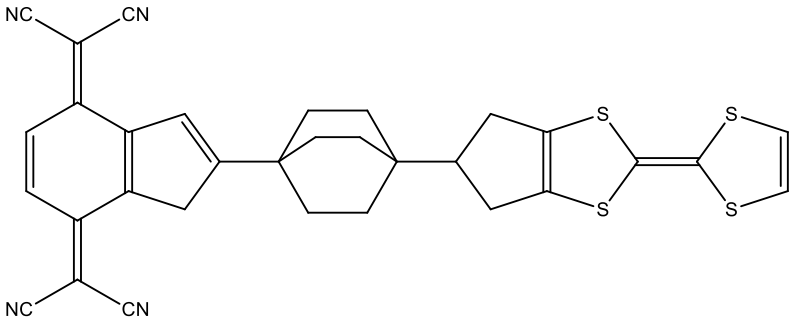


*Figure 1: In 1974 Aviram and Ratner proposed the pictured molecule as a potential molecular rectifier. By connecting the electron accepting tetracyanoquinodimethane to the electron donating tetrathiofulvalene by a molecular bridge the molecule should act as a diode.*[1]

Molecular electronics has its foundation in Aviram and Ratner's 1974 molecular diode paper,[1] in which the theoretical molecule in **Figure 1** was proposed as a potential molecular rectifier. It was proposed that by exploiting the molecular structure this molecule would allow current flow in only one direction through it. The molecular structure was carefully chosen to have isolated electron donor and acceptor units to mimic p-n semiconductor behaviour. In this diode tunnelling is predicted to occur in the direction cathode → acceptor → donor → anode, and be suppressed in the opposite direction. Although purely theoretical, this work proposed the use of molecules for their electronic behaviour for the first time, with synthesis predicted as a means to exploit the electronic properties. At the time of Aviram and Ratner's paper the idea of tunnelling through a molecule was well established, although the uses were

unclear.[20-22] Following the publication of Aviram and Ratner's paper investigation of conduction through self-assembled monolayers continued,[23] though their use in electronics devices was slow to take root.

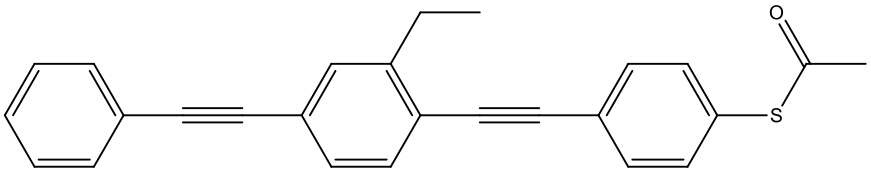


*Figure 2: 4,4'di(phenylene-ethynylene)-benzothioacetate was investigated by STM in a mixed monolayer with n-dodecanethiol on Au(111). The conductivity of 4,4'di(phenylene-ethynylene)-benzothioacetate compared to n-dodecanethiol was possible based on the difference in the brightness in the STM images.*[5]

1981 saw a turning point for molecular electronics. In this year the STM was invented, allowing for the electronic properties of molecular ensembles and isolated molecules to be probed. Although interest in molecular electronics devices did not instantly grow after the invention of the STM it was a key characterization method allowing growth in the early to mid-1990s. During this period STM measurements were particularly useful for the comparison of relative conductivities of molecular components in a monolayer. For example, the relative conductivities of 4,4'di(phenylene-ethynylene)-benzothioacetate, **Figure 2**, and n-dodecanethiol in mixed monolayers on Au(111) could be found through STM imaging.[5] More elaborate molecular conductance measurements were also performed using the STM. In 1995 the molecular electronic capabilities of $C_{60}$ were probed by measuring its resistance when in direct contact with tip and substrate.[24] These investigations showed an energetic broadening of the density of states profile of $C_{60}$ when in contact with tip and substrate allowing for flow of current. Also popular at this time was the mechanically controlled break junction technique (MCBJ),[25] in which a metallic wire is mounted on a flexible substrate, with a central notched portion, giving a nano-

contact.[26-28] When pressure is applied to the underlying flexible substrate the nano-contact breaks,[26-28] the molecular wire can span the gap, allowing current to flow.[28, 29] While molecular electronics experiments were popular in this period the number of investigations is significantly less than after the turn of the century.

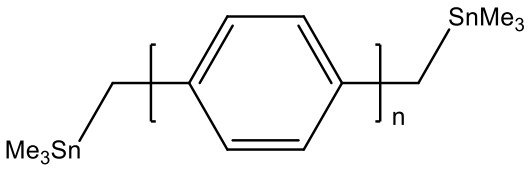


*Figure 3: The single molecule conductance of xylene between the Au STM tip and substrate were measured. These molecules contacted the tip and substrate with a C-Au bond, through loss of the $SnMe_3$ groups. The junctions gave high conductance values of 0.9 $G_0$ when n=1.*[7]

The invention of the STM was monumental for molecular electronics investigations, allowing for repeatable, statistically significant, single molecule conductance measurements. The latest turning point in molecular electronics came in 2003 when Tao's break junction technique[19] and Haiss' *I*(*s*) technique[18] were established. Both techniques measure the conductance of a single molecule attached to both a metal substrate and STM tip. The presence of the molecule significantly alters the conductance decay, causing a molecular conductance plateau in the exponential decay curve. The main difference between the break junction and the *I*(*s*) technique is that in the former the tip initially contacts the metal substrate. Since 2003 there have been nearly 1,500 papers on 'single molecule electronics' and over 10,000 papers on 'molecular electronics.' Initial investigations showed molecular conductance values many orders of magnitude smaller than traditional semiconductor devices. Recently, however, the future possibility of integration of molecules into semiconductor roles has been revitalized by careful study of a variety of end groups.

By starting with a trimethylstannyl group, which cleaves to give a direct Au-C bond, a highly promising series of xylene molecules was measured, **Figure 3**.[7] The direct Au-C bond allows strong coupling with the xylene π system resulting in large conductance values for a molecular system. When the single phenyl containing xylene molecule was measured a conductance of 0.9 $G_0$ was seen. $G_0$ is the quantum of conductance, which arises when there is a metallic point contact a single atom thick. The value of $G_0$ is equivalent to $2e^2/h$, where *e* is the charge of an electron, and *h* is Planck's constant, or 77400 nS.[30] If the hurdles present to molecular electronics can be overcome this could be a molecular system with potential technological applicability.

Molecular electronics has been used in a demonstration of non-volatile random access memory devices, through the use of alkythiolate tethered Ru(II) terpyridine molecular layers.[31] Investigations showed these RAM devices were highly stable to repeated write-read-erase-read cycles. While the ON/OFF ratio of these devices is lower than bulk organic RAM devices, they are promising for devices requiring a fast response time. Flexible electronic devices have been formed with self-assembled monolayers on flexible substrates, showing promising electrical behaviour.[32] The conductance of a variety of alkanethiol monolayers were investigated on flexible substrates as the substrates were bent. Not only was a stable current measured with bending for at least 1000 cycles, but near constant current was seen. This investigation is reflective of the new trend in molecular electronics to investigate their characteristics which have no comparable CMOS function. The use of molecular electronics can open the way for more than just carrying charge, such as optoelectronics, and spintronics.[33] Investigations into these avenues could in the future allow for a radical approach to electronics devices.

The future possibilities of molecular electronics are becoming clear. While complete replacement of traditional CMOS technologies is unlikely at present, hybrid devices based on molecular electronics are a possibility, though more work must be done before such devices become commercially realized. Molecular electronics investigations also open the opportunity to form novel electronic devices.

## Molecular Spintronics

While molecular electronics exploits the charge of an electron in spintronics conductance is controlled through control of the spin state. This can be done by aligning the electrode spin parallel and spin antiparallel, generally causing a high and low conductance state, respectively, **Figure 4**. The sister field of molecular spintronics is highly interesting, as seen recently in editorials by leaders in the field of molecular

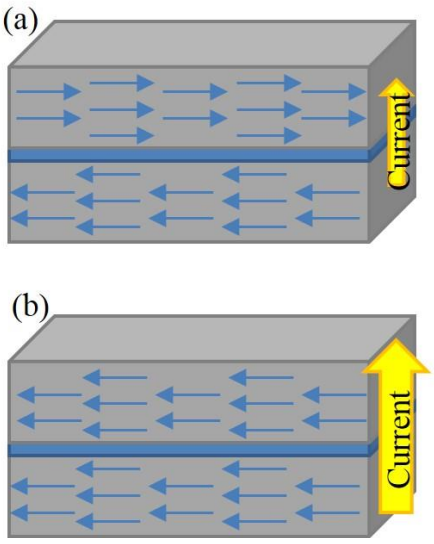


*Figure 4: Spintronics controls the current flow through a magnetic/non-magnetic/magnetic system by controlling the alignment of the electron spins of the magnetic layers. (a) Generally when the spin is opposite in the two magnetic layers the charge flow is hindered, and therefore current is of comparatively low magnitude. (b) Ideally when the spin of the two magnetic layers is aligned charge transfer is enhanced causing a relative increase in current.*

electronics.[34] From these editorials it is clear molecular spintronics is a favoured front of molecular electronics.

Spintronics is a fairly recent field, with swift commercialisation of such devices. Initial research towards spintronics was presented in 1971, with investigations of the tunnelling conductance of Al-$Al_2O_3$-Ni structures showing magnetic field dependent conductance.[35] At the time, however, the potential of spin dependent tunnelling was not fully understood. The turning point for spintronics, however, came in 1988, when Giant Magnetoresistance (GMR) was discovered by Peter Grünberg,[36] and Albert Fert.[37] Grünberg *et al.*[36] formed alternating films of ferromagnetic Fe and antiferromagnetic Cr, resulting in layered structures with hitherto unique characteristics, and a strong magnetoresistance effect. At a similar time Fert *et al.*[37] were investigating the coupling between Fe layers separated by intervening Cr layers. This work showed antiferromagnetic coupling between the separated Fe layers, again with a large magnetoresistance measured. While initially citations of these pioneering works were minimal, in 1996 the number of total citations increased by almost 75-fold, coinciding with the release of commercial GMR devices. In 1994 Nonvolatile Electronics Inc. reported the first commercially viable GMR based sensor,[38] while in the same year IBM presented the first commercial GMR read head device.[39] Intense interest in GMR devices continued, eventually leading to a multi-order of magnitude increase in magnetic memory recording density, while reducing the component size.[40] While GMR devices were pivotal in revolutionizing magnetic memory, improvements both in the magnetoresistance and performance of these devices were achieved through the exploitation of tunnelling magnetoresistance (TMR).[41] In TMR devices the two ferromagnetic electrodes are separated by a tunnel junction through which spin travels.[40] TMR allowed great enhancement of the modest magnetoresistance of the

first commercial GMR devices. In 2004 TMR values of about 200% were published,[42, 43] while three years later these values were superseded by reports of TMR values of 500%,[44] making commercialization inevitable. In 2006 Seagate Technology announced the production of a TMR based read head, which not only outperformed GMR devices but also had a longer lifetime.[41] The following year (2007) both Grünberg and Fert were awarded the Noble Prize in Physics for the discovery of Giant Magnetoresistance. Research in this area is still strong, although investigations are no longer limited to traditional metallic and semi-conductor systems.

It is possible future phases in spintronics will come from investigations of molecular spintronics. The concept of molecular spintronics began to appear in the early 2000s. Organic molecules are well suited for roles in spintronic devices, particularly as they can be tailored to suit the needs of the device. As with molecular electronics the use of molecules could give rise to a cheap, high density, production technique.[45] Even more appealing are the surprisingly large magnetoresistances possible when using molecules,[40, 46] due to their long spin relaxation times.[45, 47-50]

In recent years the experimental ability to investigate single molecule spintronics has grown. Previously conclusions about single molecule spin transport arose only from theoretical molecular spintronic investigations. Recently, one of the first single molecule spintronic systems investigated by theoretical means, has been experimentally investigated. In 2002 Emberly *et al.* investigated from a theoretical standpoint Ni-benzenedithiol-Ni junctions as envisaged in mechanically controlled break junction or STM experiments.[51] In this work they calculated the transport properties of the Ni-benzenedithiol-Ni system in both the parallel and anti-parallel alignments. These calculations showed the spin-up and spin-down electrons give rise to *d* bands of different energies, causing the parallel spin alignment to give rise to the

highest conductance. Just over a decade later this theoretical work was experimentally tested.[49] The *I-V* characteristics of the Ni-benzenedithiol-Ni system were measured by mechanically controlled break junction, at 4 and 77 K, and a variety of magnetizations. These measurements verified Emberly's theoretical findings. The Ni-benzenedithiol-Ni system was seen to give a magnetoresistance of ~150 % and 80-90 % at 4 and 77 K, respectively. This is not the only system for which the original theoretical inferences have recently been confirmed experimentally. In 2012, experimental work on $C_{60}$ between two ferromagnetic contacts showed the system to exhibit a magnetoresistance of 100 %.[46] This effort confirmed earlier theoretical work showing larger conductance in the parallel than the antiparallel magnetization state of the contacts.[52]

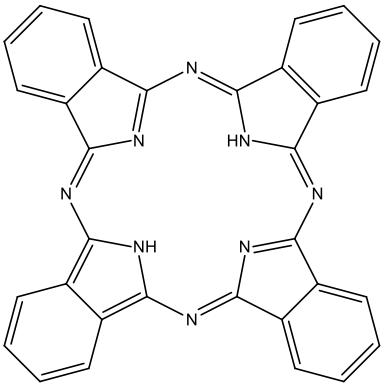


*Figure 5: Hydrogen phthalocyanine was used in molecular spintronics investigations on Co. These systems showed a magnetoresistance of over 60 %.*[2]

When dealing with single molecule spintronic devices the position of the molecular orbitals with respect to the metal Fermi level is key in controlling the resulting magnetoresistance. The role of the molecular orbitals has been established by comparing theoretical calculations with targeted single molecule spintronics experiments. For example the relationship between the molecular orbitals of hydrogen phthalocyanine, **Figure 5**, and the Co substrate Fermi levels was investigated by Schmaus *et al.*[2] The experimental measurements of this system showed a MR of over

60 %. Theoretical computations demonstrated that this MR arose from the broadening of the charge carrying LUMO during interaction with the Co Fermi level. When the tip and substrate are spin aligned the LUMO is broadened at both contacts allowing for the increased molecular conductance measured. A further explanation for the increased conductance in the spin aligned system is the reduced contribution from the majority spin containing HOMO compared to minority spin electrons.[53] The positive magnetoresistances have also been explained by changes in the DOS, which is higher for the parallel than the anti-parallel alignment, allowing a more facile flow of electrons.[50] There has been a drive to fully understand the magnetoresistance values of single molecule spintronic systems through combined theoretical and experimental work. This approach shows the measured magnetoresistances arise from the interaction of the molecular orbital with the contact Fermi level. This implies that correct tailoring of the molecular wire may one day allow for magnetoresistances which are competitive with those of solid state devices.

While molecular spintronics is a promising field more work is clearly needed. A shortfall of molecular spintronics is the often unfavourable temperature dependence of the magnetoresistance. For a molecular spintronic device to be of practical use it must show a strong magnetoresistance at room temperature. Unfortunately many experiments have only been performed at ultra-low temperatures.[2, 48, 49] In some cases attempts to measure the magnetoresistance near room temperature have been made, however the strong magnetoresistance is typically lost before room temperature is reached.[45] This shortcoming of molecular spintronic devices must be addressed for future technological applications.

The field of molecular spintronics has potential as a future application of molecular electronics. Moreover it is foreseeable that it could play a role in the

revolutionary magnetic memory technologies. At this time work must be done before molecular spintronic devices are commercially viable, not least because of the strong temperature dependence seen. However, the exponential rise in the number of papers on single molecule and molecular spintronics make it undeniable that the field is quickly gaining importance.

## Self-Assembled Monolayers

The future success of molecular electronics depends on the ability to easily contact molecules at both termini. A straightforward route to the first electrode-molecule contact is molecular self-assembly. Molecular self-assembly has a large presence in molecular electronics because the molecular layer is simply adsorbed by introduction of the electrode substrate to a solution of the molecule of interest. Not only is this technique straightforward, but it is also relatively inexpensive, and allows a degree of control over the resulting layer.

Molecular self-assembly is a multi-step process. When the substrate is introduced into the adsorption solution the adsorbed molecules are highly mobile and isolated.[54] Coverage increases with adsorption time, reducing molecular mobility, particularly if there is an associated change from a physisorbed to chemisorbed state.[54] This second phase is the low coverage 'crystalline' phase, of intermediate surface density with disordered molecules.[54, 55] Over time the third and final high-coverage 'crystalline' phase, which sees the full coverage and final ordering of the monolayer develop,[28, 54, 55] occurs. It should be noted that the adsorption process is rapid to near full coverage of the monolayer, while the final monolayer restructuring and ordering can take hours.[28, 54, 56] Thiol terminated molecules are by far the most prominent in molecular electronics studies, and as such their self-assembly mechanism will be

addressed. It is generally accepted that the self-assembly of thiol terminated molecules occurs with the loss of the S-H proton giving rise to a S-Au bond.[56-60] The mechanism by which the thiol loses its proton is questionable, however, the following chemical reactions having been proposed:[58, 60]

$$RSH + Au(0)_s + \frac{1}{2}O_2 \rightarrow RSAu(I)_s + \frac{1}{2}H_2O \qquad (Eq.\ 1)$$

$$RSH + Au(0)_s \rightarrow RSAu(I)_s + \frac{1}{2}H_2 \quad (Eq.\ 2)$$

Theoretical investigations substantiate the idea that the thiol adsorbs to the surface as a thiolate species, with loss of the proton. A theoretical study in 2000 showed that proton loss can occur with $H^+$ coadsorbed on the Au, and eventually lost as molecular hydrogen.[60] This mechanism results in a more favourable binding energy for the thiolate compared to the thiol. Exceptions to this rule do occur. When monolayers of thiol terminated alkanes were investigated on Au nanoparticles it was found that the loss of the thiol proton occurred by a slow process, for high coverage monolayers.[59] This was evident as ligand substitution of thiol protected NPs showed the loss of intact thiol molecules, even after 18 hours. However, the loss of the thiol hydrogen was rapid when there was low coverage. The behaviour of the thiol termination in this study is the exception rather than the rule.

The use of self-assembled monolayers is important for molecular electronics investigations, allowing a high degree of control over the system structure. The ease of use, and high degree of control makes molecular assembly a robust process.

## Ionic Liquids

Ionic liquids are ‘green solvents’ generally composed of an inorganic anion and organic cation. Although they have been documented in the literature for at least

a century,[61, 62] their true potential is only just being realized because of the discovery of virtually limitless air and water stable varieties.[63] In 2013 this potential was appreciated in a public vote which saw ionic liquids voted as the British Innovation which could most influence the next century.[64]

Ionic liquids are low melting point molten salts, with those that exist as liquids at room temperature and are stable upon exposure to air and water of particular interest. As an ionic liquid is composed solely of ions there is a huge variety of anion and cation combinations, however these must be carefully chosen. The anion controls the ability of the ionic liquid to mix with water,[65] its thermal stability,[65] the solvating ability,[66] the electrochemical window[67] and the viscosity.[68, 69] The cation controls the melting point,[65] viscosity[70] and the electrochemical window.[67] To achieve RTILs the organic cation tends to have low symmetry, and the inorganic anion tends to be weakly basic, a combination leading to a low lattice energy, and a liquid range encompassing room temperature.[71] The ability to tune the properties of the ionic liquid by altering the cation and anion is just one of the many reasons ionic liquids are gaining popularity as a replacement for traditional solvent and aqueous media.

The allure of ionic liquids as replacements for traditional solvent and aqueous media is growing for more than just their chemical tunability. Ionic liquids, unlike organic solvents, are considered ‘green’ solvents because of their vanishingly low vapour pressures causing no polluting vapour, and the future possibility of recycling ionic liquids after their use.[61, 72] It should be noted though, that regardless of this ‘green’ label ionic liquids should be treated with the same level of caution as other solvents, as little data exists on their toxicity and biodegradability.[73] Unlike traditional solvents ionic liquids have a wide liquid range[74] and high thermal stability, with some remaining stable up to 400 °C and higher.[75] These properties are particularly desirable

because ionic liquids also have the ability to dissolve a wide range of materials,[62] even though the kinetics of dissolution of solids into ionic liquids can be incredibly slow.[76] To overcome these slow dissolution kinetics sonication, heating and/or carrier solvents may be used, adding a degree of complexity to the experimental setup. Furthermore in the case of the carrier solvent, the solvent must be removed, which can make the solution composition questionable. In order to replace standard solvents the ability of ionic liquids as solvents must be quantified, a characteristic on which much work has been done.[62, 66, 74, 77] Ionic liquids can be thought of as polar solvents, like methanol, DMSO, and acetonitrile, which act as both hydrogen bond donors and acceptors, although this is heavily reliant on the ions composing the ionic liquid.[63, 66] One must be careful not to apply too many rules from standard solvents to ionic liquids, as often the differences between these classes of liquids mean such rules cannot be transferred across. A noticeable difference between ionic liquids and traditional solvents is their viscosity, which is 20 times larger than water even for the lowest viscosity ionic liquid.[63] Regardless of these differences, however, the potential for ionic liquids to replace or at least complement traditional systems cannot be ignored.

Before using ionic liquids, however, an understanding of their disadvantages is necessary to adequately design experiments. Some of these disadvantages have already been touched upon. The toxicity of ionic liquids has not been fully addressed,[73] therefore their long term health effects are questionable. The viscosity of ionic liquids is an obvious disadvantage. With regards to neat ionic liquids the high viscosity counteracts the fully ionic nature to reduce the conductivity.[78] When the ionic liquid is used in electrochemistry this viscosity can cause issues for the measurement of a redox reaction. The viscous nature of ionic liquids causes a reduction in the diffusion coefficient of the redox species compared to traditional electrolytes,[79, 80] in turn

causing a reduced current response. While a reduction in current can be counteracted by increasing the concentration of the redox species, when this is sparingly soluble in the ionic liquid the response can be difficult to improve. Though many ionic liquids are commercially available they are expensive compared to other electrolytes, a factor which must be accounted for in an experimental setup. To factor in the cost of the ionic liquid a small volume cell is used in electrochemistry and STM measurements, and only the quantity of ionic liquid/redox molecule solution needed for the experiment is made up at a time. As this must done for every experiment the time needed for an experiment in ionic liquid is greater than in other non-aqueous solvents. At the end of the experiment the removal of the ionic liquid must also be accounted for, this can be difficult, and subsequent disposal can be expensive.[81] All of these disadvantages are fairly straightforward to work around, by far however the greatest difficulty when using ionic liquids is the purification of the ionic liquid prior to use. This purification can range from removing water and solvents used during synthesis[78, 81] to removing halide impurities in the system.[81, 82] Although this can be a lengthy process it is necessary nonetheless. If water and solvent are not removed prior to use for electrochemistry the electrochemical window can be greatly reduced.[78] The standard method for removing solvent from ionic liquid is to vacuum dry with heat for an extended period, which requires a degree of experimental pre-planning. However for the purest ionic liquids they should ideally be made in house, from purified starting products.[81] Regardless of these disadvantages the experimental opportunities afforded by the use of ionic liquids means they are gaining popularity regardless. With respect for their disadvantages ionic liquids can be exploited to maximise their benefits.

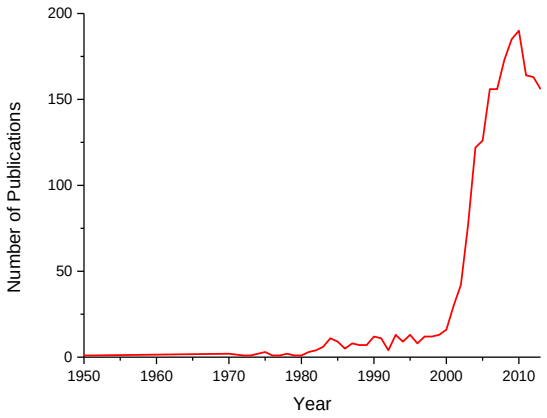


*Figure 6: Although ionic liquids have been known since the beginning of the last century little had been published on 'ionic liquid electrochemistry' until the start of this century. The sharp increase in research in this area coincides with the introduction and increased commercial availability of the second generation of ionic liquids, which are much easier to handle.*

Just as ionic liquids have an increased role in general science, their role in electrochemistry is also on the rise, as witnessed by an almost exponential increase in the number of papers dedicated to 'Ionic Liquid Electrochemistry' at the turn of the century, **Figure 6**. Long before the preparation of the first non-haloaluminate ionic liquids, the first generation of ionic liquids were exploited for their favourable electrolyte characteristics.[83] The introduction of the first non-haloaluminate ionic liquids, however, allowed for the exponential growth in their use.[84] Ionic liquids are naturally suited to electrochemistry because of their intrinsically high conductivity,[63, 68] wide electrochemical window limited by the reduction of the cation and oxidation of the anion,[74, 81] high thermal stability[61] and low vapour pressure.[61, 74] As with all electrolyte systems there are of course disadvantages to using ionic liquids, most specifically the high viscosities. The high viscosity of ionic liquids counteracts their

high intrinsic conductivity leading to conductivity values similar to those for traditional carrier electrolytes dissolved in organic solvents.[61] The high viscosity of ionic liquids also hinders mass transport, giving rise to reduced diffusion coefficients. As a result acceptable Faradaic-to-background currents may only be possible with larger concentrations of redox active molecules.[81] Impurities in the ionic liquid, particularly water, can drastically affect their performance in electrochemical studies, therefore their widespread use is hindered by difficulties associated with purification. While the addition of water reduces the viscosity of ionic liquids, increasing conductivity, it also drastically reduces their renowned electrochemical window, through the introduction of hydrogen and oxygen evolution to the electrochemical processes. Regardless of the problems associated with utilizing ionic liquids in electrochemistry their advantages far outweigh their disadvantages. As more ionic liquids become commercially available their use in electrochemistry will only become more prevalent, meaning a deep understanding of ionic liquids is necessary.

It is a misnomer to think that rules applicable to traditional electrolytes will be transferable to ionic liquid systems. Throughout the literature there are examples of ionic liquids breaking steadfast rules for traditional systems. In traditional electrolytes it is expected that if an electrode is passivated with an organic monolayer electron transfer is hindered, this is not necessarily the case for ionic liquids. Instead when an electrode is passivated by an alkane monolayer the ionic liquid can intercalate into the passivating layer, assisting electron transfer to the redox species in solution.[85] As will be discussed later the electrochemical double layer cannot be explained in the same way for ionic liquids as for traditional systems. Briefly, this occurs because ionic liquids do not contain solvent molecules,[86] and they can overscreen charges in the electrochemical double layer until charge neutrality is achieved.[87] A final example of

the differences in the electrochemistry of ionic liquids and traditional electrolytes is the effect of having two redox species in solution together. In traditional electrolytes regardless of whether the redox species are measured individually or together the resulting electrochemistry is generally unaffected. When similar experiments are performed in ionic liquids, however, the double layer capacitance and diffusion coefficients are affected, as a result of the fundamental ionic characteristics of the system, which cause distinct restructuring of the solvent system, which changes in redox state.[88] Many of the key differences of electrochemistry in ionic liquids compared to that in traditional electrolytes directly result from the ionic, solvent free, nature of the system, consequently great care is needed to analyse electrochemical systems in ionic liquids before their further use in molecular electronics investigations.

Ionic liquids provide a unique opportunity for electrochemical investigations in a low volatility, high thermal stability, non-aqueous electrolyte. The use of ionic liquids in electrochemistry is on the rise and it is expected that their role in electrochemical studies will continue to grow for some time.

## Ionic Liquids in Electrodepostion

Given the growing use of ionic liquids in electrochemistry, they have also naturally been used for electrodeposition. There are seemingly endless combinations of ions composing an ionic liquid, a trait worth using when the effect of ionic liquid composition on the size and morphology of an electrodeposit are considered.[89] Furthermore, while traditional plating methods often require additives the correct choice of the ionic liquid ions can remove the need for additives of any kind. The wide potential window for which ionic liquids are used in electrochemistry means that metals and alloys, usually requiring potentials outside of the realm of standard plating

baths, are a distinct possibility for electrodeposition. This wide potential window is due to the lack of hydrogen evolution, which can only be exploited when the ionic liquids are well dried. Correctly prepared ionic liquids have been used to electrodeposit the reactive elements Li, Mg, Al, Ge, Si, Ta, and Nb, none of which can be electrodeposited through aqueous plating baths.[90] Hydrogen evolution is a concern for all electroplating baths, however, because it can have a deleterious effect on plating baths otherwise well equipped for deposition. A direct result of hydrogen evolution is hydrogen embrittlement, often evidenced by a black deposit. Due to the detrimental effects of hydrogen evolution, any method which avoids it is highly sought after. As with other industrial applications ionic liquids are also lauded as 'green' solvents for electrodeposition. Unlike many current industrial scale deposition methods ionic liquids do not require the toxic compounds often necessary.[61, 90] The advantages of using ionic liquids as solvents for electroplating are being noted by industry, as evidenced by a recently established pilot plant for Cr plating from ionic liquid by Scionix Ltd.[91] This field is, however, still in its infancy. As with electrochemistry in ionic liquids, when using these systems one must err on the side of caution as rules well established for traditional plating methods are not necessarily transferable to electroplating from ionic liquids.

The advantages of ionic liquids in general science have been exploited in electrodeposition. Ionic liquids present not only a possible green alternative to current aqueous electroplating methods, but also provide the only means of electroplating some metals. As more information is garnered about ionic liquid electroplating systems their role in this application will undoubtedly increase.

Ionic Liquids in Molecular Electronics

The first investigation of molecular electronics in ionic liquids appeared in 2006, when Albrecht *et al*. investigated an Os bisterpyridine monolayer on Au in BMIM-$PF_6$ (**Figure 7**) by scanning tunnelling spectroscopy.[3] The Os bisterpyridine system showed a ~50-fold increase in tunnel current from the off to the on state, demonstrating the potential of ionic liquids as environments for molecular electronics studies. Spurred on by this capability the *I*(*s*) technique was used in proof of concept measurements on a series of alkanedithiols in BMIM-OTf.[92] The alkanedithiols demonstrated similar conductances to those in ambient conditions. Recently BMIM-OTf has been used to investigate the electrochemical switching capabilities of 6-pTTF-6, **Figure 8**.[6] For the first time both molecular switching events were seen, in an off-on-off-on-off transition. Ionic liquids are quickly proving viable environments for molecular electronics investigations.

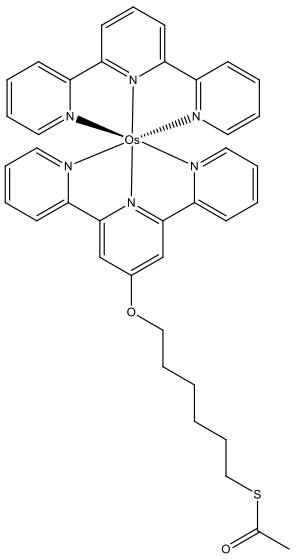


*Figure 7: The Os bisterpyridine molecule shown was measured by STS in BMIM-$PF_6$ showing a near 50-fold increase in conductance in the on state. This was the first molecular conductance measurement performed in ionic liquid.*[3]

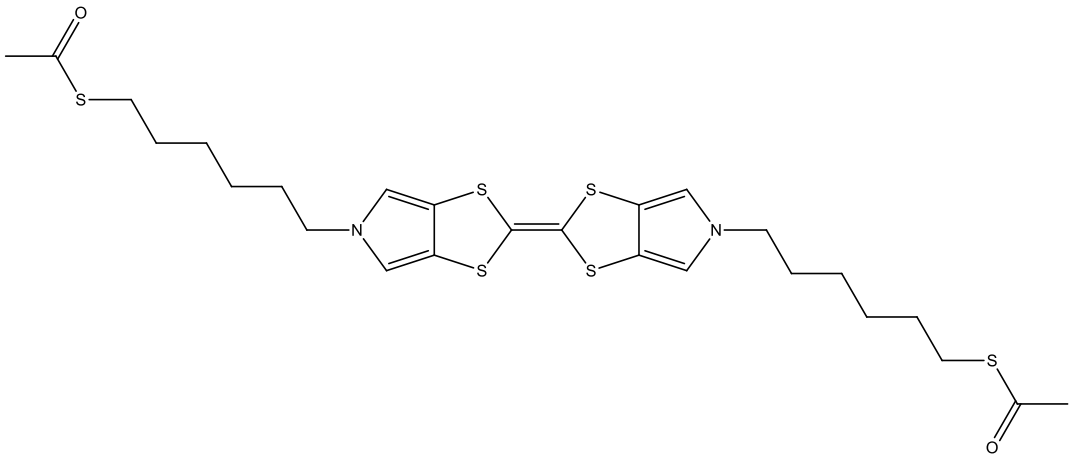


*Figure 8: Recently 6-pTTF-6 was measured by the I(s) technique in BMIM-OTf. This system showed the ability to control conductance switching using electrochemical control. This system showed off-on-off-on-off switching.*[6]

## Charge Transport Mechanisms

When studying molecular electronics an understanding of the general conductance mechanisms is important. There are four classes of charge transfer mechanisms, which can be divided into those without thermal activation and those with thermal activation.[99, 100] Only conductance by tunnelling does not requires thermal activation.[100] The three thermally activated conductance mechanisms are hopping conduction, thermionic emission, and Poole-Frankel emission.[99, 100] The conductance mechanisms discussed are visualized in **Figure 9**.

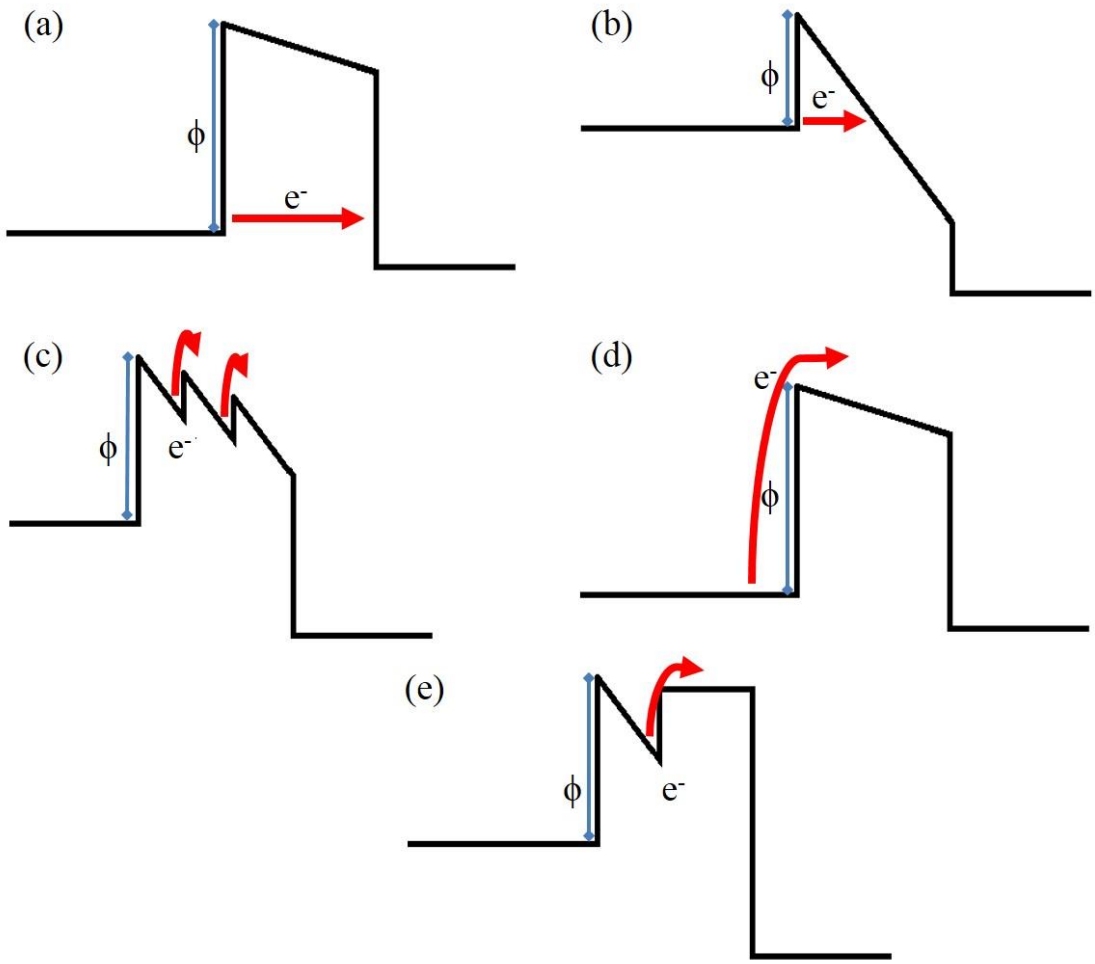


*Figure 9: The conductance mechanisms discussed are shown. These mechanisms are as follows: direct (a) and Fowler-Nordheim (b) tunnelling, hopping (c), thermionic emission (d), and Poole-Frankel emission (e).*

## Tunnelling

Tunnelling is important for molecular electronics as this is the mechanism seen for short, saturated molecules like alkanethiols.[93, 94] In tunnelling electrons are transmitted from one electrode to the other often without any charge residing on the molecular bridge in the process, and without the need for thermal activation.[95, 96] As tunnelling current transmitted through a barrier decays exponentially with distance, these systems display conductance which is exponentially dependent on distance.[94, 97] It should be noted that systems with conventional tunnelling mechanisms are often

synonymous with relatively large $\beta$ values.[98] The tunnelling mechanism itself can be divided into two regimes, which are dependent on the bias voltage and the barrier height. When the applied bias is much smaller than the potential barrier direct tunnelling occurs.[99-101] In direct tunnelling the system is most simply represented by a trapezoidal tunnel barrier.[99] The resulting current, *I*, flowing through the junction is given by the following equation:[100]

$$I \propto V \exp\left(-\frac{2d}{\hbar}\sqrt{2m\Phi}\right) \qquad \textit{(Eq. 3)}$$

Where $V$ is the bias voltage, $d$ is the barrier distance, $\hbar$ is equal to $h/2\pi$, $m$ is the effective mass, and $\Phi$ is the barrier height. When the applied voltage is much larger than the barrier height Fowler-Nordheim tunnelling occurs,[99-101] which is represented by a triangular barrier shape.[99] To account for the change in barrier shape the current of the system is now modelled by:[100]

$$I \propto V^2 \exp\left(-\frac{4d\sqrt{2m}\Phi^{3/2}}{3q\hbar V}\right) \qquad \textit{(Eq. 4)}$$

All variables have the previously given meanings, and $q$ is the charge of an electron. These equations show that while the conductance of a tunnelling system is not temperature dependent it is voltage dependent. Though a system may be satisfactorily described by the tunnelling equations it is important to understand the temperature dependent conductance regimes, because if temperature dependent studies are not performed a charge transfer cannot be conclusively determined to be tunnelling. Furthermore systems may be described by more than one conduction mechanism depending on the conditions at the time.

Hopping

Hopping has been seen in investigations of DNA,[102] oligo(aryleneethynylene)s,[103] a series of organic polymers,[104] oligo(*p*-pheneyleneethenylene)s,[105] and more. In this charge transfer mechanism the charge moves from the donor to acceptor electrode by residing on localized areas of the molecular bridge.[98, 106, 107] The multistep nature of this mechanism causes a weaker length dependence than for tunnelling.[98, 108] Unlike tunnelling, hopping is a thermally activated mechanism and can therefore be established by investigating the temperature dependence of conductance.[95, 96, 100, 108, 109] As with tunnelling the resulting current can be modelled.[100]

$$I \propto V \exp\left(-\frac{\Phi}{kT}\right) \qquad \textit{(Eq. 4)}$$

All variables have their previously listed meanings. Unlike other thermally activated mechanisms current is directly proportional to bias voltage, and there is a logarithmic dependence of current on the inverse temperature.

Thermionic Emission

Thermionic emission is another thermally activated charge transport mechanism.[99, 100, 110, 111] This mechanism describes charge transport across 1,4-phenylene diisocyanide, **Figure 10**, where it is the dominant mechanism at all biases.[9] Thermionic emission proceeds by thermal activation of the charge giving it the energy to proceed over, rather than through, the tunnel barrier.[99, 110, 111] The following equation allows the current to be modelled.[100]

$$I \propto T^2 \exp\left(-\frac{\Phi\sqrt{qV/4\pi\varepsilon d}}{kT}\right) \qquad \textit{(Eq. 5)}$$

All variables have the previously listed meanings, and $\varepsilon$ is the insulator permittivity. From this equation the current is seen to be dependent on bias voltage by $\ln(I) \propto \sqrt{V}$ and related to temperature by $\ln\left(I/T^2\right) \propto 1/T$ . By measuring the voltage dependence and/or the temperature dependence of the molecular system it should be easy to identify as thermionic emission or hopping conduction.


*Figure 10: 1,4-phenylene diisocyanide has been shown to undergo electron transfer via thermionic emission.*[9]

Poole-Frankel Emission

The final conduction mechanism possible is Poole-Frankel emission, which while observed in semi-conductor systems,[112] has not yet been noted for molecular systems. In this thermally activated mechanism defect sites act as electron traps which contribute to the resulting current.[99] As with the other mechanisms described it can be modelled to show the effects of temperature and voltage, as shown in the following equation:[113]

$$I \propto V \exp\left(\frac{-q\left(\Phi-\sqrt{qV/\pi\varepsilon}\right)}{kT}\right) \quad \textit{(Eq. 6)}$$

All variables have been previously defined. The current arising from Poole-Frankel emission is related to bias voltage by $\ln(I/V) \propto V^{1/2}$, and temperature by $\ln(I) \propto 1/T$.[99, 112]

By careful design of experiments the charge transfer mechanism of a molecular junction can be determined. An understanding of the charge transport mechanism is important to fundamentally understanding the conductance characteristics of a molecular system. Knowledge of these mechanisms is essential for the progression of molecular electronics.

## Metal-Molecule Contact Effects

In molecular electronics the identity of the metal-molecule interface is important. The interaction of the metal with the molecular end group has a significant impact on the resulting conductance. In this respect the electronic coupling between the metal Fermi level and the molecular orbitals is of importance. This coupling is easily controlled through the metal-molecule combination. Gold is relatively easy to prepare therefore it is often the molecular anchor group which is changed to alter the metal molecule interaction,[114-124] however, there have been a growing number of investigations on the effect of changing the metal contact on the conductance.[4, 93, 118-120, 125, 126]

### Anchor Group Effect

Gold is by far the most popular contact material in molecular electronics studies. Unlike other choices gold is stable to ambient exposure and easily prepared for use in standard laboratory conditions. Rather than altering the metal contact the molecular anchor group is often changed to determine the effects of the metal-molecule interaction on the molecular conductance measurements. Over the years a large library of molecular anchor groups has been amassed, including, but not limited to: thiol (-SH),[4, 114, 115, 117, 119-122, 124] isocyanide (-NC),[114] cyano (-CN),[118, 123] amine ($-NH_2$),[115-118, 121] carboxylic acid (-COOH),[115, 117] sulphide ($-S^{2-}$),[115] phosphide

(-$P^-$),[115] hydroxyl (-OH),[116, 123] fluoride (-F),[123] benzyl (-$C_6H_5$),[116] pyridyl (-$C_5H_4N$),[116] sulphonate (-$SO_3^-$),[116] selenide (-Se),[4] and nitro (-$NO_2^-$).[118] Determining the abilities of different contact groups to Au is not only important for determining the highest conductance arrangement, but also to understand how the molecule-electrode interaction affects molecular conductance. The molecular end group affects the degree of interaction between the metal contact and the molecule. At the most extreme end of the scale is the comparison of molecules physisorbed and chemisorbed on the metal substrate. It has been seen that when a molecule interacts with the metal by only a physisorbed contact the conductance is lower and less stable than that by a chemisorbed contact, due to the reduced electronic interaction between metal and molecule.[124] In the case of chemisorbed contacts the choice of molecular anchor group affects the interaction with the metal, thereby affecting molecular conductance. When series of molecular end groups have been examined in the literature it has been noted that molecules which bind more strongly to the Au give rise to high conductance values.[115, 117] Aside from altering the binding strength to Au, the choice of anchor group is also important because it directly affects the molecular orbitals of the molecule.[116, 121-123] The change in energy of the molecular orbitals as a result of changing the molecular end group, can affect the interaction with the metal Fermi levels. The effect of a concerted upward shift in the HOMO and LUMO energies was seen when the end groups of α,α'-xylyl-dithiol, **Figure 11**, were changed from –S to –O to –Se.[4] –Se showed increased conductance compared to the others because the energy of the conduction orbitals moves closer to the Au Fermi level. Changes in the molecular orbital energies do not always bring more favourable interactions with the gold Fermi level. When a –H anchor group was used in an alkane molecule the result was an increase the HOMO-LUMO gap of the molecule, resulting in a lack of levels

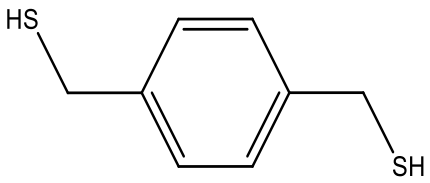


*Figure 11: The conductance of α,α'-xylyl-dithiol, and related –O and –Se terminated molecules were measured on Au, showing the effect of changing the molecular end group. As the end group changes from –S to –O to –Se the conductance increases, due to the increased interaction of the end group with the Au Fermi level.*[4]

around the Fermi level, and much lower conductance than the similar thiol terminated molecule.[122] Similar results were seen when changing from a –NC terminated benzene, with LUMOs near resonance to the Fermi level, to the –F terminated analogue.[123] It should be noted that the molecular structure itself also impacts on the effect of changing the end group. In 2013 the effect of changing the end group on highly conjugated free base porphyrins was investigated, as this effect had been mostly ignored for unsaturated molecules.[116] This investigation showed that for highly conjugated molecules the use of conjugated end groups, like pyridyl, is extremely useful as this retains the conjugation across the molecular bridge. As with other investigations the end group was seen to affect the strength of the metal-molecule interaction and the molecular orbital-Fermi level alignment. When choosing a molecular anchor group it is important to account for the effect of the end group on the structure of the molecule. The effect of the end group on the molecular orbital alignment with the metal Fermi level, and the interaction with the metal contact should also be accounted for. Unfortunately just because a molecule is a good molecular wire on gold does not mean it will be effective on other metals. Due to the inherent differences between metal surfaces the effect of the changing the metal contact on molecular conductance should be taken into account.

Metal Substrate Effect

Au has been extensively used as the contact in molecular electronics studies, even though it may not be the best choice for such measurements. Compared to other metals Au results in some of the lowest conductance values in molecular electronics.[125, 127] Furthermore, its use in hybrid electronics using semiconductor surfaces, and its ability in sister fields, like spintronics, are limited. The limitations of Au mean the effect of different metal surfaces on the conductance must be understood. Other contact materials studied include Ag,[93, 119, 125-127] Cu,[125, 127] Ni,[118, 127] Pd,[127] Pt,[93, 126, 127] Ir,[118] In,[118] and GaAs.[120] The molecular conductance on different metal surfaces is influenced by the following key factors: Fermi level position,[93, 119] orbitals involved and their DOS,[127] and bond strength.[125] In 2002 the resistances of alkanethiols of varying lengths on Au and Ag were investigated,[119] showing the Au system to have a lower resistance than Ag, a direct result of the higher Fermi energy of Au. With alkanethiols hole transport occurs through the HOMO. When the Fermi level energy increases, decreasing the gap to the HOMO, there is a decrease in the height of the energy barrier to electron transport, and a decrease in molecular resistance. A more substantial investigation on Ni, Pd, Pt, Cu, Ag, and Au has been carried out comparing group 10 and group 11 metals.[127] This study showed that while group 10 metals are dominated by *s* contribution, group 11 are dominated by *p* and *d* contributions. The character of the metals is important because this affects the metal-molecule bond angle which impacts on the conduction channels around the Fermi energies. In this case it was seen that the group 10 metals, Ni, Pd, and Pt, give rise to higher conductivities than the group 11 metals. Focusing on only the group 11 metals the jump-to-contact method was used to measure the single molecule conductance of succinic acid on Cu, Ag, and Au.[125] Conductance decreased in this investigation in the order Cu > Ag > Au

as a direct result of the decreasing metal-molecule binding energy. These three sets of results show that while it can be difficult to precisely describe the factors which contribute to the molecular conductance measured, the choice of metal is incredibly important.

An understanding of the metal-molecule interactions is important for molecular electronic devices. For the best systems the metal-molecule combination must be optimised for the strongest metal-molecule interaction and the largest metal Fermi level–molecular orbital overlap.

## Attenuation Factor ($\beta$)

The distance dependence of the system conductance is important in molecular electronics. This characteristic can be quantified through the use of the attenuation factor, $\beta$. The system conductance, $G$, length, $L$, and attenuation factor are all related by the equation:[117, 128-130]

$$G = G_0 \exp(-\beta L) \qquad (Eq.\ 7)$$

$G_0$ is the contact conductance based on the metal-anchor group coupling. There are a few possible ways noted in the literature to measure distance dependent charge transport. The first is the measurement of the change in rate constant of electron transfer between the working electrode and a surface bound redox species, with changes in molecular length.[131, 132] This requires the molecule to be synthesized with an anchor group allowing self-assembly at one end, and a redox species, like Fc, at the other end. Another method is to measure the rate of electron recombination through a molecule terminated at one end by a donor species, and at the other end an acceptor species.[133] This requires a stable molecular wire with a donor and acceptor on either

end of the molecule. One of the terminal groups can be excited driving electron/hole transfer through the molecular bridge.[133] The final technique is the use of the STM break junction (STM-BJ) or *I*(*s*) technique,[117, 128, 134-136] which requires a molecular wire terminated at both ends by anchoring groups attached to the tip and substrate. Of interest for this work is the use of the STM based techniques to measure the $\beta$-value.

The $\beta$-value is system dependent. When dealing with metal wires a $\beta$-value of 0 can be measured, while for molecules $\beta$-values larger than 0 are expected.[129] The best studied molecular systems, those with the alkane backbone, give relatively high $\beta$-values of around 1.0 $Å^{-1}$,[131] due to the large HOMO-LUMO gap of these systems. Recently there has been a push to identify molecules with low $\beta$-factors. The observation of carotenoid molecules with conductances 7 orders of magnitude larger than simple alkane molecules motivated a 2005 STM-BJ study on a series of thiol terminated carotenoid molecules.[136] When the length dependent conductance of these molecules was assessed a $\beta$ of (0.22 ± 0.04) $Å^{-1}$ was determined, which arises from the full conjugation of the carotenoid molecules. The following year even lower $\beta$-values were determined for porphyrin wires. Sedghi *et al.*[137] investigated the length dependent conductance of Zn oligoporphyrin bridges, terminated with thiol anchor groups. They witnessed surprisingly low $\beta$-factors of (0.04 ± 0.006) $Å^{-1}$. The $\beta$-value measured here is lower than in previous charge separation measurements utilizing the same backbone,[133] implying the contact to the molecular wire is also important.

While the molecular bridge has the strongest effect on the $\beta$-value measured, the contact of the molecular wire is also of great importance. The effect of the end group on the distance dependent conductance of molecular wires has been investigated for a variety of systems. In 2006 the distance dependent conductance of a series of alkane chains terminated in thiol, amine, or carboxylic acid end groups was measured,

allowing comparison of the $\beta$-values.[117] Although the $\beta$-values of all three were similar they were observed to decrease in the order thiol > amine > carboxylic acid. While similar the length dependence is exponential and therefore the effect of $\beta$-value over long-range electron transport can be high. In 2013 the distance dependent conductance of a series of highly conjugated diaryloligoynes, with different terminations was examined.[128] The terminations used were dihydrobenzo[*b*]thiophene, cyano, amino, thiol, and pyridyl. Comparison of the measured conductance values showed $\beta$ decreases in the order thiol > pyridine ≈ dihydrobenzo[*b*]thiophene > amine > cyano, due to the effect of the molecular anchor group on the ability of the molecular wire to couple to the metal. Stronger coupling occurs between the metal Fermi level and the molecular orbitals closest to it, therefore changing the molecular anchor group changes the metal-molecule interaction, altering the $\beta$-factor.[117, 137]

When investigating molecular electronics systems the $\beta$-value of the system is important for potential applications. It would be a mistake to assume that by simply choosing a molecular wire with a small HOMO-LUMO band gap this will give the most favourable $\beta$-value. Instead the whole system should be accounted for, including the metal-molecule contact. By carefully selecting the whole system, including metal, anchor group, and molecular backbone, a robust control over the electrical properties of single molecules should be possible.

## PM-IRRAS

Polarization modulation-infrared reflection absorption spectroscopy is a surface sensitive IR technique. Through the modulation of the polarization of the incident beam the sensitivity of the standard IRRAS experiment is improved allowing higher quality spectra of monolayers of adsorbed species.

Principles

PM-IRRAS works on the same premise as standard IRRAS techniques. In these measurements an incident IR beam is reflected off of the surface of interest into the detector resulting in a surface sensitive spectra. IRRAS experiments are performed in two steps, with the spectra from the *p*- and *s*-light measured separately. This procedure means long periods for the experiment, this is further extended by the time scale needed to achieve a high signal-to-noise (SNR) ratio.[138] The long time scale of the IRRAS experiments allow system instabilities to degrade the quality of the resulting spectra.[138] PM-IRRAS, on the other hand, allows performance of the IR measurements in a single step, with good SNR achieved in only tens of minutes. These advantages make PM-IRRAS the preferred technique for surface IR investigations.

PM-IRRAS experiments are performed by rapidly modulating the incident IR beam between *p*- and *s*-polarized light. Electronic signal processing and computational analysis results in a differential reflectance spectrum given by:

$$\frac{\Delta R}{R} = \frac{(R_p - R_s)}{(R_p + R_s)} \quad \textit{(Eq. 8)}$$

Where *R* denotes the reflectivity of the *p*- or *s*-polarized light. The resulting differential spectrum contains only information about the surface species, due to the combined use of *p*- and *s*-polarized light. This selectivity arises because of the reflectivities of the incident light on the substrate. The reflectivity equations are:[139]

$$R_s = \frac{(n - sec\phi)^2 + k^2}{(n + sec\phi)^2 + k^2} \quad \textit{(Eq. 9)}$$

$$R_p = \frac{(n - cos\phi)^2 + k^2}{(n + cos\phi)^2 + k^2} \quad \textit{(Eq. 10)}$$

In these equations *n* and *k* are components of the index of refraction and $\phi$ is the angle of incidence. These equations show that regardless of $\phi$ the reflectivity of the *s*-polarized light is negligible, due to the 180 ° phase shift on reflection. The *p*-polarized light, however, tends to undergo an enhancement in reflectivity, though this is dependent on $\phi$. As depicted in **Figure 12**, the largest enhancement occurs for near grazing incidence. The surface insensitivity of *s*-polarized light, coupled with the surface sensitivity of *p*-polarized light is key to the success of all IRRAS experiments. All but the surface species are probed by *s*-polarized light, whereas *p*-polarized is less

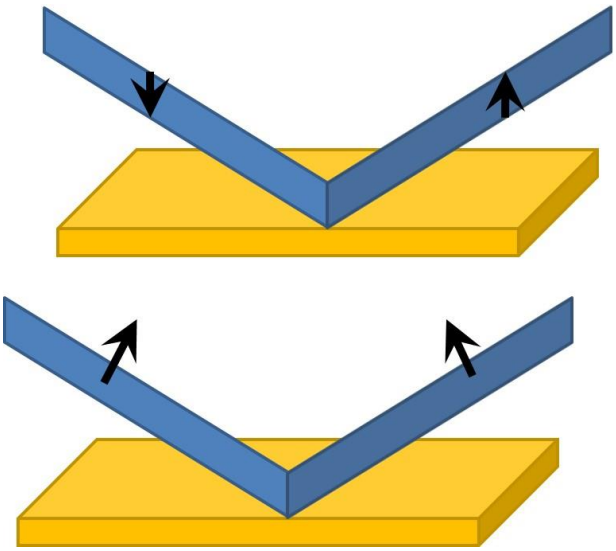

*Figure 12: PM-IRRAS experiments exploit p- and s-polarized light. When s-polarized light is reflected off of the substrate surface it undergoes a 180 ° phase change, effectively cancelling out any surface signal (a). On the other hand p-polarized light undergoes a phase change dependent on the angle of incidence (b). When near grazing incidence is used the p-polarized light undergoes its maximum enhancement, leading to the strongest surface signals. Through the use of p- and s-polarized light a spectrum with high sensitivity to surface species can be achieved, without undue influence from atmospheric species.*

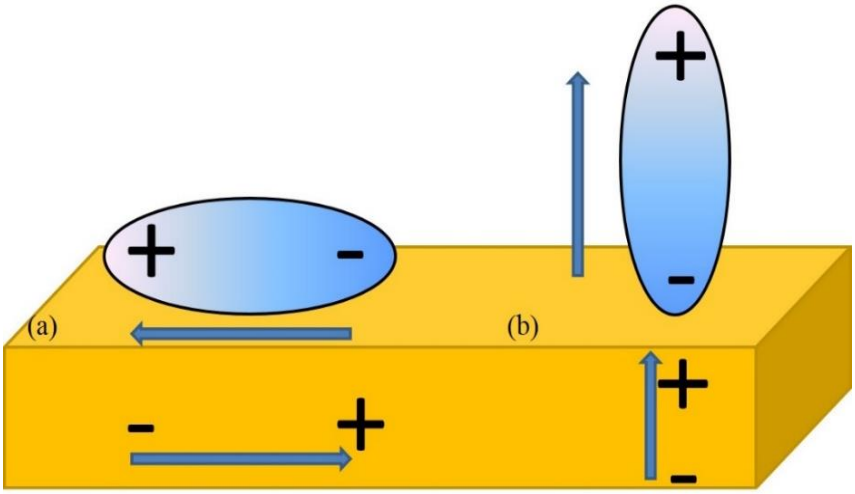


*Figure 13: In metal surfaces charge is free to move throughout, an advantageous property when using PM-IRRAS. The free movement of charge throughout the metal means that when a charge adsorbs at the surface an equal but opposite charge appears in the metal surface region. When dealing with dipole changes this translates to an equal but opposite dipole change within the metal, known as the image dipole. When the dipole change exists parallel to the surface (a), the image dipole cancels the resulting signal. On the other hand when the dipole change is perpendicular to the metal surface the image dipole causes an enhancement in signal. The signal intensity allows a reference of the molecular ordering.*

selective measuring all IR active species. The *s*-polarized spectrum can be subtracted from that of *p*-polarized light to give a final surface sensitive spectrum.

The conceptual operation of PM-IRRAS and its surface sensitivity is governed by the selection rules. When probing the IR vibrational spectra of molecules only those with a dipole change resulting from vibrational excitation are measured, with stronger responses for larger dipole changes. IRRAS measurement of adsorbed molecules on metal substrates are further limited by the surface selection rule. The surface selection rule arises because charge moves freely within a metal. Therefore, when a charge exists above the metal surface, an equal but opposite image charge forms within the

metal maintaining charge neutrality across the polarisable interface.[140] The dipole of the adsorbed molecules is countered by the 'image dipole' formed in the metal. If a dipole change is parallel to the metal surface the 'image dipole' causes mutual cancellation.[140] While, if the dipole change is perpendicular to the surface the 'image dipole' enhances the net dipole change.[140] This surface selection rule, which is exploited by PM-IRRAS is illustrated in **Figure 13**. The most intense response arises when the dipole change is perpendicular to the surface, and is non-existent when parallel to the surface. The orientation of an adsorbed molecule can be determined by detailed considerations of the intensity of its IR response.

Instrumentation

The PM-IRRAS experiment is outlined in **Figure 14**. The IR beam from the source is of random, mixed polarization. The light undergoes two polarization modulations. The first occurs as it travels through the grid polarizer, giving rise to *p*-polarized light only. Following this the beam goes through the photoelastic modulator, resulting in *p*- or *s*-polarized light. The polarized light then hits the sample, at near grazing incidence, and reflects off into the detector. The resulting signal is finally adjusted through the lock-in amplifier. The role of each component is as follows.

- *IR Source*: For PM-IRRAS experiments the IR source is often a Globar, which is more stable than other source methods.[139]
- *Grid Polarizer*: The first modulation of the IR beam occurs at the grid polarizer, which is more reliable and compact than other polarizers.[141] For optimum performance the wire width and spacing should be smaller than the incident light wavelength.[142]

- *Photoelastic Modulator*: The photoelastic modulator is the second modulation step, resulting in *p*- and *s*-polarized light. The PEM is composed of a piezoelectric crystal which is expanded and contracted with applied voltage. The expansion and contraction of the crystal changes its refractive index, causing modulation of the light. [143] When using the PEM the applied voltage must be carefully chosen to give a maximum at the region of interest, because while the outgoing *p*-polarized light is linear at all wavelengths, the *s*-polarized light is only linear at specific wavelengths.[138] The use of the PEM is advantageous as it ensures the *p*- and *s*-light follow the same path to the detector,[139] thereby removing any error arising from divergent paths. At this point there are two resulting interferograms. The first is the $(R_p+R_s)$, and the second is $J_2(\varphi_0)(R_p+R_s)$, where $J_2(\varphi_0)$ is the second order Bessel function resulting from polarization modulation.[138]
- *Lock-In Amplifier*: The lock-in amplifier is the final step to achieve the PM-IRRAS spectrum. The role of the lock-in amplifier is to demodulate the incoming $J_2(\varphi_0)(R_p+R_s)$ signal.[138, 139, 144, 145] The demodulation at the LIA occurs through the use of a reference signal provided by the PEM controller, resulting in a useable interferogram.[143, 144, 146]

This process is repeated many times for each measurement, allowing for high quality, low noise spectra. These spectra allow for IR analysis of systems which would be difficult to achieve otherwise.

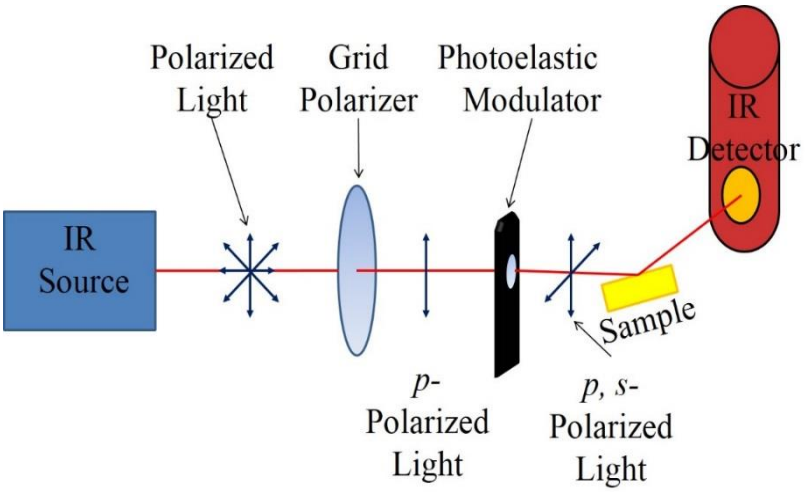


*Figure 14: During the PM-IRRAS experiment the incident IR beam goes through multiple stages before the IR detector. The beam first leaves the IR source with mixed polarization. The beam then passes through a grid polarizer resulting in p-polarized light only. When the p-polarized beam passes through the photoelastic modulator resulting in either p- or s-polarized light before hitting the sample at grazing incidence, and finally being reflected into the IR detector. The use of the PEM ensures that the p- and s-polarized light follow the same path to the sample and detector.*

## Uses for Molecular Electronics

PM-IRRAS is of great use for molecular electronics as it allows characterization of the monolayers adsorbed on the surface. The most obvious use of PM-IRRAS is to identify the adsorbed molecule. PM-IRRAS can also be used to follow the mixing of two molecules in a monolayer, by following the change in peaks with changing adsorption solution compositions. Aside from these uses PM-IRRAS allows for more sophisticated analysis, providing information about the quality of the resulting monolayer. The position and bandwidth of the $CH_2$ stretching peaks at 2825-

3000 $cm^{-1}$ provides information about the relative ordering of the monolayer. The position of these stretches relates to the crystallinity of the monolayer. When the monolayer is well ordered there is strong intermolecular interaction between the alkyl chains, while when the monolayer is liquid like the intermolecular interactions are vastly reduced. The higher the degree of intermolecular interaction the lower the wavenumber, and vice versa.[147] By comparing the peak positions of different monolayers their relative ordering can be assessed. It is, however, possible to judge the crystallinity of a single monolayer. In the assessment of a monolayer when peak position is less than 2920 $cm^{-1}$ for the $CH_2$ asymmetric stretch, and 2850 $cm^{-1}$ for the $CH_2$ symmetric stretch the monolayers are viewed as crystalline.[148, 149] This rule does not, however, hold true in all cases. Investigations of SDS systems by Sperline showed the benchmark crystallinity values are not always an accurate assessment.[150] Sperline saw that for a poorly ordered monolayer of SDS monohydrate known to have a single *gauche* defect, a peak position of 2915.7 $cm^{-1}$ was measured. When the similar RbDS system was investigated a peak position of 2919.6 $cm^{-1}$ was measured, regardless of the monolayer's all-*trans* nature. For an accurate description of the monolayer ordering the peak position is also often assessed in tandem with the FWHM of the measured $CH_2$ peaks. When a monolayer is well-ordered and crystalline it is expected to exist in the all-*trans* state, giving rise to a sharp peak, of small FWHM. As the system becomes less ordered with more *gauche* defects, more orientations contribute to the respective signal, causing peak broadening. Therefore, while, a qualitative assessment of monolayer ordering is possible using the FWHM, it should not be used as a standalone assessment. The FWHM is less accurately measured than peak position because of the possibility of peak overlap, and errors in assessment of the baseline.[147]

The combined measurement of peak position and FWHM is a powerful and straightforward means of assessing monolayer ordering.

It should be noted, that PM-IRRAS assesses the high coverage structures of molecular electronics systems, therefore it is not transferable to the sub-monolayer coverages usually used in single molecule conductance studies. PM-IRRAS is, however, useful for the structures of the pure and mixed monolayers sometimes used in single molecule conductance studies. Furthermore, some future molecular electronics devices will use ensemble structures. It is important to assess the monolayer ordering of these devices to avoid electronic shorts from highly disordered devices. Finally PM-IRRAS can provide information about the final form of the adsorbed structure and as such can be a useful measurement prior to single molecule conductance measurements.

## Electrochemistry

Electrochemistry allows the investigation of the electrochemical responses of species both in solution and on surfaces. This field is well established, with some of its fundamental principles having been presented in the 19$^{th}$ century.[151] The current boom of the electronics and renewable energies industries mean electrochemistry will become more prevalent in everyday life.

### Nernst Equation

Key to the understanding of electrochemical reactions is the Nernst equation, introduced in 1889.[151] The Nernst equation is applicable to reversible electron transfers of the form $O + ne^- \rightleftharpoons R$. In its simplest form, the Nernst equation relates the concentration of the electroactive species to the potential of electron transfer for a

given half-cell reaction. When the activities of the system are assumed to be $a_R = a_O = 1$ the Nernst equation is given by the expression:[152-154]

$$E = E^{\circ} + \frac{RT}{nF} \ln \frac{[O]}{[R]} \qquad (Eq.\ 11)$$

All variables have their usual meanings, and $E^{\circ}$ is the formal potential. When performing electrochemical measurements the Nernst equation will be applicable for reversible electron transfers where the system can return to its equilibrium state in the time frame of the process.[148] It should be noted that when [O]=[R] the standard potential of the system should equal the formal potential of the system.

Electrochemical Double Layer

When performing electrochemical experiments knowledge of the electrochemical double layer is important, because its structure affects the kinetics of an electrochemical system.[155] The electrochemical double layer is affected by the electrolyte used, and the electrode material, therefore changes in these can indirectly cause changes in the electrochemical kinetics of the system. Today a double layer model accounting for the electrolyte charges both near and far from the electrode, as well as the effect of solvent is used to explain the electrochemical double layer.

The first description of the electrochemical double layer was that of Helmholtz. In the Helmholtz model only those ions at the electrode surface are accounted for. The Helmholtz model predicts that at the charged electrode surface there will exist a layer of oppositely charged ions, causing charge neutrality, **Figure 15**.[156-158] Based on this model the capacitance of the system remains constant regardless of the potential or concentration of the system,[157] a shortcoming later addressed by the Gouy-Chapman model. Unlike the Helmholtz model, the Gouy-Chapman model accounts for the

inherent ability of charge to migrate throughout an electrolyte, **Figure 16**. In this model the ions are treated as point charges which can be infinitely close to the electrode surface. Charge neutrality is achieved by a gradient of the counter charge into the electrolyte.[156-158] Due to the reduced electrostatic interaction with the electrode surface the concentration of the counter ion decreases with increasing distance from the electrode. This model was later improved in the Gouy-Chapman-Stern model, which combined both the Helmholtz and the Gouy-Chapman model, **Figure 17**. In the Gouy-Chapman-Stern model there exists both a monolayer of counter ions, of known size, at the electrode surface, and a diffuse layer in which the concentration of counter ions decreases with increasing distance from the electrode, until the bulk electrolyte layer is met.[156, 158] The double layer model used today was finalized by Grahame, **Figure 18**.[156, 158] The counter ions can exist adsorbed on the electrode surface and as solvated species which interact with the electrode. These two ion states give rise to two planes of closest approach, the outer and inner Helmholtz plane, as well as the diffuse layer, and the bulk electrolyte. While this final description is well suited to traditional electrochemical systems, the double layers of ionic liquids are more difficult to model.

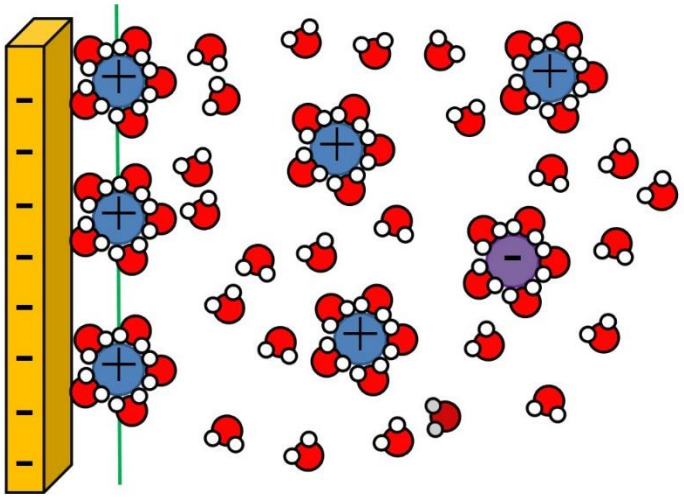

*Figure 15: The Helmholtz model was the first description of the electrochemical double layer. This description only accounts for the ions at the surface of the electrode. A layer of ions exists at the electrode of opposite charge to the electrode in order to neutralise the electrode charge.*

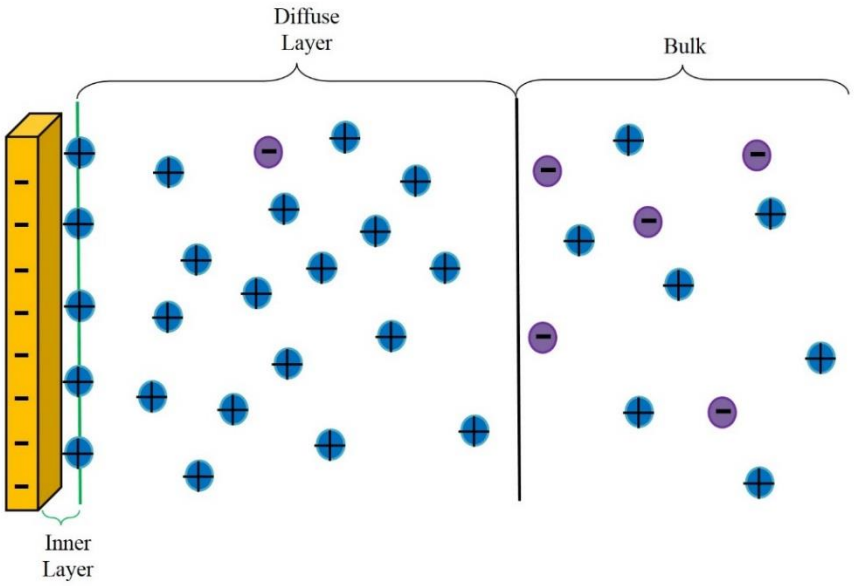


*Figure 16: The Guoy-Chapman model expands on the Helmholtz model. Oppositely charged ions form a layer at the electrode to counter the electrode charge. Unlike the Helmholtz model the ions are treated as point charges which are infinitely close to the electrode surface.*

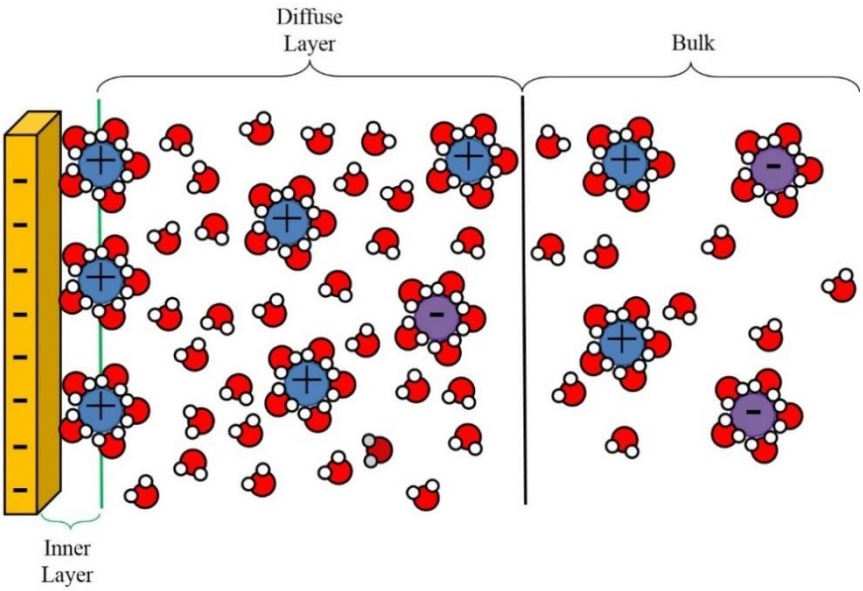


*Figure 17: The Guoy-Chapman-Stern model combines traits of the Helmholtz and Guoy-Chapman models. In this model ions are of a distinct size. The Guoy-Chapman-Stern Model has a diffuse layer with an ion concentration decreasing with distance from the electrode, until reaching the bulk electrolyte.*

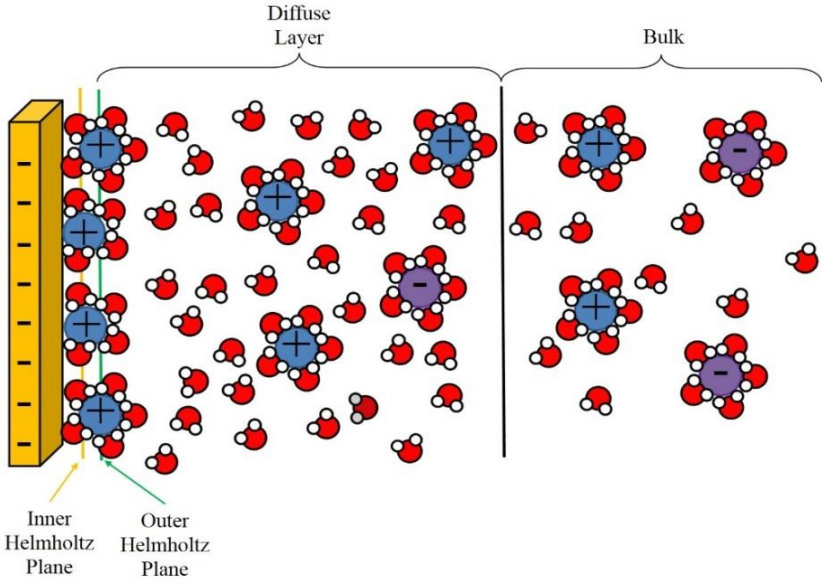


*Figure 18: The Guoy-Chapman-Stern-Grahame model is the model used today. In this model the ions have two planes of closest approach dependent on whether the molecules adsorb at the surface, the inner Helmholtz plane, or if the solvated species approaches the surface, the outer Helmholtz plane. As with prior models a diffuse layer and bulk solution layer are present.*

Work to determine the structure of the electrochemical double layer in an ionic liquid has been carried out in recent years by Kornyshev[87, 159, 160] and Oldham.[86] From these studies it is clear the Gouy-Chapman-Stern model, applied to ionic liquids in the past, does not appropriately model the ionic liquid double layer. While the Gouy-Chapman-Stern model predicts a decrease in capacitance at the point of zero charge, this instead increases at the PZC, due to the inherent differences between the ionic liquids and traditional solvent based electrolytes.[86, 159] Investigation has shown when the electrode potential changes in traditional electrolytes the ions move throughout the system, trading places with the solvent molecules.[86] In ionic liquids, however, there are no solvent molecules, therefore the ions of opposite charge must trade places. This lack of uncharged sites in ionic liquids causes a maximum capacitance at the PZC. The work of Kornyshev shows the ionic liquid is not completely free from voids, however.[159] The current generation of ionic liquids contains cations with long neutral chains, which replace the voids of traditional electrolytes by acting as spacer groups. Changes in electrode potential cause molecular orientation to change in order to move the neutral spacers and allow the ions to replace them. At moderate potentials the double layer is more compact, while at high potentials the double layer is expanded, giving rise to the decrease in capacitance away from the PZC seen for ionic liquids. Kornyshev also saw charge screening at the electrode differs for ionic liquids.[87] When dealing with ionic liquids the charge of the counter ions at the electrode surface is larger than that of the electrode itself. This overscreening of charge translates through the ionic liquid, until electroneutrality is achieved. It should be noted that this overscreening is most pronounced nearest the PZC. These fundamental differences in ionic liquids and traditional electrolytes cause obviously different electrochemical double layers. The difference in electrochemical double layer in ionic liquids is one of

many factors giving rise to the differing electrochemistry compared to traditional electrolytes.

Cyclic Voltammetry

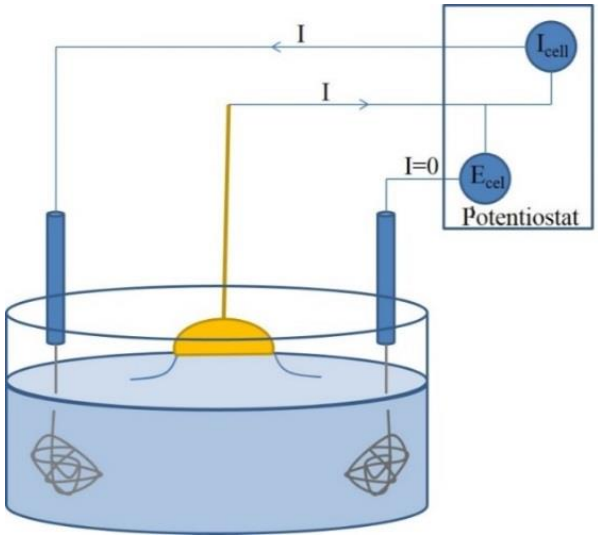


*Figure 19: Cyclic voltammetry uses a three-electrode cell, composed of a reference, counter, and working electrode. The working electrode here is a Au(111) bead which interacts with the electrolyte by a hanging meniscus. The potential of the working electrode is controlled with respect to the reference electrode. The resulting current which flows between the working and counter electrode with changing potential are measured by the potentiostat.*

Cyclic voltammetry has found widespread use in electrochemical experiments because of its ease of use and analysis. CV provides information about the kinetics of an electron transfer reaction, and the number of species involved in the experiment. Cyclic voltammetry uses a three-electrode cell connected to a potentiostat, which controls the system potential and measures the resulting current. The cell is composed of a working, reference and counter electrode, **Figure 19**. The reaction of interest occurs at the working electrode. Current flows between the working electrode and the large area counter electrode, to avoid the iR drop associated with current flow through

the reference electrode. No current flows through the reference electrode, which is chosen to undergo stable, reversible electron transfer. In cyclic voltammetry the potential of the system is changed in a saw-tooth manner with time, as shown in **Figure 20**. Faradaic current flows as a result of passing through the redox potential of the electroactive species. As the scan rate is known the change in current can be plotted as a function of potential, typically resulting in a cyclic voltammogram as shown in **Figure 21**.

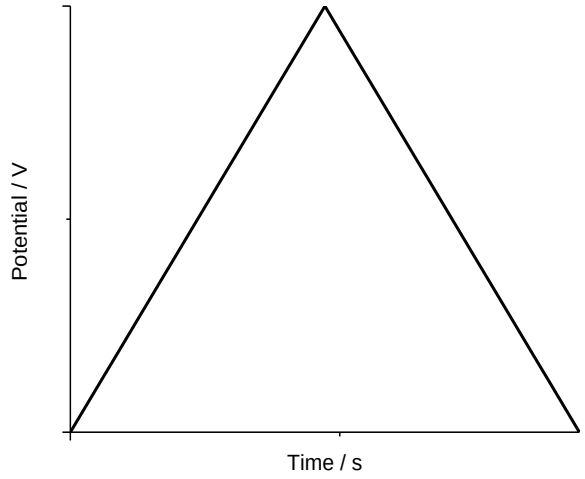


*Figure 20: In cyclic voltammetry the electrode potential varies in a saw-toothed manner with time.*

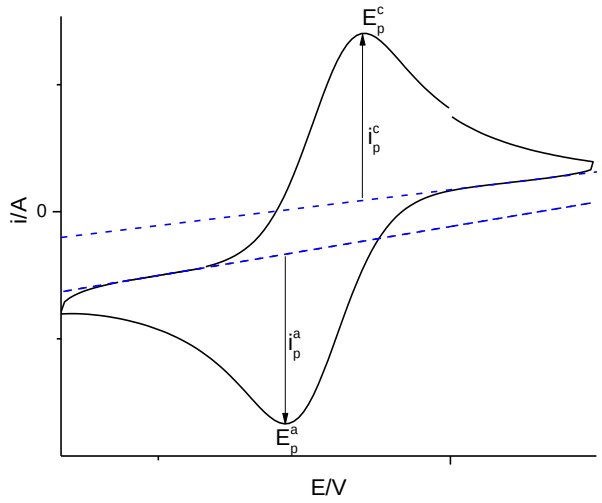


*Figure 21: Ideal reversible electrochemical reactions have the form shown. The resulting cyclic voltammograms hold important information about the electrochemical system. In order to determine the electrochemical parameters of a system. The location of the peak potentials of the system,* $E_p$*, are marked. The peak currents of the system,* $i_p$*, may also be found. To determine accurate* $i_p$ *values the voltammogram baselines must be accurately measured.*

The shape of the voltammogram in **Figure 21** is typical of electron transfers of electrochemically active solution species, which proceed by the mechanism: $R+ne^- \rightleftharpoons O$. The shape of the peaks are dependent on the diffusion controlled mass transport of the electroactive species to the electrode surface,[161-164] which controls the number of species available for electron transfer. The initial increase in current arises from the increase in the concentration gradient of the electroactive species as it converts to the product at the electrode surface.[164] The current eventually plateaus and decreases as the concentration of the electroactive species becomes increasingly small. The final current decay arises from the expansion of the diffusion layer, with increased electrolysis of the electroactive species, which causes a decrease in concentration

gradient.[162, 165] Eventually, if the experimental length allows, the concentration gradient of the electroactive species would become so low that the Faradaic current would drop to zero. The peak separation of the voltammogram is dependent on the rate of electron transfer between the electrode and the electroactive species. Depending on the rate constant of electron transfer the electrochemical reaction is broken into three regimes: reversible with $k > 1 \times 10^{-1}$ cm $s^{-1}$, quasi-reversible with $10^{-1} > k > 10^{-5}$ cm $s^{-1}$, and finally irreversible with $k < 10^{-5}$ cm $s^{-1}$.[162] It should be noted though that these rate values are dependent on the scan rate used and the diffusion of the redox species to the electrode. When the electron transfer is reversible the reduction and oxidation potentials do not change with scan rate, and the reaction fully adheres to the Nernst equation.[164] This is possible because the electron transfer is faster than the rate of mass transport, allowing the concentrations of the electroactive species to be maintained at the electrode surface.[161, 164] Unlike the reversible system the rate of electron transfer in the quasi-reversible system is not fast enough to allow a steady state concentration of electroactive species at the electrode surface. As a result the

quasi-reversible systems do not strictly adhere to the Nernst equation,[164] and scan rate dependent peak separations occur. The irreversible case is similar to that of the quasi-reversible case, although electron transfer is slower. When measuring adsorbed electroactive species the voltammetry shown in **Figure 22** is encountered. Unlike for the solution based electrochemistry the redox species is already present at the electrode surface. Furthermore, in this electrochemistry the number of species which undergo electron transfer is limited to the number present at the electrode surface, causing the peak symmetry seen.[164] As mass transport is not involved in the electrochemistry the current maxima occur at the redox potential of the species. By investigating the

resulting voltammetry valuable information about the electrochemical processes occurring can be determined.

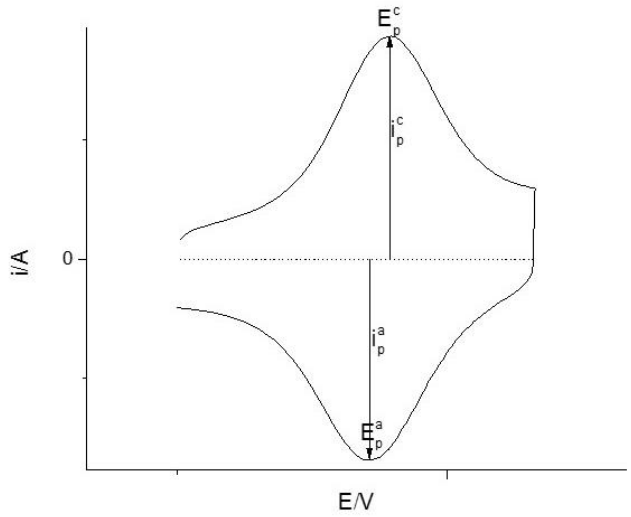


*Figure 22: Cyclic voltammetry of absorbed species results in a distinctly different shape. Unlike solution electrochemistry an ideal system shows symmetric voltammetry, with equal anodic and cathodic peak potentials. Offsets in the peak potentials, as seen here, occur for slower rates of electron transfer. The symmetric nature of the adsorbed species voltammetry is due to the presence of all of the redox molecule at the electrode surface at the start of and during the experiment. This means electron transfer to the redox species is not diffusion controlled.*

Differential Pulse Voltammetry

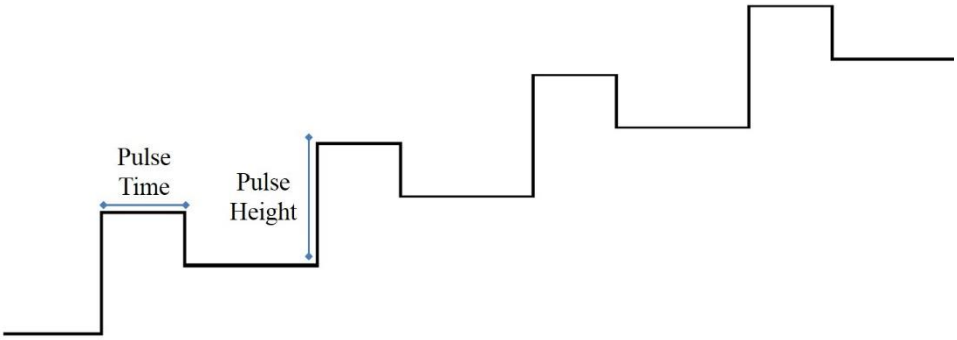


*Figure 23: The DPV potential program is shown. DPV proceeds with a known, changing baseline potential over which a 10-100 mV voltage pulse is applied. After application of the pulse, the voltage drops to a new baseline potential.*

When using redox active species which have a difficult to observe electrochemical response cyclic voltammetry may be inadequate. In electrochemical experiments, particularly cyclic voltammetry, there is always a background charging current,[166] which can hide the Faradaic current related to the redox couple. A convenient method to remove the charging current is differential pulse voltammetry. Pulse voltammetries are useful for the removal of charging currents because these currents decay much faster than the Faradaic currents of interest.[166] The potential versus time form of the DPV experiments, shown in **Figure 23**, proceeds in a staircase manner with a pulse superimposed over the changing baseline potential.[154, 167] During these experiments the baseline potential is applied for a known time, after which a voltage pulse of 10-100 mV is applied for a much shorter time period,[167, 168] before dropping to the new baseline potential. The duration of the voltage pulse is a balancing act, as it must be long enough to allow the decay of the charging current, but not so long that the Faradaic current fully decays.[166] When working with differential pulse the current value is measured just before the application of the pulse, and then late in

the pulse.[154, 167] The difference of these values is then plotted as a function of potential, giving rise to a voltammogram ideally free from background current.

## Electrochemical Impedance Spectroscopy

The impedance of an electrochemical system can be measured using electrochemical impedance spectroscopy, which is particularly useful for investigation of organic monolayers formed on an electrode surface. Through the use of EIS the comparative resistance of the systems with and without the monolayer can be determined, allowing an assessment of the passivation ability of the monolayer. EIS measurements are performed at a known potential. The system is perturbed by an applied AC sine wave,[169-171] with information about the system garnered from the change in amplitude and potential of the applied wave.[172, 173] The typical method for measuring electrochemical impedance spectra is the use of a Frequency Response Analyser (FRA). Using the FRA technique a DC current potential is applied to the working electrode of the system with an AC wave of known frequency and amplitude superimposed on this signal.[169, 174] The resulting AC response is recorded, and the process repeated at different frequencies.[174] Through measurement of the response at different frequencies a Nyquist plot of Z', the resistance, versus –Z", the reactance can be prepared. Z' and Z" are related to the impedance, $|Z|$, by the equation $|Z|^2 = (Z')^2 + (Z")^2$.[171] The Nyquist plot can be fitted to an equivalent circuit diagram, usually the Randles circuit, to determine the solution and electrode resistances. When dealing with monolayers on electrode the electrode resistance can be compared to that of the bare electrode to determine relative surface coverage.

Electrochemistry in Molecular Electronics Investigations

Electrochemistry, particularly cyclic voltammetry, is insightful for molecular electronics investigations. The most straightforward experiments allow for determination of the monolayer coverage, and the redox activity of the species to be assessed. Electrochemistry also allows in depth analysis of a molecular electronics system by enabling assessment of the rate constant of electron transfer between the electrode, and a surface bound redox species. There is general consensus that the rate constant of electron transfer and the molecular conductance of analogous systems are related.[175-178] Recently there have been experimental efforts to understand the relationship between molecular conductance and the rate constant of electron transfer. In 2011 Zhou *et al.*[175] investigated a series of redox active monolayers of different structure, including an Os terpyridine complex, a phenylenvinylene, and a series of Fc containing molecules, **Figure 24**. These molecules were investigated by fast scan CV and STM-BJ. Whilst these investigations showed a general trend of molecules with faster rates of electron transfer being more conductive, there were some discrepancies. The differences seen likely arise because of the different nature of the CV and the STM-BJ systems. In CV electron transfer occurs by localization of the electron or hole on a localized state, whereas in STM measurements the charge traverses the molecule through tunnelling. Furthermore the CV measurements are generally performed on a monolayer, while those of the STM-BJ are performed on a single molecule. In the STM-BJ junction it is possible that the molecule is not fully upright, as in the CV, causing a higher conductance than expected. Whilst showing that molecules with high values of electron transfer rate constant lead to high conductance little was done to form an overall relation. In 2013 Wierzbinski et al.[178] investigated single and double strand PNA molecules, of varying length, bound by cysteine to Au. These molecules

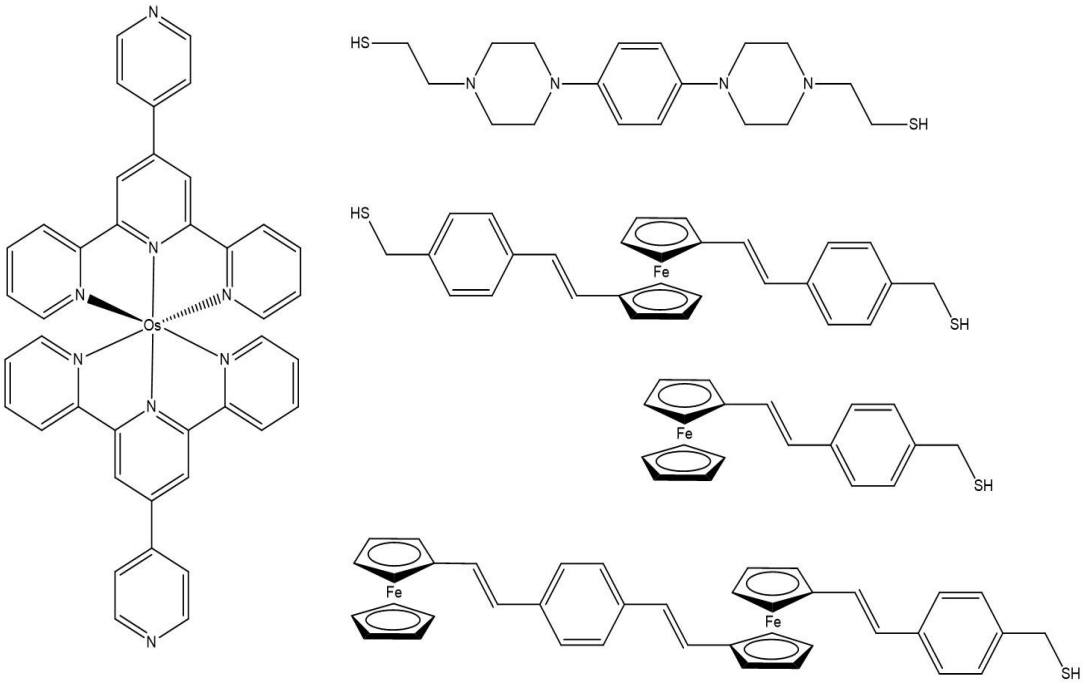


*Figure 24: To determine the relationship between the rate constant of electron transfer and molecular conductance the pictured molecules were measured by fast scan CV and STM-BJ. It was generally seen that the faster the rate of electron transfer the greater the molecular conductance.*[175]

were examined by STM-BJ and CV, although for this they were terminated with Fc. In this investigation it was expected that the *k* and *G* values would have a linear relationship due to the similarities between the Landauer conductance of a molecular junction and the rate equation for charge transfer across a molecular bridge:

$$g_{MJ} = \frac{e^2}{\pi\hbar}\Gamma_{LB}\Gamma_{RB}|G_B|^2 \text{ (Eq. 12)}$$

$$k_{DA} = \frac{2\pi}{\hbar}|V_{DB}V_{AB}|^2|G_B|^2F \quad \text{(Eq. 13)}$$

Based on the linear relationship expected for *k* and *G* it is determined that $\beta_k=\beta_g$, where $\beta_k$ and $\beta_g$ are the attenuation factors found from the electrochemical rate constant and molecular conductance, respectively. Comparison of the rate constant of electron transfer, and the conductance of the systems demonstrated that faster rates of electron

transfer correlate with higher conductance values. It was also determined that *k* and *G*, for each series of molecules, have a non-linear relationship given by $G = Ak^B$. Again this more complex relationship between *k* and *G* is attributed to inherent differences in CV and STM-BJ investigations, more specifically differences in the barrier height to electron transfer in the two investigation types. Wierzbinski concluded that these differences in apparent barrier height arise from differences in work function between the two set-ups, differences in solvation environment, and the charging of the molecular bridge and metal-molecule contact which can occur in STM-BJ. Unfortunately based on these publications it appears the relationship between *k* and *G* is difficult to predict, however, it is clear the two are related, albeit in a complex manner. To conclude this section CV on redox active monolayers is a promising technique in molecular electronics. By using CV it may be possible to screen systems first by electrochemistry to allow those with clear electrochemical response and where desired the highest rates of electron transfer to be determined. Using the CV data it is then possible to make an informed decision about the best redox active systems to perform molecular conductance studies on.

## STM

The invention of the scanning tunnelling microscope in the early 1980s revolutionized surface science. While initially used by only a select few groups,[179] the STM has found use in many scientific fields. The STM is particularly important for molecular electronics investigations as it provides a method for quickly forming repeatable molecular junctions.

## Background

Accounts of the STM first appeared in *Applied Physics Letters* in January of 1982.[180] By the time of this publication, however, Gerd Binnig, and Heinrich Rohrer had already submitted a patent disclosure on the STM.[179] While the exploitation of vacuum tunnelling had been envisaged before,[181, 182] the work of Binnig and Rohrer represented a departure from previous investigations because they aimed to measure the vacuum tunnelling, utilise it as a spectroscopic technique and measure its changes as the probe moved across the surface. They were indeed successful at harnessing measurement of the vacuum tunnelling current and in 1982 published the first current versus distance measurements performed with the STM.[180] This publication showed for the first time the exponential decay in tunnelling in an expanding tunnel junction, over four orders of magnitude. In the same year the advantages of being able to scan the tip over the surface, while measuring current, were presented. For the first time the substrate structure of (110) $CaIrSn_4$, and Au surfaces were imaged by STM.[183] While Binnig and Rohrer made great strides in the exploitation of vacuum tunnelling for scanning tunnelling microscopy, there was doubt about the quality of the results as atomic scale resolution was not achieved in the earliest studies.[179] This changed in 1985, however, when atomic resolution of the 7 x 7 and 2 x 2 reconstructions of Ge on Si(111) was achieved by Becker *et al.*[184] The demonstration of the ability of the STM to achieve atomic scale resolution cemented the STM in scientific studies. Following the achievement of atomic resolution by the STM Binnig and Rohrer were awarded the Nobel Prize in Physics in 1986. Today the STM is a diverse technique allowing both imaging and spectroscopy of systems in chemistry, materials, biology and more. The STM is a widely used technique which has been cited in tens of thousands of publications.

Quantum Tunnelling

Key to the function of the STM is the quantum mechanical phenomena of tunnelling. Tunnelling is incredibly important in physics, with work towards experimental understanding of tunnelling awarded the Nobel prize in physics in 1973.[185] In classical physics when a particle encounters a potential barrier its motion is impeded by the barrier unless it has more energy than the barrier itself. In quantum mechanics, however, the particle's progression is not necessarily halted by a potential barrier, as a direct result of wave-particle duality. When dealing with a potential barrier of higher energy than the electron, the wave function of the electron from the left to the right of the barrier exists as shown **Figure 25**. Key to determining the probability of the electron traversing the barrier is the Schrödinger equation, which can be rearranged to give:[186]

$$\frac{d^2\psi}{dx^2} = \frac{2m}{\hbar^2}(E - V)\psi \quad \textit{(Eq. 14)}$$

For this equation to be solved the wavefunction, ψ, must be known. When dealing with a potential barrier, where by definition V > E, the wavefunctions are given by:[186]

$$\psi = Ae^{ikW} + Be^{-ikW} \qquad \textit{(Eq. 15)}$$

For the left side of the barrier. Where $k\hbar = (2me)^{1/2}$

$$\psi = Ce^{\kappa W} + De^{-\kappa W} \quad \textit{(Eq. 16)}$$

For the electron through the barrier, with $\kappa\hbar = \{2m(V - E)\}^{1/2}$.

$$\psi = A'e^{ikW} + B'e^{-ikW} \qquad \textit{(Eq.17)}$$

For the electron on the right side of the barrier.

The Schrödinger equation shows that electrons can tunnel through the barrier because in all allowed cases the solution is non-zero,[187] with 0 expected for disallowed states. Based on the Schrödinger equation the probability of tunnelling through the potential, $T$, can be found, and related to the barrier height and width.[188]

$$T \propto \frac{16E(V_0-E)}{V_0^2}\exp\left(-2\sqrt{\frac{2m^*(V_0-E)}{\hbar^2}}W\right) \qquad \textit{(Eq. 18)}$$

Where $E$ is the potential of the electron, $V_0$, is the potential of the barrier, and $W$ is the width of the barrier. This probability equation dictates the tunnelling probability is exponentially related to barrier width, with larger barrier widths decreasing tunnelling probability. The dependence of tunnelling on barrier width will be seen to be a key premise of STM investigations.

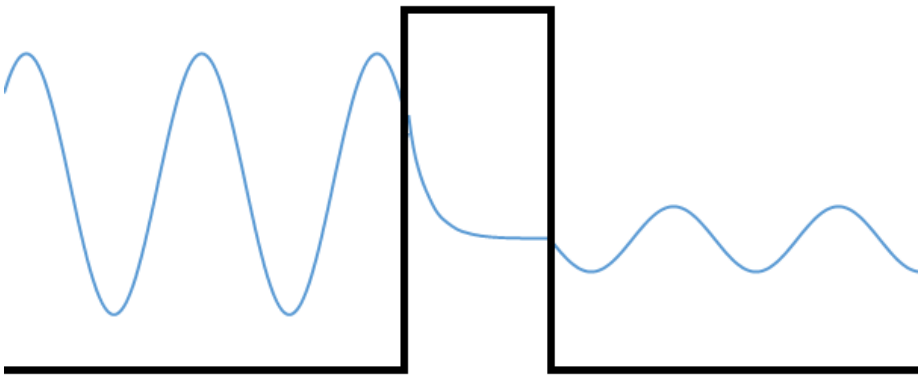

*Figure 25: In quantum mechanics electrons exhibit wave-particle duality. This characteristic means that even when the energy barrier is larger than the energy of the electron there is still a probability of the electron tunnelling through the barrier. On the left-side of the barrier the electron has wave like properties, in the barrier there is an exponential decay of the electron energy, and on the right-hand side of the barrier the wave-like properties return, however, with reduced amplitude.*

## Principles

STM measurements exploit vacuum tunnelling between an atomically sharp tip and substrate, both of which are conductive. The driving force of the STM

technique is the strong distance dependence of the current which flows between the tip and substrate. The relation between tip-substrate distance, *s*, and the current, $I_T$, is given by the equation:[183, 189]

$$I_T \propto (V_{bias}/s)\exp(-A\Phi^{1/2}s) \qquad \textit{(Eq. 19)}$$

In this equation $V_{bias}$ is the bias voltage, $A$ is 1.025 Å$^{-1}$ eV$^{-1/2}$ for a vacuum, and $\Phi$ is the work function. $A$ is found from $A = \left(\left(\frac{4\pi}{h}\right)2m\right)^{1/2}$, where h is Planck's constant, and $m$ the free electron mass. This equation shows that as the tip-substrate distance increases the tunnel current decays exponentially, and therefore small height changes in the substrate cause noticeable current changes. It should be noted that changes in the work function of the system also cause the current to change. The current-distance relationship of tunnelling is combined with the movement of the tip across the surface to allow imaging of the substrate.

As there is a strong current-distance relationship between tip and substrate of the STM the tip should be atomically sharp with a single protrusion. When tunnelling occurs through an STM tip most of the current flows through the tip protrusion closest to the surface, and current rapidly falls away to the side of this.[189, 190] A piezoelectric system controls the movement of the STM tip across the substrate. While this used to be composed of a piezo tripod,[184] a piezo tube is now used, giving better performance, with less effect from the ambient vibrations, faster scan speeds, and smaller STM components.[191] The fine control of the STM tip across the surface allows for atomic scale imaging of the substrate. There are two modes in which the STM can be used to image the substrate, as shown in **Figure 26**. The first, and most common, is the constant current mode. In this method the tip is scanned across the surface with the tip height dictated by the chosen current. As changes in the substrate cause changes in the

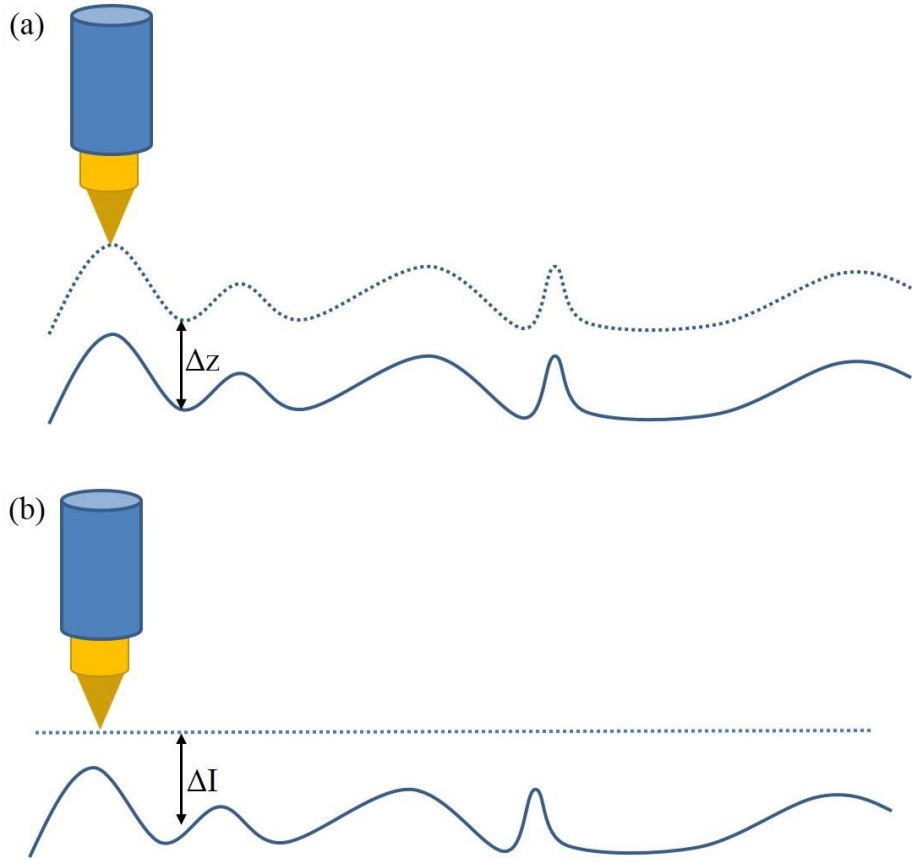


*Figure 26: The STM can be used for imaging in one of two modes. (a) In constant current mode the STM measures the topography of the surface by measuring changes in the z-position of the tip. These changes occur to maintain a constant current, (b) In constant height mode the STM measures the surface topography by measuring the change in the current measured at the tip. In this mode the tip is held at a constant z-position, therefore as the surface topography changes, and the distance between the tip and substrate changes the current changes.*

current the feedback loop of the STM causes the tip to move in the z-direction.[190, 192] In this method the z-displacement of the tip is recorded throughout. If the substrate is extremely flat the STM can be used in constant height mode, in which the changes in current between tip and substrate are recorded as the tip is moved across the surface.[190, 192] This is only suitable for flat surfaces because the tip does not correct for protrusions in the surface, and will instead crash into them. Aside from imaging STM also allows

for the measurement of the current versus distance characteristics of a system,[180, 193] an ability later shown to be important to molecular electronics studies.

EC-STM

Of particular use in molecular electronics investigations is the ability to use the STM in conjunction with the control of the electrochemical potential of the system, as in EC-STM. The general setup for an EC-STM experiment is shown in **Figure 27**. These experiments are setup as a four electrode system, composed of a reference electrode, a counter electrode, and two working electrodes, the tip and substrate. Through the use of a built in bipotentiostat the tip and substrate potentials, $E_T$ and $E_S$ respectively, can be separately controlled.[192, 194, 195] It is standard, however, to keep the bias between the tip and the substrate constant, therefore the tip potential is based on the substrate potential.[192, 195]

When working with EC-STM one of the biggest difficulties presented is the fact that the current measured by the tip is a combination of the tunnel current and the faradaic current of the system.[195] One of the simplest ways to ensure the effect of the faradaic contribution is minimized is to insulate the tip, so only a minimal area is exposed, thereby restricting the conductive area of the tip.[192, 194-196] This technique has been used throughout to ensure accurate measurements

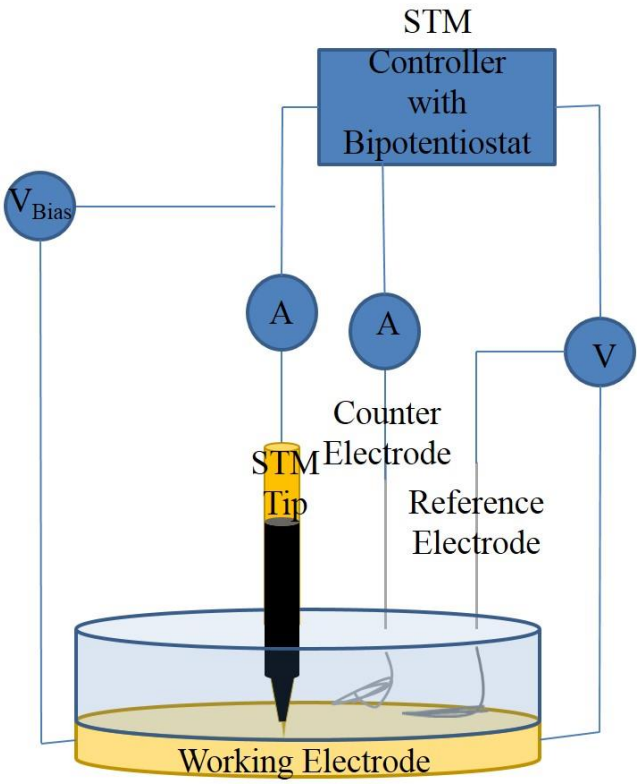


*Figure 27: EC-STM experiments are performed with the setup pictured. These experiments work with a four-electrode system composed of two working electrodes, a reference electrode, and a counter electrode. The working, counter and reference electrodes are controlled in the manner outlined for the standard three-electrode cell setup. The use of a bipotentiostat allows separate control of the two working electrodes which are the STM tip and substrate. By using a bipotentiostat control of the bias potential, $V_{bias}$, between the STM tip and substrate is possible. To avoid faradaic contributions to the current measured by the tip, arising from charge transfer through the electrolyte, the tip must be coated (e.g. with Apiezon wax) allowing only a minimum tip surface area.*

## STM in Molecular Electronics Measurements

### Break Junction

In 2003 Tao's break junction technique, the first STM method allowing for symmetric contact to a molecular wire, was published.[19] In the break junction technique it is possible to form thousands of junctions in a short time, allowing measurement of statistically significant conductances.[197] In the break junction experiment the STM tip is moved in and out of contact with the substrate surface in a solution with the molecular wire. During retraction the tip pulls a metallic wire out of

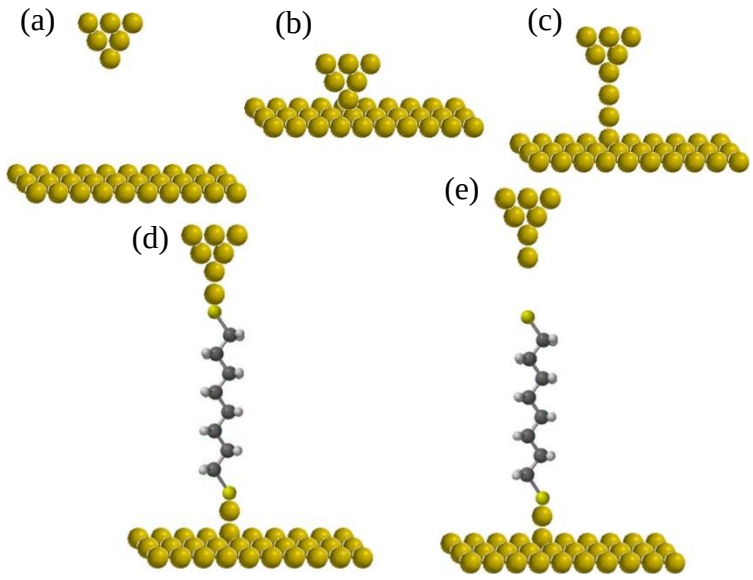


*Figure 28: The STM break junction technique is a multi-step process. (a) The tip begins a known distance away from the substrate. This distance is controlled by the set point current of the STM. (b) The tip is approached to the substrate allowing contact to be made. (c) When the tip is retracted from the substrate a metal nanowire forms. (d) Further retraction of the tip results in breaking of the nanowire. If the tip-substrate junction breaks in the presence of the molecular wire of interest it can span the tip-substrate gap. (e) Finally further retraction of the tip causes the molecular junction to break. This breakage may occur at the metal-anchor group bond as pictured, or it may occur at a metal-metal bond.*

the surface, and with further retraction this nanowire breaks. As the measurement is performed in the presence of the molecular wire it can span the gap between the tip and substrate allowing measurement of its conductance. The steps of the break junction technique are shown in **Figure 28**. This process can be followed throughout the retraction using the *I*(*s*) curves, which show stepwise decreases in conductance, assigned to different conductance events. Those high conductance plateaus occurring at integer values of $G_0$ are due to the breaking of the wires of the metallic contacts. Lower conductance values due to the molecular wire are also apparent in the *I*(*s*) traces.[19] The break junction method is useful for determining the highest conductance values of a molecular system.

*I*(*s*) Technique

In 2003 Haiss *et al.* published the first work using the *I*(*s*) technique in which the molecular conductance of 6V6 was measured between two Au contacts.[18] Like the break junction technique, in the *I*(*s*) technique both ends of the molecular wire are contacted to form a symmetric junction. The *I*(*s*) technique is visualized in **Figure 29**. In the *I*(*s*) technique the STM tip approaches the substrate surface by an increase in the setpoint current, $I_0$. The close proximity of the tip to the molecular wire coated substrate can result in the spontaneous attachment of the molecule to the tip. On retraction of the STM tip the molecule moves from a flat lying to an upright position, with the junction eventually breaking. At no point in this process do the tip and substrate contact. The retraction can be followed in the simultaneously measures *I*(*s*) characteristics. Two general trace types can be distinguished, as in **Figure 30**, depending on whether the nano-gap forms with or without the presence of a molecular wire. When a molecular wire is not present a clean exponential curve results, due to through space tunnelling.[18] If a molecule spans the gap, however, a characteristic

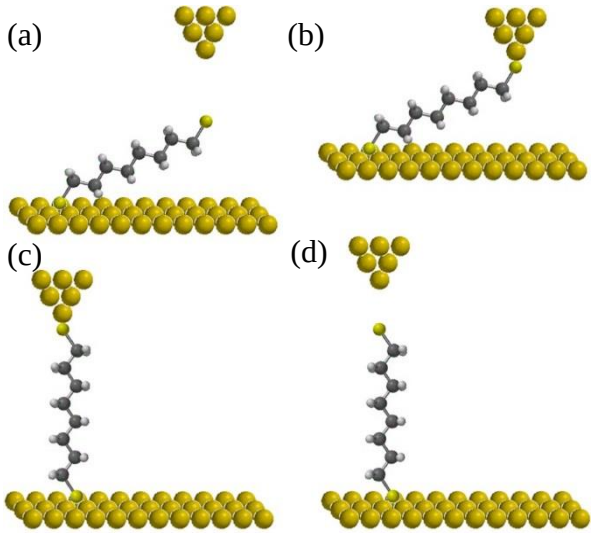


*Figure 29: The* I(s) *technique proceeds in a similar manner to the break junction technique, except contact between tip and substrate is not made. The* I(s) *technique proceeds as follows: (a) The tip approaches the substrate surface which has the molecular wire pre-adsorbed, retraction of the tip follows. (b) The molecular wire spans the tip-substrate gap aiding charge transfer between the two. (c) Retraction of the tip continues pulling the molecular wire upright in the junction. (d) Full retraction of the tip occurs with the breaking of the tip-molecule-substrate junction. The junction may break at the metal-molecule bond, as shown, or at a metal-metal bond.*

plateau is seen in the exponential current decay. The current of the plateau, $I_w$, is due to the enhanced current through the molecular junction. $I_w$ is easily converted to molecular conductance, $G$, by $G = {I_w}/{V_{bias}}$. In the resulting $I(s)$ curves the plateau length, $s_w$, corresponds to the length at which the tip-molecule-substrate junction breaks. This can be added to the set point distance, $s_0$, calibrated specifically for the setup, to find the total break-off distance. Comparison of the break-off distance to the molecular length gives information about the molecular junction. As the $I(s)$ technique allows the measurement of molecules adsorbed on the surface it is advantageous for

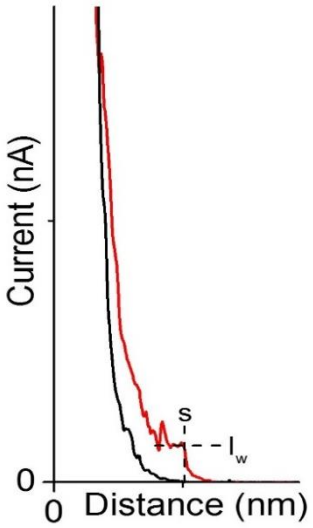


*Figure 30: When STM-BJ and I(s) measurements are performed the current between tip and substrate decays exponentially, as shown. If the tip retracts from the substrate without a molecule present between tip and substrate then pure exponential decay, as in the black curve, occurs. If a molecule spans the gap, however, the substrate-molecule-tip junction modifies the current-distance characteristics. When charge transfer occurs through the molecule there is a conductance plateau such as that in the red curve. The plateau current value,* $I_w$*, can be correlated to the molecular conductance. The length of the current plateau can be correlated to the junction breakoff distance,* s.

molecules of limited solubility. The last point is particularly important as it means even molecules of low solubility can be investigated with the *I*(*s*) technique.

Jump-to-Contact

The jump-to-contact break junction technique, outlined in **Figure 31**, was introduced in 2008 to measure the point contacts of non-noble metals,[198] and was later adapted for single molecule conductance studies.[125, 199] In the jump-to-contact technique the tip and substrate are composed of the same metal ($M_1$) which does not alloy with the metal of interest ($M_2$). During the jump-to-contact process $M_2$ is continually electrodeposited to the STM tip. During the electrodeposition a short

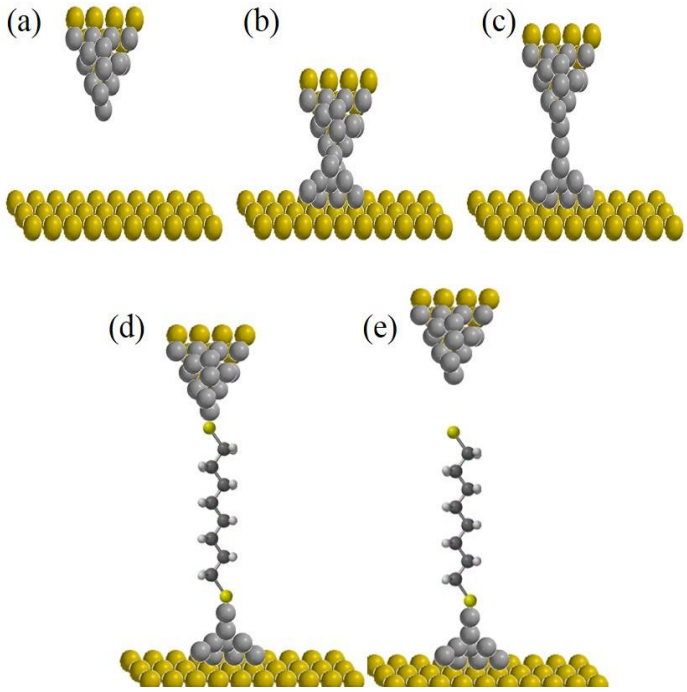


*Figure 31: The jump-to-contact STM technique is a further development of the STM-BJ technique. In this method the metal of interest is plated onto an inert metal tip, (a) which is composed of the same material as the substrate. Following this plating the jump-to-contact technique proceeds as follows. (b) A voltage pulse is applied driving the tip to the surface and allowing transfer of the electrodeposited metal to the surface. (c) The STM feedback loop forces the tip to retract, forming a nanowire in the process. (d) Further retraction of the STM tip causes the nanowire to break, allowing the molecular wire of interest to span the gap, aiding charge transfer. (e) Further tip retraction causes the metal-molecule-metal junction to break.*

voltage pulse is applied to the system, $Z_{piezo}$, which drives the tip towards the substrate. When the tip is close to the substrate the electrodeposited $M_2$ spans the gap from tip to substrate forming a nanoconstriction. From here the setup behaves in the same manner as a break junction experiment. The large current flowing through the nanoconstriction causes the feedback loop to force the retraction of the STM tip, which eventually breaks the metal contact. If this experiment is performed in the presence of

a molecular wire it can span the gap, allowing its conductance to be measured.[198] The jump-to-contact method is particularly useful for the measurement of metal surfaces which are highly reactive under ambient conditions, such as Fe and Ni.[198]

Scanning Tunnelling Spectroscopy (STS)

Scanning tunnelling spectroscopy allows measurement of the conductance properties of an asymmetric junction of a monolayer of redox active molecules. In STS measurements the change in tunnel current is measured as a function of substrate potential,[200-203] and is therefore only useful for redox active molecular wires. In this technique the tip is held at a fixed bias voltage above the monolayer, and the potential of the tip, $E_T$, and substrate, $E_S$, are swept with the feedback loop off, keeping the tip from retracting with changes in tunnel current during the potential scan.[200-203] Care must be taken in the choice of potentials as $E_S$ and $E_T$ must start at a value at which there is no redox process, with changes in tunnel current seen when the potential sweeps through the redox potential of the molecular wire.[200, 203] As the feedback loop is off during these measurements the system must be stable and the measurement time short, to avoid erroneous changes in tunnel current.[203] The STS technique has proven useful in molecular electronics investigations, and was the basis for the first conductance measurements in ionic liquid.[3]

## Karl Fisher Titration

One of the merits of ionic liquids are their wide electrochemical windows, gained through the lack of hydrogen evolution. The degree of hydrogen evolution which can occur is dependent, however, on the water content of the ionic liquid, therefore a means of quantifying this is necessary. A simple method for the determination of the water content of a system is the Karl Fischer titration, a

potentiostatic titration based on the reaction of water with iodine. Originally established in 1935[204] the Karl Fischer titration technique has grown into a straightforward and accurate technique to determine the water content of a sample.[205] Karl Fischer titration was revolutionized with the advent of a potentiostatic means of determining the titration endpoint, which has allowed automation of the technique.

The Karl Fischer titration is based on the reaction of iodine and water, which can be monitored electrochemically. Titration can be performed volumetrically, with the iodine added from a burette, or coulometrically, with the iodine formed in the titration cell.[206] For the small volumes of water present in ionic liquids, as well as the small sample sizes available coulometric titration was used in this work.[207, 208] This titration is performed with a mix of sulphur dioxide, diethanolamine, 1H-imidazole monohydriodide, and imidazole, in a methanol solution.[209] Iodine forms from 1H-imidazole monohydriodide electrochemically in the titration cell. The titration can then proceed through the following reaction:[206, 207]

$$H_2O + I_2 + SO_2 + CH_3OH + 3RN \rightarrow [RNH]SO_4CH_3 + 2[RNH]I \qquad \textit{(Eq. 20)}$$

In these titrations the iodine is the limiting factor,[205] and is therefore rapidly used up on introduction to the cell. When there is water present the rapid consumption of iodine, means only iodide species are ever present in the cell. When the end point is reached the iodine is no longer consumed and builds up in the cell. The appearance of both species is monitored potentiostatically. During the titration the presence of iodide alone means that current does not flow between the electrodes in the titration cell, however, at the endpoint when both species are present the current rapidly increases.[208, 210] It should be noted though, that in modern titrators addition of the titrating reagent can be slowed based on given control parameters.[207] The reaction of

iodine with water in this method allows for an accurate measurement of water because they react with 1:1 stoichiometry and 100 % electrical efficiency is achieved.[205, 208] Based on these assumptions the amount of water in the sample can be determined based on the charge necessary to form the iodine used in the titration.[208]

The Karl Fischer titration is a straightforward method allowing the determination of the water content in an ionic liquid sample. Through the use of coulometric titration the water content of even small samples can be found. The automated procedure now standard for Karl Fischer titration allows this analysis to be performed with little time used by the operator.

When working with ionic liquids it is possible to achieve water contents of 1 ppm or less,[211, 212] however, this is not the usual working water content. The water content of ionic liquids is often around 100 ppm,[78, 213, 214] but can be 1000 ppm or more depending on the ionic liquid used.[65, 73, 78] As this trait affects the electrochemical window of the ionic liquid this work aimed to achieve a low water content. Karl Fischer titrations on the BMIM-OTf used throughout showed drying the ionic liquid for at least 18 hours at 120 °C resulted in a final water content of around 100 ppm.

## References


1. A. Aviram and M. A. Ratner, *Chemical Physics Letters*, 1974, **29**, 277-283.
2. S. Schmaus, A. Bagrets, Y. Nahas, T. K. Yamada, A. Bork, M. Bowen, E. Beaurepaire, F. Evers and W. Wulfhekel, *Nature Nanotechnology*, 2011, **6**, 185-189.
3. T. Albrecht, K. Moth-Poulsen, J. B. Christensen, J. Hjelm, T. Bjørnholm and J. Ulstrup, *Journal of the American Chemical Society*, 2006, **128**, 6574-6575.
4. S. N. Yaliraki, M. Kemp and M. A. Ratner, *Journal of the American Chemical Society*, 1999, **121**, 3428-3434.
5. L. A. Bumm, J. J. Arnold, M. T. Cygan, T. D. Dunbar, T. P. Burgin, L. Jones, D. L. Allara, J. M. Tour and P. S. Weiss, *Science*, 1996, **271**, 1705-1707.
6. N. J. Kay, S. J. Higgins, J. O. Jeppesen, E. Leary, J. Lycoops, J. Ulstrup and R. J. Nichols, *Journal of the American Chemical Society*, 2012, **134**, 16817-16826.

7. W. Chen, J. R. Widawsky, H. Vázquez, S. T. Schneebeli, M. S. Hybertsen, R. Breslow and L. Venkataraman, *Journal of the American Chemical Society*, 2011, **133**, 17160-17163.
8. G. E. Moore, *Solid-State Circuits Society Newsletter, IEEE*, 2006, **11**, 33-35.
9. J. Chen, L. C. Calvet, M. A. Reed, D. W. Carr, D. S. Grubisha and D. W. Bennett, *Chemical Physics Letters*, 1999, **313**, 741-748.
10. V. M. Donnelly and A. Kornblit, *Journal of Vacuum Science & Technology A*, 2013, **31**, 050825.
11. H. Iwai, Industrial and Information Systems, 2007. ICIIS 2007. International Conference on, 2007.
12. M. Haselman and S. Hauck, *Proceedings of the IEEE*, 2010, **98**, 11-38.
13. H. Iwai, *Solid-State Electronics*, 2004, **48**, 497-503.
14. *International Technology Roadmap for Semiconductors: 2012 Update Overview*, 2012.
15. E. Lortscher, *Nature Nanotechnology*, 2013, **8**, 381-384.
16. M. Tsutsui and M. Taniguchi, *Sensors*, 2012, **12**, 7259-7298.
17. J. Y. Son and H. Song, *Current Applied Physics*, 2013, **13**, 1157-1171.
18. W. Haiss, H. van Zalinge, S. J. Higgins, D. Bethell, H. Höbenreich, D. J. Schiffrin and R. J. Nichols, *Journal of the American Chemical Society*, 2003, **125**, 15294-15295.
19. B. Xu and N. J. Tao, *Science*, 2003, **301**, 1221-1223.
20. H. M. McConnell, *The Journal of Chemical Physics*, 1961, **35**, 508-515.
21. H. Kuhn and D. Möbius, *Angewandte Chemie International Edition in English*, 1971, **10**, 620-637.
22. B. Mann and H. Kuhn, *Journal of Applied Physics*, 1971, **42**, 4398-4405.
23. E. E. Polymeropoulos and J. Sagiv, *The Journal of Chemical Physics*, 1978, **69**, 1836-1847.
24. C. Joachim, J. K. Gimzewski, R. R. Schlittler and C. Chavy, *Physical Review Letters*, 1995, **74**, 2102-2105.
25. M. A. Reed, C. Zhou, C. J. Muller, T. P. Burgin and J. M. Tour, *Science*, 1997, **278**, 252-254.
26. J. Moreland and J. W. Ekin, *Journal of Applied Physics*, 1985, **58**, 3888-3895.
27. J. M. van Ruitenbeek, A. Alvarez, I. Piñeyro, C. Grahmann, P. Joyez, M. H. Devoret, D. Esteve and C. Urbina, *Review of Scientific Instruments*, 1996, **67**, 108-111.
28. G. Speyer, R. Akis and D. K. Ferry, in *Nano and Molecular Electronics Handbook*, ed. S. E. Lyshevski, CRC Press, Taylor & Francis Group, Editon edn., 2007, pp. 21:21-21:33.
29. J. Reichert, R. Ochs, D. Beckmann, H. B. Weber, M. Mayor and H. v. Löhneysen, *Physical Review Letters*, 2002, **88**, 176804.
30. L. M. Ballesteros, S. Martin, G. Pera, P. A. Schauer, N. J. Kay, M. C. Lopez, P. J. Low, R. J. Nichols and P. Cea, *Langmuir*, 2011, **27**, 3600-3610.
31. J. Lee, H. Chang, S. Kim, G. S. Bang and H. Lee, *Angewandte Chemie*, 2009, **121**, 8653-8656.
32. S. Park, G. Wang, B. Cho, Y. Kim, S. Song, Y. Ji, M.-H. Yoon and T. Lee, *Nature Nanotechnology*, 2012, **7**, 438-442.
33. S. V. Aradhya and L. Venkataraman, *Nature Nanotechnology*, 2013, **8**, 399-410.

34. S. J. van der Molen, R. Naaman, E. Scheer, J. B. Neaton, A. Nitzan, D. Natelson, N. J. Tao, H. van der Zant, M. Mayor, M. Ruben, M. Reed and M. Calame, *Nature Nanotechnology*, 2013, **8**, 385-389.
35. P. M. Tedrow and R. Meservey, *Physical Review Letters*, 1971, **26**, 192-195.
36. G. Binasch, P. Grunberg, F. Saurenbach and W. Zinn, *Physical Review B*, 1989, **39**, 4828-4830.
37. M. N. Baibich, J. M. Broto, A. Fert, F. N. Vandau, F. Petroff, P. Eitenne, G. Creuzet, A. Friederich and J. Chazelas, *Physical Review Letters*, 1988, **61**, 2472-2475.
38. J. Daughton, J. Brown, E. Chen, R. Beech, A. Pohm and W. Kude, *Magnetics, IEEE Transactions on*, 1994, **30**, 4608-4610.
39. T. Ching, R. E. Fontana, T. Lin, D. E. Heim, V. S. Speriosu, B. A. Gurney and M. L. Williams, *Magnetics, IEEE Transactions on*, 1994, **30**, 3801-3806.
40. A. Fert, *Angewandte Chemie International Edition*, 2008, **47**, 5956-5967.
41. S. Mao, C. Yonghua, F. Liu, C. Xingfu, X. Bin, L. Puling, M. Patwari, X. Haiwen, C. Clif, B. Miller, D. Menard, B. Pant, J. Loven, K. Duxstad, S. Li, Z. Zhengyong, A. Johnston, R. Lamberton, M. Gubbins, T. McLaughlin, J. Gadbois, J. Ding, B. Cross, X. Song and P. Ryan, *Magnetics, IEEE Transactions on*, 2006, **42**, 97-102.
42. S. Yuasa, T. Nagahama, A. Fukushima, Y. Suzuki and K. Ando, *Nature Materials*, 2004, **3**, 868-871.
43. S. S. P. Parkin, C. Kaiser, A. Panchula, P. M. Rice, B. Hughes, M. Samant and S. H. Yang, *Nature Materials*, 2004, **3**, 862-867.
44. Y. M. Lee, J. Hayakawa, S. Ikeda, F. Matsukura and H. Ohno, *Applied Physics Letters*, 2007, **90**, 21250
45. M. Galbiati, C. Barraud, S. Tatay, K. Bouzehouane, C. Deranlot, E. Jacquet, A. Fert, P. Seneor, R. Mattana and F. Petroff, *Advanced Materials*, 2012, **24**, 6429-6432.
46. S. L. Kawahara, J. Lagoute, V. Repain, C. Chacon, Y. Girard, S. Rousset, A. Smogunov and C. Barreteau, *Nano Letters*, 2012, **12**, 4558-4563.
47. S. Pramanik, C. G. Stefanita, S. Patibandla, S. Bandyopadhyay, K. Garre, N. Harth and M. Cahay, *Nature Nanotechnology*, 2007, **2**, 216-219.
48. J. Camarero and E. Coronado, *Journal of Materials Chemistry*, 2009, **19**, 1678-1684.
49. K. Horiguchi, T. Sagisaka, S. Kurokawa and A. Sakai, *Journal of Applied Physics*, 2013, **113**, 144313.
50. S. Chakrabarti and A. J. Pal, *Applied Physics Letters*, 2014, **104**, 013305.
51. E. G. Emberly and G. Kirczenow, *Chemical Physics*, 2002, **281**, 311-324.
52. A. Saffarzadeh, *Journal of Applied Physics*, 2008, **104**, 123715.
53. A. Bagrets, *Journal of Chemical Theory and Computation*, 2013, **9**, 2801-2815.
54. D. K. Schwartz, *Annual Review of Physical Chemistry*, 2001, **52**, 107-137.
55. G. E. Poirier and E. D. Pylant, *Science*, 1996, **272**, 1145-1148.
56. W. Wang, T. Lee and M. Reed, in *Nano and Molecular Electronics Handbook*, ed. S. E. Lyshevski, CRC Press, Taylor & Francis Group, Editon edn., 2007, pp. 1:1-1:41.
57. J. Hautman and M. L. Klein, *The Journal of Chemical Physics*, 1989, **91**, 4994-5001.

58. C. D. Bain, H. A. Biebuyck and G. M. Whitesides, *Langmuir*, 1989, **5**, 723-727.
59. M. Hasan, D. Bethell and M. Brust, *Journal of the American Chemical Society*, 2002, **124**, 1132-1133.
60. H. Grönbeck, A. Curioni and W. Andreoni, *Journal of the American Chemical Society*, 2000, **122**, 3839-3842.
61. M. Armand, F. Endres, D. R. MacFarlane, H. Ohno and B. Scrosati, *Nature Materials*, 2009, **8**, 621-629.
62. T. Welton, *Chemical Reviews*, 1999, **99**, 2071-2084.
63. H. Weingärtner, *Angewandte Chemie International Edition*, 2008, **47**, 654-670.
64. http://www.topbritishinnovations.org/, *Great British Innovation Vote*, Accessed 18/04/14, 2014.
65. J. G. Huddleston, A. E. Visser, W. M. Reichert, H. D. Willauer, G. A. Broker and R. D. Rogers, *Green Chemistry*, 2001, **3**, 156-164.
66. L. Crowhurst, P. R. Mawdsley, J. M. Perez-Arlandis, P. A. Salter and T. Welton, *Physical Chemistry Chemical Physics*, 2003, **5**, 2790-2794.
67. E. I. Rogers, B. Šljukić, C. Hardacre and R. G. Compton, *Journal of Chemical & Engineering Data*, 2009, **54**, 2049-2053.
68. M. C. Buzzeo, R. G. Evans and R. G. Compton, *ChemPhysChem*, 2004, **5**, 1106-1120.
69. J. Jacquemin, P. Husson, A. A. H. Padua and V. Majer, *Green Chemistry*, 2006, **8**, 172-180.
70. A. P. Abbott and K. J. McKenzie, *Physical Chemistry Chemical Physics*, 2006, **8**, 4265-4279.
71. B. Clare, A. Sirwardana and D. MacFarlane, in *Ionic Liquids*, ed. B. Kirchner, Springer Berlin Heidelberg, Editon edn., 2010, vol. 290, pp. 1-40.
72. C. G. Hanke, A. Johansson, J. B. Harper and R. M. Lynden-Bell, *Chemical Physics Letters*, 2003, **374**, 85-90.
73. M. E. Zakrzewska, E. Bogel-Łukasik and R. Bogel-Łukasik, *Energy & Fuels*, 2010, **24**, 737-745.
74. N. Tachikawa, Y. Katayama and T. Miura, *Electrochemical and Solid State Letters*, 2009, **12**, F39-F41.
75. H. Ohno, in *Electrodeposition from Ionic Liquids*, eds. F. Endres, D. R. MacFarlane and A. P. Abbott, Wiley-VCH, Editon edn., 2008, pp. 47-82.
76. J. Zhang and A. M. Bond, *Analytical Chemistry*, 2003, **75**, 2694-2702.
77. J. K. D. Surette, L. Green and R. D. Singer, *Chemical Communications*, 1996, 2753-2754.
78. A. M. O'Mahony, D. S. Silvester, L. Aldous, C. Hardacre and R. G. Compton, *Journal of Chemical & Engineering Data*, 2008, **53**, 2884-2891.
79. L. Xiao, E. J. F. Dickinson, G. G. Wildgoose and R. G. Compton, *Electroanalysis*, 2010, **22**, 269-276.
80. D. Y. Kim, J. C. Yang, H. W. Kim and G. M. Swain, *Electrochimica Acta*, 2013, **94**, 49-56.
81. J. Zhang and A. M. Bond, *Analyst*, 2005, **130**, 1132-1147.
82. J. A. Widegren, E. M. Saurer, K. N. Marsh and J. W. Magee, *The Journal of Chemical Thermodynamics*, 2005, **37**, 569-575.
83. H. L. Chum, V. R. Koch, L. L. Miller and R. A. Osteryoung, *Journal of the American Chemical Society*, 1975, **97**, 3264-3265.

84. J. S. Wilkes and M. J. Zaworotko, *Journal of the Chemical Society, Chemical Communications*, 1992, 965-967.
85. A. D. Le and L. Yu, *Journal of the Electrochemical Society*, 2011, **158**, F10-F14.
86. K. B. Oldham, *Journal of Electroanalytical Chemistry*, 2008, **613**, 131-138.
87. M. Z. Bazant, B. D. Storey and A. A. Kornyshev, *Physical Review Letters*, 2011, **106**, 046102.
88. M. J. A. Shiddiky, A. A. J. Torriero, C. Zhao, I. Burgar, G. Kennedy and A. M. Bond, *Journal of the American Chemical Society*, 2009, **131**, 7976-7989.
89. M. Drüschler, B. Huber, S. Passerini and B. Roling, *The Journal of Physical Chemistry C*, 2010, **114**, 3614-3617.
90. T. Schubert, H. A. A. El-Rahman, A. P. Abbott, K. J. McKenzie, K. S. Ryder and F. Endres, in *Electrodeposition from Ionic Liquids*, eds. F. Endres, D. R. MacFarlane and A. P. Abbott, Wiley-VCH, Editon edn., 2008, pp. 83-123.
91. http://www.scionix.co.uk/index.php?option=com_content&view=article&id=58&Itemid=77, *Plating General - Technology - Scionix*, Accessed 03/02/14, 2014.
92. N. J. Kay, R. J. Nichols, S. J. Higgins, W. Haiss, G. Sedghi, W. Schwarzacher and B.-W. Mao, *The Journal of Physical Chemistry C*, 2011, **115**, 21402-21408.
93. V. B. Engelkes, J. M. Beebe and C. D. Frisbie, *Journal of the American Chemical Society*, 2004, **126**, 14287-14296.
94. L. Luo, S. H. Choi and C. D. Frisbie, *Chemistry of Materials*, 2010, **23**, 631-645.
95. A. H. Flood, E. W. Wong and J. F. Stoddart, *Chemical Physics*, 2006, **324**, 280-290.
96. D. Segal, A. Nitzan, W. B. Davis, M. R. Wasielewski and M. A. Ratner, *The Journal of Physical Chemistry B*, 2000, **104**, 3817-3829.
97. K. Liu, G. Li, X. Wang and F. Wang, *The Journal of Physical Chemistry C*, 2008, **112**, 4342-4349.
98. F. C. Grozema, Y. A. Berlin and L. D. A. Siebbeles, *Journal of the American Chemical Society*, 2000, **122**, 10903-10909.
99. D. K. Aswal, S. Lenfant, D. Guerin, J. V. Yakhmi and D. Vuillaume, *Analytica Chimica Acta*, 2006, **568**, 84-108.
100. W. Wang, T. Lee and M. A. Reed, *Physical Review B*, 2003, **68**, 035416.
101. J. G. Simmons, *Journal of Applied Physics*, 1963, **34**, 2581-2590.
102. C. H. Wohlgamuth, M. A. McWilliams and J. D. Slinker, *Analytical Chemistry*, 2013, **85**, 8634-8640.
103. X. Zhao, C. Huang, M. Gulcur, A. S. Batsanov, M. Baghernejad, W. Hong, M. R. Bryce and T. Wandlowski, *Chemistry of Materials*, 2013, **25**, 4340-4347.
104. T. Hines, I. Diez-Perez, J. Hihath, H. Liu, Z.-S. Wang, J. Zhao, G. Zhou, K. Müllen and N. Tao, *Journal of the American Chemical Society*, 2010, **132**, 11658-11664.
105. Q. Lu, K. Liu, H. Zhang, Z. Du, X. Wang and F. Wang, *ACS Nano*, 2009, **3**, 3861-3868.
106. Y. A. Berlin, G. R. Hutchison, P. Rempala, M. A. Ratner and J. Michl, *The Journal of Physical Chemistry A*, 2003, **107**, 3970-3980.
107. E. A. Weiss, M. R. Wasielewski and M. A. Ratner, in *Molecular Wires: From Design to Properties*, ed. L. DeCola, Editon edn., 2005, vol. 257, pp. 103-133.
108. L. Luo, S. H. Choi and C. D. Frisbie, *Chemistry of Materials*, 2011

**23**, 631-645.
109. C. Zhou, M. R. Deshpande, M. A. Reed, L. Jones and J. M. Tour, *Applied Physics Letters*, 1997, **71**, 611-613.
110. A. Vilan, J. Ghabboun and D. Cahen, *The Journal of Physical Chemistry B*, 2003, **107**, 6360-6376.
111. A. Salomon, D. Berkovich and D. Cahen, *Applied Physics Letters*, 2003, **82**, 1051-1053.
112. R. N. Sharma, S. T. Lakshmikumar and A. C. Rastogi, *Thin Solid Films*, 1991, **199**, 1-8.
113. S. M. Sze and K. K. Ng, in *Physics of Semiconductor Devices*, Wiley-Interscience, Editon edn., 2007, pp. 197-242.
114. A. Tan, J. Balachandran, S. Sadat, V. Gavini, B. D. Dunietz, S.-Y. Jang and P. Reddy, *Journal of the American Chemical Society*, 2011, **133**, 8838-8841.
115. X. Y. Feng, Z. Li and J. Yang, *The Journal of Physical Chemistry C*, 2009, **113**, 21911-21914.
116. Z. Li, M. Smeu, M. A. Ratner and E. Borguet, *The Journal of Physical Chemistry C*, 2013, **117**, 14890-14898.
117. F. Chen, X. Li, J. Hihath, Z. Huang and N. Tao, *Journal of the American Chemical Society*, 2006, **128**, 15874-15881.
118. F.-R. F. Fan, Y. Yao, L. Cai, L. Cheng, J. M. Tour and A. J. Bard, *Journal of the American Chemical Society*, 2004, **126**, 4035-4042.
119. J. M. Beebe, V. B. Engelkes, L. L. Miller and C. D. Frisbie, *Journal of the American Chemical Society*, 2002, **124**, 11268-11269.
120. G. Nesher, H. Shpaisman and D. Cahen, *Journal of the American Chemical Society*, 2007, **129**, 734-735.
121. G. Kim, S. Wang, W. Lu, M. Buongiorno Nardelli and J. Bernholc, *The Journal of Chemical Physics*, 2008, **128**, 024708.
122. R. N. Wang, X. H. Zheng, Z. X. Dai, H. Hao, L. L. Song and Z. Zeng, *Physics Letters A*, 2011, **375**, 657-660.
123. Y. Xue and M. A. Ratner, *Physical Review B*, 2004, **69**, 085403.
124. X. D. Cui, A. Primak, X. Zarate, J. Tomfohr, O. F. Sankey, A. L. Moore, T. A. Moore, D. Gust, G. Harris and S. M. Lindsay, *Science*, 2001, **294**, 571-574.
125. X.-S. Zhou, J.-H. Liang, Z.-B. Chen and B.-W. Mao, *Electrochemistry Communications*, 2011, **13**, 407-410.
126. B. Kim, S. H. Choi, X. Y. Zhu and C. D. Frisbie, *Journal of the American Chemical Society*, 2011, **133**, 19864-19877.
127. J. M. Seminario, C. E. De La Cruz and P. A. Derosa, *Journal of the American Chemical Society*, 2001, **123**, 5616-5617.
128. P. Moreno-García, M. Gulcur, D. Z. Manrique, T. Pope, W. Hong, V. Kaliginedi, C. Huang, A. S. Batsanov, M. R. Bryce, C. Lambert and T. Wandlowski, *Journal of the American Chemical Society*, 2013, **135**, 12228-12240.
129. H. Meier, *Angewandte Chemie International Edition*, 2009, **48**, 3911-3913.
130. M. Magoga and C. Joachim, *Physical Review B*, 1997, **56**, 4722-4729.
131. H. O. Finklea, L. Liu, M. S. Ravenscroft and S. Punturi, *The Journal of Physical Chemistry*, 1996, **100**, 18852-18858.
132. J. F. Smalley, H. O. Finklea, C. E. D. Chidsey, M. R. Linford, S. E. Creager, J. P. Ferraris, K. Chalfant, T. Zawodzinsk, S. W. Feldberg and M. D. Newton, *Journal of the American Chemical Society*, 2003, **125**, 2004-2013.

133. M. U. Winters, E. Dahlstedt, H. E. Blades, C. J. Wilson, M. J. Frampton, H. L. Anderson and B. Albinsson, *Journal of the American Chemical Society*, 2007, **129**, 4291-4297.
134. G. Sedghi, V. M. Garcia-Suarez, L. J. Esdaile, H. L. Anderson, C. J. Lambert, S. Martin, D. Bethell, S. J. Higgins, M. Elliott, N. Bennett, J. E. Macdonald and R. J. Nichols, *Nature Nanotechnology*, 2011, **6**, 517-523.
135. V. Kaliginedi, P. Moreno-García, H. Valkenier, W. Hong, V. M. García-Suárez, P. Buiter, J. L. H. Otten, J. C. Hummelen, C. J. Lambert and T. Wandlowski, *Journal of the American Chemical Society*, 2012, **134**, 5262-5275.
136. J. He, F. Chen, J. Li, O. F. Sankey, Y. Terazono, C. Herrero, D. Gust, T. A. Moore, A. L. Moore and S. M. Lindsay, *Journal of the American Chemical Society*, 2005, **127**, 1384-1385.
137. G. Sedghi, K. Sawada, L. J. Esdaile, M. Hoffmann, H. L. Anderson, D. Bethell, W. Haiss, S. J. Higgins and R. J. Nichols, *Journal of the American Chemical Society*, 2008, **130**, 8582-8583.
138. T. Buffeteau, B. Desbat and J. M. Turlet, *Appl. Spectrosc.*, 1991, **45**, 380-389.
139. F. M. Hoffmann, *Surface Science Reports*, 1983, **3**, 107,109-192.
140. H. A. Pearce and N. Sheppard, *Surface Science*, 1976, **59**, 205-217.
141. S. Mitsunori, Y. Tatsuya, Y. Itsunari, N. Junji, M. Susumu and U. Masashi, *Japanese Journal of Applied Physics*, 2010, **49**, 052503.
142. M. Saito, T. Kano, T. Seki and M. Miyagi, *Infrared Physics & Technology*, 1994, **35**, 709-714.
143. K. W. Hipps and G. A. Crosby, *The Journal of Physical Chemistry*, 1979, **83**, 555-562.
144. L. Nafie, N.-S. Lee, G. Paterlini and T. Freedman, *Mikrochim Acta*, 1987, **93**, 93-104.
145. D. Blaudez, J.-M. Turlet, J. Dufourcq, D. Bard, T. Buffeteau and B. Desbat, *Journal of the Chemical Society, Faraday Transactions*, 1996, **92**, 525-530.
146. W. G. Golden, D. D. Saperstein, M. W. Severson and J. Overend, *The Journal of Physical Chemistry*, 1984, **88**, 574-580.
147. C. Nogues and P. Lang, *Langmuir*, 2007, **23**, 8385-8391.
148. J. E. Sadler, D. S. Szumski, A. Kierzkowska, S. R. Catarelli, K. Stella, R. J. Nichols, M. H. Fonticelli, G. Benitez, B. Blum, R. C. Salvarezza and W. Schwarzacher, *Physical Chemistry Chemical Physics*, 2011, **13**, 17987-17993.
149. G. Fonder, F. Cecchet, A. Peremans, P. A. Thiry, J. Delhalle and Z. Mekhalif, *Surface Science*, 2009, **603**, 2276-2282.
150. R. P. Sperline, *Langmuir*, 1997, **13**, 3715-3726.
151. T. Stock John, in *Electrochemistry, Past and Present*, American Chemical Society, Editon edn., 1989, vol. 390, pp. 1-17.
152. K. Izutsu, in *Electrochemistry in Nonaqueous Solutions*, Wiley-VCH Verlag GmbH & Co. KGaA, Editon edn., 2009, pp. 89-110.
153. A. J. Bard and L. R. Faulkner, in *Electrochemical Methods: Fundamentals and Applications*, John Wiley & Sons, Inc., Editon edn., 2001, pp. 44-86.
154. D. Pletcher, R. Greef, R. Peat, L. M. Peter and J. Robinson, in *Instrumental Methods in Electrochemistry*, Horwood Publishing, Chichester, Editon edn., 2001, pp. 42-75.
155. M. Breiter, M. Kleinerman and P. Delahay, *Journal of the American Chemical Society*, 1958, **80**, 5111-5117.

156. Z. Stojek, in *Electroanalytical Methods*, ed. F. Scholz, Springer Berlin Heidelberg, Editon edn., 2010, pp. 3-9.
157. A. J. Bard and L. R. Faulkner, in *Electrochemical Methods: Fundamentals and Applications*, John Wiley & Sons, Inc., Editon edn., 2001, pp. 534-579.
158. D. Pletcher, R. Greef, R. Peat, L. M. Peter and J. Robinson, in *Instrumental Methods in Electrochemistry*, Horwood Publishing, Chichester, Editon edn., 2001, pp. 149-177.
159. M. V. Fedorov, A. A. Georgi and A. A. Kornyshev, *Electrochemistry Communications*, 2010, **12**, 296-299.
160. A. A. Kornyshev, *The Journal of Physical Chemistry B*, 2007, **111**, 5545-5557.
161. G. A. Mabbott, *Journal of Chemical Education*, 1983, **60**, 697.
162. J. Heinze, *Angewandte Chemie International Edition in English*, 1984, **23**, 831-847.
163. F. Marken, A. Neudeck and A. Bond, in *Electroanalytical Methods*, ed. F. Scholz, Springer Berlin Heidelberg, Editon edn., 2010, pp. 57-106.
164. D. Pletcher, R. Greef, R. Peat, L. M. Peter and J. Robinson, in *Instrumental Methods in Electrochemistry*, Horwood Publishing, Chichester, Editon edn., 2001, pp. 178-228.
165. P. T. Kissinger and W. R. Heineman, *Journal of Chemical Education*, 1983, **60**, 702.
166. J. Osteryoung, *Journal of Chemical Education*, 1983, **60**, 296.
167. A. J. Bard and L. R. Faulkner, in *Electrochemical Methods: Fundamentals and Applications*, John Wiley & Sons, Inc., Editon edn., 2001, pp. 261-304.
168. J. G. Osteryoung and R. A. Osteryoung, *Analytical Chemistry*, 1985, **57**, 101A-110A.
169. A. Amirudin and D. Thieny, *Progress in Organic Coatings*, 1995, **26**, 1-28.
170. D. D. Macdonald, *Electrochimica Acta*, 2006, **51**, 1376-1388.
171. U. Retter and H. Lohse, in *Electroanalytical Methods*, ed. F. Scholz, Springer Berlin Heidelberg, Editon edn., 2010, pp. 159-177.
172. H. G. L. Coster, T. C. Chilcott and A. C. F. Coster, *Bioelectrochemistry and Bioenergetics*, 1996, **40**, 79-98.
173. E. Azzarello, E. Masi and S. Mancuso, in *Plant Electrophysiology*, ed. A. G. Volkov, Springer Berlin Heidelberg, Editon edn., 2012, pp. 205-223.
174. B.-Y. Chang and S.-M. Park, *Annual Review of Analytical Chemistry*, 2010, **3**, 207-229.
175. X.-S. Zhou, L. Liu, P. Fortgang, A.-S. Lefevre, A. Serra-Muns, N. Raouafi, C. Amatore, B.-W. Mao, E. Maisonhaute and B. Schöllhorn, *Journal of the American Chemical Society*, 2011, **133**, 7509-7516.
176. A. Nitzan, *The Journal of Physical Chemistry A*, 2001, **105**, 2677-2679.
177. M. C. Traub, B. S. Brunschwig and N. S. Lewis, *The Journal of Physical Chemistry B*, 2007, **111**, 6676-6683.
178. E. Wierzbinski, R. Venkatramani, K. L. Davis, S. Bezer, J. Kong, Y. Xing, E. Borguet, C. Achim, D. N. Beratan and D. H. Waldeck, *ACS Nano*, 2013, **7**, 5391-5401.
179. G. Binnig and H. Rohrer, *Reviews of Modern Physics*, 1987, **59**, 615-625.
180. G. Binnig, H. Rohrer, C. Gerber and E. Weibel, *Applied Physics Letters*, 1982, **40**, 178-180.
181. W. A. Thompson and S. F. Hanrahan, *Review of Scientific Instruments*, 1976, **47**, 1303-1304.
182. I. Giaever, *Reviews of Modern Physics*, 1974, **46**, 245-250.

183. G. Binnig, H. Rohrer, C. Gerber and E. Weibel, *Physical Review Letters*, 1982, **49**, 57-61.
184. R. S. Becker, J. A. Golovchenko and B. S. Swartzentruber, *Physical Review Letters*, 1985, **54**, 2678-2680.
185. http://www.nobelprize.org/nobel_prizes/physics/laureates/1973/, *The Nobel Prize in Physics 1973*, Accessed 18/04/14, 2013.
186. P. Atkins and J. de Paula, in *Atkins' Physical Chemistry*, Editon edn., 2006, pp. 243-276.
187. L. Esaki, *Science*, 1974, **183**, 1149-1155.
188. S. M. Sze and K. K. Ng, in *Physics of Semiconductor Devices*, Wiley-Interscience, Editon edn., 2007, pp. 7-78.
189. G. Binnig and H. Rohrer, *Helvetica Physica Acta*, 1982, **55**, 726-735.
190. J. Tersoff and N. D. Lang, *Methods in Experimental Physics*, 1993, **27**, 1-29.
191. G. Binnig and D. P. E. Smith, *Review of Scientific Instruments*, 1986, **57**, 1688-1689.
192. A. J. Bard and L. R. Faulkner, in *Electrochemical Methods: Fundamentals and Applications*, John Wiley & Sons, Inc., Editon edn., 2001, pp. 659-679.
193. G. Binnig, H. Rohrer, C. Gerber and E. Weibel, *Physica B+C*, 1982, **109-110**, 2075-2077.
194. M. Wilms, M. Kruft, G. Bermes and K. Wandelt, *Review of Scientific Instruments*, 1999, **70**, 3641-3650.
195. Z. W. Tian, X. D. Zhuo, J. Q. Mu, J. H. Ye, Z. D. Fen and B. W. Mao, *Ultramicroscopy*, 1992, **42-44**, 460-463.
196. A. Shkurankov, F. Endres and W. Freyland, *Review of Scientific Instruments*, 2002, **73**, 102-107.
197. F. Chen, J. Hihath, Z. Huang, X. Li and N. J. Tao, *Annual Review of Physical Chemistry*, 2007, **58**, 535-564.
198. X.-S. Zhou, Y.-M. Wei, L. Liu, Z.-B. Chen, J. Tang and B.-W. Mao, *Journal of the American Chemical Society*, 2008, **130**, 13228-13230.
199. Z.-L. Peng, Z.-B. Chen, X.-Y. Zhou, Y.-Y. Sun, J.-H. Liang, Z.-J. Niu, X.-S. Zhou and B.-W. Mao, *The Journal of Physical Chemistry C*, 2012, **116**, 21699-21705.
200. A. V. Rudnev, I. Pobelov and T. Wandlowski, *Journal of Electroanalytical Chemistry*, 2011, **660**, 302-308.
201. I. V. Pobelov, Z. Li and T. Wandlowski, *Journal of the American Chemical Society*, 2008, **130**, 16045-16054.
202. P. Petrangolini, A. Alessandrini, L. Berti and P. Facci, *Journal of the American Chemical Society*, 2010, **132**, 7445-7453.
203. Z. Li, Y. Liu, S. F. L. Mertens, I. V. Pobelov and T. Wandlowski, *Journal of the American Chemical Society*, 2010, **132**, 8187-8193.
204. K. Fischer, *Angewandte Chemie*, 1935, **48**, 394-396.
205. A. S. Meyer and C. M. Boyd, *Analytical Chemistry*, 1959, **31**, 215-219.
206. http://uk.mt.com/gb/en/home/supportive_content/application_editorials/Moisture_determination_by_Karl_Fischer_1.html?cnty=gb, *Mettler Toledo: Moisture Determination with Karl Fischer Titration*, Accessed 18/04/14, 2014.
207. C. A. De Caro, A. Aichert and C. M. Walter, *Food Control*, 2001, **12**, 431-436.
208. S. K. MacLeod, *Analytical Chemistry*, 1991, **63**, 557A-566A.
209. Private correspondence with I. Aldous.
210. H. A. Frediani, *Analytical Chemistry*, 1952, **24**, 1126-1128.

211. F. Endres, N. Borisenko, S. Z. El Abedin, R. Hayes and R. Atkin, *Faraday Discussions*, 2012, **154**, 221-233.
212. R. Atkin, S. Z. E. Abedin, R. Hayes, L. H. S. Gasparotto, N. Borisenko and F. Endres, *The Journal of Physical Chemistry C*, 2009, **113**, 13266-13272.
213. H. Li, F. Endres and R. Atkin, *Physical Chemistry Chemical Physics*, 2013, **15**, 14624-14633.
214. C. Gaillard, I. Billard, A. Chaumont, S. Mekki, A. Ouadi, M. A. Denecke, G. Moutiers and G. Wipff, *Inorganic Chemistry*, 2005, **44**, 8355-8367.

# Chapter 2:

# PM-IRRAS

# Introduction

Molecular spintronics is of great contemporary interest due to the drive to miniaturise computational devices. Spintronic devices, in which the spin state of the electrons is controlled, are ever present in daily life as the memory devices in computers, phones and a plethora of electronic equipment. However, the amount of information which can be written onto a single device is reaching its limits, with more and more creative methods to increase device memory needed. A widely discussed, but still futuristic, way to increase device miniaturization beyond the current limit would be to switch from a top-down to a bottom-up fabrication technique. Molecular spintronics is such a bottom-up platform, but such concepts remain far from practical implementation at this time. Aside from allowing for more components per device molecular spintronics would also eventually allow for greater spin coherence, as the spin-relaxation time of the molecules tends to be less than the length of time it takes the electron to travel between the two ferromagnetic contacts.[1, 2] A wealth of fundamental data exists for molecular electronics junctions and to a certain extent for devices also, whereas the development of defined molecular spintronic devices and junctions is at a much earlier stage. Forming well defined and well characterized molecular adlayers and junctions with ferromagnetic metals like Ni is a prerequisite for molecular spintronics studies. Therefore to gain better insight into these junctions and devices, the formation of various monolayers on Ni has been investigated using PM-IRRAS.

In the past Ni has found use in molecular spintronic devices, both those composed of large molecular assemblies, such as SAMs, and of the single molecule variety. As early as 2004 self-assembled monolayers of octanethiol on Ni were used to investigate the effect of different magnetic alignments on the conductance of the

molecular assembly.[3] In this work Petra *et al.* formed and measured multiple Ni-octanethiol-Ni devices at 4.2 K, with the majority of these devices showing transport by tunnelling through the molecular layer. The devices exhibiting tunnelling transport were further investigated for their ability to tune conductance with magnetic alignment. Amongst those devices showing different conductance values for the parallel and antiparallel configuration the highest magnetoresistance seen was 16 %. This is indicative of a high degree of spin polarization during the tunnelling process, an observation which is exciting for the future of molecular electronics and spintronics. The low device yield means this work is far from commercialization. Progressing from here the formation of monolayers on Ni and their ability in large scale arrays has been investigated. In 2009 a method for forming an array device for molecular spintronics was implemented.[4] This method used self-assembly on freshly prepared Ni surfaces to form the first nickel-molecule contact. To form the second contact Ni was deposited on a PFPE stamp which was pressed onto the prepared monolayer to form a highly stable metal-molecule-metal sandwich. Unfortunately, however, Ni is a metal which oxidises quickly in ambient conditions, and so formation of the oxide layer during measurement of the *I-V* characteristics caused variable resistances for the system. Nevertheless this technique is promising as repeatable results have been seen for Au-dodecanethiol-Au systems, and the method may be improved through the enhanced monolayer formation proposed for molecular spintronics by Sadler et al.[5] In this the Ni surface was reduced *in-situ,* and potential assisted deposition was used to form well-ordered monolayers of octanethiol. Although the film formed was ascertained by EQCM to arise from a multilayer of octanethiol on Ni, the more weakly adsorbed multilayer could be rinsed off to leave the monolayer. The monolayer was characterized by XPS, PM-IRRAS and a change

in electrochemistry. Furthermore, a well-ordered monolayer was indicated by the PM-IRRAS results as well as the inhibition of re-oxidation of the Ni surface. More recently single molecule devices with Ni contacts have been investigated. In 2012 computational methods were used to investigate the negative TMR value being reported in the literature, for a Ni-benzenediethenylenethiol-Ni (Ni-BDET-Ni) system.[2] Both parallel and antiparallel magnetizations were examined at a variety of contact distances and biases. It was seen that the TMR was distance dependent, as would be expected on the basis that the Ni contact can impart some of its magnetic character to the BDET molecule. Furthermore, it was found that a negative TMR value could arise if the distance was small enough. The negative TMR arises because of a change in the antiparallel configuration, which at large distances has mainly the Ni (*s*, *p*) character contributing to the unoccupied orbitals of the molecule, while at short distances this changes to have mainly *d*-character contributing. This implies that small changes in the junction distance can give rise to a large change in the TMR, which can act as a means of controlling conductance. In 2013 experimental measurements were performed on a single molecule of $C_{60}$ between 2 Ni contacts in feedback-controlled electrical break junction experiments at 0.3 K.[1] The measured *I-V* characteristics of these junctions showed negative TMR, which was as large as -80%, much larger than had been expected. As before the negative TMR arose because of the hybridization between $C_{60}$ and Ni. While these fundamental investigations have provided insight into the functionality of Ni in molecular spintronics, they still remain very far from any demonstration of a commercially viable device. Experiments must first be performed at or near room temperature. Furthermore a means of preparing an oxide free contact is needed for practical device fabrication and subsequent handling under ambient conditions.

Following the method outlined by Sadler[5] the use of electrochemical potential assisted monolayer deposition, after *in-situ* Ni oxide reduction, was utilized in monolayer formation on Ni. The monolayers have been characterized by PM-IRRAS. It has been demonstrated that this method results in well-ordered monolayers and it could be possible to extend its use to single molecule investigations on Ni by forming mixed monolayers of insulating and wire molecules. The use of mixed monolayers in molecular electronics is well documented.[6-9] Mixed monolayers are particularly useful for aromatic molecules because the insertion of these molecules does not affect the order of the surrounding alkanethiol monolayer.[8] In molecular electronics mixed monolayers are appealing because conductance switching can occur due to conformational changes and molecular tilting.[7] By isolation of the molecules in a highly ordered matrix the molecule is held in conformation causing a reduction in conductance switching, with the high conductance state favoured.[6, 7, 9] For the investigations on Ni the use of mixed monolayers is beneficial because the overall monolayer is expected to be well-ordered. Therefore, the Ni surface will be passivated during the measurement process, while locking the molecule into a high conductance state. The formation of mixed monolayers of benzenedimethane dithiol (BDMT) and hexanethiol (HT) on Ni has been investigated by PM-IRRAS to determine whether the monolayer composition can be controlled. While in most cases the alkanethiol monolayer is formed and then the molecular wires added to defect sites,[6-10] for these investigations the risk of re-oxidation of the Ni at defect sites means the mixed monolayers are formed from mixed molecule adsorption solutions.

To investigate the quality of the monolayers formed on the Ni surface from potential assisted assembly PM-IRRAS was used. PM-IRRAS is a surface sensitive technique which exploits the surface selection to allow for both qualitative, and in

more rigorous experiments, quantitative investigations of the surface species. Utilizing both surface sensitive *p*-polarized light, and surface insensitive *s*-polarized light, PM-IRRAS affords the measurement of high quality, spectra of surface species, free of any atmospheric signals.[11] The investigative power of this technique, makes it an ideal method to probe monolayer ordering on the Ni surface.

## Aim

While Ni has been reported in the literature as a potential ferromagnetic contact for molecular spintronics the resulting investigations have shown that there is a need to better understand the formation of molecular films on Ni to eventually facilitate the fabrication of more robust devices.[1-4] This work utilizes PM-IRRAS to probe the ordering of the various monolayers formed on the Ni surface. To aid in the analysis of monolayer formation on Ni, analogous investigations on Au have also been carried out. Following these investigations on Au, simple alkanethiol monolayers on Ni formed by the method outlined by Sadler[5] have been investigated by PM-IRRAS to ensure they are well ordered before moving to the more complex mixed monolayer. Using PM-IRRAS it will be shown that by controlling the adsorption solution the resulting mixed monolayer composition can be controlled.

## Methods

PM-IRRAS was performed using a Bruker Instruments PMA 37 module attached to an IFS 66v/S spectrophotometer. This instrument was controlled by a computer running the Bruker Instruments OPUS software. The angle of incidence for all samples was 81.25 °. Polarization modulation was performed with a Hinds Instruments PEM-90 photoelastic modulator. An Infrared Associates liquid nitrogen cooled, mercury cadmium telluride infrared detector was used. Resolution was set to

2 $cm^{-1}$. Data was analysed using the OPUS software, and unless otherwise stated all spectra were corrected against a spline function.

## Thiol Monolayers on Au

Au(111) Arrandee™ slides were rinsed with ethanol and Milli-Q® water, and dried under nitrogen, before flame annealing. Once cooled the slide was placed in a 0.1 mM organothiol in ethanol solution. When investigating the mixed monolayers the total organothiol concentration was kept constant, although the ratios of compounds in the mixed adsorption solution was changed. The compositions of the adsorption solutions are shown in **Table 1**. After 1 hour of adsorption the Au slide was rinsed with ethanol followed by Milli-Q® water and dried under nitrogen.

*Table 1: Concentrations used for adsorption solutions for monolayers on Au.*

| Molecule A | Molecule B | Concentration A (mM) | Concentration B (mM) | Total Concentration (mM) |
|---|---|---|---|---|
| Octanethiol | * | 0.1 | * | 0.1 |
| Hexanethiol | * | 0.1 | * | 0.1 |
| Hexanethiol | TFBM | 0.08 | 0.02 | 0.1 |
| Hexanethiol | TFBM | 0.06 | 0.04 | 0.1 |
| Hexanethiol | TFBM | 0.04 | 0.06 | 0.1 |
| Hexanethiol | TFBM | 0.02 | 0.08 | 0.1 |
| * | TFBM | * | 0.1 | 0.1 |

## Thiol Monolayers on Ni

Using an Autolab PGSTAT30 computer controlled instrument, running GPES, Ni was plated onto Au(111) Arrandee™ slides, which had been cleaned twice with piranha solution to remove any trace of previous Ni deposits. Plating was performed at a potential of -0.9 V vs SCE from an aqueous solution of 0.2 M $NiSO_4$/ 0.5 M $B(OH)_3$ to a charge limit of 300 mC. A flattened crocodile clip made contact to the corner of the Arrandee™ slide to ensure good electrical connection; this was wrapped with PTFE tape to ensure isolation from the plating solution, a Pt mesh CE was used.

The Ni surface oxide was removed *in-situ* in 0.05 M $Na_2SO_4$, which unless otherwise stated was made up to a pH just less than 3 with $H_2SO_4$, by running a CV from -0.4 to -0.85 V vs SCE, followed by holding the potential at -0.6 V. To this aqueous solution 1 mL of the desired thiol in ethanol solution per 100 mL of electrolyte was added, the initial and final concentrations are listed in **Table 2**. During the thiol adsorption process the surface was held for 1 hour at -0.6 V vs SCE. If the multilayer is desired the surface is briefly rinsed with ethanol, followed by Milli-Q® water. Whereas if the monolayer is desired then the surface is rinsed for 2 minutes with ethanol, followed by 30 seconds of Milli-Q® water.

*Table 2: Initial and final concentrations used for solutions used in monolayer formation on Ni.*

| Molecule A | Molecule B | Initial Concentration A (mM) | Initial Concentration B (mM) | Final Concentration A (mM) | Final Concentration B (mM) | Total Concentration (mM) |
|---|---|---|---|---|---|---|
| Octanethiol | * | 10 | * | 0.1 | * | 0.1 |
| Hexanethiol | * | 10 | * | 0.1 | * | 0.1 |
| Hexanethiol | BDMT | 8 | 2 | 0.08 | 0.02 | 0.1 |
| Hexanethiol | BDMT | 6 | 4 | 0.06 | 0.04 | 0.1 |
| Hexanethiol | BDMT | 4 | 6 | 0.04 | 0.06 | 0.1 |
| Hexanethiol | BDMT | 3.5 | 6.5 | 0.035 | 0.065 | 0.1 |
| Hexanethiol | BDMT | 3 | 7 | 0.03 | 0.07 | 0.1 |
| Hexanethiol | BDMT | 2 | 8 | 0.02 | 0.08 | 0.1 |
| Hexanethiol | BDMT | 1.5 | 8.5 | 0.015 | 0.085 | 0.1 |
| Hexanethiol | BDMT | 1 | 9 | 0.01 | 0.09 | 0.1 |
| Hexanethiol | BDMT | 0.5 | 9.5 | 0.005 | 0.095 | 0.1 |
| * | BDMT | * | 10 | * | 0.1 | 0.1 |
| Hexanethiol | TFBM | 8 | 2 | 0.08 | 0.02 | 0.1 |
| Hexanethiol | TFBM | 7 | 3 | 0.07 | 0.03 | 0.1 |
| Hexanethiol | TFBM | 6 | 4 | 0.06 | 0.04 | 0.1 |
| Hexanethiol | TFBM | 5 | 5 | 0.05 | 0.05 | 0.1 |
| Hexanethiol | TFBM | 4 | 6 | 0.04 | 0.06 | 0.1 |
| Hexanethiol | TFBM | 2 | 8 | 0.02 | 0.08 | 0.1 |
| * | TFBM | * | 10 | * | 0.1 | 0.1 |

# Results and Discussion

## Octanethiol

Octanethiol monolayers were investigated on Au and electrodeposited Ni using PM-IRRAS allowing the qualitative ordering of these monolayers on Au and Ni

to be determined and compared. Furthermore PM-IRRAS shows that by slightly changing the method of formation the octanethiol layers formed on Ni can be altered. Alkanethiol monolayers are well studied[12-19] and as such are a good reference system before measuring more complex systems, with regards to both the metal substrate and the monolayer material. The reference Au/octanethiol system was investigated before moving on to examine octanethiol on Ni. **Figure 1** shows a PM-IRRAS spectrum of a self-assembled monolayer of octanethiol is formed on a Au(111) Arrandee™ substrate. With regards to monolayer ordering the peaks from about 2825-3000 $cm^{-1}$ are the most informative. This set of peaks arises from the $CH_2$ backbone and the $CH_3$ end group of the octanethiol. Based on the peak position and relative bandwidth the relative monolayer ordering can be determined. The peak position changes depending on whether the system is in a liquid- or crystalline-like phase, with higher frequencies indicating a liquid-like monolayer and lower frequencies a crystalline-like structure.[20]

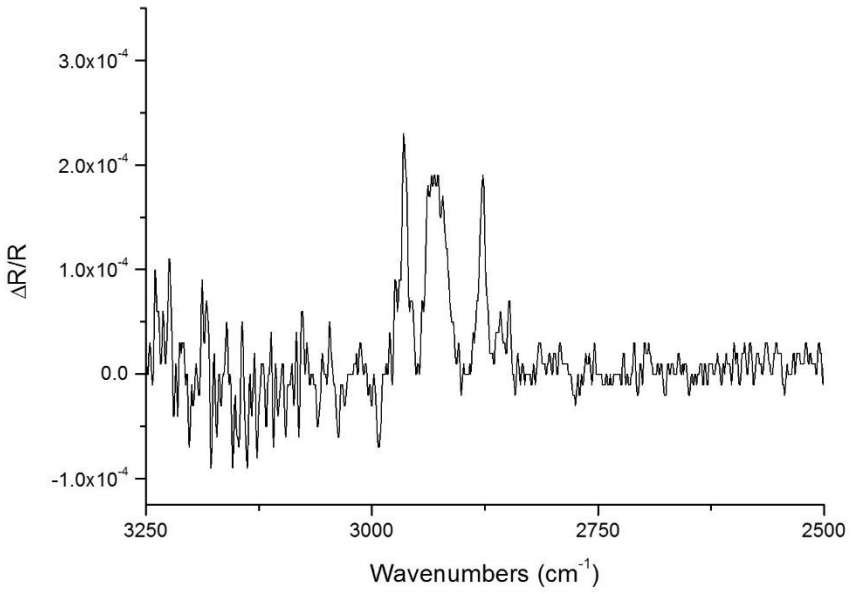


*Figure 1: The PM-IRRAS spectra of ordered octanethiol monolayers on Au is shown. By using an appropriate adsorption method for each metal similarly ordered monolayers can be formed.*

The shift in peak position towards values more characteristic of the crystalline structure arises because of the strong interactions holding neighbouring molecules together. Longer chain alkanes give rise to more crystalline-like structures. When assessing a single monolayer the degree of ordering can be determined using the $CH_2$ stretches. Frequencies of less than 2920 $cm^{-1}$ for the asymmetric stretch, and less than 2850 $cm^{-1}$ for the symmetric stretch indicate a crystalline-like structure, with all-*trans* configuration.[5, 21] While this method is not without its critics,[22] it allows for a picture of the monolayer ordering to be formed. The peak positions measured for this system are 2965, 2858 2917, and 2877 $cm^{-1}$ for the symmetric and asymmetric $CH_2$ and the symmetric and asymmetric $CH_3$ stretches, respectively. Comparison of the $CH_2$ stretching peak positions are to the benchmark values show this monolayer has crystalline-like ordering. Along with peak position the FWHM of these peaks is also used to assess the ordering of the alkane system. When a monolayer is well ordered the system is composed of nearly all *trans* oriented molecules causing a sharp well-defined peak, as is seen in **Figure 1**, however as the system becomes more disordered more *gauche* oriented molecules are incorporated. The multiple orientations occurring in each peak, from the *gauche* molecules, broadens the peak. Assessment of the FWHM is more difficult than assessment of peak position, because FWHM is not measured as accurately. In this respect uncertainties arise from peak overlap and errors introduced from a non-flat baseline.[20] The peak width is assessed as 4, 7, 7 and 6 $cm^{-1}$ for the symmetric and asymmetric $CH_2$ and symmetric and asymmetric $CH_3$ peaks. These values are indicative of a well ordered monolayer. Alkanethiols on Au are known to form well-ordered and dense monolayers therefore the ordering of octanethiol on Au will be used as a benchmark for assessing the same monolayers on Ni.

*Table 3: Comparison of peak positions and FWHM values for octanethiol on Au and Ni.*[17, 20, 23]

| Au | | Ni pH < 3, Extensive Rinsing | | Ni pH < 3, Brief Rinsing | | Ni pH ≥ 3 | | Assignment | Literature Position ($cm^{-1}$) |
|---|---|---|---|---|---|---|---|---|---|
| Peak Position ($cm^{-1}$) | FWHM ($cm^{-1}$) | Peak Position ($cm^{-1}$) | FWHM ($cm^{-1}$) | Peak Position ($cm^{-1}$) | FWHM ($cm^{-1}$) | Peak Position ($cm^{-1}$) | FWHM ($cm^{-1}$) | | |
| 2965 | 6 | 2965 | 10 | 2963 | 14 | 2962 | 16 | $\nu_{as}(CH_3)$ | 2966-2964 |
| 2917 | 7 | 2920 | 5 | 2927 | 3 | 2926 | 19 | $\nu_{as}(CH_2)$ | 2923-2918 |
| 2877 | 7 | 2878 | 3 | 2879 | 20 | 2873 | 11 | $\nu_{s}(CH_3)$ | 2880-2877 |
| 2858 | 4 | 2850 | 8 | 2854 | 13 | 2854 | 13 | $\nu_{s}(CH_2)$ | 2854-2848 |
| 1528 | | 1469, 1243, 1166 | | 1734, 1609, 1467 | | 1469, 1249, 1163 | | CH Backbone | |

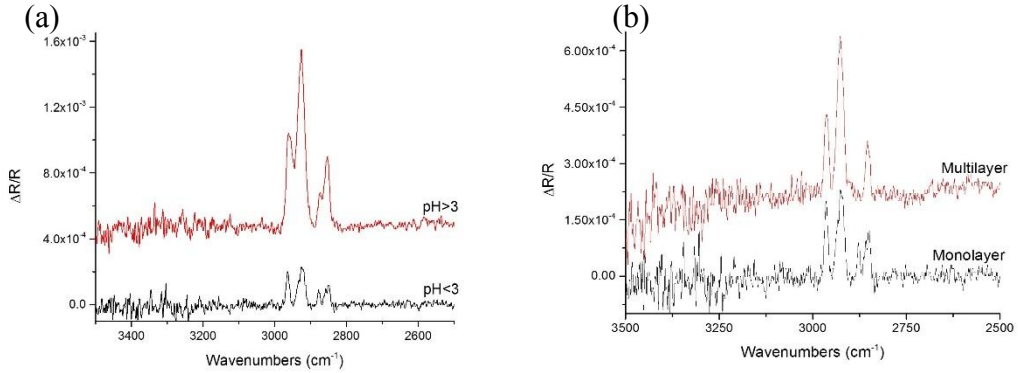


*Figure 2: (a) Octanethiol monolayers on Ni were formed in adsorption solutions of differing pHs. Comparing the monolayers formed at pH ≥ 3 (Method (1)) and pH < 3 (Method (3)) it can be seen that at lower pH the monolayer is more ordered. (b) Octanethiol monolayers on Ni were rinsed with ethanol for different lengths. A brief rinse with ethanol gave the multilayer (Method (2)), while a long rinse (Method (1)) gave the monolayer.*

Following the control experiments on octanethiol on Au, similar experiments can be performed on octanethiol on electrodeposited Ni. Unlike Au, Ni quickly oxidises on exposure to ambient conditions, therefore standard self-assembly is inadequate for the formation of octanethiol monolayers. The use of standard self-assembly is a two-fold problem, firstly NiO rather than pure Ni would be investigated and second the metal oxide layer causes poor monolayers. Furthermore, this work has

shown that by altering the method of potential assisted assembly the resulting alkanethiol deposit can be controlled. Three different methods of formation were used, these are (1) a pH ≥ 3 solution with extensive ethanol and water rinsing, (2) a pH < 3 solution with brief rinsing, and (3) a pH < 3 solution with extensive ethanol and water rinsing. For clarity the spectra from Method (1) and (3), and Method (2) and (3) are compared separately in **Figures 2a** and **2b**, respectively. As with the analogous octanethiol on Au system the peak position and FWHM are used to assess the octanethiol ordering, these values are compared in **Table 3**. For comparison the Au values are tabulated. Comparing peak position it can be seen that ordering increases in the sequence below:

$$\text{Method (2)} < \text{Method (1)} < \text{Method (3)} \approx \text{Au}$$

Using the FWHM to assess the system ordering it increases in the succession shown:

(a) pH < 3 (b) pH > 3

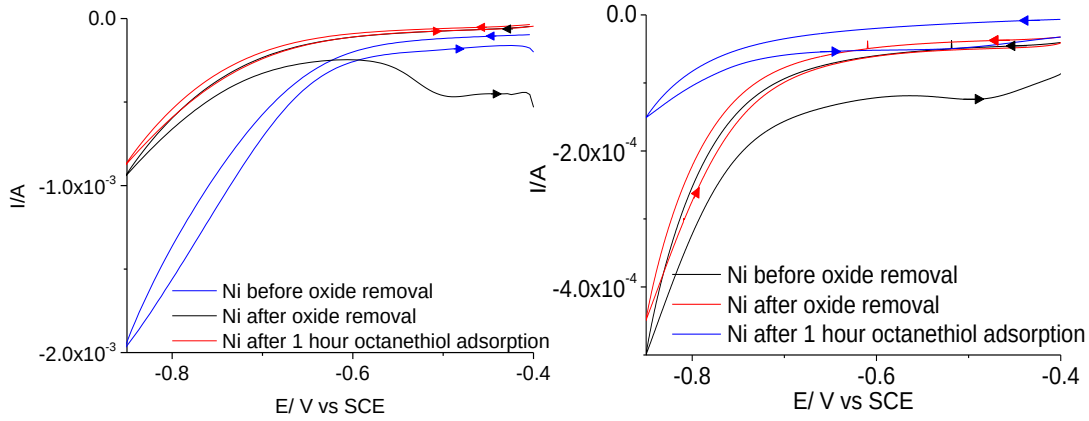


*Figure 3: (a) When pH < 3 0.05 M $Na_2SO_4$ is used the Ni can be fully oxidised allowing a well formed octanethiol monolayer to form. This monolayer leads to an enhancement of hydrogen evolution as can be seen through cyclic voltammetry. (b) Unlike when the pH is less than 3, when pH > 3 0.05 M $Na_2SO_4$ is used hydrogen evolution is suppressed, and there is slight return of the oxide peak.*

Method (2) ≈ Method (1) < Method (3) ≈ Au

These comparisons show that while the monolayer formed from Method (3) has similar ordering to that seen for octanethiol on Au, those from Methods (2) and (3) are always more disordered. The difference in monolayer order from Methods (2) and (3) arises because Method (2) uses a pH ≥ 3 electrolyte, whereas in Method (3) a pH < 3 electrolyte is used. When comparing the monolayers formed by these methods it is useful to look at the electrochemistry of these surfaces both before and after monolayer adsorption. **Figure 3a** and **3b** shows similar results for the first and second scans of the initial Ni surface. In the first scan the peak at ~ -0.5 V vs SCE pertains to the reduction of the Ni surface oxide.[24] From this peak average surface coverage of surface oxide of about 0.4 ML is calculated,[24] although this is highly dependent on the specific experiment. The other universal feature of the voltammetry is the curvature of the current, and sharp increase in current. This feature is a direct result of the hydrogen evolution reaction. In acidic solutions, like that used here, hydrogen evolution occurs by the reaction $2H^+ + 2e^- \rightarrow H_2$.[25] When Ni is used hydrogen adsorption precedes the hydrogen evolution reaction, $H^+_{(sol)} + e^- \rightarrow H_{ad(Ni)}$.[26] This step alters the free energy of the electron transfer in the HER allowing it to occur positive of the equilibrium potential of the HER.[25] Hydrogen evolution can then proceed through the $H_{ad(Ni)}$ species. HER occurs through one of two pathways:[25, 26]

1) $H_{ad(Ni)} + H^+_{(sol)} + e^- \rightarrow H_{2(gas)}$ *(Eq. 1)*

2) $2H_{ad(Ni)} \rightarrow H_{2(gas)}$ *(Eq. 2)*

The result of these reactions is the characteristic sharp, curved increase in the electrochemistry seen. In both cases the oxide reduction peak does not reappear on the second scan. After the adsorption of the octanethiol monolayer, however, the electrochemistry is obviously different. In the pH < 3 system the electrochemistry is

uneventful aside from the enhancement of the hydrogen evolution reaction. For the pH ≥ 3 system, however, the hydrogen evolution is reduced, but more importantly the peak related to the reduction of the surface oxide starts to reappear. The appearance of the oxide reduction peak in the pH ≥ 3 system occurs because the Ni system does not undergo its full reduction at pH 3 and higher.[27] The presence of the oxide layer on Ni does not preclude the formation of an ordered alkanethiol monolayer, nonetheless it does cause difficulties. It has been seen that the presence of a metal oxide can hinder the formation of the sulphur-metal bond, particularly since the oxide layer can oxidise the incoming thiol end group to the poor anchor groups sulphonate, sulphonite,[28] or disulphides.[29] However, this can be taken advantage of, over an extended period, to form well-ordered monolayers, because the metal is simultaneously reduced allowing fresh thiol to bond to a pure metal surface.[29] Furthermore, on a metal oxide surface more disorder has been seen because of the physisorption, rather than chemisorption of the alkanethiols.[30]

Having established that the pH < 3 solution gives rise to more ordered monolayers than the pH ≥ 3 solution the rinsing methods can be compared. Upon examination of the spectra from brief and extended rinsing with ethanol and water it is apparent that the extended rinsing reveals a more ordered monolayer. It has been established that when a monolayer is formed on Ni with potential assisted assembly the monolayer forms from micelles of octanethiol. After the formation of a monolayer these micelles promote multilayer formation, which can be removed by extensive rinsing.[5] As the octanethiol exists in many directions in the micelle structure the disorder seen in the PM-IRRAS exists from the many molecular contributions from the micelle structure on the monolayer. Furthermore, multilayer systems have shown more disorder than those of monolayers.[13] Based on this investigation the most ordered

monolayers on Ni occur with use of a pH < 3 adsorption solution, and to rinse with copious amounts of ethanol followed by Milli-Q® water. In summary, by using this technique the Ni is fully reduced to its metallic state allowing the formation of well-ordered layers. The multilayer system which forms during assembly is subsequently fully rinsed off.

Mixed Monolayers

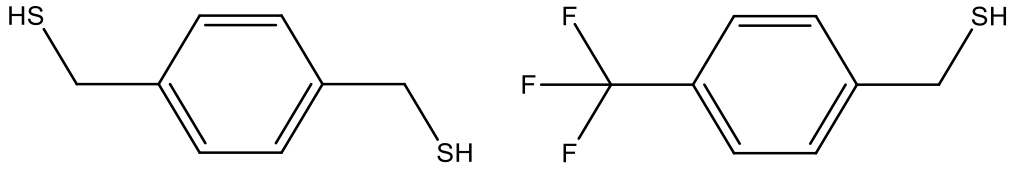


(a) (b)

*Figure 4: (a) The molecular wire of interest 1,4-benzenedimethanedithiol. (b) The chromophore molecule [4-(trifluoromethyl)phenyl]methanethiol.*

Benzenedimethanedithiol (BDMT), **Figure 4a**, is an interesting molecule for molecular electronics because the HOMO-LUMO gap, from the benzene centre, is smaller than in more traditional alkanedithiols.[31] Moreover, theoretical studies on BDMT demonstrate that the existence of the π-bond in the system gives rise to stronger hybridization between the molecular orbitals and the Au.[32] Both the reduced HOMO-LUMO gap, and the delocalization of the molecular orbitals give rise to an improved conductance in these benzene containing molecules than in standard alkanedithiols. Driven by the improved conductance BDMT and related molecules have been well studied as molecular wires.[31-34] The large portfolio of background literature for BDMT on Ni makes it an interesting pairing for fundamental investigation of molecular spintronics. If BDMT is to be investigated on Ni then the Ni surface must be protected from oxidation on transfer to the STM, a simple way to do this is to protect the surface with a monolayer. As BDMT is a relatively bulky molecule the surface could be better protected by the use of a mixed monolayer composed mostly of an insulating

alkanethiol. Furthermore the use of a mixed monolayer should separate the BDMT molecules to avoid the measurement of multiple rather than single BDMT molecules. When forming a mixed monolayer for molecular conductance studies it is important that the "insulating" molecule is chosen to be a similar length or shorter than the target molecular wire to allow for subsequent contact to the STM tip. Using Spartan® it was calculated that BDMT is 0.79 nm in length, consequently hexanethiol which has a molecular length of 0.80 nm, was chosen as the insulator molecule. For *I*(*s*) and break junction investigations this tiny difference in size is acceptable as the STM tip will penetrate the insulating alkanethiol monolayer slightly to contact the molecular wire. The differing rates of adsorption of molecules means the composition of the adsorption solution is not necessarily an accurate reflection of the mixed monolayer, therefore the composition and the ability to control the composition of this mixed monolayer should be experimentally ascertained. When investigating a mixed monolayer on Au a straightforward way to quantitatively measure the composition of the mixed monolayer is to use reductive desorption experiments. Unfortunately reductive desorption is not possible for mixed monolayers on Ni as this process is hidden by hydrogen evolution. As an alternative PM-IRRAS can be used. By investigating the growth and loss of characteristic peaks for each molecule a semi-quantitative analysis of the monolayer composition can be made. For successful analysis the vibration modes investigated should be carefully chosen. For example, while only BDMT in a mixed monolayer BDMT/HT monolayer contains the aromatic ring the stretches of the C-H bonds in this occur in a similar location to and are weaker than those of the stretches for the alkanethiol backbone. In this case little information will be garnered by using with these mixed monolayers. Moreover, the aromatic C-H peaks can be missing from spectra of adsorbed phenyl species.[35] For the purposes of investigating

the ability to control the mixing of the monolayer a means around this is to replace BDMT by a chromophore molecule, such as the [4-(trifluoromethyl)phenyl]methanethiol (TFBM) molecule in **Figure 4b**. The C-F stretches are very intense, and well removed from the alkanethiol backbone stretches. A simple way to study the ability to control mixed monolayer composition is by following the growth of the C-F peak as the concentration of the chromophore molecule changes. As before the mixed monolayer was investigated on the Au substrate to gain insight into the system, prior to investigation on the electrodeposited Ni, using the proven technique of a potential assisted deposition in a pH < 3 electrolyte followed by extended rinsing by ethanol and Milli-Q® water.

(a) (b)

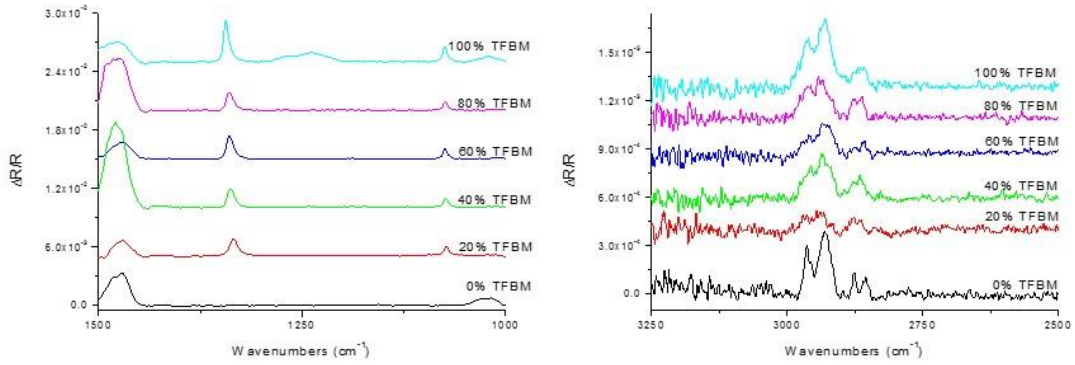


*Figure 5: PM-IRRAS was used to follow the composition of the mixed monolayers of TFBM/6-HT on Au, the percentage of TFBM in solution is listed (a). Following the growth of the $CF_3$ peaks it is seen that the intensity of the peaks varies the most at the extreme solutions, but there is little change in between. (b) The $CH_3$ peaks are followed.*

Mixed monolayers of TFBM and hexanethiol (HT) were investigated on Au by Simon Harris. These mixed monolayers were formed by changing the ratio of TFBM:HT in the adsorption solution, which results in monolayers of different

compositions as followed by PM-IRRAS. The resulting spectra of these investigations are presented in **Figure 5**. From these spectra it is clear the $\nu_s$(C-$F_3$) peak at 1345 $cm^{-1}$ [36] and the $\nu_s$(CF) peak at 1076 $cm^{-1}$,[37] are strongest at 100 % TFBM, and non-existent at 0 % TFBM as expected. A plateau in peak intensities between these two concentration extremes is also apparent. Somewhat surprisingly, intense peaks due to C-H stretches of $CH_3$ (2962 and 2865 $cm^{-1}$) are seen for the 100 % TFBM layer; this likely results from co-adsorption of the ethanol solvent used. It is well-known that the solvents used in molecular adsorption can intercalate into the monolayer,[38] however given the proven track record of ethanol as a solvent for monolayer formation the intercalation of solvent species is a compromise for the well-ordered monolayers. By integrating the area under these peaks the peak intensities, for different solution composition, can be compared, **Figure 6**. The resulting stacked bar charts demonstrate that based on the peak intensity the composition of the resulting monolayer should be broadly similar for all cases of mixed composition solution between 20-80 %. The $CH_3$ peaks can also be used to investigate the insertion of the TFBM molecule, as in theory this group is only present on the hexanethiol molecules. While a similar result is seen as with the $CF_3$ peaks, these results are more difficult to interpret. While the $CH_3$ peaks are insightful the co-adsorption of the solvent makes the values less accurate than those from the $CF_3$ analysis. Based on this work it is apparent that TFBM:HT mixed monolayers can be formed on Au, but the monolayer composition does not necessarily follow the adsorption solution composition. Nevertheless, this investigation has prompted similar experiments on Ni.

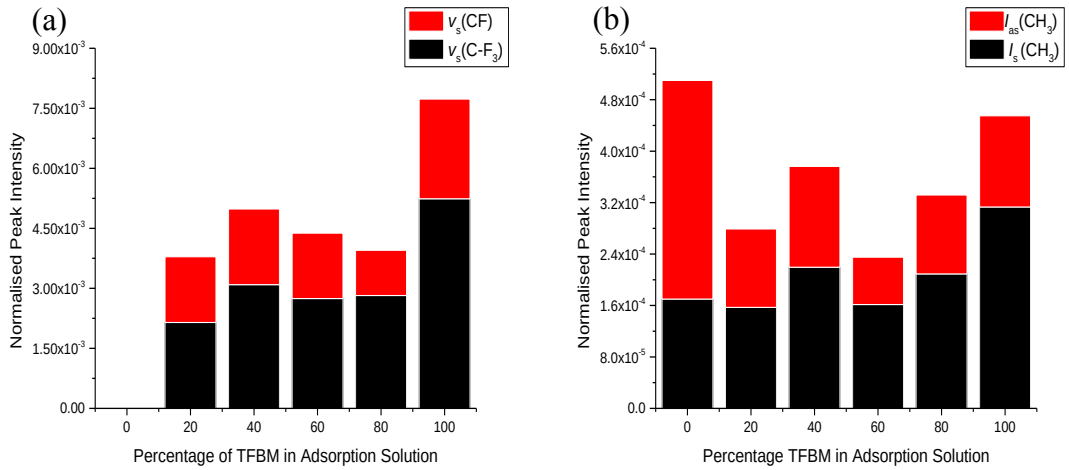


*Figure 6: (a) Comparison of the intensities of the $CF_3$ peaks from mixed monolayers of TFBM/6-HT on Au. The intensity is a maximum at 100% TFBM in adsorption solution. When TFBM is present the peak intensities have similar values regardless of the solution composition. (b) Comparison of the intensities of the $CH_3$ peaks. The $CH_3$ intensity is highest when there was no TFBM in solution, though there is not a plateau of intensities.*

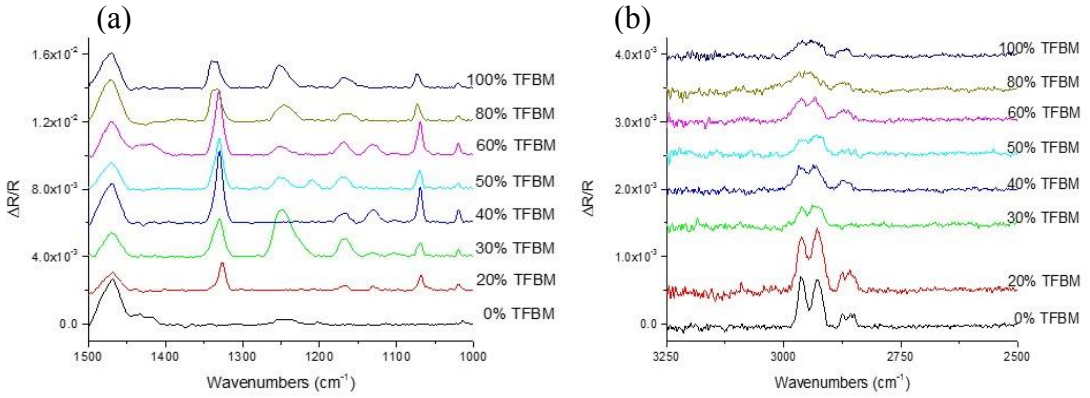


*Figure 7: PM-IRRAS spectrum of mixed monolayers of TFBM/6-HT on Ni. The percentage of TFBM in the adsorption solution is listed to the right of both spectra. (a) The intensity of the peaks relating to $CF_3$ reach a maximum at 40-60 % TFBM in the adsorption solution. The spectrum at 100 % is that formed after 1 hour adsorption. (b). Focussing on the $CH_3$ stretching peaks shows the amount of 6-HT in the resulting monolayer to decrease with increasing TFBM in solution. The spectrum shown for 100 % is that measured after 1 hour adsorption.*

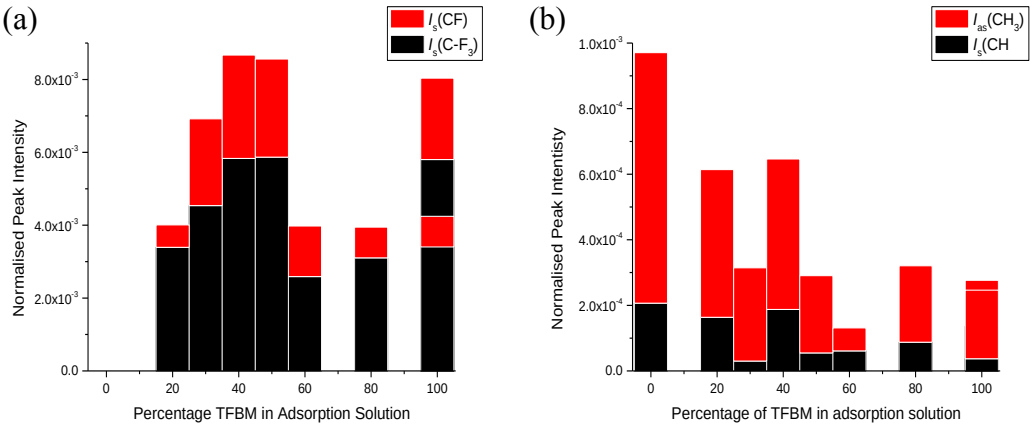


*Figure 8: (a) Comparison of the intensities of the $CF_3$ peaks from mixed monolayers of TFBM/6-HT on Ni. The intensity can be seen to be at a maximum at 40 % TFBM in adsorption solution. When compared to 100 % TFBM with 1 hour adsorption the total intensity is almost double. The values become more comparable when a 65 hour adsorption time is used. (b) Comparison of the intensities of the $CH_3$ peaks. As expected $CH_3$ intensity is highest when there was no TFBM in solution.*

Having established these sorts of measurements are possible on mixed monolayer on gold substrate the same measurements on electrodeposited Ni could be performed. In this case the monolayers were formed by electrode potential assisted assembly. The spectra resulting from the TFBM:HT mixed monolayer investigations are presented in **Figure 7**. As with Au the intensity of both the $CH_3$ and $CF_3$ stretches can be followed to gain insight into the monolayer system on Ni, **Figure 8**. Looking at the $CH_3$ region it is clearly apparent that the intensity of the CH peaks decreases from the 0 % TFBM solution to the 30 % TFBM solution. However, for TFBM concentrations greater than 30 % the differences in intensity do not follow a clear pattern. As with the Au system there are peaks apparent from $CH_3$ even for 100 % TFBM, likely due to the co-adsorption of solvent. When the intensity of these peaks is determined by integration and represented in stacked bar charts against the composition of the adsorption solution it is apparent that the peak intensity does not

change in a consistent manner. On increasing TFBM concentration the peak intensity seems to be completely random. Since there can be some confusion between the CH peaks of the monolayer species, and those of the solvent species which may be incorporated into the monolayer, $CF_3$ stretches must also be followed. As expected no $CF_3$ peaks from the 0 % TFBM solution can be seen, surprisingly, however, the CF stretch for the 100 % TFBM solution is visibly not the most intense, with the maximum intensity occurring for the 40 % TFBM solution. When the normalized peak intensity is plotted against the composition of the adsorption solution it becomes apparent that it is not just the CH region which shows a seemingly random change in intensities but also the $CF_3$ region. The random change in intensity in the $CF_3$ region as well means the change must be due to the mixed monolayer itself and not the inclusion of solvent into the monolayer, although this may be a contributing factor to some of the peaks. It is known that alkanethiol monolayers can reach near full coverage after just 1 hour, and then over longer periods they become more organized.[17] It is possible, however, that the bulkier TFBM molecule takes more time to form a full monolayer. A reduced surface concentration due to incomplete monolayer formation could explain the reduced peak intensity of the monolayer formed on Ni, therefore an increased adsorption time of 65 hours for the 100 % TFBM solution was investigated. When the intensities of these peaks for this long adsorption time are added to the plot against solution concentration it can be seen that the intensity is still not higher than the 40 % TFBM case. Nevertheless, the long adsorption time system now gives amongst the highest intensities. This implies that the time for a full TFBM monolayer to form plays a role in the seemingly random intensities seen for both the CH and CF peaks. Regardless, however, the 100 % TFBM monolayer should give rise to the most intense peaks for the CF stretches, as was the case for Au, therefore there must be another

cause. The surface selection rule dictates that peak intensity becomes stronger as the dipole change moves into a perpendicular position, therefore the intensity changes seen in the investigation may arise from changes in orientation of the monolayer species on the surface. It is conceivable that this may be an issue for Ni, but not for Au, as different substrates can give rise to different angles of orientation of molecules in the monolayer.[39, 40] Therefore, the intensity on Ni with composition may be more closely dictated by the surface selection rule. A further explanation for the difficult to explain progression of peak intensities arises from visual inspection of the Ni surface after monolayer formation. It was observed that although the Ni surface was always of mirror-like quality at the start of the adsorption process during this time the quality of the Ni surface visibly deteriorated, but only in the presence of TFBM. When BDMT was used in place of TFBM no visible deterioration of the Ni surface occurred. This implies that the addition of the trifluoromethyl group causes the deterioration of the Ni surface. While there is no account in the literature of the interaction of trifluoromethyl substituted aromatic compounds with metallic Ni, it should be noted that in electrocatalytic reactions to form trifluoromethyl aromatic molecules the intermediate complex is Ni with the aromatic and trimethylfluoro group of interest acting as ligands.[41] Therefore it is possible that the combination of the Ni surface, and the very negative electrode potential are acting to cause the breakdown of TFBM. It has also been noted in the literature that when the adsorption of I-$CF_3$ was investigated on Ni surfaces at low temperature, –$CF_3$ fragments do in fact adsorb on the Ni surface.[37] Furthermore, the Ni surface can activate the C of the C-F bond, allowing the formation of $NiF_2$. The presence of the $I^-$ does mean, however, that this system does not necessarily behave in the manner in which TFBM does. Unfortunately, while the TFBM molecule acted as a successful spectroscopic probe molecule on Au its complex

interaction with the Ni surface meant its use on Ni has provided no evidence as to the ability of this mixed monolayer formation.

Due to the problems encountered when using TFBM as a chromophore molecule for the investigation of the ability of BDMT type molecules to insert into alkanethiol monolayers on Ni, BDMT itself in a mixed monolayer with HT was investigated. As with the TFBM mixed monolayer investigations the intensity change of the $CH_3$ peaks with changing adsorption solution composition was followed to gain insight into the monolayer composition. A series of adsorption solution compositions from 0 % BDMT to 100 % BDMT was investigated with the resulting spectra shown in **Figure 9**. By visually inspecting these spectra one observes a decrease in intensity of the $CH_3$ peak (2955 and 2874 $cm^{-1}$) on increasing the solution composition from 0 to 40 % BDMT, after which changes in intensity are difficult to perceive without integration of the peaks. The intensities of the $CH_3$ stretching peaks are plotted against the composition of the adsorption solution in **Figure 10**. In this plot the $\nu_{as}(CH_3)$ peak intensity decreases linearly on going from 0 to 60 % BDMT, and then becomes less consistent on going from 60 to 100 % BDMT. This implies there is control of the composition of the monolayer at least up to 60 % BDMT in solution, after this point, however, control of the monolayer composition becomes questionable. It is likely the changes in peak intensity in the region 60 to 100 % BDMT arise not just because of changes in monolayer composition, but also because of changes in the orientation of the molecules comprising the monolayer. The change in orientation has in the literature been linked to proportionately more intense $CH_3$ peaks.[20]

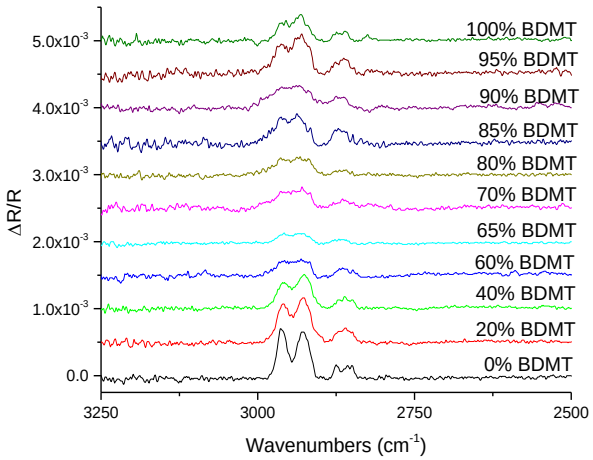


*Figure 9: PM-IRRAS spectra of mixed monolayers of BDMT/6-HT on electroplated Ni surfaces. The $CH_3$ stretching peaks are focused on, showing their reduction with increasing BDMT. The percentage of BDMT in the adsorption solution is quoted.*

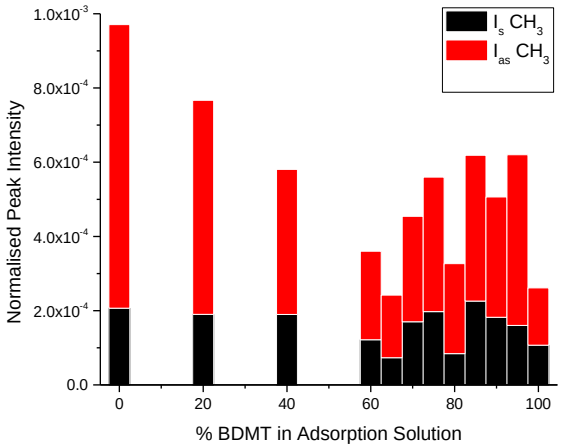


*Figure 10: Normalised peak intensity of the $I_s$ and $I_{as}$ $CH_3$ peaks plotted as a function of percentage of BDMT in the adsorption solution for mixed monolayers of BDMT/HT on Ni. The composition of the resulting monolayer can be controlled up to 60 % BDMT in solution. After 60 % the make-up of the resulting monolayer cannot be accurately controlled.*

*Table 4: Comparison of peak positions for 100 % aromatic molecule on Au and Ni. (a)[17, 20, 23] (b)[42] (c)[36] (d)[37]*

| Au/TFBM Peak Position ($cm^{-1}$) | Ni/TFBM Peak Position ($cm^{-1}$) | Ni/BDMT Peak Position ($cm^{-1}$) | Assignment | Literature Position ($cm^{-1}$) | |
|---|---|---|---|---|---|
| 2962 | 2959 | 2955 | $\nu_{as}(CH_3)$ | 2966-2964 | (a) |
| 2930 | 2931 | 2931 | $\nu_{as}(CH_2)$ | 2923-2918 | (a) |
| 2865 | 2866 | 2874 | $\nu_{s}(CH_3)$ | 2880-2877 | (a) |
| | 2848 | 2861, 2825 | $\nu_{s}(CH_2)$ | 2854-2848, 2838 | (b) |
| 1345 | 1343 | | $\nu_{s}(C\text{-}F_3)$ | Expt:1372/ Calc:1343 | (c) |
| | 1164 | | $\nu_{as}(CF)$ | 1172 | (d) |
| 1076 | 1075 | | $\nu_{s}(CF)$ | 1072 | (d) |
| 1729, 1615, 1470 | 2118, 1469, 1247 | 1606, 1511, 1470, 1349 | CH Backbone | | |

Using the peak positions of the $CH_2$ stretches a comparison of the ordering between the three systems can be made. Because of the differences in the way the solution composition affected the apparent composition of the resulting monolayer only 3 solution compositions were compared. The systems with 100 % and 0 % of the molecular wire of interest in solution were used, (**Table 3** and **4**) as well as those with 40 % of the molecular wire in solution. The 40 % solution was chosen because this is the last solution composition where any control over the monolayer composition was seen for the Ni/BDMT system. When the analogous systems for 100 % of the molecular wire of interest are compared it was seen that the resulting monolayers increase in the order Au/TFBM < Ni/TFBM < Ni/BDMT. This order changes on going to the analogous 40 % molecular wire in solution systems whose order increases in the manner Ni/TFBM < Ni/BDMT < Au/TFBM. From these comparisons it is obvious

that the monolayer formed from BDMT on Ni is more ordered than that formed from TFBM. This is unsurprising, however, given the variability between experiments on the same adsorption solutions implying little control over the formation of monolayers. Comparison of the ordering of different adsorption solution compositions with each metal-molecule series shows that for both Au/TFBM and Ni/BDMT the ordering increases in the manner 100 % molecular wire solution < 0 % molecular wire solution < 40 % molecular wire solution. The increase in monolayer ordering on going from 0 % BDMT in solution to 40 % BDMT in solution for the Ni system is encouraging because a more ordered monolayer with less defect sites should protect the surface better from re-oxidation than a less ordered one. This means the insertion of the molecular wire into the hexanethiol monolayer will allow for molecular conductance measurements to be made, while still protecting the Ni surface.

From these investigations it has been seen that while chromophore molecules like TFBM allow for insight into monolayer composition on Au their interaction with the Ni surface is too complex to be useful when investigating mixed monolayers on Ni. Although chromophore molecules allow for easier analysis, it was possible to use BDMT for analysis of the monolayers formed with hexanethiol. Investigations of these mixed monolayers showed that if a BDMT:HT monolayer were to be used for investigation of BDMT single molecule conductance on a Ni substrate it is possible to control the composition of the monolayer by using an adsorption solution of composition 0 to 60 % BDMT.

## Conclusion

Metallic Ni is of interest in molecular electronics because of its access to control of electron spin. Unfortunately, as with other ferromagnetic metals, Ni easily

oxidizes on exposure to air. A simple way to avoid this while still maintaining the ability to perform single molecule conductance measurements is to form molecular monolayers on the Ni surface which have included the molecular wire of interest. In this work PM-IRRAS was successfully used to assess the ability of various methods in monolayer formation. Using potential assisted adsorption in a pH < 3 electrolyte high quality octanethiol monolayers, with an ordering similar to those on Au, could be formed. Building on this knowledge mixed monolayers on Ni were formed with the aim of controlling the adsorption of the molecular wire of interest in the monolayer. While a simple technique to investigate the insertion of these molecules is to use a chromophore molecule to ensure intense peaks in the IR spectra from the molecular wire this was not possible with Ni. The formation of mixed TFBM monolayers on Ni was surprisingly complex and therefore an alternative means of following molecular wire insertion was needed. Although not a chromophore the $CH_3$ end group of BDMT was successfully used to follow the change in monolayer composition as a result of adsorption layer composition, showing controllability when the solution is 60-100 % BDMT. This controllability allows confidence in the future use of these mixed monolayers for molecular electronics studies on Ni systems. The isolation of the BDMT molecule in insulating monolayers on Ni provides a unique approach to measure molecular conductance by $I(s)$ or break junction methods on a metal other than Au.

## Declaration

*Simon Harris performed PM-IRRAS measurements on TFBM:HT monolayers on Au under my supervision as part of his 3$^{rd}$ year research project.*

# References


1. K. Yoshida, I. Hamada, S. Sakata, A. Umeno, M. Tsukada and K. Hirakawa, *Nano Letters*, 2013, **13**, 481-485.
2. S. Mandal and R. Pati, *ACS Nano*, 2012, **6**, 3580-3588.
3. J. R. Petta, S. K. Slater and D. C. Ralph, *Physical Review Letters*, 2004, **93**, 136601.
4. J. R. Niskala and W. You, *Journal of the American Chemical Society*, 2009, **131**, 13202-13203.
5. J. E. Sadler, D. S. Szumski, A. Kierzkowska, S. R. Catarelli, K. Stella, R. J. Nichols, M. H. Fonticelli, G. Benitez, B. Blum, R. C. Salvarezza and W. Schwarzacher, *Physical Chemistry Chemical Physics*, 2011, **13**, 17987-17993.
6. A. S. Hallback, B. Poelsema and H. J. W. Zandvliet, *ChemPhysChem*, 2007, **8**, 661-665.
7. Z. J. Donhauser, B. A. Mantooth, T. P. Pearl, K. F. Kelly, S. U. Nanayakkara and P. S. Weiss, *Japanese Journal of Applied Physics Part 1-Regular Papers Brief Communications & Review Papers*, 2002, **41**, 4871-4877.
8. F. v. Wrochem, F. Scholz, A. Schreiber, H.-G. Nothofer, W. E. Ford, P. Morf, T. Jung, A. Yasuda and J. M. Wessels, *Langmuir*, 2008, **24**, 6910-6917.
9. Z. J. Donhauser, B. A. Mantooth, K. F. Kelly, L. A. Bumm, J. D. Monnell, J. J. Stapleton, D. W. Price, A. M. Rawlett, D. L. Allara, J. M. Tour and P. S. Weiss, *Science*, 2001, **292**, 2303-2307.
10. H. Tokuhisa, H. Suga, E. Koyama, T. Ishida, A. Belaissaoui, Y. Nishioka and M. Kanesato, *Japanese Journal of Applied Physics Part 2-Letters & Express Letters*, 2006, **45**, L332-L334.
11. W. G. Golden, D. D. Saperstein, M. W. Severson and J. Overend, *The Journal of Physical Chemistry*, 1984, **88**, 574-580.
12. E. Ito, J. Noh and M. Hara, *Chemical Physics Letters*, 2008, **462**, 209-212.
13. S. F. Bent, M. L. Schilling, W. L. Wilson, H. E. Katz and A. L. Harris, *Chemistry of Materials*, 1994, **6**, 122-126.
14. Y. T. Tao, *Journal of the American Chemical Society*, 1993, **115**, 4350-4358.
15. Y. Jun, X. Y. Zhu and J. W. P. Hsu, *Langmuir*, 2006, **22**, 3627-3632.
16. W. A. Marmisollé, D. A. Capdevila, E. de la Llave, F. J. Williams and D. H. Murgida, *Langmuir*, 2013, **29**, 5351-5359.
17. R. H. Terrill, T. A. Tanzer and P. W. Bohn, *Langmuir*, 1998, **14**, 845-854.
18. Y.-F. Liu and Y.-L. Lee, *Nanoscale*, 2012, **4**, 2093-2100.
19. E. Ito, H. Kang, D. Lee, J. B. Park, M. Hara and J. Noh, *Journal of Colloid and Interface Science*, 2013, **394**, 522-529.
20. C. Nogues and P. Lang, *Langmuir*, 2007, **23**, 8385-8391.
21. G. Fonder, F. Cecchet, A. Peremans, P. A. Thiry, J. Delhalle and Z. Mekhalif, *Surface Science*, 2009, **603**, 2276-2282.
22. R. P. Sperline, *Langmuir*, 1997, **13**, 3715-3726.
23. H. Ron, H. Cohen, S. Matlis, M. Rappaport and I. Rubinstein, *The Journal of Physical Chemistry B*, 1998, **102**, 9861-9869.
24. T. Suzuki, T. Yamada and K. Itaya, *The Journal of Physical Chemistry*, 1996, **100**, 8954-8961.
25. *Instrumental Methods in Electrochemistry / Southampton Electrochemistry Group*, Horwood Publishing, Chichester, 2001.
26. I. Bianchi, E. Guerrini and S. Trasatti, *Chemical Physics*, 2005, **319**, 192-199.

27. B. Macdougall and M. Cohen, *Journal of the Electrochemical Society*, 1976, **123**, 191-197.
28. Z. Mekhalif, J. Riga, J. J. Pireaux and J. Delhalle, *Langmuir*, 1997, **13**, 2285-2290.
29. Z. Mekhalif, G. Fonder, D. Auguste, F. Laffineur and J. Delhalle, *Journal of Electroanalytical Chemistry*, 2008, **618**, 24-32.
30. F. Sinapi, T. Issakova, J. Delhalle and Z. Mekhalif, *Thin Solid Films*, 2007, **515**, 6833-6843.
31. Xiao, Xu and N. J. Tao, *Nano Letters*, 2004, **4**, 267-271.
32. Z. Ning, J. Chen, S. Hou, J. Zhang, Z. Liang, J. Zhang and R. Han, *Physical Review B*, 2005, **72**, 155403.
33. C. Brooke, PhD Thesis, University of Liverpool, 2012.
34. E. Leary, S. J. Higgins, H. van Zalinge, W. Haiss, R. J. Nichols, S. Nygaard, J. O. Jeppesen and J. Ulstrup, *Journal of the American Chemical Society*, 2008, **130**, 12204-12205.
35. H. Tokuhisa and R. M. Crooks, *Langmuir*, 1997, **13**, 5608-5612.
36. N. Bonalumi, A. Vargas, D. Ferri and A. Baiker, *The Journal of Physical Chemistry C*, 2007, **111**, 9349-9358.
37. K. B. Myli and V. H. Grassian, *The Journal of Physical Chemistry*, 1995, **99**, 5581-5587.
38. J. Dai, J. Cheng, J. Jin, Z. Li, J. Kong and S. Bi, *Electrochemistry Communications*, 2008, **10**, 587-591.
39. T. Kasahara and K. Itoh, *Surface Science*, 2007, **601**, 1054-1063.
40. H. Hoffmann, U. Mayer, H. Brunner and A. Krischanitz, *Vibrational Spectroscopy*, 1995, **8**, 151-157.
41. M. Khrizanforov, T. Gryaznova, O. Sinyashin and Y. Budnikova, *Journal of Organometallic Chemistry*, 2012, **718**, 101-104.
42. H. Hamoudi, M. Prato, C. l. Dablemont, O. Cavalleri, M. Canepa and V. A. Esaulov, *Langmuir*, 2010, **26**, 7242-7247.

# Chapter 3:

# Electrochemistry in Ionic Liquids

# Introduction

Ionic liquids are an exciting environment for electrochemical investigations. Although ionic liquids have been known since 1914,[1-4] their initial use for electrochemical analysis of redox species was slow, taking over half a century for the use of a chloroaluminate ionic liquid to investigate a metal redox centre to be reported.[5] Even after this investigation was published, studies on the use of ionic liquids as electrolytes were minimal, although by the 1980s and 1990s, the tide was turning and the first generation of ionic liquids, haloaluminates, were becoming active areas of electrochemical research.[6] Although ionic liquids had become more prominent, their ease of use in ambient conditions was very limited, hindering their overall applicability. This changed in 1992, when the first of the second generation of ionic liquids was reported.[7] The second generation started with the investigation of 1-ethyl-3-methylimidazolium ($EMIM^+$) ionic liquids. Unlike the prior generation, the anion was specifically chosen to form an inert ionic liquid which was easily handled under ambient conditions. By combining the $EMIM^+$ cation with $NO_3^-$, $NO_2^-$, $BF_4^-$, $MeCO_2^-$, or $SO_4^-$ the resulting ionic liquid could be synthesized without any special care aside from drying under vacuum at elevated temperatures.[7] The introduction of an easily handled second generation of ionic liquids opened the door for the explosion of work on electrochemistry in ionic liquids in the 2000s.[3] Ionic liquids are now used in electrochemical investigations because of their wide potential window, high thermal stability, low volatility, high conductivity, and the limitless variety of ionic liquids available by changing the combination of anion and cation.

Redox active monolayers are important in molecular electronics measurements for several reasons. 1) In-depth analysis of the electrochemistry of redox active monolayers is often the first step in assessing a molecule for further analysis by

molecule conductance studies. 2) The interpretation of the electrochemistry of monolayers can allow for determination of electron transfer between the substrate and redox centre and assessment of the linking groups. 3) Redox active monolayers may themselves be important in the formation of hybrid molecular electronics systems.

When looking at redox active molecular wires, investigation of the electrochemical activity of the adsorbed species is often the first step in assessing the molecules' potential as a molecular wire. This has been the case for many redox active molecules including, although not limited to, viologen wires,[8-12] pTTF containing wires,[10, 13] and redox active Ru wires.[14, 15] By assessing the electrochemistry of a redox active molecule adsorbed on the electrode, electron transfer to and from that molecule can be assessed which has eventual implications on the conductance behaviour of the molecule. This is particularly true when the conductance is investigated as a function of the electrochemical potential. At a more simplistic level, the initial assessment of the electrochemistry of an adsorbed redox species is necessary to ensure the redox chemistry is stable in the electrochemical potential measurement window.

The investigation of the interaction of an electrode surface with a bound redox molecule is insightful in itself for studies of relevance to molecular electronics. These sorts of studies are important in determining not only the rate of electron transfer,[16, 17] but also the mechanism of electron transfer,[18] whilst also allowing the effect of changing the molecular wire on electron transfer, to be determined.[17, 19] By investigating the electron transfer between a bound redox species and the electrode, the electron transfer through a saturated alkane molecular bridge has been seen to give rise to an attenuation factor of ~1.0 Å.[16, 17] The same technique of measuring electron transfer from electrode to redox active group shows more favourable electron transfer through OPV and OPE molecules with noticeably lower $\beta$-values.[17, 19] The capabilities

of using redox active monolayers to investigate electron transfer for future exploitation in molecular electronics were demonstrated in 2011, when electron transport through a monolayer of a 120 Å 80mer helical peptide bound to Au by a disulphide, and terminated in a ferrocene group was measured.[20] This work showed long-range charge transfer through the peptide to the ferrocene to produce a voltammetric response, and allowed the rate of charge transfer and the charge transport mechanism to be determined. Through this work charge transfer through the self-assembled monolayer of peptide was determined to occur by a hopping mechanism in which a hole is transferred from amide to amide, forming and removing radical amide cations until the ferrocene is oxidised. This study demonstrated that redox active monolayers have facilitated charge transfer to be measured through very long helical peptides, which are one of the longest molecular electron transfer systems investigated. While redox active monolayers hold great potential for investigating molecular electronics, they also hold great potential for the use in final devices in molecular electronics.

Self-assembled monolayers have been envisaged as potential components in futuristic molecular electronics devices, although technological implementation still seems a long way off. More fundamental studies have been performed with this envisaged aim by investigating the ability of various redox active monolayers in memory devices.[21-23] Measurements of hybrid molecular devices, *i.e.* those composed of molecular monolayers on Si, are being made to assess their potential as computational memory. The investigation of a Co-porphyrin for a Flash memory gate structure showed improvements over similar porphyrin free structures with better memory retention, and negligible memory loss.[22] DRAM, a non-volatile memory requiring power for storage, has also shown improvements when molecular monolayers are used.[21] Self-assembled monolayers terminated in ferrocene have been

proposed as a good molecular alternative for DRAM devices. It has been contended that ferrocene terminated monolayers may allow lower power consumption, as this is related to the potential needed to oxidise ferrocene, while having higher charge density on a unit area basis because of the small size of the ferrocene.[21] These investigations were aimed at a first level demonstration that self-assembled monolayers can be competitive in computational memory.

The electrochemistry of redox active self-assembled monolayers has been investigated as the first stage for molecular electronics studies of redox active molecular wires. These studies have assessed electron transfer to/from the electrode to the tethered redox moiety, as assisted by a molecular wire, in a straightforward manner. Ionic liquids have allowed for investigations on the redox active monolayers which are not otherwise possible, particularly in aqueous electrolytes. With use of room temperature ionic liquids, the redox properties of a viologen containing molecular wire, through both electron transfer processes have been investigated. Furthermore, the use of ionic liquids have allowed the rate of electron transfer through covalent and hydrogen bonded ferrocene to be assessed, with the effect of electrolyte environment seen.

## Aim

The second generation of ionic liquids is an interesting area of research for electrochemistry. The unique characteristics afforded by using an ionic liquid rather than an aqueous or organic electrolyte can be exploited for investigations in molecular electronics, particularly with redox active molecules. By utilizing ionic liquids, this work aims to study the electrochemistry of redox active monolayers on Au. In this chapter it will be demonstrated that ionic liquids allow the investigation of multiple

redox states of molecules, as well as monolayers functionalized with redox active molecules by exploitation of hydrogen bonding. The electrochemistry of various redox systems in ionic liquids will be compared with their aqueous electrochemistry.

## Methods

Cyclic voltammetry was performed on an Autolab PGSTAT30 computer controlled instrument running GPES. Analysis of resulting voltammograms was performed in GPES, and/or Origin 8.9, depending on limitations of the former. All CVs were performed between at least 0.05 $Vs^{-1}$ and 1.0 $Vs^{-1}$.

For aqueous investigations, a three electrode setup with an Au(111) bead WE, Pt mesh CE, and SCE RE was used. Both the CE and WE were prepared through annealing in a Bunsen flame. All 3 electrodes were in separate compartments of a 50 ml cell, with the reference electrode separated by a Luggin capillary, and the WE contacted the electrolyte with a hanging meniscus. Aqueous electrochemistry was performed after at least 20 minutes bubbling with oxygen free nitrogen. Aqueous electrolytes were prepared using Milli-Q® water (18 MΩ)

Ionic liquid based studies were performed with a three electrode setup composed of a Au(111) bead, and Pt wire CE and QRE. The WE was placed so as to achieve a stable hanging meniscus. It should be noted the ionic liquid Fc experiments were performed using an Arrandee™ slide sealed at the bottom of the electrochemical cell. All cells used were > 1.5 ml in capacity, prepared in a nitrogen atmosphere glovebox, and sealed prior to removal. All potentials are quoted against a $Fc/Fc^+$ internal reference, after all necessary measurements were performed. To dissolve Fc in the ionic liquids, gentle heating was necessary. Ionic liquids were prepared by vacuum drying for at least 18 hours at 120 °C, with stirring.

Ferrocene

The electrochemistry of ferrocene was measured as a 2.5 mM solution in BMIM-TFSA and BMIM-$PF_6$, and a 5 mM solution in BMIM-OTf. Fc was dissolved by gentle heating of the ionic liquid. Analogous aqueous electrochemistry was performed on 2.5 mM FcCOOH in 0.2 M sodium phosphate buffer.

Viologen Compounds

The aqueous electrochemistry of paraquat was studied using a 1 mM paraquat/0.3 M KCl solution, made from Milli-Q® water. A three electrode, three compartment cell was employed, in which a Luggin capillary connected the reference and working electrode compartments. The working electrode was a Au(111) bead, with a hanging meniscus, a Pt mesh counter electrode, and the reference electrode was SCE. Before carrying out measurements, the system was bubbled with oxygen free nitrogen for 20 minutes, and kept under nitrogen throughout the duration of the experiment.

The electrochemistry of the viologen compounds in ionic liquid were all performed in the same manner. All compounds were measured as 7.5 mM in BMIM-OTf solutions. On their own, these compounds are sparingly soluble in BMIM-OTf, therefore, to form a solution, they were dissolved in the smallest amount of methanol possible and to this 1 ml of BMIM-OTf was added. As the addition of any solvent to BMIM-OTf can reduce the potential window, the methanol was heated off by the 'sweeping method.'[24] To do this, the solution was heated, in the glovebox, at about 100 °C with nitrogen bubbled directly into the solution, for 1 hour.

Monolayers of 6V6 were formed on the surfaces of a Au(111) bead electrode and investigated in aqueous and ionic liquid electrolytes. To successfully form

monolayers of 6V6 the thioacetate protecting group was removed to reveal the free thiol. To deprotect the 6V6 a 1:1 1 mM solution of 6V6 and KOH in methanol was made and left for 2 hours, after which point a colour change in the solution had occurred. The Au(111) bead was prepared by annealing in a Bunsen flame and immersed in the solution, after cooling, for 1.5 hours. Upon removal the electrode was rinsed with ethanol and Milli-Q® water and dried with nitrogen. Aqueous electrochemistry was performed in 0.1 M $Na_2SO_4$. Ionic liquid electrochemistry was performed in vacuum dried BMIM-OTf.

Laviron Analysis for Ferrocene Terminated Monolayers

The electrochemistry of a series of Fc terminated monolayers on a Au(111) bead electrode was investigated in aqueous 0.1 M $HClO_4$ and BMIM-OTf. The monolayers fall into two categories, covalently bonded Fc, and hydrogen bonded Fc. The covalently bonded Fc monolayers are $FcC_{11}SH$, $FcC_6SH$, and FcCOOH, the hydrogen bonded Fc monolayers are 6-mercaptohexanoic acid, 8-mercaptooctanoic acid, and 11-mercaptoundecanoic acid monolayers with FcCOOH hydrogen bonded to the carboxylic acid end group. The ferrocenyl alkanethiol monolayers were formed by 1 hour adsorption in a mixed adsorption solution of 1 mM: 3 mM ferrocenyl alkanethiol: alkanethiol in ethanol, where the alkanethiol has one less $CH_2$ unit. A 0.25 mM FcCOOH in DCM solution was used to form the FcCOOH monolayer with 45 minutes adsorption. To form the hydrogen bonded series, the carboxylic acid terminated thiol monolayer was first formed from 1 hour adsorption in a 10 mM in methanol solution. The electrode was then rinsed with ethanol and water and transferred to the FcCOOH in DCM solution for 45 minutes. All monolayers were rinsed with ethanol and Milli-Q® water after removal from the adsorption solution

used. All systems were investigated in the ionic liquid BMIM-OTf, only the $FcC_{11}SH$/10-decanethiol monolayer was investigated in the aqueous electrolyte.

## Methods of Analysis

### Randles-Ševčik Analysis

The Randles-Ševčik equation is extensively used in electrochemistry to determine the diffusion coefficient of a dissolved system. The diffusion coefficient is related to the scan rate by:[25-28]

$$|I_p| = 0.4463\left(\frac{F^3}{RT}\right)^{1/2} Ac^* D^{1/2} v^{1/2} \quad (Eq.\ 1)$$

Where $I_p$ is the peak current, $F$ Faraday's constant, $R$ the gas constant, $T$ the absolute temperature, $A$ the area of the electrode, $c^*$ the bulk concentration, $D$ the diffusion coefficient and $v$ the scan rate. This equation shows a linear relation between $I_p$ and $v^{1/2}$. As a result of this relationship, by plotting $I_p$ as a function of $v^{1/2}$ the diffusion coefficient of the system can be found from the slope of this plot. The Randles-Ševčik equation allows for the diffusion coefficient to be easily determined from cyclic voltammetry using a range of scan rates.

### Nicholson Analysis

The Nicholson analysis allows for the determination of the rate constant of electron transfer for a quasi-reversible system. This analysis allows cyclic voltammetry to be used to accurately measure the rate constant of electron transfer, with the assumption that only the soluble oxidised and reduced species are formed as a result of charge transfer.[29] The Nicholson analysis relates $k_0$ to $\Delta E_p$ through the use of a standard working curve.[29-31] The working curve directly links the charge transfer parameter, $\Psi$, to $\Delta E_p$, allowing $\Psi$ to be read from the curve when $\Delta E_p$ is known.[29-32] If

the diffusion coefficients are known, once $\Psi$ is determined the rate constant of electron transfer can be found. $\Psi$ is related to *k* by the following equation:[29, 33]

$$\Psi = \frac{\gamma^{\alpha} k}{(\pi a D_O)^{\frac{1}{2}}} \quad \textit{(Eq. 2)}$$

Where $\gamma = \left(\frac{D_O}{D_R}\right)$, $\alpha$ is the transfer coefficient, $a = nFv/RT$, and $D_O$ and $D_R$ are the diffusion coefficients of the oxidised and reduced species. For this analysis to be successful $\Delta E_p$ values linked to intermediate values of $\Psi$ should be used.[29] Also $\alpha$ must be between 0.3 and 0.7, as in this range peak separation is only dependent on $\Psi$.[32] In most cases, however, the effect of $\alpha$ is small and therefore is assumed to be 0.5.[33] Finally, the success of this analysis is dependent on there being minimal *iR* drop.[29, 32] If these assumptions hold true then the Nicholson analysis is a powerful technique for the determination of the rate constant of electron transfer from cyclic voltammetry.

Laviron Analysis

Utilizing the Laviron analysis, the rate constant of electron transfer between an adsorbed redox species and the substrate can be easily determined using cyclic voltammetry.[34] The Laviron analysis works by relating the peak separation of a system over a range of scan rates. The aim of the range of scan rates is to probe both the fully reversible and fully irreversible domains. In the fully reversible domain there is little change in peak separation as scan rate increases, whereas in the fully irreversible domain small changes in scan rate result in large changes in peak separation.[35] By plotting peak separation of the system as a function of $v^{1/2}$ the two domains become readily apparent in the form of a trumpet plot. To determine *k* a straight line is fitted to both domains in the trumpet plot, and the scan rate at which these intercept is noted. Using the intercept scan rate, *k* can be found from the following relationship:[35]

$$\left(\frac{\alpha nFv}{RTk_s}\right) = 1 \quad \textit{(Eq. 3)}$$

It should be noted though, that a number of assumptions are made when using this treatment. The assumptions made include: 1) The oxidized and reduced species are strongly adsorbed with minimal desorption.[34, 36] 2) Only the adsorbed species are involved in the measured electrochemistry.[34, 36] 3) All adsorption sites are equal, with the oxidized and reduced species having the same surface area occupancy.[36] 4) All adsorbed redox active species take part in the electron transfer reaction.[36] 5) The adsorbed redox centres do not interact with one another.[36, 37] By making these assumptions the Laviron analysis allows a straightforward determination of the rate constant of electron transfer between the electrode and an adsorbed species.

# Results and Discussion

## Ferrocene Solution Electrochemistry

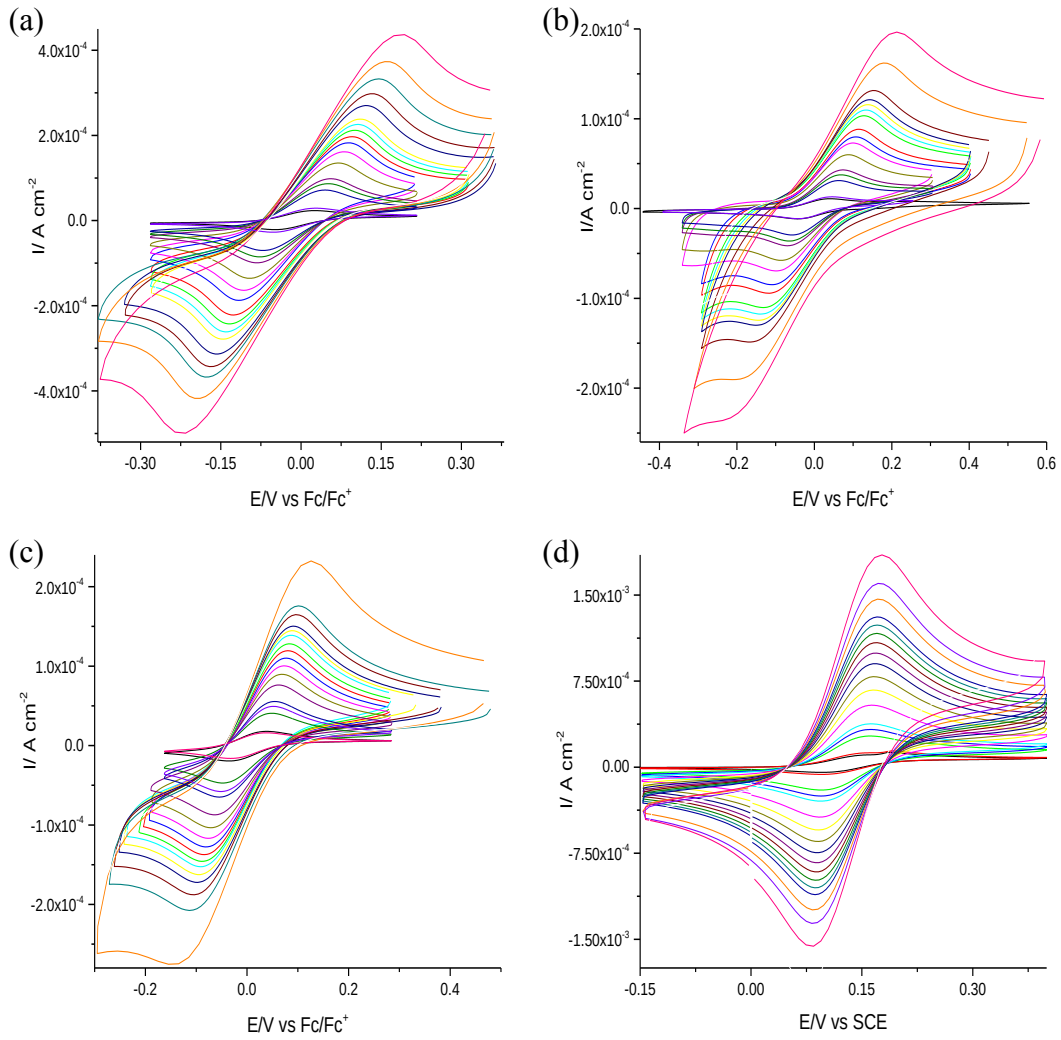


*Figure 1: The electrochemistry of Fc in (a) BMIM-OTf, (b) BMIM-$PF_6$, and (c) BMIM-TFSA. (d) The electrochemistry of FcCOOH in 0.2 M sodium phosphate buffer. All ionic liquid electrochemistry is performed at a Au(111) Arrandee$^{TM}$ slide WE, against Pt wire CE and QRE. The result was referenced to $Fc/Fc^+$. Aqueous electrochemistry was performed at a Au(111) bead electrode, with a Pt CE, and SCE RE. Scan rates ranged from 0.005 to 3.0 V $s^{-1}$ for all systems.*

*Table 1: Diffusion coefficients and rate constants of electron transfer for Fc systems.*

| System | $D_a$ / $cm^2$ $s^{-1}$ | $D_c$ / $cm^2$ $s^{-1}$ | $k$ / cm $s^{-1}$ |
|---|---|---|---|
| 5 mM Fc in BMIM-OTf | $2.27 \times 10^{-8}$ | $3.63 \times 10^{-8}$ | $1.95 \times 10^{-4}$ |
| 2.5 mM Fc in BMIM-TFSA | $3.06 \times 10^{-8}$ | $4.97 \times 10^{-8}$ | $4.38 \times 10^{-4}$ |
| 2.5 mM Fc in BMIM-$PF_6$ | $8.82 \times 10^{-9}$ | $1.50 \times 10^{-8}$ | $1.20 \times 10^{-4}$ |
| 2.5 mM FcCOOH in 0.2 M Sodium Phosphate Buffer | $3.40 \times 10^{-6}$ | $3.52 \times 10^{-6}$ | $2.26 \times 10^{-2}$ |

To gain a better understanding of electrochemistry in ionic liquids, ferrocene was investigated in BMIM-OTf, BMIM-TFSA, and BMIM-$PF_6$. For comparison aqueous investigations were performed on ferrocene carboxylic acid, because ferrocene is not soluble in aqueous electrolytes. Based on the literature, the solubility of ferrocene in ionic liquids is questionable,[38] however, with just some gentle heating relatively high concentration ferrocene solutions could be made. The electrochemistry of all four solutions against Au(111) is shown in **Figure 1**. These voltammograms show a degree of sloping, dependent on the ionic liquid. This sloping likely arises from residual water content. As different ionic liquids have different hydrophobicities it is unsurprising that the sloping changes with ionic liquid. The large range of scan rates used allowed determination of the diffusion coefficient and rate constant of electron transfer using the Randles-Ševčik equation and Nicholson analysis, respectively. **Table 1** shows the diffusion coefficients and rate constants for the three ionic liquid systems and those for the aqueous system. The diffusion coefficients seen in this investigation are in line with values previously measured for ferrocene in a variety of ionic liquids.[39-41] Low rate constants of electron transfer for ferrocene in ionic liquids, have been seen in the literature.[42, 43] The diffusion coefficients for the ionic liquids are

also less than for the aqueous system. When the diffusion coefficients and rate constants of the three ionic liquid systems are compared it is seen that both values decrease in the order:

$$\text{BMIM-TFSA} > \text{BMIM-OTf} > \text{BMIM-PF}_6$$

It is known that diffusion in an ionic liquid is associated with its viscosity based on a modified Stokes-Einstein equation. This assumes the redox species in an ionic liquid behaves as a perfectly sliding sphere, rather than a species with perfect sticking to the surface.[40] The modified Stokes-Einstein equation related to ionic liquids is:

$$D = \frac{kT}{4\pi\eta a} \qquad \textit{(Eq. 4)}$$

Where $k$ is the Boltzmann constant, $T$ the absolute temperature, $\eta$ the dynamic viscosity of the ionic liquid and $a$ the "hydrodynamic radius" of the redox species in the ionic liquid. This equation predicts the diffusion coefficient is inversely related to the viscosity of the ionic liquids. This is the trend seen, with viscosity decreasing in the order:[44]

$$\text{BMIM-PF}_6 > \text{BMIM-OTf} > \text{BMIM-TFSA}$$

The rate constant of electron transfer changes as a result of the change in anion of the species. Changing the anion alters the interaction of the ionic liquid with the Au electrode,[45] which can lead to changes in the double layer structure. By changing the double layer, the distance of closest approach and effective concentration profile of the electroactive species in the interfacial region changes, in turn altering the rate of electron transfer.[46] With an understanding of the electrochemistry of ferrocene in ionic liquids more complex systems can then be investigated.

## Viologens

Viologen molecules undergo a two electron transfer process, **Figure 2**, with only the first electron transfer visible in aqueous solutions. While the second electron transfer can be elucidated in organic electrolytes, these are often poor environments for use in the STM because of their high vapour pressure and volatility. Ionic liquids provide a unique opportunity for the investigation of redox active molecules, particularly as their negligible vapour pressure allows for their use in the STM. Due to their lack of hydrogen evolution, ionic liquids allow for both electron transfer processes to be seen under circumstances where $H_2$ would be evolved in aqueous systems.

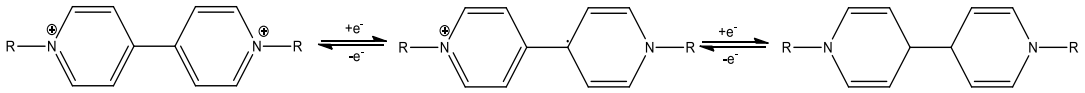


*Figure 2: Paraquat undergoes 2 electron transfers as shown.*

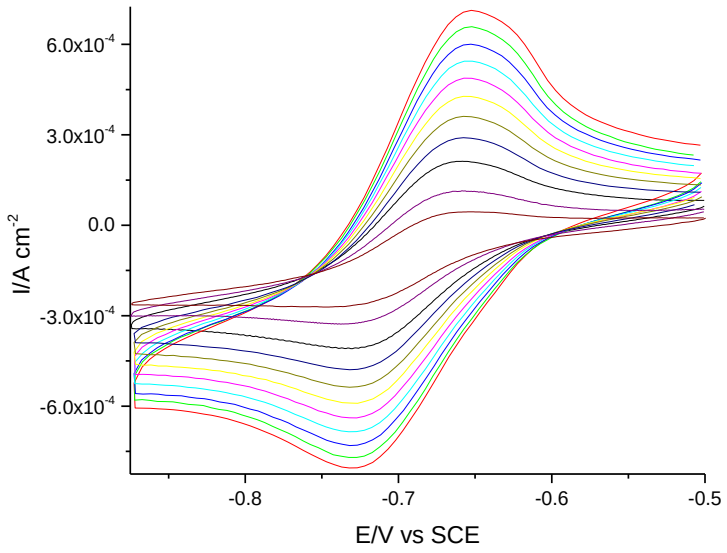


*Figure 3: Aqueous electrochemistry of paraquat was performed at a Au(111) bead electrode using a 1 mM paraquat in 0.3 M KCl solution. A Pt CE and SCE RE were used. From the brown to the red cycle the scan rate increases from 0.1 to 1 V $s^{-1}$.*

Paraquat (dimethylviologen) is the simplest of viologen compounds available. As with other viologens, it undergoes a 2 electron transfer process to go from the $V^{2+}$ to $V^0$ species. For better understanding, paraquat was first investigated in aqueous electrolyte before investigation in the ionic liquid BMIM-OTf. The electrochemistry of paraquat in aqueous electrolyte is shown in **Figure 3**. Only the first redox wave, at -(0.700 ± 0.004) V vs SCE, is seen in this potential range. The $V^{2+} \rightarrow V^{+\cdot}$ electron transfer is an electrochemically reversible process. This is evidenced by the independence of $E_p$ with the scan rate, and the dependence of the peak current on the square root of the scan rate. There is some quasi-reversibility and/or non-ideality in the system, however, as the peak separation is slightly larger than the expected 59/*n* mV, and $I_p^A \neq I_p^C$.[47] By plotting the change in peak potential as a function of the square root of the scan rate, the diffusion coefficients are determined to be 4.13 x $10^{-6}$ and 8.38 x$10^{-6}$ $cm^2$ $s^{-1}$. The rate constant of electron transfer was determined using the Nicholson analysis, with $\Psi$ values between 0.23 and 2.5 used. The rate constant of electron transfer was measured as 4.27 x $10^{-2}$ $s^{-1}$. With an understanding of the electrochemistry of paraquat in aqueous electrolytes, its electrochemistry in BMIM-OTf could be carried out, shown in **Figure 4**. With the larger electrochemical window in BMIM-OTf, both electron transfer curves are apparent. The measured redox potentials are –(0.63 ± 0.07) and –(1.04 ± 0.06) V vs $Fc/Fc^+$ for the $V^{2+} \rightarrow V^{+\cdot}$ and $V^{+\cdot} \rightarrow V^0$ electron transfers, respectively. Using the Randles-Ševčik equation, the diffusion coefficients are seen to be 1.59 x $10^{-9}$, 5.02 x $10^{-9}$, 1.90 x $10^{-9}$, and 3.41 x $10^{-9}$ $cm^2$ $s^{-1}$ for the first anodic and cathodic electron transfers, and second anodic and cathodic electron transfers. The two orders of magnitude difference between these and the aqueous measurements are similar to the change seen on moving to ionic liquids for ferrocene. These values are an order of magnitude less than the diffusion

coefficients seen for ferrocene. This is expected based on the modified Stokes-Einstein equation, as the diffusion coefficient is inversely proportional to the effective radius of the molecule which is expected to be larger for the paraquat species. The rate constants for electron transfer were measured as 1.23 x $10^{-6}$ and 8.20 x $10^{-7}$ cm $s^{-1}$.

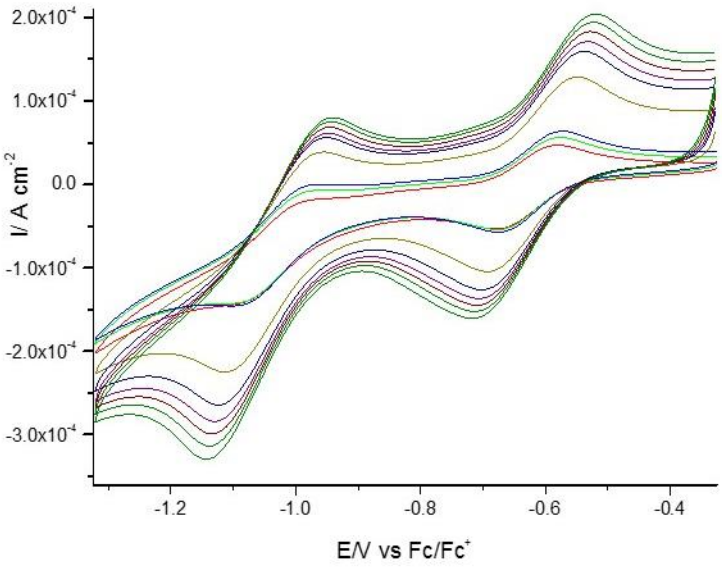


*Figure 4: Cyclic voltammetry of 7.5 mM Paraquat in BMIM-OTf vs Au(111) WE. A Pt CE and QRE were used, with an $Fc/Fc^+$ internal reference. The scan rate increased from 0.05 to 0.9 V $s^{-1}$ going from the red to the black scan. When the ionic liquid is well dried both redox waves can be seen, whereas in aqueous electrolytes only the first reduction is apparent.*

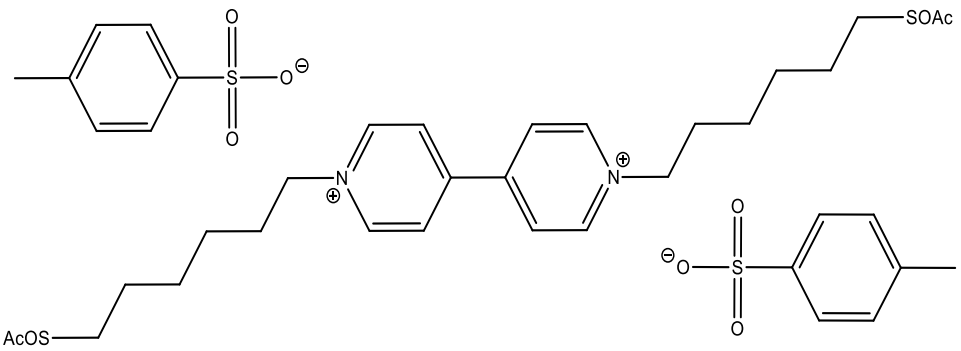


*Figure 5: 6V6, as synthesized by Dr. Carly Brooke is shown. The tosylate anions counter the charge of the viologen core.*

6V6, **Figure 5**, is interesting for molecular electronics studies. The electrochemistry of viologen moieties attached to Au by alkyl thiol linkers has been well studied in aqueous electrolytes.[8, 9, 12, 48-50] These systems show reversible electron transfer for the first redox process, with the second process measureable under some conditions, although because of solubility and the stability of the $V^0$ state, this is less reversible.[49, 51] Because of the thiol end group of 6V6 it can easily bond to Au surfaces and therefore, the electrochemistry of the surface bound molecule is easily studied. Before investigating 6V6 in an ionic liquid it was investigated in an aqueous environment, allowing for a benchmark of the electrochemistry in ionic liquids. 6V6 was provided by Dr. Carly Brooke, as the tosylate salt, with a thioacetate protecting group. Deprotection of the thioacetate group in a 1:1 mixture with KOH was necessary for molecular adsorption. After deprotecting the 6V6 molecule it was adsorbed on the Au(111) surface, and electrochemistry performed in 0.1 M $Na_2SO_4$. As has been discussed, in the aqueous electrolyte, 6V6 only shows one electron transfer wave, at –(0.53 ± 0.01) V vs. SCE, **Figure 6**. By looking at the charge associated with this electron transfer wave the coverage of the 6V6 molecule on Au can be found to be (1.22 ± 0.05) mol $cm^{-2}$. This coverage is about three times less than that seen for a high coverage monolayer in the literature, although this difference is likely due to the much shorter adsorption time.[8, 12, 48, 52]

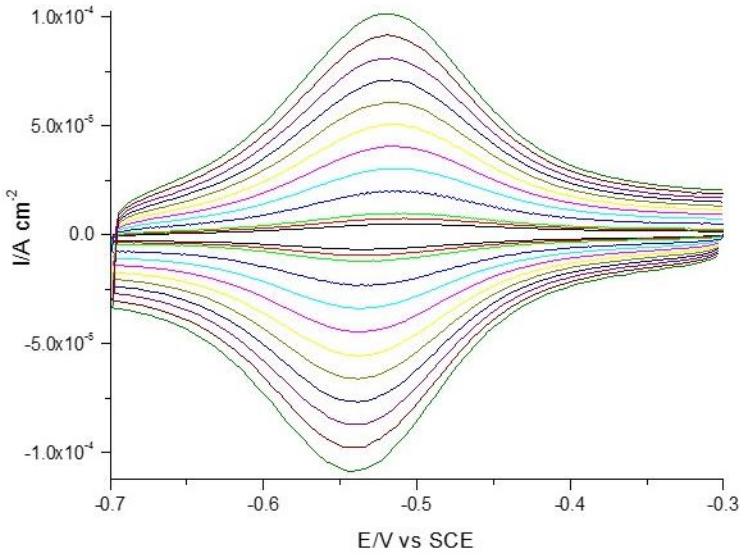


*Figure 6: A 6V6 monolayer was formed on Au(111) bead through deprotection of the thioacetate group and 1.5 hours adsorption, then investigated in 0.1 M $Na_2SO_4$. The CE was a Pt mesh, and the RE was SCE. The scan rates are 0.05 to 1 V $s^{-1}$.*

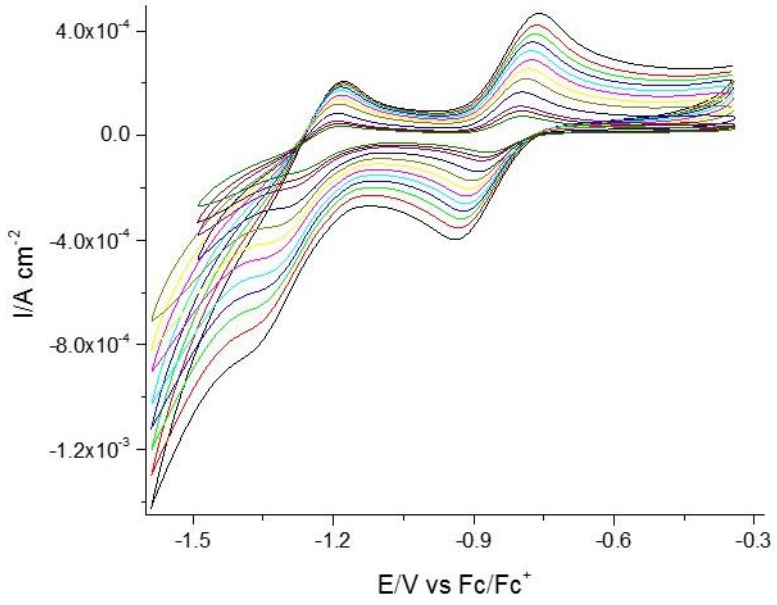


*Figure 7: Solution electrochemistry was performed on 7.5 mM 6V6 in BMIM-OTf at a Au (111) WE. The CE and QRE used were both Pt wire electrodes. The system was referenced against a $Fc/Fc^+$ internal reference. From the inner green curve to the outer black curve the scan rate increases from 0.05 to 1.0 V $s^{-1}$.*

As BMIM-OTf is a novel environment for 6V6, it was investigated both in solution and adsorbed on the Au surface. When investigated in a BMIM-OTf solution, 6V6 gives rise to the electrochemistry shown in **Figure 7**. This electrochemistry shows a sloped baseline, particularly apparent at the second redox wave. With the viologens if the ionic liquid is not dry enough the second redox wave cannot be measured, therefore while this slope may be due to a minute amount of residual water, it is unlikely the underlying cause. The use of the highly conductive ionic liquids, with the close placement of the reference to working electrode, and the small area of the working electrode makes iR drop unlikely. Furthermore iR drop is expected to be exacerbated in fast scan CV, causing erroneous peak potentials. As will be seen later, this does not occur, at least not in BMIM-OTf, ruling out iR drop as the cause of the slope. The sloping of the CV occurs in a similar location to the potential limit of the ionic liquid measured, therefore this downward curve is likely a natural reflection of the potential limit of BMIM-OTf. This electrochemistry shows redox waves at –(0.65 ± 0.01) and –(1.25 ± 0.01) V vs. $Fc/Fc^+$, with growing peak separations indicative of a quasi-reversible electron transfer. The peak potentials measured for 6V6 in solution are negative of those seen for the paraquat molecule in BMIM-OTf. This change in peak potential arises because of the change in the 1,1'-substituents from –Me to $–(CH_2)_6SH$, which makes the system harder to reduce.[51] By accurately measuring the current of the redox peak, the Randles-Ševčik equation can be used to determine the diffusion coefficient. The diffusion coefficient for 7.5 mM 6V6 in BMIM-OTf was found to be 2.70 x $10^{-8}$, 3.89x $10^{-8}$ $cm^2$ $s^{-1}$ for the anodic and cathodic first electron transfer, and 1.08 x $10^{-8}$ and 8.59 x $10^{-9}$ $cm^2$ $s^{-1}$ for the anodic and cathodic second electron transfer, respectively. As a quasi-reversible electrochemical reaction, the rate constant of electron transfer was found, using the Nicholson analysis, to be 2.20 x

$10^{-6}$ and 7.10 x $10^{-7}$ cm $s^{-1}$ for the first and second electron transfers, respectively. Based on the modified Stokes-Einstein equation, one would predict the larger 6V6 molecule would have a lower diffusion coefficient than the comparatively small paraquat molecule. The increased diffusion coefficient, and the resulting improvement in the rate of electron transfer, seen for 6V6, however, is likely due to the ability of ionic liquids to solvate different molecules. It is expected that the long alkyl chain 1,1'-substituents of the 6V6 give rise to a more soluble molecule than paraquat. This is in line with investigations carried out on gaseous alkane chains which saw solubility increasing with molecular chain length.[53] It should also be noted that the decreased solubility of paraquat compared to 6V6 may give rise to a difference in the predicted and actual concentration of the systems, thereby reducing the accuracy of the determined diffusion coefficient and rate constant of electron transfer of these systems.

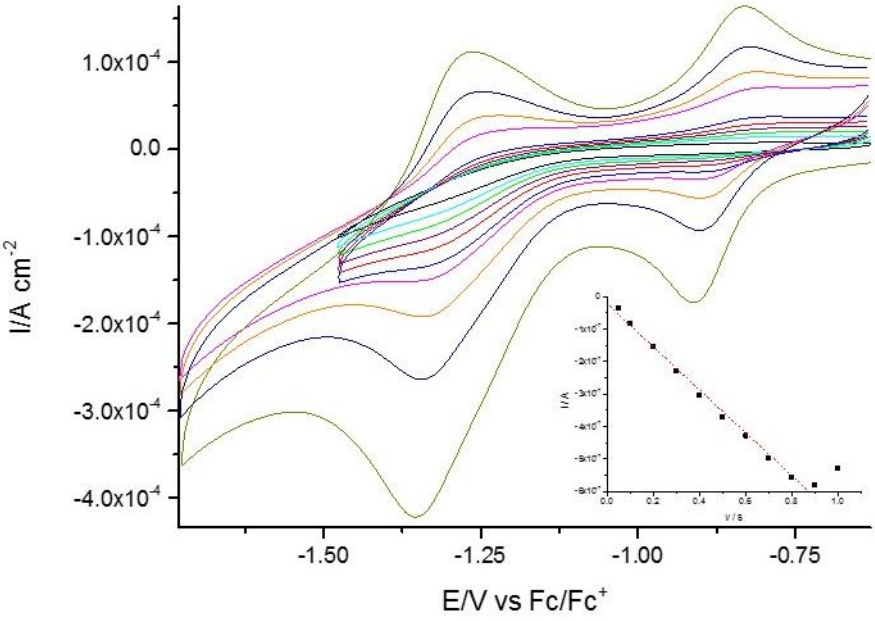


*Figure 8: A 6V6 monolayer on Au(111) investigated in BMIM-OTf. A Pt wire QRE and CE were used, and the system was referenced to Fc/Fc$^+$. The scan rate increases from 0.05 to 1 V $s^{-1}$ from the inner black to outer olive curves. The larger potential window of the ionic liquid allows both reductions to be witnessed. The linear* i-v *dependence is shown in the inset. The outlier at 1 V $s^{-1}$ was not used in the linear fit.*

Monolayers of 6V6 were prepared on Au(111) using the deprotection technique established for the investigation of this monolayer in aqueous electrolyte. From **Figure 8** the differences in electrochemistry of adsorbed 6V6 in aqueous electrolyte and in BMIM-OTf become obvious. First and foremost, unlike in aqueous electrolyte, both electron transfers are apparent, at –(0.85 ± 0.03) and –(1.28 ± 0.04) V vs. $Fc/Fc^+$. The peak separation is seen to change with scan rate, indicating the system is quasi-reversible, due to the decreased rate of electron transfer in ionic liquids. Though not ideal electrochemistry for an adsorbed species, the direct dependence of $I_P$ on $v$, is indicative of this being adsorbed and not solution electrochemistry. The difference in electrochemistry of the 6V6 in $Na_2SO_4$ and BMIM-OTf is likely due to the different interaction of the viologen with the different electrolytes. Even in aqueous electrolytes the viologen moiety has been seen to interact differently with different anions, with some anions even intercalating into the monolayer.[50] As in the aqueous investigations, the coverage of the 6V6 on the Au(111) was determined through integration of the peaks in the cyclic voltammogram. When the surface coverage of the monolayer is determined from the first electron transfer, a coverage of (2.2 ± 0.2) x $10^{-10}$ mol $cm^{-2}$ was seen. The robust electrochemistry seen for viologen containing molecules in ionic liquids is evidence of their potential in molecular electronics studies. By utilizing the ionic liquid environment it could be possible to investigate both electron transfers associated with viologens which may be promising for future studies of molecular switching.

Fc bound to Au

Ferrocene is a simple redox active molecule with stable electrochemistry, which has been actively investigated as a terminal redox probe on alkanethiol monolayers.[54-62] By looking at the electrochemistry of the ferrocene bound to Au, the

effects of altering the alkanethiol link to the Au surface, for example by changing the alkyl chain length, and bonding mechanism, can be ascertained. Insight into the effect of the electrolyte on the system, can also be gained. The ionic liquid BMIM-OTf provides a unique opportunity for the study of the effect of hydrogen bonding ferrocene to the alkanethiol through COOH end groups on both the SAM and the ferrocene derivative. Such measurements are difficult to perform in aqueous, or even organic electrolytes, due to the weak bonding between the end groups, which allows only a single scan rate to be investigated at a time.[63] For a better understanding of the effect of these hydrogen bonds, the ferrocene alkanethiol system in which ferrocene is covalently bonded to the thiol backbone, has also been studied. Unlike the hydrogen bonded systems these molecules can be studied in aqueous electrolytes, thereby providing a good starting point for these experiments. By looking at both the covalently bonded and hydrogen bonded systems, the effect of going from a system where the interactions are through bond rather than through space, can be ascertained.[60]

Covalently Bonded Ferrocene Systems

The covalently bonded ferrocene systems investigated were 11-ferrocenyl undecanethiol, and 6-ferrocenyl hexanethiol, which have the structures depicted in **Figure 9**. The literature shows that when a full monolayer of the ferrocenyl alkanethiol is used, the results are poor because the bulky ferrocene end group hinders the formation of an ordered monolayer, and the lateral interactions between the ferrocene moieties cause peak broadening.[54, 61] This broadening is exacerbated in the anodic peak because of the unfavourable interactions of the positively charged ferrocene end groups.[58] To improve the electrochemistry of the covalently bonded ferrocene systems, the ferrocenyl alkanethiol molecules should be diluted by a shorter

alkanethiol molecule. In order to perform measurements on these covalent systems a dilute monolayer of 25 % $FcC_6SH$ in pentanethiol, and 25 % $FcC_{11}SH$ in decanethiol, were utilized.[61] Whilst both systems were measured in the ionic liquid BMIM-OTf only the $FcC_{11}SH$ system was investigated in the aqueous electrolyte.

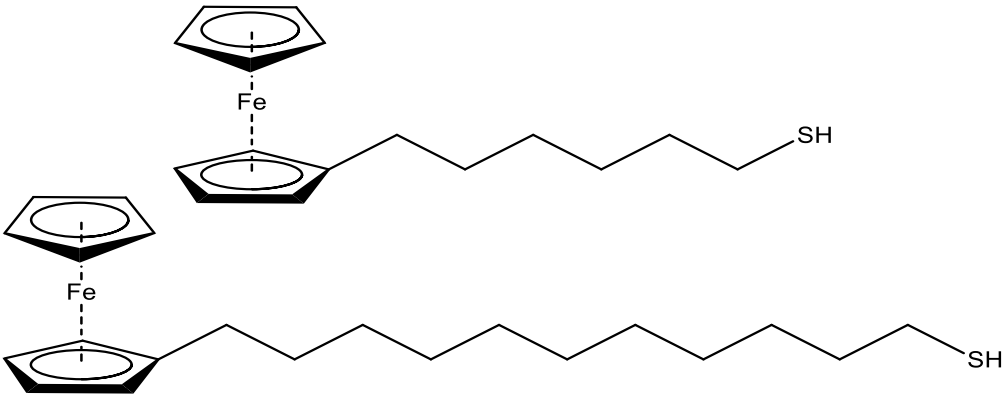


*Figure 9: Monolayers of $FcC_{11}SH$ and $FcC_6SH$ on Au(111) have been investigated. The structure of these molecules are shown.*

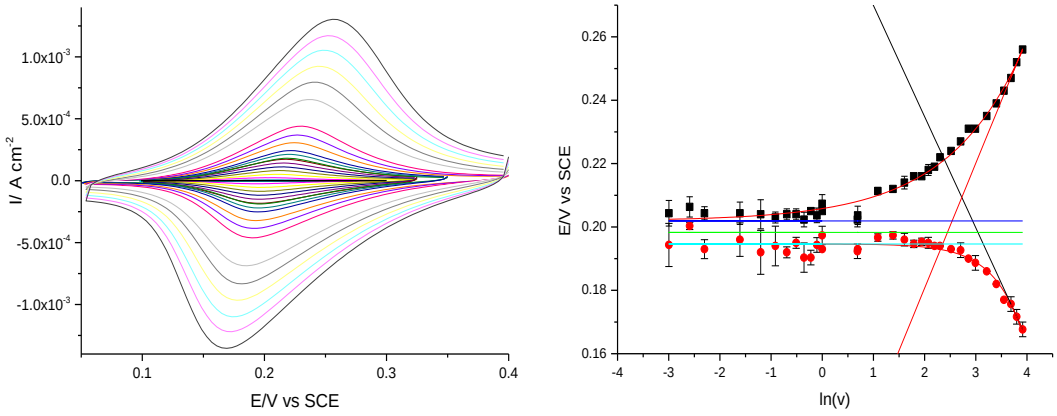


*Figure 10: The electrochemistry of a mixed 1:3 $FcC_{11}SH$:decanethiol monolayer on Au(111) in 0.1 M $HClO_4$ aqueous electrolyte was investigated. Measurements were performed using a Pt mesh CE, and a SCE RE. The scan rate increases to the outer black curve from 0.05 to 50.0 V $s^{-1}$. The peak potential was plotted as a function of ln(v) to determine* k.

A 1:3 $FcC_{11}SH$: decanethiol monolayer on Au(111) was investigated in an aqueous 0.1 M $HClO_4$ electrolyte. This electrolyte was chosen because it has been shown in the literature that the anion of the electrolyte can interact with the ferrocene end moiety through ion pairing, altering the stability of the system. The $ClO_4^-$ anion is known to interact less than others, particularly at low pH values.[62] The electrochemistry of this system was investigated from a scan rate of 0.05 to 50 V $s^{-1}$, **Figure 10a**. When the redox chemistry of the $FcC_{11}SH$ molecule bound to Au was investigated, it was seen to undergo electron transfer at (0.20 ± 0.02) V vs. SCE. Using the slowest scan rates, 0.05 to 2 V $s^{-1}$, the surface coverage of the $FcC_{11}SH$ molecules, was found. In the mixed monolayer, a coverage of (1.9 ± 0.6) x $10^{-12}$ mol $cm^{-2}$ of $FcC_{11}SH$ was determined. By investigating the charge transfer between the Au surface and the ferrocene end group at fast scan rates, the system is forced into irreversibility. Recording CVs for this system in both the reversible and irreversible charge transfer regime allows determination of the rate of charge transfer from the Au surface to the ferrocene using the Laviron analysis. In this analysis, the peak potential of the charge transfer is plotted as a function of the natural log of the scan rate, resulting in a trumpet plot, like that shown in **Figure 10b**. By determining the intercept of the linear portion of the trumpet, i.e. at the fastest scan rates, with the baselines of the trumpet, the rate of charge transfer can be found. This is a somewhat flawed technique when the system does not behave ideally, but it allows determination of the general trends in *k*. The baseline of the trumpet could be taken as either the individual baselines of each branch, or an average of these baselines, unfortunately, because the branches are not mirror images, the extrapolated lines will not meet at the same point. Using the intercept the rate constants can be determined. The average rate constant for the average baseline is 316 $s^{-1}$, and for the individual baselines is 349 $s^{-1}$. Though not strikingly different, the

differences in the values from the two baselines dictate that a somewhat arbitrary choice must be made about the baseline used for analysis. It was decided that, moving forward, the average baseline would be used. The rate constant of 316 $s^{-1}$ is the same order of magnitude as measurements presented in the literature.[56, 60, 62] By measuring the electrochemistry of the 1:3 $FcC_{11}SH$:decanethiol system in a well-known aqueous electrolyte, the ability of the technique and analysis was proven, and a reference system for comparison with the following BMIM-OTf data has been established.

As the preparation and analysis method has proven itself in aqueous electrolytes it could be extended to use in BMIM-OTf. Both the $FcC_{11}SH$ and $FcC_6SH$ systems were investigated by cyclic voltammetry, the results of which can be seen in **Figure 11**. From the cyclic voltammetry, the coverage of the systems was found to be $(1.0 \pm 0.5) \times 10^{-11}$ mol $cm^{-2}$ and $(1.4 \pm 1.2) \times 10^{-12}$ mol $cm^{-2}$ for the $FcC_{11}SH$ and $FcC_6SH$, respectively The apparently larger coverage of $FcC_{11}SH$ in the ionic liquid, compared to the aqueous electrolyte may arise because of a reduced risk of nucleophilic attack presented by the poorly nucleophilic ionic liquids on the terminal Fc.[64] The coverage of $FcC_{11}SH$ is larger than that of the $FcC_6SH$ system because it is composed of longer alkyl chains. The longer the alkyl chain, the stronger the van der Waals interactions of the monolayer, causing a monolayer of higher ordering and surface coverage.[65] It also seems likely that the increased ordering leads to a lower recorded error in the monolayer coverage for $FcC_{11}SH$, because the more disordered $FcC_6SH$ monolayer will be more susceptible to incoming nucleophiles which can remove the Fc end group.[59, 66] The charge transfer processes occur at $-(0.10 \pm 0.04)$ V and $-(0.03 \pm 0.06)$ V vs. $Fc/Fc^+$ for the $FcC_6SH$ and $FcC_{11}SH$ systems, respectively. When the Laviron analysis of these monolayers is performed, the rate constant for charge transfer are 263 and 166 $s^{-1}$ for the $FcC_6SH$ and $FcC_{11}SH$, respectively. On

moving to the shorter alkanethiol chain, the electrochemistry obviously changes, with increasing chain length showing an increase in peak separation, a direct result of the reduction in the rate constant of charge transfer. It should be noted that while this is an intuitive result, it is descriptive of the BMIM-OTf environment, as it means that, as is the case with an aqueous electrolyte, the ionic liquid does not disorder the alkanethiol system to the point that the polymethylene chain no longer keeps the ferrocene a constant distance from the electrode.[54] Directly comparing the electrochemistry of the surface bound $FcC_{11}SH$ in the $HClO_4$ and the BMIM-OTf, it can be seen that the peak separation is obviously larger in the ionic liquid system transfer. The rate constant ($k$) for $FcC_{11}SH$ measured in the ionic liquid is half that in aqueous electrolyte. This is likely due to an increased reorganization energy of the ionic liquid system.[54] Although these are the only two ferrocenealkanethiol systems measured in the ionic liquid, a $\beta$-value can be found to allow for comparison with the hydrogen bonded system. $\beta$ is found from the equation $k=\exp(-\beta d)$ where $d$ is the distance from the surface to the redox centre.[66] Using the $k$ values determined for these systems, a $\beta$ value of 0.7 $nm^{-1}$ is found.

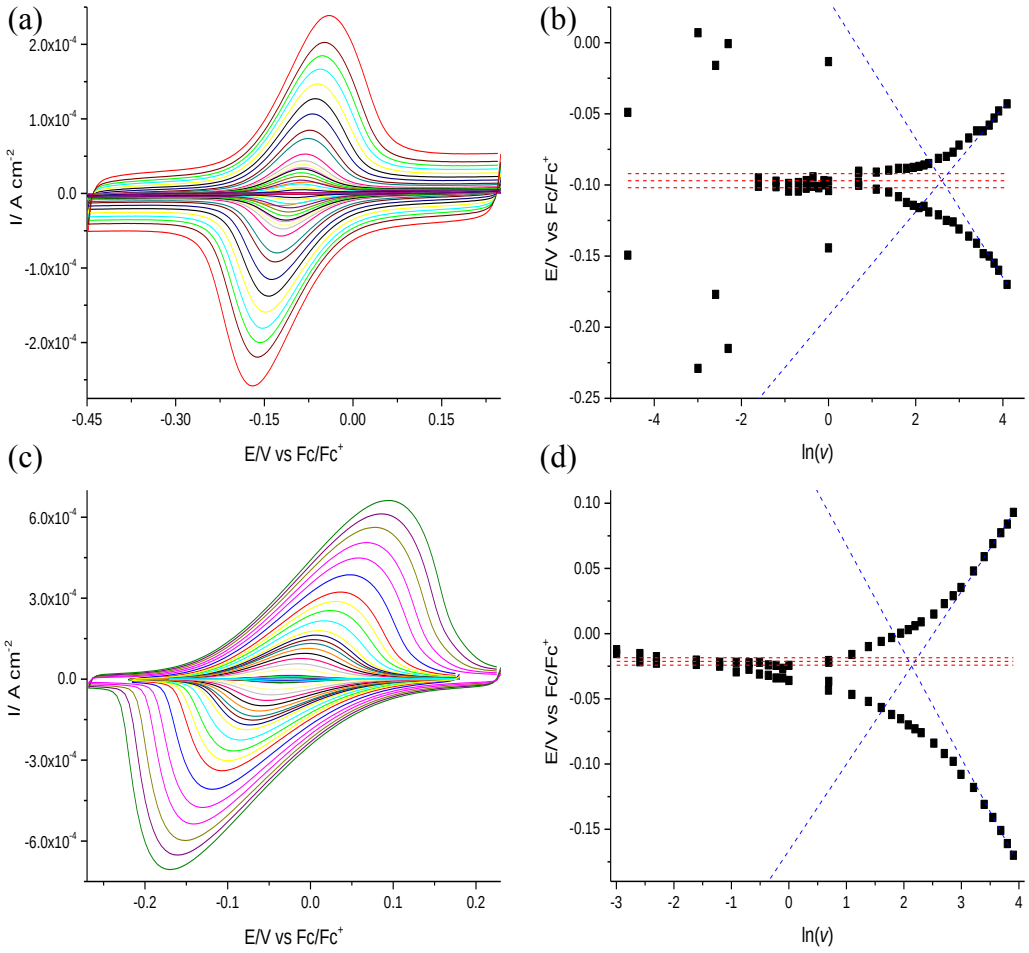


*Figure 11: (a) The electrochemistry of a mixed 1:3 $FcC_6SH$: pentanethiol monolayer on Au(111) in BMIM-OTf was investigated. (b) The peak potential was plotted as a function of* ln(v) *to determine* k. *(c) The electrochemistry of a mixed 1:3 FcC11SH:decanethiol monolayer on Au(111) in BMIM-OTf was investigated. (d) To determine k the peak potential was plotted as a function of ln(v). All experiments were performed with a Au(111) bead WE, and Pt wire QRE and CE. Systems were referenced to $Fc/Fc^+$. Scan rates ranged from 0.05 to 50.0 V $s^{-1}$, from the inner to the outer curves for both experiments.*

Hydrogen Bonded Ferrocene Systems

*Table 2: Peak potentials and coverages of FcCOOH hydrogen bonded to –COOH terminated monolayers.*

| System | Coverage / mol $cm^{-2}$ | Peak Potential / V vs $Fc/Fc^{+}$ |
|---|---|---|
| FcCOOH-6-MHA | $(8.8 \pm 1.8) \times 10^{-11}$ | 0.13 |
| FcCOOH-8-MOA | $(1.3 \pm 0.3) \times 10^{-11}$ | 0.13 |
| FcCOOH-11-MUA | $(3.8 \pm 2.2) \times 10^{-11}$ | 0.10 |

Moving on to a more complex system, a series of monolayers with ferrocene hydrogen bonded to the surface were investigated. While the ferrocene species in this investigation was always ferrocene carboxylic acid, the system was altered by changing the length of the mercaptoalkanoic acid monolayer. The monolayers investigated were 6-mercaptohexanoic acid, 8-mercaptoocatnoic acid, and 11-mercaptoundecanoic acid, the resulting electrochemistry of these three systems, is shown in **Figure 12**. The redox potentials of these systems, and the coverage of the ferrocene, is shown in **Table 2**. Unlike for the system with covalent attachment of ferrocene to the polymethylene chain, when the redox target is hydrogen bonded through carboxylic acid groups complex electrochemistry is seen. For all three systems the electrochemistry at the slowest scan rate exhibit a single peak, but as the scan rate is increased the peak broadens, eventually resolving itself into two. The break-away peak in all three systems quickly reaches a point where its peak separation is larger than the potential range of the voltammogram. Shoulders have been seen in the literature, with these attributed to a difference in packing density in the monolayer, due to liquid-like and crystalline-like regions.[66] The presence of liquid-like regions gives rise to slower charge transfer,[66] like that of the 'break- away' peak. As this

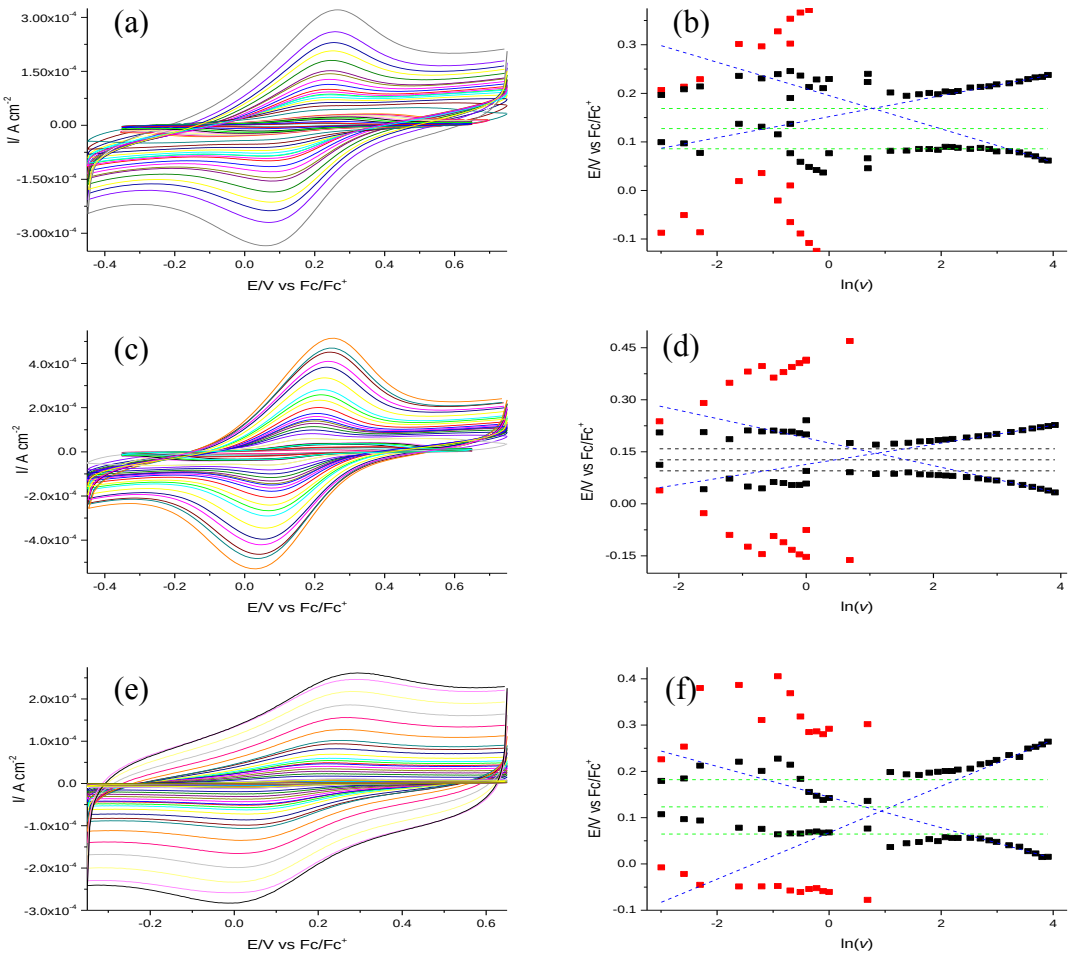


*Figure 12: (a) The electrochemistry of a mixed FcCOOH-mercaptohexanoic monolayer was investigated on Au(111) in BMIM-OTf. (b) Plotting peak potential as a function of* ln(v) *allows determination of* k. *(c) The electrochemistry of FcCOOH-mercaptooctanoic monolayer on Au(111) in BMIM-OTf was investigated. (d) To determine* k *the peak potential was plotted as a function of ln(v). (e) A FcCOOH-mercaptoundecanoic acid monolayer was investigated on Au(111) in BMIM-OTf. (f)* k *was determined by a plot of peak potential as a function of* ln(v). *All experiments were performed using a Au(111) bead working electrode, and Pt wire QRE and CE. Systems were referenced to* $Fc/Fc^+$. *From the inner to the outer curve of all systems the scan rate increased from 0.05 to 50 V* $s^{-1}$.

'break-away' peak is not witnessed for the covalently bonded system, this may be a direct result of the hydrogen bonding. As the structure of the hydrogen bonded interface is unknown, it is possible that there are regions of singly and doubly hydrogen-bonded ferrocene. Singly hydrogen bonded ferrocene could give rise to the 'break-away' peak, while doubly hydrogen-bonded ferrocene gives rise to the main peak as a result of the increased conductance in the doubly hydrogen bonded systems.[67] These peaks can be individually analysed using the Laviron analysis, though this is not as straightforward as for the better-behaved ferrocenyl alkanethiols. To fully resolve the characteristics of the two redox waves, Gaussian fittings were used for both peaks, underpinning the idea that two separate electron transfers were occurring. Using the positions determined by the Gaussian fittings, these electron transfers were investigated by application of the Laviron analysis, giving rise to two separate trumpet plots, like that seen in **Figure 12**. In order for the Laviron analysis to be applied to a system, it should have an exponential relationship between the natural log of the scan rate and the peak position, whereas for the 'break-away peak' of all three systems, the relationship is closer to linear, as such, the Laviron analysis will only be applied to the second peak. Due to the non-ideality of both peak positions during the presence of both electron transfers, the baseline of the trumpet plot was extrapolated by fitting an exponential curve to the regions where only the main peak is apparent in the trumpet plot, thereby allowing *k* to be determined. When the Laviron analysis is applied in this manner, the *k* values determined for these systems are 74, 63, and 48 $s^{-1}$ for the 6-MHA, 8-MOA, and 11-MUA systems, respectively, an order of magnitude lower than those seen for the covalently bonded systems. This reduction of rate constant of electron transfer on going to a through space system is consistent with literature investigations on singly hydrogen bonded ferrocene-alkanethiol

systems,[57] and Langmuir-Blodgett film ferrocene on alkanethiols.[60] When taken as a series, and the change in length of the mercaptanoic acid molecules is accounted for, these systems give rise to a $\beta$-value of 6.7 $nm^{-1}$, similar to what has been seen in the literature for single molecule conductance measurements between two carboxylic acid terminated alkanes which interact through hydrogen bonding.[68] The larger $\beta$-value of the hydrogen bonded systems, compared to the covalently bonded systems, arises because of the H-bonds which force tunnelling to occur between molecules.

For completeness, the electrochemistry of the surface bound ferrocene carboxylic acid molecule was investigated in BMIM-OTf. Unlike when FcCOOH is bonded to the carboxylic acid terminated monolayers, only one peak from the electron transfer is apparent, indicating the two peaks described for the H-bonded system are not due to the FcCOOH species itself. The position of this redox peak is (0.15 ± 0.04) V vs. $Fc/Fc^{+}$, which is within error of those hydrogen bonded to the mercaptoalkanoic acids. By investigating the charge of this layer, the coverage can be seen to be (9.0 ± 0.3) x $10^{-12}$ mol $cm^{-2}$, lower than that seen for the FcCOOH on the –COOH terminated surfaces. The lower coverage is likely a result of the poor interaction of carboxylic acid with Au.[69] As before, the Laviron analysis was applied to the system to determine the rate constant of electron transfer. When the Laviron analysis is performed, as in **Figure 13**, the rate constant of electron transfer is determined to be 189 $s^{-1}$. It should be noted this value is lower than that measured for the $FcC_6SH$ (263 $s^{-1}$) even though the redox centre is closer to the Au surface. This lower *k* value is a result of the fact that the binding group is a carboxylic acid rather than a thiol. A 2006 study on the effect of molecular anchor group on conductance saw that on going from a thiol to a carboxylic acid anchor, the contact resistance increases as a result of the 20-fold decrease in bond strength with the Au surface.[69] While measurement of the FcCOOH

molecule on Au was necessary for comparison to the longer chain measurements, the –COOH end group is a poor anchor group for molecular electronics, and therefore, if possible, should be avoided.

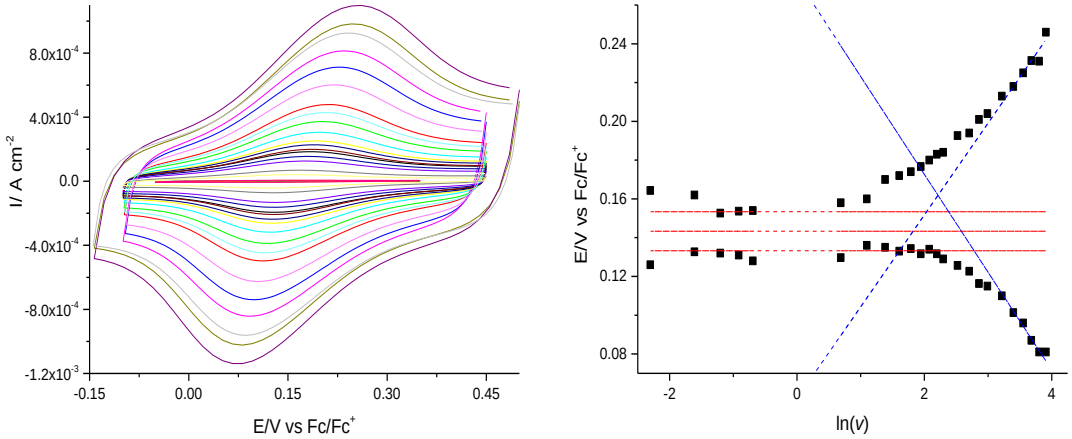


*Figure 13: The electrochemistry of a FcCOOH monolayer adsorbed on Au(111) bead was investigated in BMIM-OTf. The system was measured using Pt wire CE and QRE, and referenced to* $Fc/Fc^{+}$. *On going to the outer purple curve the scan rate changes from 0.05 to 50.0 V* $s^{-1}$. *The peak potential was plotted as a function of* ln(v) *to determine* k.

## Conclusion

Ionic liquids present a unique environment for electrochemical studies, and as a direct result, molecular electronics studies. Although ionic liquids result in reduced rates of charge transfer, their enhanced electrochemical window allows for investigations not possible in aqueous electrolytes. By exploiting the wider electrochemical window, BMIM-OTf has been successfully used to measure both electron transfers of the viologen redox centre. This ability is useful for molecular electronics as it presents the possibility of investigating the capacity of a redox molecule to induce conductance switching in multiple states. The ionic liquid environment has also been exploited here to investigate the electron transfer process

through a hydrogen bonded system, something which is difficult to achieve in other environments. It was seen that compared to the covalently bonded system, the hydrogen bonded system has a slow rate of electron transfer. Although the rate of electron transfer is reduced, this is an exciting prospect for molecular electronics, as it implies that the functionality of a system can be changed not only by traditional synthesis methods, but also by non-covalent attachment after the formation of a monolayer system.

## Declaration

*The 6V6 measured in this chapter was synthesized at the University of Liverpool by Dr. Carly Brooke of Professor Simon Higgins' group.*

## References


1. Y.-Z. Su, Y.-C. Fu, Y.-M. Wei, J.-W. Yan and B.-W. Mao, *ChemPhysChem*, 2010, **11**, 2764-2778.
2. M. Armand, F. Endres, D. R. MacFarlane, H. Ohno and B. Scrosati, *Nature Materials*, 2009, **8**, 621-629.
3. F. Endres and S. Zein El Abedin, *Physical Chemistry Chemical Physics*, 2006, **8**, 2101-2116.
4. P. E. Laibinis, G. M. Whitesides, D. L. Allara, Y. T. Tao, A. N. Parikh and R. G. Nuzzo, *Journal of the American Chemical Society*, 1991, **113**, 7152-7167.
5. H. L. Chum, V. R. Koch, L. L. Miller and R. A. Osteryoung, *Journal of the American Chemical Society*, 1975, **97**, 3264-3265.
6. K. Izutsu, *Journal of Solid State Electrochemistry*, 2011, **15**, 1719-1731.
7. J. S. Wilkes and M. J. Zaworotko, *Journal of the Chemical Society, Chemical Communications*, 1992, 965-967.
8. Z. Li, B. Han, G. Meszaros, I. Pobelov, T. Wandlowski, A. Blaszczyk and M. Mayor, *Faraday Discussions*, 2006, **131**, 121-143.
9. W. Haiss, T. Albrecht, H. van Zalinge, S. J. Higgins, D. Bethell, H. Höbenreich, D. J. Schiffrin, R. J. Nichols, A. M. Kuznetsov, J. Zhang, Q. Chi and J. Ulstrup, *The Journal of Physical Chemistry B*, 2007, **111**, 6703-6712.
10. E. Leary, S. J. Higgins, H. van Zalinge, W. Haiss, R. J. Nichols, S. Nygaard, J. O. Jeppesen and J. Ulstrup, *Journal of the American Chemical Society*, 2008, **130**, 12204-12205.
11. I. V. Pobelov, Z. Li and T. Wandlowski, *Journal of the American Chemical Society*, 2008, **130**, 16045-16054.
12. Z. H. Li, I. Pobelov, B. Han, T. Wandlowski, A. Blaszczyk and M. Mayor, *Nanotechnology*, 2007, **18**.

13. N. J. Kay, S. J. Higgins, J. O. Jeppesen, E. Leary, J. Lycoops, J. Ulstrup and R. J. Nichols, *Journal of the American Chemical Society*, 2012, **134**, 16817-16826.
14. Kim, J. M. Beebe, C. Olivier, S. Rigaut, D. Touchard, J. G. Kushmerick, X. Y. Zhu and C. D. Frisbie, *The Journal of Physical Chemistry C*, 2007, **111**, 7521-7526.
15. K. Seo, A. V. Konchenko, J. Lee, G. S. Bang and H. Lee, *Journal of the American Chemical Society*, 2008, **130**, 2553-2559.
16. H. O. Finklea, L. Liu, M. S. Ravenscroft and S. Punturi, *The Journal of Physical Chemistry*, 1996, **100**, 18852-18858.
17. J. F. Smalley, H. O. Finklea, C. E. D. Chidsey, M. R. Linford, S. E. Creager, J. P. Ferraris, K. Chalfant, T. Zawodzinsk, S. W. Feldberg and M. D. Newton, *Journal of the American Chemical Society*, 2003, **125**, 2004-2013.
18. G. Che, Z. Li, H. Zhang and C. R. Cabrera, *Journal of Electroanalytical Chemistry*, 1998, **453**, 9-17.
19. J. F. Smalley, S. B. Sachs, C. E. D. Chidsey, S. P. Dudek, H. D. Sikes, S. E. Creager, C. J. Yu, S. W. Feldberg and M. D. Newton, *Journal of the American Chemical Society*, 2004, **126**, 14620-14630.
20. Y. Arikuma, H. Nakayama, T. Morita and S. Kimura, *Langmuir*, 2011, **27**, 1530-1535.
21. B. Fabre, *Accounts of Chemical Research*, 2010, **43**, 1509-1518.
22. T. Shaw, X. Qianyin, S. Rajwade, T.-H. Hou and E. C. Kan, *Electron Devices, IEEE Transactions on*, 2012, **59**, 1189-1198.
23. T. Pro, J. Buckley, H. Kai, A. Calborean, M. Gely, G. Delapierre, G. Ghibaudo, F. Duclairoir, J. C. Marchon, E. Jalaguier, P. Maldivi, B. De Salvo and S. Deleonibus, *Nanotechnology, IEEE Transactions on*, 2009, **8**, 204-213.
24. S. Ren, Y. Hou, W. Wu and W. Liu, *Journal of Chemical & Engineering Data*, 2010, **55**, 5074-5077.
25. M. C. Henstridge, E. Laborda, E. J. F. Dickinson and R. G. Compton, *Journal of Electroanalytical Chemistry*, 2012, **664**, 73-79.
26. K. B. Oldham, *Journal of Electroanalytical Chemistry and Interfacial Electrochemistry*, 1979, **105**, 373-375.
27. A. Lewandowski, L. Waligora and M. Galinski, *Journal of Solution Chemistry*, 2013, **42**, 251-262.
28. S. Chanfreau, B. Yu, L.-N. He and O. Boutin, *The Journal of Supercritical Fluids*, 2011, **56**, 130-136.
29. R. S. Nicholson, *Analytical Chemistry*, 1965, **37**, 1351-1355.
30. I. Lavagnini, R. Antiochia and F. Magno, *Electroanalysis*, 2004, **16**, 505-506.
31. A. Degli Esposti, V. Fattori, C. Sabatini, G. Casalbore-Miceli and G. Marconi, *Physical Chemistry Chemical Physics*, 2005, **7**, 3738-3743.
32. A. J. Bard and L. R. Faulkner, in *Electrochemical Methods: Fundamentals and Applications* John Wiley & Sons, Inc., Editon edn., 2001, pp. 226-260.
33. R. Parsons, *Surface Science*, 1964, **2**, 418-435.
34. E. Laviron, *Journal of Electroanalytical Chemistry and Interfacial Electrochemistry*, 1979, **101**, 19-28.
35. L. Bouffier, K. E. Lister, S. J. Higgins, R. J. Nichols and T. Doneux, *Journal of Electroanalytical Chemistry*, 2012, **664**, 80-87.
36. M. J. Honeychurch and G. A. Rechnitz, *Electroanalysis*, 1998, **10**, 285-293.

37. A. Ricci, C. Rolli, S. Rothacher, L. Baraldo, C. Bonazzola, E. Calvo, N. Tognalli and A. Fainstein, *Journal of Solid State Electrochemistry*, 2007, **11**, 1511-1520.
38. R. A. Ballinger and C. A. W. Marshall, *Journal of Physics F: Metal Physics*, 1973, **3**, 735.
39. A. Lewandowski, L. Waligora and M. Galinski, *Electroanalysis*, 2009, **21**, 2221-2227.
40. M. A. Vorotyntsev, V. A. Zinovyeva and M. Picquet, *Electrochimica Acta*, 2010, **55**, 5063-5070.
41. O. Fontaine, C. Lagrost, J. Ghilane, P. Martin, G. Trippé, C. Fave, J. C. Lacroix, P. Hapiot and H. N. Randriamahazaka, *Journal of Electroanalytical Chemistry*, 2009, **632**, 88-96.
42. L. Xiao, E. J. F. Dickinson, G. G. Wildgoose and R. G. Compton, *Electroanalysis*, 2010, **22**, 269-276.
43. D. Y. Kim, J. C. Yang, H. W. Kim and G. M. Swain, *Electrochimica Acta*, 2013, **94**, 49-56.
44. N. E. Christensen and B. O. Seraphin, *Physical Review B*, 1971, **4**, 3321-3344.
45. H. Li, F. Endres and R. Atkin, *Physical Chemistry Chemical Physics*, 2013, **15**, 14624-14633.
46. J. O. Bockris, apos, M, R. J. Mannan and A. Damjanovic, *The Journal of Chemical Physics*, 1968, **48**, 1898-1904.
47. D. Galizzioli and S. Trasatti, *Journal of Electroanalytical Chemistry and Interfacial Electrochemistry*, 1973, **44**, 367-388.
48. B. Liu, A. Blaszczyk, M. Mayor and T. Wandlowski, *ACS Nano*, 2011, **5**, 5662-5672.
49. B. Han, Z. Li, T. Wandlowski, A. Błaszczyk and M. Mayor, *The Journal of Physical Chemistry C*, 2007, **111**, 13855-13863.
50. H. C. De Long and D. A. Buttry, *Langmuir*, 1990, **6**, 1319-1322.
51. C. L. Bird and A. T. Kuhn, *Chemical Society Reviews*, 1981, **10**, 49-82.
52. D. I. Gittins, D. Bethell, R. J. Nichols and D. J. Schiffrin, *Journal of Materials Chemistry*, 2000, **10**, 79-83.
53. A. A. H. Pádua, M. F. Costa Gomes and J. N. A. Canongia Lopes, *Accounts of Chemical Research*, 2007, **40**, 1087-1096.
54. L. S. Curtin, S. R. Peck, L. M. Tender, R. W. Murray, G. K. Rowe and S. E. Creager, *Analytical Chemistry*, 1993, **65**, 386-392.
55. L. Tender, M. T. Carter and R. W. Murray, *Analytical Chemistry*, 1994, **66**, 3173-3181.
56. L. H. Dubois and R. G. Nuzzo, *Annual Review of Physical Chemistry*, 1992, **43**, 437-463.
57. C. Miller, P. Cuendet and M. Graetzel, *The Journal of Physical Chemistry*, 1991, **95**, 877-886.
58. D. J. L. Brett, R. Williams and C. P. Wilde, *Journal of Electroanalytical Chemistry*, 2002, **538–539**, 65-74.
59. M. M. Rahman and I. C. Jeon, *Journal of Organometallic Chemistry*, 2006, **691**, 5648-5654.
60. L.-H. Guo, J. S. Facci and G. McLendon, *The Journal of Physical Chemistry*, 1995, **99**, 8458-8461.
61. J. F. Smalley, S. W. Feldberg, C. E. D. Chidsey, M. R. Linford, M. D. Newton and Y.-P. Liu, *The Journal of Physical Chemistry*, 1995, **99**, 13141-13149.

62. G. Valincius, G. Niaura, B. Kazakevičienė, Z. Talaikytė, M. Kažemėkaitė, E. Butkus and V. Razumas, *Langmuir*, 2004, **20**, 6631-6638.
63. S. R. Catarelli, MChem Dissertation, University of Liverpool, 2010.
64. M. Hromadová and W. R. Fawcett, *The Journal of Physical Chemistry A*, 2000, **104**, 4356-4363.
65. M. D. Porter, T. B. Bright, D. L. Allara and C. E. D. Chidsey, *Journal of the American Chemical Society*, 1987, **109**, 3559-3568.
66. Y. Xiaoling and Z. Guigen, *Nanotechnology*, 2008, **19**, 465504.
67. M. Das and B. D. Dunietz, *The Journal of Physical Chemistry C*, 2006, **111**, 1535-1540.
68. T. Nishino, N. Hayashi and P. T. Bui, *Journal of the American Chemical Society*, 2013, **135**, 4592-4595.
69. F. Chen, X. Li, J. Hihath, Z. Huang and N. Tao, *Journal of the American Chemical Society*, 2006, **128**, 15874-15881.

# Chapter 4:

# STM in Ionic Liquids

# Introduction

The limits of current technology will be reached as the demand for smaller and faster computational devices expands. Although solid state electronic devices are the current norm, this field looks to be revolutionized by the use of bottom up techniques, such as the vigorously investigated molecular electronics. To implement molecular electronics the conductance characteristics of single molecules must be understood. A common method for probing the conductance of molecular systems is the use of the STM based single molecule conductance measurements, the *I*(*s*) and break junction techniques. In these methods the molecule is directly connected to the tip and substrate, allowing the effects of the entire metal-molecule unction to be assessed.

Of particular interest is the behaviour of molecular conductance in different environments. Single molecule conductance measurements have been performed in a variety of environments, including ambient conditions,[1] dry and doped gases,[2] organic solvents,[3] UHV conditions,[4] and more. The environment has been seen to affect the measurement of metal-molecule-metal junctions, and therefore must be carefully chosen. Venkataraman *et al.*[3] investigated the conductance of benzenediamine in 13 different organic electrolytes, with a variation in conductance of up to 50 % seen. Their investigation showed the adsorption of different solvents on the surface affect the electrode work function differently, in turn altering the molecular conductance. Recently the effects of more exotic environments have been investigated. In 2011 a series of alkanedithiol molecules of different length were investigated in ionic liquids.[5] Although the conductance of the alkanethiols in BMIM-OTf were similar to those seen for ambient measurements, the high conductance group is not seen, which may be because of the interaction of the ionic liquid with the Au surface, which blocks adsorption sites. In 2013 a similar series of experiments were performed on a series of

alkanedithiol molecules of varying length under UHV.[4] These measurements showed similar conductance values as the analogous systems in ambient and ionic liquid environments. The library of possible environments for molecular electronics studies is continually growing. It is important investigations on more complex systems are performed on the back of these successes.

In this work a variety of molecular wires with different end groups and backbones are investigated in ionic liquids. Ionic liquids are ideal for single molecule conductance experiments, because unlike organic solvents they have negligible volatility, making them safe for use in the STM. Furthermore their negligible volatility means that unlike some organic solvents used, they do not evaporate off during the experiment, which can cause noticeable conductance changes.[3] While aqueous environments are also less volatile than organic solvents, they can solvate the molecular backbone and alter the conductance.[2] Furthermore, if electrochemical control is to be used, ionic liquids are more promising than aqueous electrolytes because of their wider electrochemical window. The wide electrochemical window of ionic liquids allows for measurements which would not be possible otherwise. By measuring a variety of molecules in ionic liquids the potential of these environments can be further assessed. At this time only thiol terminated molecular wires have been investigated in ionic liquids in the literature,[5-7] therefore, it is important to determine if ionic liquids allow for the same variety of molecular end groups as other environments.

## Aim

Ionic liquids hold great potential for molecular electronics investigations. To date, however, they have been used to measure a very limited number of molecules.

In order to determine the usefulness of this environment in future investigations it is necessary to build up a catalogue of molecules measured in these systems. Furthermore, the usefulness of ionic liquids as a class of solvents must be assessed. This work looks to measure a series of molecules in ionic liquids. Branching out from alkanedithiol molecules, a variety of end groups and molecular structures are measured. Furthermore, this work investigates these molecules in two different $BMIM^+$ ionic liquids, allowing the effect of the anion to be assessed.

## Methods

### PM-IRRAS of 4,4'-Bipyridine

4,4'-bipyridine was measured by PM-IRRAS prior to SMC investigations. PM-IRRAS was performed on a Bruker Instruments PMA 37 module, with an IFS 66v/S spectrophotometer. The instrument was controlled by a computer running the Bruker Instruments OPUS software. The IR beam had an angle of incidence of 81.25 $^\circ$ on the sample. Polarization modulation was performed using a Hinds Instruments PEM-90 photoelastic modulator. The detector was a liquid nitrogen cooled, mercury cadmium telluride infrared detector from Infrared Associates. The resulting data was analysed using the OPUS software, and spectra were corrected against a spline function. Bipyridine was adsorbed on a Au(111) Arrandee$^{TM}$ slide from a 0.1 mM bipyridine in BMIM-OTf solution with 1 hour adsorption. The slide was rinsed with water and dried with nitrogen. Based on the results of the initial PM-IRRAS measurements, it was determined the bipyridine should be purified before SMC measurements were performed. Purification was achieved by dissolving the bipyridine in 0.1 M $H_2SO_4$ and precipitating it out by adding 1 M NaOH to raise the pH to 8, and repeating. Finally the bipyridine was recrystallized from ethanol. The PM-IRRAS was repeated with the purified bipyridine.

Electrochemistry of Porphyrins

The electrochemistry of a monolayer of AcOS-Zn-SOAc, **Figure 1**, was investigated on a Au(111) bead electrode in 0.025 M potassium phosphate buffer solution against a SCE RE, with a Pt CE, and in BMIM-OTf, using a Pt wire CE and RE. The aqueous electrochemistry was performed after 20 minutes of nitrogen bubbling. The ionic liquid electrochemistry was performed in a sealed cell, prepared in a nitrogen filled glovebox. The monolayer was formed by first cleaving the S-OAc bond by the addition of KOH to a 0.05 mM AcOS-Zn-SOAc in chloroform solution, to give a 1:1 solution. The solution was left to react for 2 hours before immersing the Au bead for 1 hour.

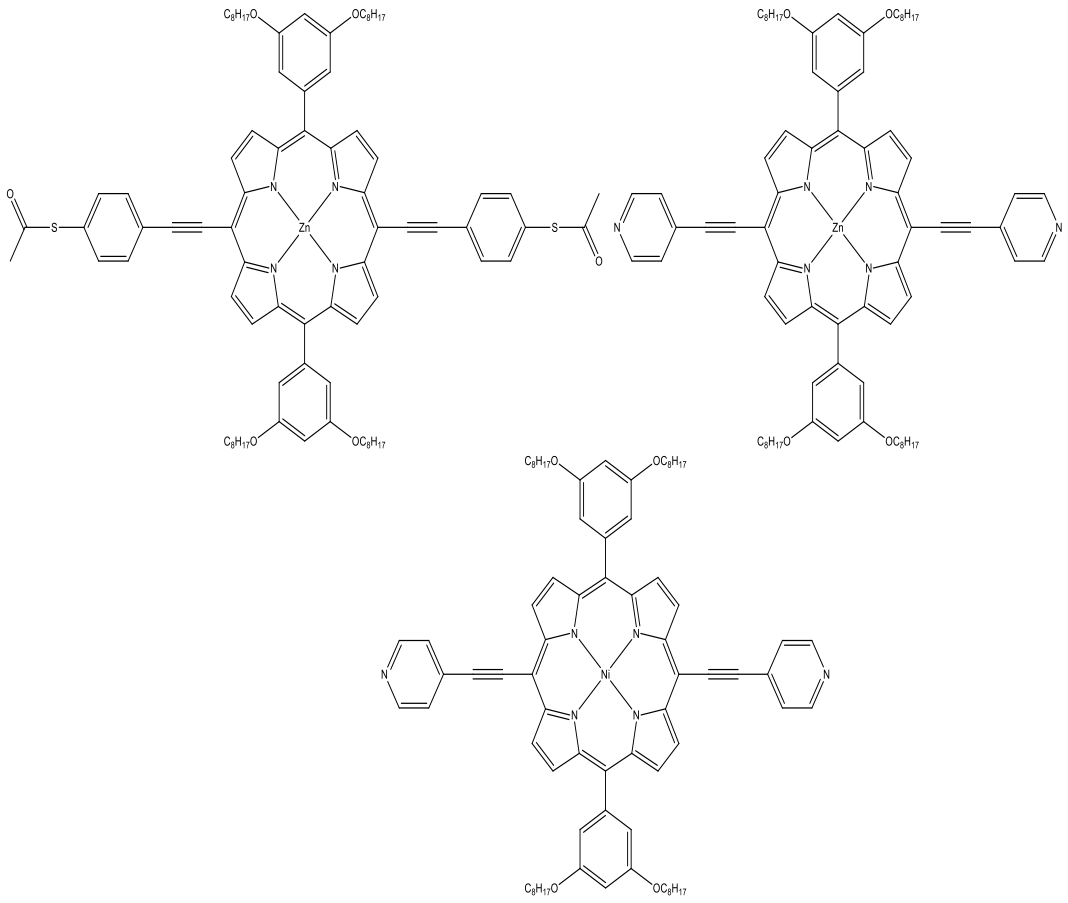


*Figure 1: The three porphyrin molecules measured are shown. The molecules were all prepared and supplied by Prof. Harry Anderson's group at the University of Oxford.*

Solution electrochemistry of 0.25 mM Py-Ni-Py solution in both 0.1 M tertrabutyl ammonium hexafluorophosphate in DCM, and BMIM-OTf was performed. The electrochemistry in DCM was performed after 20 minutes of nitrogen purging. To form the BMIM-OTf solution Py-Ni-Py was dissolved in a minimal amount of DCM, which was heated off with nitrogen bubbling, after the addition of the ionic liquid. The BMIM-OTf electrochemistry was performed in a cell prepared and sealed in a nitrogen containing glovebox. Both experiments were performed using a Au(111) bead WE, and Pt QRE and CE, and referenced to $Fc/Fc^{+}$.

## SMC Measurements

### Sample Preparation

Arrandee$^{TM}$ Au(111) on glass slides were prepared by annealing in a Bunsen flame, and immersing in the adsorption solution of choice for a given length of time, dependent on the anchoring group and coverage desired. Concentrations, adsorption solvents, and adsorption lengths are listed in **Table 1**. Slides were removed from solution, rinsed and dried in nitrogen. Gold tips were freshly cut or etched from 0.25 mm wire and coated in Apiezon wax for use in ionic liquids. The ionic liquid was vacuum dried at 120 °C for 18 hours before use. Ionic liquid measurements were performed in a nitrogen atmosphere, with nitrogen purging for at least 1 hour before measurements were carried out.

*Table 1: The composition of the STM adsorption solutions, and adsorption times, are shown.*

| Molecule | Solvent | Concentration | Adsorption Time | Notes |
|---|---|---|---|---|
| Azelanitrile | Acetone | 10 mM | 10 minutes | |
| 4,4'-Bipyridine | Toluene | 0.5 mM | 20 seconds | Purified |
| 1,2 –Bis(4-pyridyl)ethane | Toluene | 0.5 mM | 2-2.5 minutes | |
| 6V6 | MeOH | 1 mM | 1.5 hours | S-OAc bond cleaved with 1 eq. KOH 2 hours prior to use. Synthesized by Dr C. Brooke |
| AcOS-Zn-SOAc | Chloroform | 0.05 mM | 1-1.5 minutes | Synthesized by Prof H. Anderson's Group, University of Oxford |
| Py-Zn-Py | Chloroform | 0.05 mM | 1-1.5 minutes | Synthesized by Prof H. Anderson's Group, University of Oxford |
| Py-Ni-Py | Chloroform | 0.05 mM | 1-1.5 minutes | Synthesized by Prof H. Anderson's Group, University of Oxford |

### *I*(*s*) Measurements

*I*(*s*) measurements were performed on an Agilent Technologies 2500 or 5500 controller, with a 10 nA/V scanner fitted. All measurements were performed using the *I*(*s*) spectroscopy function of PicoScan 5.0. The sample bias was 0.6 V, and the set point current was 20 mA. Only those spectra showing plateaus were saved and analysed using a program written in-house for the Labview software, allowing all points to be collated and exported to Origin 8.6, and for a histogram of the current to be plotted. Around 500 scans were used to form each histogram.

## Analysis of Histograms

The large number of molecular conductance events from an *I*(*s*) investigation, requires a statistically significant means of dealing with the data. A common method for determining molecular conductance is to use a 1D histogram composed of the number of times a conductance is measured versus the conductance. It should be noted the entire *I*(*s*) trace is included in these histograms, so not every conductance represented is due to the metal-molecule-metal junction. The peaks arising in the histograms represent an average conductance of all the junctions, while the peak height is a representation of the probability of a particular conductance event.[8] It would be a

mistake in these analyses to assume the conductance histogram peak width is due to errors within the measurement. It is regularly seen that the peak width can be 30-100% of the peak position itself.[9] This intrinsic broadness arises from a plethora of different configurations sampled. Each $I(s)$ trace samples an individual molecular junction and there are generally many possible substrate-molecule-substrate configurations. When constructing the histogram, each event is weighted, based on the length of the event, and included, with more probable conductance events causing larger counts. Based on this, the peak width may be dependent on factors such as the tilt angle of the molecule,[10, 11] the binding site of the molecule,[12-14] the configuration of the molecule in the junction,[9, 12, 14] and more. Aside from causing slight changes in the conductance, these different molecule junction interactions affect the length of the measured conductance plateau. The length of the conductance plateau affects the degree to which it adds to the histogram peak, with longer plateaus contributing to higher counts in the histogram.[9, 15] This length dependence means the final peak shape relates to the stabilities of different molecular junctions. Aside from being sensitive to the metal-molecule interactions, the peak width may also reflect the different conductance channels. While it is assumed the conductance event in a molecular junction is fully through the molecule, this is not necessarily the case. Depending on the molecule's position relative to the tip apex direct tunnelling between the tip and substrate can occur, giving rise to a background tunnelling current. When included in the conductance histograms, this background current can cause increased broadening of the molecular conductance peak.[9, 15] Finally, although not necessarily contributing to the overall peak width, the change in peak weighting with resonant versus non-resonant tunnelling should be noted, as this can cause an asymmetric peak shape.[13, 16] While for resonant tunnelling the peak is asymmetric with the weighting towards

lower conductance values, in nonresonant tunnelling, as is expected for molecular conductance, the peak is asymmetric and sloped towards large conductance values.[13, 16] The histogram peak width and shape holds a large degree of information about the molecular conductance event, indeed, more detail than can be generally interpreted.

The peak seen in the 1D molecular conductance histogram should be thought of as a representation of the probability of a specific conductance event occurring. The peak position is the average conductance event which will occur based on a variety of factors such as the interaction of the molecular junction and its overall stability. The peak width reflects the spread of the data rather than the error in the measurement. This spread arises from the vast number of molecular junctions which give differing conductance values. The weights of these junctions in the histogram reflects the probability of their formation. The quoted peak width and spread in conductance are the range of values arising from the most probable molecular junctions.

## Determination of $s_0$

The correlation of junction distance and molecular conductance allows further information about the molecule in the junction to be gathered. The measured length of the plateau, compared to the length of the molecule, holds information about the interaction of the molecule in the junction. When the plateau length is shorter than the molecular length, the molecule may be tilted in the junction,[11, 17] there may be *gauche* defects in the molecule,[18, 19] or there may be a weak molecule-electrode interaction with the junction breaking before it is fully elongated.[11] If the plateau length is similar to the molecular length, the molecule must be fully upright in the junction, as it is impossible to span the gap otherwise.[10, 11] Somewhat surprisingly, it is also possible to measure break-off distances longer than the molecular length. Longer break-off

lengths arise when the end group electrode interaction is so strong that atoms are pulled out of the surface before the junction breaks.[11] This discrepancy may also arise when molecular stacking occurs, allowing multiple molecules to span the gap at once.[11] When multiple conductance pathways are available in a molecule, the break off distance holds information about the conductance pathway.[20] Furthermore, longer molecules can give rise to proportionately longer plateaus due to their ability to move along the atoms of the electrodes, and bond to sites away from the apex unlike shorter molecules.[19] To accurately determine the junction distance, the measurements must be calibrated.

To determine the total break-off distance, the initial distance of the STM tip from the substrate at the start of the $I(s)$ measurement, $s_0$, must be calibrated. In order to determine $s_0$ multiple $I(s)$ scans, free from evidence of a molecular bridge, are collected, and re-plotted as $\ln(I)$ vs. $s$, allowing determination of the slope of this measurement.[10, 21, 22] When the STM tip just touches the substrate, in most cases both are Au, the conductance of the system is assumed to be the quantum of conductance, $G_0$, 77400 nS.[23] From this assumption, the tip position at a given set point current can be determined by extrapolating backwards.[22] To determine $s_0$ the following equation is used:[21, 23]

$$s_0 = \frac{\ln\left(G_0 \times \frac{V_{bias}}{I_0}\right)}{d \ln I / d s} \qquad (Eq.\ 1)$$

Where $V_{bias}$ is the tip bias voltage, and $I_0$ the set point current.

The calibration of $s_0$, although useful, assumes ideal behaviour, which is not always the case. In these analysis it is assumed the junction is completely free of adsorbates, and therefore the empty tip-substrate gap conductance is monitored. As

will be seen in this work, the use of ionic liquids often led to break-off distances noticeably larger than expected for the molecular length. It is well known that when using ionic liquids the cation interacts strongly with the Au surface.[24, 25] As a result of the strong ionic liquid network which forms on the substrate and the tip, it is unlikely the gap can be thought of as 'molecule free.' Rather than probing the change in conductance of tip and substrate system, it is, instead, tip-ionic liquid-substrate, which leads to a $d\ln I/ds$ value which decays more slowly than that of a completely molecule free system. Ionic liquids may further contribute to the $d\ln I/ds$ value as a result of their mobility on the Au surface or even in the tip-substrate gap. At room temperature ionic liquids have been seen to diffuse and rotate along the Au surface, causing fluctuations in the measured tunnelling current.[26, 27] In scanning probe imaging experiments the interaction of the ions with the Au has manifested itself as an unresolvable surface.[27] In this work it is likely the interaction of the Au with the ionic liquid complicates the conductance decay.

# Results and Discussion

## Ambient Environment Investigations

Prior to performing $I(s)$ investigations in ionic liquids, it is useful to investigate a simple system under ambient conditions.

### Azelanitrile

Azelanitrile, **Figure 2**, was investigated under ambient conditions by the $I(s)$ technique. Azelanitrile is interesting because it uses a C≡N anchor group rather than the most commonly used thiol, pyridyl, or amine anchor groups, which will affect the coupling between the metal-molecule contact, thereby affecting the molecular

conductance.[28] To build on the understanding of molecular conductance it is important to fully explore the available molecular terminations.

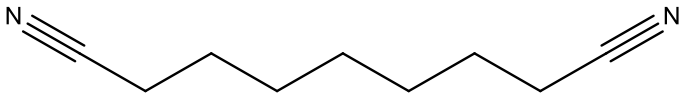


*Figure 2: The structure of azelanitrile is shown.*

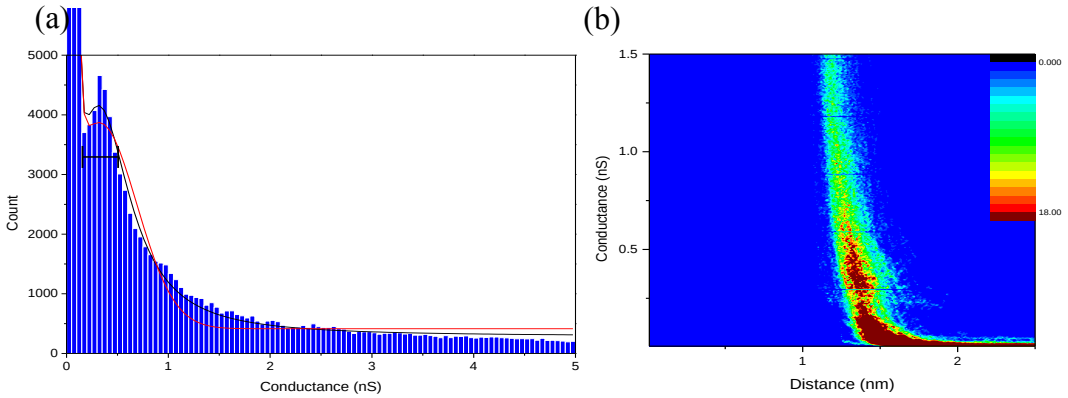


*Figure 3: Azelanitrile was investigated by the I(s) technique using a sample bias of 0.6 V and set point current of 20 nA. The 1D (a), and 2D (b) histograms shown were formed from 458 plateau containing scans. The different methods of analysis of the peak conductance are shown. The black curve is the Lorentzian fit, while the red curve is the Guassian fit.*

The conductance of the Au-azelanitrile-Au system was determined using the *I*(*s*) technique. 458 scans, with a plateau indicative of the azelanitrile molecule contacting the STM tip and substrate, were collected and used to form the histogram in **Figure 3a**. A conductance value can be found using the histogram by averaging the conductance of the upper boundaries of the peak, as marked in **Figure 3a**. Using this method a conductance of 0.32 nS was found. A more rigorous analysis of the conductance peak for azelanitrile is performed with peak fitting. The azelanitrile conductance could be fitted to both a Gaussian and a Lorentzian peak, marked in **Figure 3a**. Using Gaussian fitting, the conductance is 0.32 nS, while using a Lorentzian fit, gives a conductance of 0.31 nS. Both of these fitted values are similar

to that found by taking an average of the conductance values composing the peak. Comparison of the two fit types shows that, in this instance, the Lorentzian gives the best fit to the data.

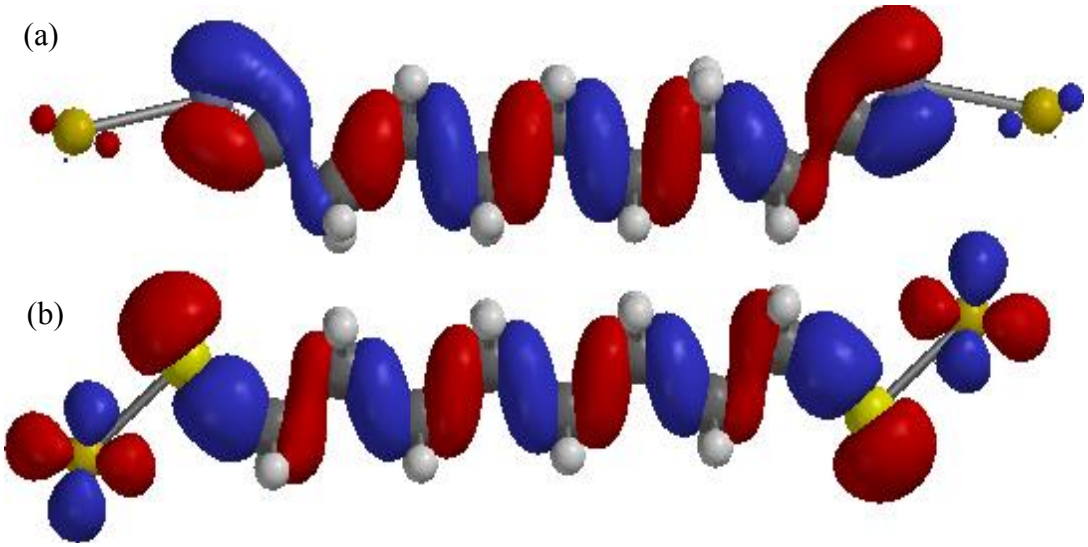


*Figure 4: The frontier orbitals of azelanitrile (a), and octanedithiol (b), contacted at both ends by Au, were determined through Spartan®. Both conduct through HOMO orbitals, however it is obvious that the HOMO orbital of azelanitrile is localized on the molecule, whereas that of octanedithiol spans the entire metal-molecule-metal junction.*

For the measurements performed on azelanitrile it is also useful to determine the current-distance relationship, which is easily shown using a 2D histogram, **Figure 3b**. The 2D histogram shows most conductance events occur between ~1.25 and 1.5 nm, which is comparable to the break-off distance of this molecule of (1.4 ± 0.2) nm. When Spartan® calculations were performed on the azelanitrile molecule between two Au atoms, a molecular length of 1.6 nm was determined. The shorter than expected break-off distance may arise for one of two reasons. 1) The azelanitrile is tilted in the junction, with break-off occurring before full extension. This is in line with the comparatively weak **Au-N**≡C bond.[29] 2) Azelanitrile binds to Au through a flat-lying N≡C group. Surface IR studies of nitrile terminated alkanes have shown bonding to a flat lying N≡C is possible. However, because of the large footprint in this orientation,

the coverage is low.[29] The sub-monolayer coverage used for *I*(*s*) measurements, would accommodate the flat lying C≡N.

To benchmark the behaviour of the C≡N end group, azelanitrile is compared to the analogous alkanethiol system, octanedithiol. Octanedithiol has one extra methyl unit, but a similar molecular length. The conductance of azelanitrile is ~2.75 times less than that of octanedithiol.[1] In previously published work lower conductance has been measured for the C≡N end group, due to the reduced **Au-N**≡C coupling when compared to Au-S.[30] By modelling the HOMO-LUMO states of azelanitrile and octanedithiol in Spartan®, insight into the origin of the different conductance values is gained. The Spartan® calculations, **Figure 4**, show azelanitrile conducts through the HOMO (-11), whereas octanedithiol conducts through the HOMO (-4) level. Comparisons of these states show for octanedithiol the HOMO is fairly well delocalized across the whole system, whereas for azelanitrile, the HOMO is mostly localized on the azelanitrile molecule with some smaller orbital character existing on the Au contacts. The differences in molecular orbital structure are unsurprising, as the reduced relative bond strength of the **Au-N**≡C causes reduced metal-molecule coupling. The energy of the frontier orbitals of the octanedithiol and azelanitrile systems can be calculated and compared. The HOMO (-4) of the Au-octanedithiol-Au system has an energy of -8.07 eV, whereas the HOMO (-11) of the Au-azelanitrile-Au system has an energy of -9.37 eV. When predicting molecular conductance, higher conductances are expected when the energy gap between the metal work function and the frontier orbital is small. As the work function of Au is -5.4 eV the gap is smaller for the octanedithiol system, in line with the higher conductance seen.[31, 32]

The Au-azelanitrile-Au system was measured by the *I*(*s*) technique under ambient conditions. These measurements showed azelanitrile to have a conductance

much lower than for the similar length alkanedithiol. The difference in conductance arises from the use of a C≡N end group instead of the thiol end group. This substitution leads to a reduction in metal-molecule coupling which, in turn, leads to a system with reduced conductance.

## Ionic Liquid Environment

### Pyridyl Terminated Molecules

4,4'-bipyridine is the simplest pyridyl terminated molecule, composed of two covalently bonded pyridyl rings. 4,4'-Bipyridine is of interest for several reasons. It is historically significant as the first molecule measured by the break junction technique[33] and, as such, has been a testing ground for many new single molecule conductance techniques.[34-36] The interest in 4,4'-bipyridine means not only does it have a well measured molecular conductance, but there is also a wealth of information about its behaviour in the molecular junction.[35-37] As bipyridine is well-known for its high conductivity, it is ideal for initial measurements in ionic liquids as it is well removed from the STM noise level, which helps to simplify the experiments.

Prior to molecular conductance measurements, PM-IRRAS measurements were performed on the bipyridine, direct from the manufacturer, with Au substrates, **Figure 5**. This spectrum shows the presence of the $BMIM^+$ cation at the monolayer from 2954-2857 $cm^{-1}$, due to the stretches of the $CH_2$ and $CH_3$ of the alkyl side chain. There is no evidence of the OTf anion. A series of peaks due to the bipyridine itself is seen from 1743-1645 $cm^{-1}$. The most revealing peak in this spectrum is that at 1645 $cm^{-1}$, indicating the bipyridine molecule exists as the hydrolysed species $BiPyH_2^{2+}$.[38] There is no apparent documentation in the literature of the bipyridine molecule having been purified prior to use in past conductance studies. Ionic liquids are an already

complex environment on which little work has been done thus far to determine their effects on molecular conductance. While it is possible the hydrated bipyridine will behave in a manner similar to the thiol end groups, losing the $-H^+$ upon adsorption,[39, 40 41] steps were taken to cleave the N-H bond prior to performing single molecule conductance measurements. Once the NH bond was cleaved to return the bipyridine molecule the PM-IRRAS experiments were repeated, **Figure 5**. The spectrum again shows peaks from the $BMIM^+$ cation at 2960-2857 $cm^{-1}$, as well as peaks at 2359 and 2343 $cm^{-1}$ due to adsorbed $CO_2$. There is no longer any evidence of the $BiPyH_2^{2+}$ species, however a peak at 1472 $cm^{-1}$ appears due to the ring vibrations. The noticeable changes in the bipyridine on Au spectra shows that pre-cleavage of the N-H bond is possible.

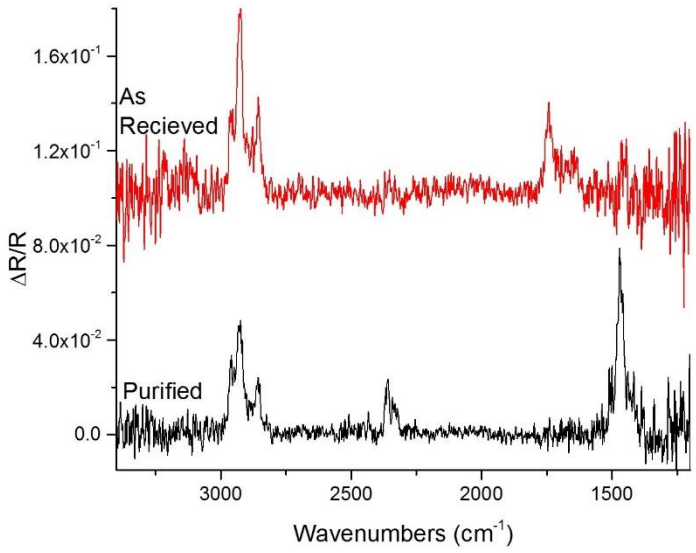


*Figure 5: 4,4'-bipyridine on Au(111) was investigated by PM-IRRAS both without and with purification. Modulation was optimized for 2200 $cm^{-1}$. Spectra were corrected against a spline function. The sample measured in both cases was formed from 1 hour of adsorption from a 0.1 mM bipyridine in BMIM-OTf solution.*

Using the treated bipyridine, single molecule conductance studies were performed in both BMIM-OTf and BMIM-TFSA using the *I*(*s*) technique. By collecting over 600 scans, containing molecular junctions, in each ionic liquid, histograms could be formed to determine the molecular conductance of bipyridine. In this case, the best agreement of the conductance between both environments was achieved using the average of the peak conductance values. The conductance of bipyridine was 7.3 and 7.2 nS in BMIM-OTf and BMIM-TFSA, respectively, **Figure 6**. Although this conductance value is lower than measured previously for bipyridine by STM,[42, 43] it is similar to that seen by Frei *et al.*[35] using conductive AFM. The break-off distance of the bipyridine junctions was determined to be (4.5 ± 1.1) nm, and (4.3 ± 0.8) nm in BMIM-OTf and BMIM-TFSA. Based on the Spartan® determined molecular length of bipyridine and the length of the pyridyl-Au bond, a break-off distance of 1.2 nm is expected.[44] As has been discussed there is likely an overestimation in $s_0$. When $s_0$ is not included, raw displacement distances of (1.7 ± 0.5) and (1.7 ± 0.4) nm are seen in BMIM-OTf and BMIM-TFSA, respectively. Although these break-offs are still long, they are within error of values expected from Spartan® molecular length calculations. While achieving such long break-off distances seems implausible, the similarities in both conductance and break-off values between the two ionic liquid systems, and the similarity to literature values, leads to confidence in the results. Care must be taken when measuring aromatic rings, as the rings can interact with each other by π-π stacking, allowing for intermolecular conductance mechanisms.[45, 46] There is a possibility, therefore, that the 4,4'-bipyridine molecules measured here can interact by π-π stacking. The resulting increase in molecular length, and reduction in conjugation, could correlate to the lower conductance than in other

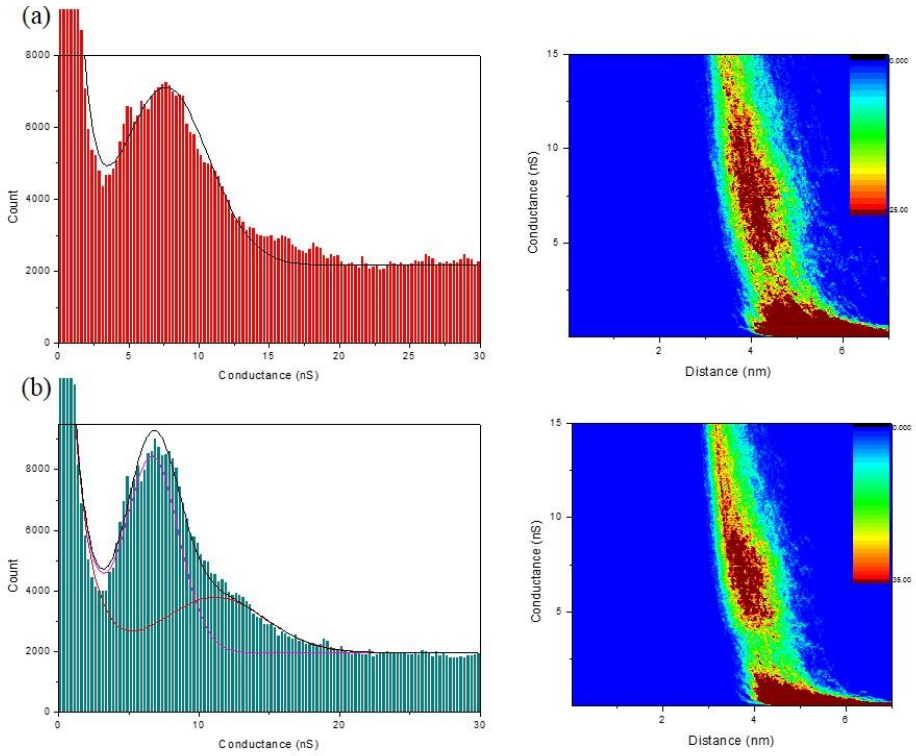


*Figure 6: The 1D and 2 D histograms of the* I(s) *measurements of 4,4'-bipyridine in BMIM-OTf (a) and BMIM-TFSA (b) are shown. The histograms from BMIM-OTf were formed from 608 scans, which those from BMIM-TFSA used 633 scans. In both cases the sample bias was 0.6 V, and the set point current was 20 nA.*

STM based studies.[42, 43] To test whether π-π stacking occurs in these junctions, bipyridyl molecules with bulky side chains could be synthesized. The bulky side chains should act to hinder the π-π interaction,[45] and allow the formation of a junction from a single bipyridine molecule. Although theoretically π-π stacking can occur with just one aromatic ring overlaps,[46] a more likely explanation for the long break-off distances is the formation of long gold chains during the junction extension. When *I*(*s*) measurements are performed on thiol terminated molecules on Au the interaction causes Au atoms to pull out of the surface.[47] A similar effect may occur for the pyridine-Au bond. Usually, only a single Au atom pulls out at the contact site,[47] however in ionic liquids it may be possible to form longer Au nanowires. What little

work has been done on the formation of atomic wires in ionic liquids has not reported the long atomic wires proposed here, although different metals and ionic liquids were used.[48] For a description of the stabilization of Au nanowires in ionic liquids, therefore, the formation of nanoparticles in ionic liquids has been reviewed. It has commonly been reported that ionic liquids can be used to form stable metal nanoparticles without the need for a capping ligand or stabilizer.[49-53] The most applicable explanation to the long nanowires is that the ionic liquids solvate the nanostructure to give a 1 ion thick layer.[49, 51] The solvation layer formed at the surface is composed of the ionic liquid anions and head group of the cation, which strongly interacts with the nanostructure.[49] The use of cations with longer alkyl chains gives rise to more stable nanostructures because of the strengthened solvation layer, from the increased van der Waals interactions of the alkyl groups.[49, 51] Strengthening the solvation layer has the secondary effect of enhancing the electrostatic interactions with the nanostructure, causing further stabilization.[49] Utilizing the same molecule/ ionic liquid system, the hypothesis that the BMIM ionic liquids allow for longer Au nanowires, through stabilization of the system, could be investigated by the break junction technique. The use of the break junction technique would allow for the $G_0$ peak to be measured in conjunction with the Au-bipyridine-Au junctions and the average length of the $G_0$ plateau could be correlated with the length of the Au wire. For comparison, the same measurements would have to be performed in mesitylene. If the $BMIM^+$ ionic liquids do, indeed, give rise to longer Au nanowires, then shorter plateaus are expected for $G_0$ in mesitylene. As a further means to investigate if an ionic liquid solvation layer arises for the Au system, break junction experiments of a Au tip and substrate could be investigated in various ionic liquids. By changing the cation of the ionic liquid to one with a shorter alkyl chain, for example $EMIM^+$, the stabilizing

effect of the ionic liquid on the Au nanowire should be diminished causing a reduced break-off distance. Summarising this part bipyridine has presented itself as an interesting model system for measurement in ionic liquids.

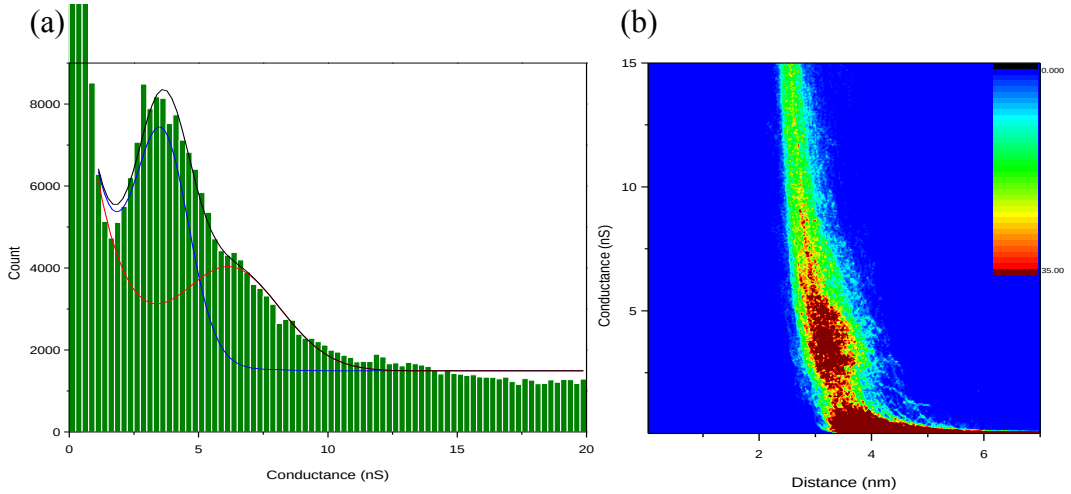


*Figure 7:* I(s) *measurements were performed on 1,2 –bis(4-pyridyl)ethane in BMIM-OTf. 493 scans were collected to form the 1D (a) and 2D (b) histograms shown. The sample bias was 0.6 V, while the set point current was 20 nA*

Pyridyl terminated molecules are an interesting class of molecular wires which allow for measurement of the conductance of short alkyl chains,[43] due to these prospects, the molecular conductance of 1,2-bis(4-pyridyl)ethane in BMIM-OTf was also investigated. A histogram was constructed from over 500 *I*(*s*) traces containing molecular bridge plateaus, allowing the conductance to be determined, **Figure 7**. When investigated in BMIM-OTf, the conductance of 1,2-bis(4-pyridyl)ethane is 3.7 nS, similar to that seen in the literature.[42, 43] The reduced molecular conductance is attributed to the increased molecular length and loss of conjugation through the molecule.[42, 43] The break-off distance of the Au-1,2-bis(4-pyridyl)ethane-Au junctions was found to be (3.5 ± 0.7) nm. From Spartan® calculations performed on this molecule, a break-off distance of 1.41 nm is expected. The raw break-off distance of the 1,2-bis(4-pyridyl)ethane was (1.4 ± 0.3) nm, similar to the molecular length.

6V6

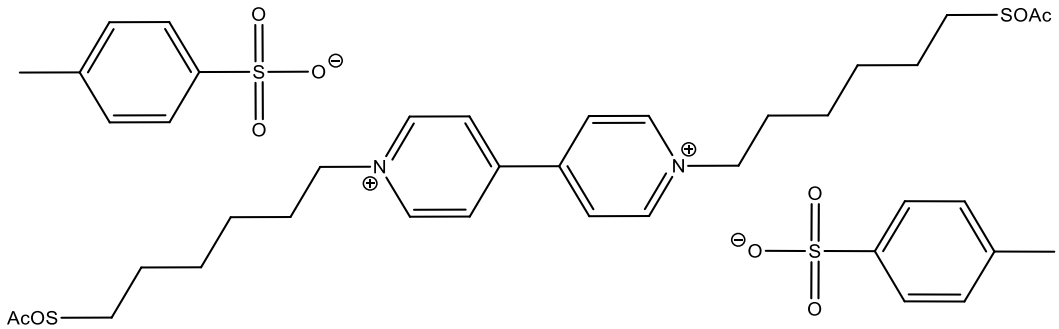


*Figure 8: The structure of 6V6 is shown. 6V6 was by Dr. Carly Brooke. The tosylate cation counters the charge of the viologen core.*

6V6, **Figure 8**, is a redox active organic molecule of interest because of its prospects as a molecular switch. Viologen containing molecules, like 6V6, undergo two reversible electron transfers between a dication and neutral state. The electrochemistry of 6V6 was discussed in depth in **Chapter 3: Electrochemistry in Ionic Liquids**. 6V6 is of particular interest because it has been well studied in the past,[54-57] and was the first molecule investigated by the *I*(*s*) technique.[58] The investigation of the 6V6 molecule in ionic liquid is interesting because it presents the opportunity to look at the effect of both the first and second electron transfers on molecular conductance.

A full monolayer of 6V6 was investigated by the *I*(*s*) technique in BMIM-OTf. 496 molecular plateau containing scans were collected to form the histograms in **Figure 9**. The 1D histogram shown has been fitted with a Lorentzian curve showing the conductance of this system to be 2.15 nS. The break-off distance is measured as (2.06 ± 0.44) nm. The molecular conductance is larger than that expected from the literature for the dication state of this molecule.[58] As the molecule is measured in BMIM-OTf, without electrochemical control the redox state of the molecule cannot be definitively determined. The conductance of the 6V6 molecule, when in the radical cation state, is known to increase to 2.8 nS,[57] similar to that seen here. More likely,

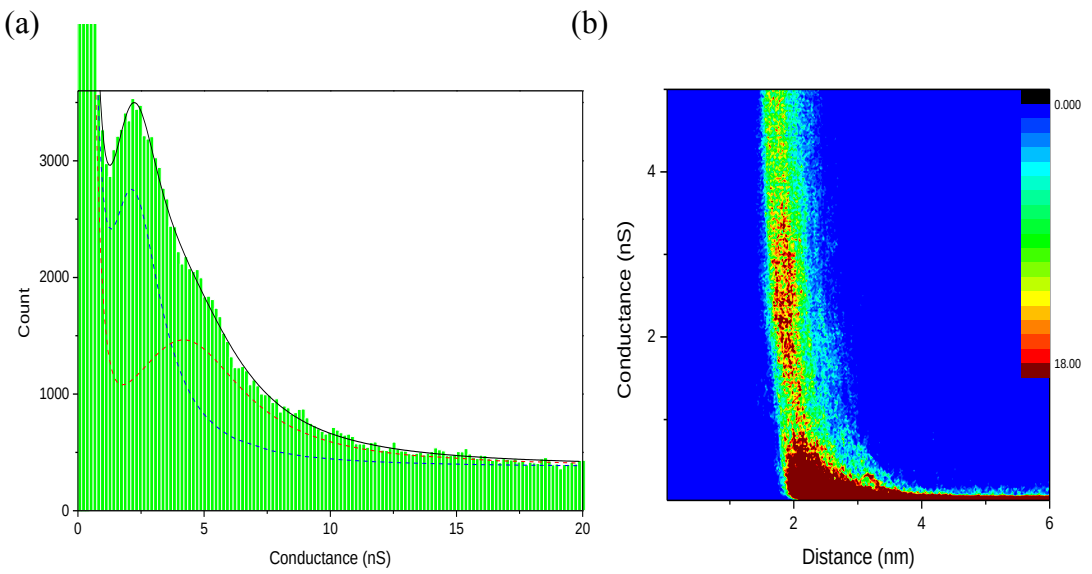


*Figure 9: The* I(s) *technique was used to investigate the single molecule conductance of 6V6 with full monolayer coverage. 496 scans were compiled in the 1D (a) and 2D (b) histograms shown. The sample bias used was 0.6 V, while the set point current was 20 nA.*

however, the lowest conductance group has not been measured. When molecular conductance measurements were performed in ionic liquids the low (A), and medium (B) conductance groups were present.[59] While the ionic liquid study of Kay *et al.*[59] used the break junction to measure the B group, it is possible to measure this group using the *I*(*s*) technique. These two groups arise because of different contact geometries, with A arising when the molecule is bound to two atop sites, whereas the B group arises when the molecules are bound between an atop site, and a step-type site, **Figure 10**.[59] In this case the step-type site can arise from the molecular anchor binding away from the tip apex. Conductance via a group B mechanism is indicated, in part, by the junction length, which is expected to be shorter than the molecular length. When compared to Spartan® calculations, the measured break-off distance is indeed shorter than that expected. The length of the break-off distance cannot be fully explained by the molecular junction forming in a B type configuration, therefore the

molecule is also likely tilted in the junction. High conductance values have been seen by Li *et al.*[55] for the 6V6 system measured by the break junction technique though these are still ~50% of the magnitude measured here. This difference is likely to result from the presence of the complete 6V6 monolayer in the present study, which can alter the conductance due to changes in molecular conformation and charge transfer properties.[60] Theoretical analysis of inelastic tunnelling spectroscopy of coherent tunnelling of molecular bridges showed cooperative effects due to the presence of multiple molecules could occur.[61] Intermolecular interactions within the monolayers measured here may occur. This investigation shows it is possible to measure the conductance of 6V6 in $BMIM^+$ ionic liquids. For direct comparison to the previous aqueous measurements, however, future investigations should be performed using submonolayer coverages.

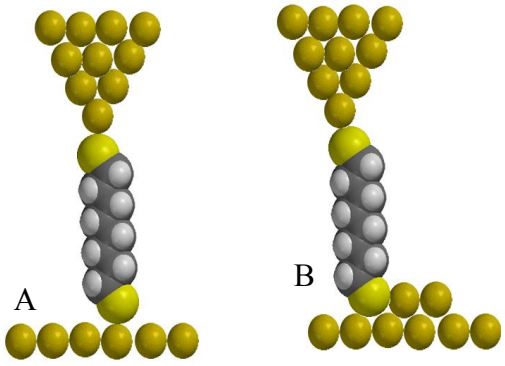


*Figure 10: When the A conductance group is seen the molecule contacts the tip apex, and an atop site. When the B conductance group is seen the molecule is contacted to a single metal atom on one side, and multiple atoms on the other.*

Porphyrin Molecules

Redox active molecules are of particular interest for molecular electronics studies because of their ability to act as conductance switches. Porphyrins, in particular, are of interest because they have well known adaptable chemistry.[62] Furthermore, porphyrins are an electrochemically and thermally stable species.[63, 64]

Even without these attributes, porphyrins are interesting as wires for molecular electronics because of their relatively narrow HOMO-LUMO gap,[63] and the low $\beta$ factor possible with these molecules.[65] The potential of porphyrin molecules has not gone unnoticed. It has been claimed that this class of redox active molecules are a possible commercial alternative for DRAM devices. Investigations of porphyrin molecules as DRAM type devices were published in 2007, with research into the ZettaCore ZettaRAM device.[66] In these molecular electronics devices, porphyrins are desirable because they have traits which allow for lower energy consumption than traditional DRAM devices,[64, 66, 67] including a lack of moving parts,[64] the ability to store information for longer periods,[64, 68] and the higher charge density of the systems.[67] As porphyrin are an exciting class of molecules, a series of these molecules was investigated in $BMIM^+$ containing ionic liquids. Ionic liquids could be of particular interest for investigations of the porphyrins since the porphyrin have an affinity for the Au surface, which may be hindered by an ionic liquid environment.[69] The molecular conductance of three porphyrin molecules, **Figure 1**, provided by Harry Anderson's group, was investigated. The molecules are referred throughout as (1) AcOS-Zn-SOAC, (2) Py-Zn-Py (3) Py-Zn-Py. Since porphyrins hold potential as molecular switches, the electrochemistry of some systems were also investigated.

*Electrochemistry*

The electrochemistry of AcOS-Zn-SOAc and the Py-Ni-Py porphyrins were investigated in BMIM-OTf to determine their redox switching characteristics. Only the oxidation was investigated because the porphyrin cation is more stable than the anion,[68] and therefore, holds the most potential in molecular electronics investigations.

The electrochemical response of a monolayer of AcOS-Zn-SOAc molecule, was recorded. Prior to investigation in BMIM-OTf, this monolayer was investigated

in aqueous phosphate buffer, **Figure 11**. Zn porphyrins, are expected to undergo two oxidations above 0.8 V.[70] Only a single oxidation peak at 1.03 V vs. SCE is seen in cyclic voltammetry which disappears on the reverse. The large reduction peak around 0.45 V vs. SCE is the reduction of the Au surface. The loss of the oxide peak indicates the porphyrin is removed from the Au surface, as had also been observed in previous investigations.[69] When investigated in BMIM-OTf, the resulting electrochemistry was less clear, with ambiguous peaks seen. The electrochemistry shows the AcOS-Zn-SOAc porphyrin is not suitable for measurements investigating the effect of redox switching on conductance.

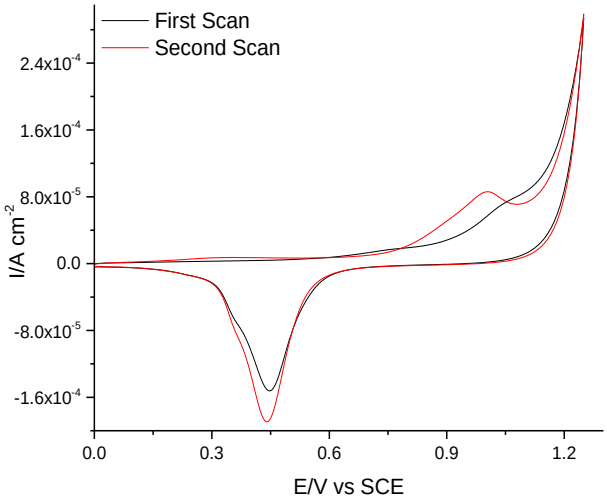


*Figure 11: A AcOS-Zn-SOAc monolayer was measured on a Au(111) bead electrode. Prior to adsorption the S-OAc bond was cleaved. Electrochemistry was performed in 0.025 M potassium phosphate buffer. A SCE RE and Pt mesh CE were used. The electrochemistry changes between the first and second cycle because of the loss of the porphyrin monolayer.*

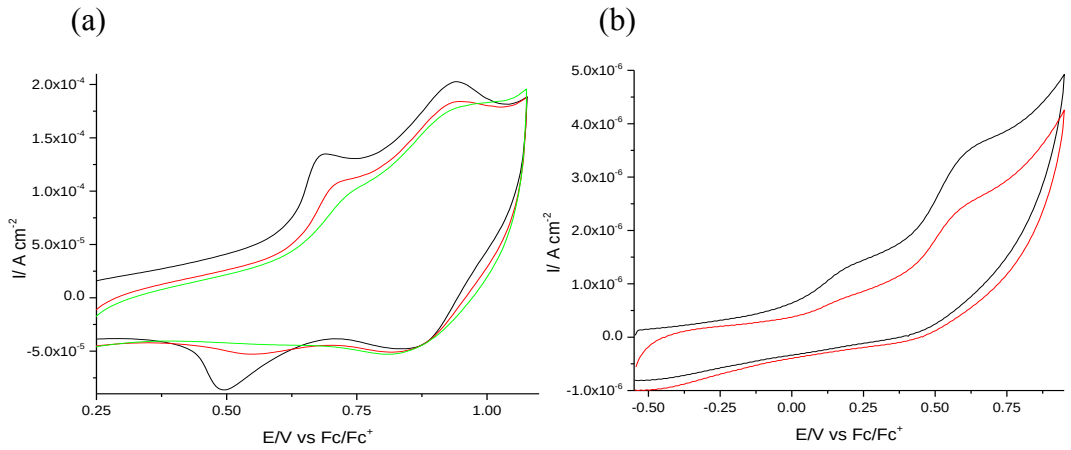


*Figure 12: Py-Ni-Py was investigated as a 0.25 mM solution in both 0.1 M tetrabutyl ammonium hexafluorophosphate (a), and BMIM-OTf (b). Electrochemistry was performed at a Au(111) bead WE, with a Pt wire RE and CE. The electrochemistry was referenced to Fc/Fc$^+$. Both cases show a loss in electrochemical response after the first cycle. This is likely to be a result of the demetallation of the porphyrin ring.*

The solution electrochemistry of the Py-Ni-Py porphyrin molecule was investigated in tetrabutyl ammonium hexafluorophosate in DCM, and in BMIM-OTf, **Figure 12**. In the DCM, two oxidation waves are seen at (0.78 ± 0.10) and (1.1 ± 0.03) V vs. SCE, although the electrochemistry is not stable, with the peak currents decreasing in successive scans. This is likely to result from demetallation of the porphyrin.[71-74] The oxidation peaks in BMIM-OTf, occur at around 0.1 and 0.5 V vs. Fc/Fc$^+$, although these are difficult to determine as the decrease of the peak current occurs faster in BMIM-OTf. The loss of electrochemical activity due to demetallation rules out Py-Ni-Py as a redox active switch.

Although the two porphyrin monomers investigated here show poor electrochemistry, they still hold promise as molecular wires. As porphyrins are interesting molecules regardless of their electrochemical attributes, the single

molecule conductance of the AcOS-Zn-SOAc and Py-Ni-Py molecules was investigated.

*Single Molecule Conductance*

Conductance of the AcOS-Zn-SOAc porphyrin was measured in both BMIM-OTf and BMIM-TFSA. This molecule has been well studied in the past,[21] and because of the thiol linkers is particularly appealing with regards to ease of measurement.

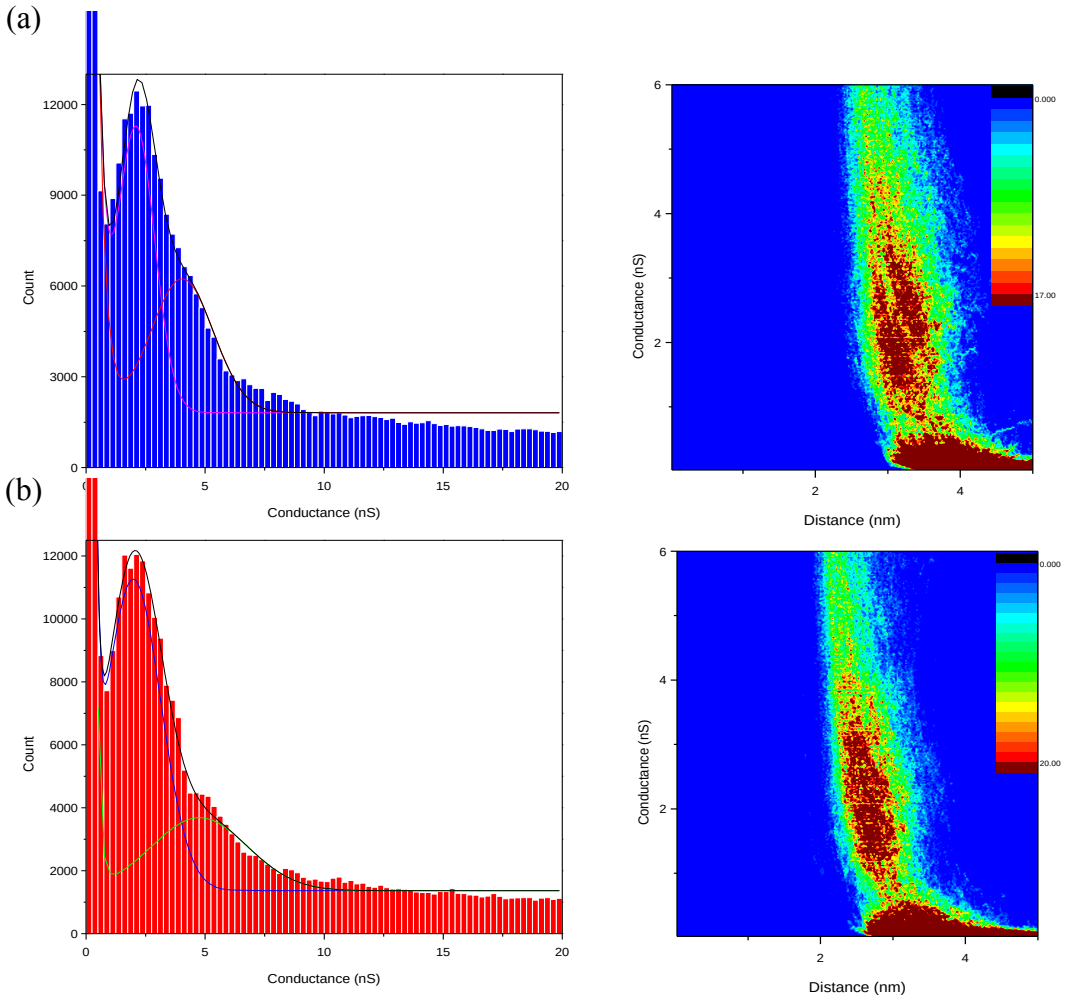


*Figure 13: The AcOS-Zn-SOAc porphyrin was measured by the* I(s) *technique in both BMIM-OTf (a), and BMIM-TFSA (b). The 1D and 2D histograms of AcOS-Zn-SOAc measured in BMIM-OTf were composed of 550 scans, while those of BMIM-TFSA were composed of 549 scans. Both sets of experiments were performed at 0.6 V sample bias, and with a 20 nA set point current.*

Although Gaussian curves fit well to the histograms of these systems, **Figure 13**, for consistency with other measurements, the average value of the conductance histogram peak was used to determine the conductance. In both ionic liquids, AcOS-Zn-SOAc has a conductance of 2.3 nS, which agrees with previously measured values in ambient conditions,[21] implying the molecular conductance is not affected by the anion. When this molecule was investigated under ambient conditions, the addition of an axial ligand, such as pyridine, was necessary to stop the strong porphyrin-Au interaction and allow formation of the molecular junction.[69] In these studies, the use of an axial ligand was unnecessary for successful junction formation. This difference is likely a result of the interaction of the ionic liquid cation with the Au surface.[25, 75, 76] As the cation of the ionic liquid can interact with the Au surface, the sites available for the interaction of the porphyrin molecule with the surface are reduced. Furthermore, as a highly aromatic compound, the porphyrin molecule is well solvated by the ionic liquid, which may also reduce its interaction with the Au surface.[77, 78] The break-off distance of this molecule was (3.5 ± 0.7) nm in BMIM-OTf, and (3.0 ± 0.5) nm in BMIM-TFSA, which is longer than seen in the literature.[79] However, the predicted S-S distance of the AcOS-Zn-SOAc molecule is 2.47 nm,[79] which when combined with the S-Au bond distance gives an expected break-off distance of 3.0 nm.[79] This is consistent with the break-off distance values seen in BMIM-TFSA. It is possible to achieve agreement with break-off seen in BMIM-OTf if it is assumed that during the pulling of the junction, a Au atom is pulled out of both the tip and substrate.[80] However, it should be noted that the $s_0$ value is 0.5 nm larger in BMIM-OTf than in BMIM-TFSA, implying that there may be an overestimation of $s_0$ in BMIM-OTf. Regardless of the cause of the larger break-off in BMIM-OTf over BMIM-TFSA, the break-off distance in ionic liquid is noticeably larger than in ambient conditions. The

increased break-off distance in ionic liquid may arise as a result of a reduced interaction between the porphyrin and Au, allowing the porphyrin to span the junction in an upright orientation. It would be interesting to repeat these experiments with a different ionic liquid cation. The interaction of the ionic liquid with the Au surface can be altered by changing the cation, which may change the interaction of the porphyrin with Au.

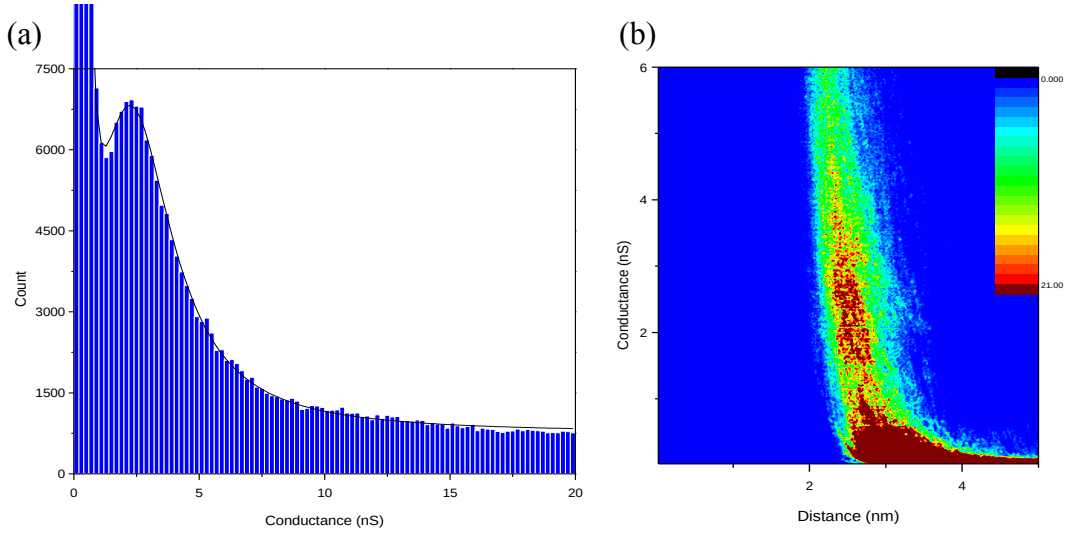


*Figure 14: The 1D (a) and 2D (b) histograms of the* I(s) *measurements of Py-Zn-Py in BMIM-OTf are shown. These histograms are composed of 538 scans. A set point current of 20 nA, and a sample bias of 0.6 V were used.*

The effect of end group on conductance could be investigated by measuring Py-Zn-Py molecule in BMIM-OTf. From the histogram compiled from the *I*(*s*) investigation of this molecule, **Figure 14**, a conductance of 2.3 nS is seen, similar to previous ambient measurements.[65] This means that for this molecule the change in end group from thiol to pyridine does not affect conductance. The break-off distance of the Au-Py-Zn-Py–Au system was found to be (2.8 ± 0.5) nm. This is longer than the N to N distance of this molecule in the literature.[65, 69] While the break-off length is still longer than expected even if the Au-Py bond length is included,[44] it is possible that the

bonding of pyridine pulls Au atoms from the surface during stretching of the junction, increasing the break-off distance. However, as it is known that the Au-Py bonding is not particularly strong is likely the $s_0$ calibration is overestimated.

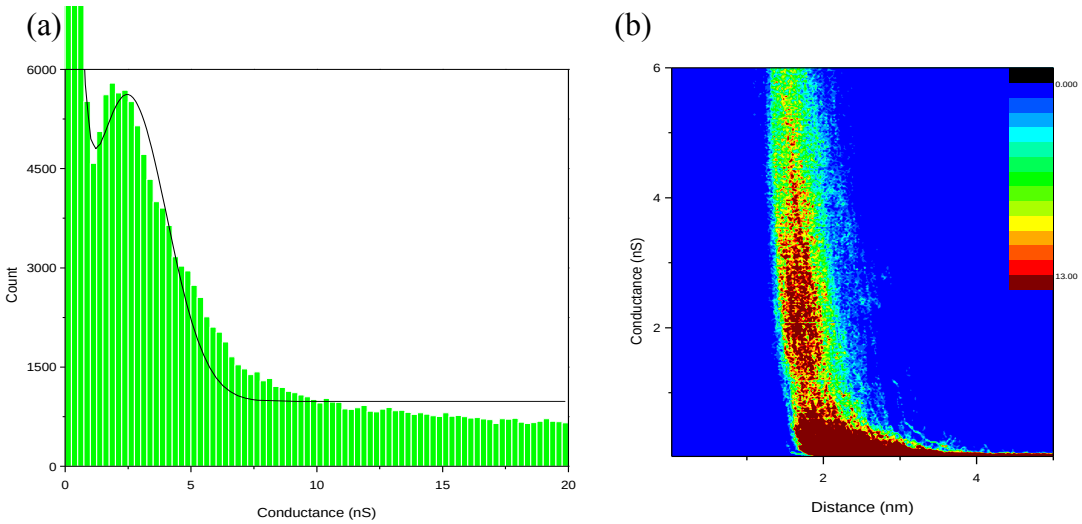


*Figure 15: The conductance of Py-Ni-Py was measured by the* I(s) *technique in BMIM-OTf. Collection of 501 scans allowed the 1D and 2D histograms to be composed. The experiments were performed at 0.6 V sample bias, and 20 nA set point current.*

The porphyrin molecules also allow the effect of changing the metal centre on conductance to be investigated, as this affects the electronic properties of the porphyrin.[63] The *I*(*s*) investigations of the Py-Ni-Py molecule showed the system to have a conductance of 2.2 nS, **Figure 15**, strikingly similar to that seen for the Py-Zn-Py molecule. The similar conductance of the analogous Zn and Ni porphyrins implies the metal centre does not affect the molecular conductance of these porphyrins. This likely occurs because the conductance mechanism is through the aromatic porphyrin frame, completely bypassing the metal centre. Investigations of the conductance of Mn porphyrin showed its molecular conductance is unaffected by the potential of the system, similar to free base porphyrin, which does not contain a metal centre, implying the Mn centre is not involved in conductance.[69] Based on this previous work, it is

unsurprising that going from a Zn to a Ni centre does not noticeably affect the porphyrin molecular conductance. The break-off distance of this system was (1.9 ± 0.4) nm, comparable to that seen for the molecular distance from Spartan® calculations.

By investigating three porphyrin monomers in $BMIM^+$ ionic liquids the molecular conductance of these systems was seen to be unaffected by the anion of the ionic liquid, the anchor group, or the metal centre. The ionic liquid environment, however, was beneficial to these measurements. The use of $BMIM^+$ ionic liquids means axial ligands are unnecessary for the molecular conductance studies of the porphyrin monomers. The improved conductance characteristics of the original porphyrins probably arises as a result of the interaction of the $BMIM^+$ cation with the Au surface, which hinders the strong interaction of the porphyrin with the Au surface. Future experiments with ionic liquids of different cations could allow the relation between porphyrin conductance and ionic liquid to be further elucidated.

## Conclusion

Ionic liquids are an interesting environment for molecular conductance studies. While their use in investigations of the molecular conductance of redox active molecules brings clear benefits, they also hold promise for molecular electronics studies of other molecular wires. The intrinsic characteristics of ionic liquids have shown surprising results. The investigation of bipyridine in $BMIM^+$ ionic liquids highlighted the apparent ability of the ionic liquid to stabilize Au nanowires, leading to longer than expected junctions. Further investigations into this system have been proposed to determine the cause of these extended break-off distance values. Proposed further investigations include examining molecular conductance in ionic liquids with

different cations. BMIM-OTf presents itself as an interesting avenue for future conductance switching measurements on 6V6. By employing ionic liquids, molecular conductance measurements on various porphyrin molecules were possible without the addition of an axial ligand. As with the bipyridine measurements, investigations using ionic liquids with different cations could be enlightening as to the interaction of the ionic liquid with the porphyrin. Although ionic liquids have great possibilities in future molecular electronics studies, more work is needed to determine how they interact with the metal-molecule-metal junctions. To fully understand these interactions the library of ionic liquid environments must be expanded.

## Declaration

*The 6V6 used here was synthesized by Dr. Carly Brooke, of Prof. Higgins' group at the University of Liverpool. All of the porphyrins measured were prepared by members of Prof. Anderson's group at the University of Oxford.*

## References


1. W. Haiss, S. Martin, L. E. Scullion, L. Bouffier, S. J. Higgins and R. J. Nichols, *Physical Chemistry Chemical Physics*, 2009, **11**, 10831-10838.
2. E. Leary, H. Höbenreich, S. J. Higgins, H. van Zalinge, W. Haiss, R. J. Nichols, C. M. Finch, I. Grace, C. J. Lambert, R. McGrath and J. Smerdon, *Physical Review Letters*, 2009, **102**, 086801.
3. V. Fatemi, M. Kamenetska, J. B. Neaton and L. Venkataraman, *Nano Letters*, 2011, **11**, 1988-1992.
4. E. Pires, J. E. Macdonald and M. Elliott, *Nanoscale*, 2013, **5**, 9397-9403.
5. N. J. Kay, R. J. Nichols, S. J. Higgins, W. Haiss, G. Sedghi, W. Schwarzacher and B.-W. Mao, *The Journal of Physical Chemistry C*, 2011, **115**, 21402-21408.
6. N. J. Kay, S. J. Higgins, J. O. Jeppesen, E. Leary, J. Lycoops, J. Ulstrup and R. J. Nichols, *Journal of the American Chemical Society*, 2012, **134**, 16817-16826.
7. N. J. Kay, PhD Thesis, University of Liverpool, 2012.
8. Y. Yang, L. Jun-Yang, C. Zhao-Bin, T. Jing-Hua, J. Xi, L. Bo, L. Xiulan, L. Zhong-Zi, L. Miao, Y. Fang-Zu, T. Nongjian and T. Zhong-Qun, *Nanotechnology*, 2011, **22**, 275313.
9. B. Gotsmann, H. Riel and E. Lörtscher, *Physical Review B*, 2011, **84**, 205408.

10. W. Haiss, C. S. Wang, I. Grace, A. S. Batsanov, D. J. Schiffrin, S. J. Higgins, M. R. Bryce, C. J. Lambert and R. J. Nichols, *Nature Materials*, 2006, **5**, 995-1002.
11. W. Hong, D. Z. Manrique, P. Moreno-García, M. Gulcur, A. Mishchenko, C. J. Lambert, M. R. Bryce and T. Wandlowski, *Journal of the American Chemical Society*, 2012, **134**, 2292-2304.
12. T. Hines, I. Diez-Perez, J. Hihath, H. Liu, Z.-S. Wang, J. Zhao, G. Zhou, K. Müllen and N. Tao, *Journal of the American Chemical Society*, 2010, **132**, 11658-11664.
13. P. D. Williams and M. G. Reuter, *The Journal of Physical Chemistry C*, 2013, **117**, 5937-5942.
14. C. Li, I. Pobelov, T. Wandlowski, A. Bagrets, A. Arnold and F. Evers, *Journal of the American Chemical Society*, 2007, **130**, 318-326.
15. S.-Y. Jang, P. Reddy, A. Majumdar and R. A. Segalman, *Nano Letters*, 2006, **6**, 2362-2367.
16. M. G. Reuter, M. C. Hersam, T. Seideman and M. A. Ratner, *Nano Letters*, 2012, **12**, 2243-2248.
17. J. S. Meisner, M. Kamenetska, M. Krikorian, M. L. Steigerwald, L. Venkataraman and C. Nuckolls, *Nano Letters*, 2011, **11**, 1575-1579.
18. M. Paulsson, C. Krag, T. Frederiksen and M. Brandbyge, *Nano Letters*, 2009, **9**, 117-121.
19. M. Kamenetska, M. Koentopp, A. C. Whalley, Y. S. Park, M. L. Steigerwald, C. Nuckolls, M. S. Hybertsen and L. Venkataraman, *Physical Review Letters*, 2009, **102**, 126803.
20. T. A. Su, J. R. Widawsky, H. Li, R. S. Klausen, J. L. Leighton, M. L. Steigerwald, L. Venkataraman and C. Nuckolls, *Journal of the American Chemical Society*, 2013, **135**, 18331-18334.
21. G. Sedghi, K. Sawada, L. J. Esdaile, M. Hoffmann, H. L. Anderson, D. Bethell, W. Haiss, S. J. Higgins and R. J. Nichols, *Journal of the American Chemical Society*, 2008, **130**, 8582-8583.
22. S. Martín, W. Haiss, S. Higgins, P. Cea, M. C. López and R. J. Nichols, *The Journal of Physical Chemistry C*, 2008, **112**, 3941-3948.
23. L. M. Ballesteros, S. Martín, G. Pera, P. A. Schauer, N. J. Kay, M. a. C. López, P. J. Low, R. J. Nichols and P. Cea, *Langmuir*, 2011, **27**, 3600-3610.
24. R. Atkin, S. Z. E. Abedin, R. Hayes, L. H. S. Gasparotto, N. Borisenko and F. Endres, *The Journal of Physical Chemistry C*, 2009, **113**, 13266-13272.
25. A. P. Abbott and K. J. McKenzie, *Physical Chemistry Chemical Physics*, 2006, **8**, 4265-4279.
26. B. Uhl, F. Buchner, D. Alwast, N. Wagner and R. J. Behm, *Beilstein Journal of Nanotechnology*, 2013, **4**, 903-918.
27. T. Waldmann, H.-H. Huang, H. E. Hoster, O. Höfft, F. Endres and R. J. Behm, *ChemPhysChem*, 2011, **12**, 2565-2567.
28. F. Chen, X. Li, J. Hihath, Z. Huang and N. Tao, *Journal of the American Chemical Society*, 2006, **128**, 15874-15881.
29. U. B. Steiner, W. R. Caseri and U. W. Suter, *Langmuir*, 1992, **8**, 2771-2777.
30. M. Kiguchi, S. Miura, K. Hara, M. Sawamura and K. Murakoshi, *Applied Physics Letters*, 2006, **89**, 213104.
31. S. Saito, T. Maeda, T. Soumura and K. Takeda, *Applied Surface Science*, 1988, **33–34**, 1088-1093.

32. M. Uda, A. Nakamura, T. Yamamoto and Y. Fujimoto, *Journal of Electron Spectroscopy and Related Phenomena*, 1998, **88–91**, 643-648.
33. B. Xu and N. J. Tao, *Science*, 2003, **301**, 1221-1223.
34. Y. Yang, Z. Chen, J. Liu, M. Lu, D. Yang, F. Yang and Z. Tian, *Nano Res.*, 2011, **4**, 1199-1207.
35. M. Frei, S. V. Aradhya, M. Koentopp, M. S. Hybertsen and L. Venkataraman, *Nano Letters*, 2011, **11**, 1518-1523.
36. Z. Liu, S. Y. Ding, Z. B. Chen, X. Wang, J. H. Tian, J. R. Anema, X. S. Zhou, D. Y. Wu, B. W. Mao, X. Xu, B. Ren and Z. Q. Tian, *Nat. Commun.*, 2011, **2**.
37. T. Konishi, M. Kiguchi, M. Takase, F. Nagasawa, H. Nabika, K. Ikeda, K. Uosaki, K. Ueno, H. Misawa and K. Murakoshi, *Journal of the American Chemical Society*, 2012, **135**, 1009-1014.
38. M. Futamata, *The Journal of Physical Chemistry B*, 2001, **105**, 6933-6942.
39. H. Grönbeck, A. Curioni and W. Andreoni, *Journal of the American Chemical Society*, 2000, **122**, 3839-3842.
40. C. D. Bain, H. A. Biebuyck and G. M. Whitesides, *Langmuir*, 1989, **5**, 723-727.
41. W. Wang, L. Takhee and M. A. Ratner, in *Nano and Molecular Electronics Handbook*, ed. S. E. Lyshevski, CRC Press, Taylor & Francis Group, Editon edn., 2007, pp. 1:1-1:41.
42. Z. Xiao-Yi, P. Zheng-Lian, S. Yan-Yan, W. Li-Na, N. Zhen-Jiang and Z. Xiao-Shun, *Nanotechnology*, 2013, **24**, 465204.
43. X.-S. Zhou, Z.-B. Chen, S.-H. Liu, S. Jin, L. Liu, H.-M. Zhang, Z.-X. Xie, Y.-B. Jiang and B.-W. Mao, *The Journal of Physical Chemistry C*, 2008, **112**, 3935-3940.
44. H. Shimin, Z. Jiaxing, L. Rui, N. Jing, H. Rushan, S. Ziyong, Z. Xingyu, X. Zenquan and W. Quande, *Nanotechnology*, 2005, **16**, 239.
45. S. Martín, I. Grace, M. R. Bryce, C. Wang, R. Jitchati, A. S. Batsanov, S. J. Higgins, C. J. Lambert and R. J. Nichols, *Journal of the American Chemical Society*, 2010, **132**, 9157-9164.
46. L.-L. Lin, J.-C. Leng, X.-N. Song, Z.-L. Li, Y. Luo and C.-K. Wang, *The Journal of Physical Chemistry C*, 2009, **113**, 14474-14477.
47. N. A. Kautz and S. A. Kandel, *Journal of the American Chemical Society*, 2008, **130**, 6908-6909.
48. Y.-M. Wei, J.-H. Liang, Z.-B. Chen, X.-S. Zhou, B.-W. Mao, O. A. Oviedo and E. P. M. Leiva, *Physical Chemistry Chemical Physics*, 2013, **15**, 12459-12465.
49. A. Podgoršek, A. S. Pensado, C. C. Santini, M. F. Costa Gomes and A. A. H. Pádua, *The Journal of Physical Chemistry C*, 2013, **117**, 3537-3547.
50. A. Banerjee, R. Theron and R. W. J. Scott, *ChemSusChem*, 2012, **5**, 109-116.
51. A. S. Pensado and A. A. H. Pádua, *Angewandte Chemie International Edition*, 2011, **50**, 8683-8687.
52. E. Vanecht, K. Binnemans, S. Patskovsky, M. Meunier, J. W. Seo, L. Stappers and J. Fransaer, *Physical Chemistry Chemical Physics*, 2012, **14**, 5662-5671.
53. E. Redel, M. Walter, R. Thomann, L. Hussein, M. Kruger and C. Janiak, *Chemical Communications*, 2010, **46**, 1159-1161.
54. B. Han, Z. Li, T. Wandlowski, A. Błaszczyk and M. Mayor, *The Journal of Physical Chemistry C*, 2007, **111**, 13855-13863.
55. Z. Li, B. Han, G. Meszaros, I. Pobelov, T. Wandlowski, A. Blaszczyk and M. Mayor, *Faraday Discussions*, 2006, **131**, 121-143.

56. Z. H. Li, I. Pobelov, B. Han, T. Wandlowski, A. Blaszczyk and M. Mayor, *Nanotechnology*, 2007, **18**.
57. W. Haiss, T. Albrecht, H. van Zalinge, S. J. Higgins, D. Bethell, H. Höbenreich, D. J. Schiffrin, R. J. Nichols, A. M. Kuznetsov, J. Zhang, Q. Chi and J. Ulstrup, *The Journal of Physical Chemistry B*, 2007, **111**, 6703-6712.
58. W. Haiss, H. van Zalinge, S. J. Higgins, D. Bethell, H. Höbenreich, D. J. Schiffrin and R. J. Nichols, *Journal of the American Chemical Society*, 2003, **125**, 15294-15295.
59. W. Haiss, S. Martín, E. Leary, H. v. Zalinge, S. J. Higgins, L. Bouffier and R. J. Nichols, *The Journal of Physical Chemistry C*, 2009, **113**, 5823-5833.
60. E. Wierzbinski, R. Venkatramani, K. L. Davis, S. Bezer, J. Kong, Y. Xing, E. Borguet, C. Achim, D. N. Beratan and D. H. Waldeck, *ACS Nano*, 2013, **7**, 5391-5401.
61. M. Galperin and A. Nitzan, *The Journal of Physical Chemistry B*, 2012, **117**, 4449-4453.
62. M. L. Perrin, F. Prins, C. A. Martin, A. J. Shaikh, R. Eelkema, J. H. van Esch, T. Briza, R. Kaplanek, V. Kral, J. M. van Ruitenbeek, H. S. J. van der Zant and D. Dulić, *Angewandte Chemie International Edition*, 2011, **50**, 11223-11226.
63. M. Jurow, A. E. Schuckman, J. D. Batteas and C. M. Drain, *Coordination Chemistry Reviews*, 2010, **254**, 2297-2310.
64. J. S. Lindsey and D. F. Bocian, *Accounts of Chemical Research*, 2011, **44**, 638-650.
65. G. Sedghi, V. M. Garcia-Suarez, L. J. Esdaile, H. L. Anderson, C. J. Lambert, S. Martin, D. Bethell, S. J. Higgins, M. Elliott, N. Bennett, J. E. Macdonald and R. J. Nichols, *Nature Nanotechnology*, 2011, **6**, 517-523.
66. R. K. Venkatesan, A. S. Al-Zawawi, K. Sivasubramanian and E. Rotenberg, *IEEE Transactions on Computers*, 2007, **56**, 147-160.
67. B. De Salvo, J. Buckley and D. Vuillaume, *Current Applied Physics*, 2011, **11**, E49-E57.
68. K. M. Roth, N. Dontha, R. B. Dabke, D. T. Gryko, C. Clausen, J. S. Lindsey, D. F. Bocian and W. G. Kuhr, *Journal of Vacuum Science & Technology B*, 2000, **18**, 2359-2364.
69. G. Sedghi, PhD Thesis, University of Liverpool, 2010.
70. J. A. Hodge, M. G. Hill and H. B. Gray, *Inorganic Chemistry*, 1995, **34**, 809-812.
71. S. Baranton, C. Coutanceau, C. Roux, F. Hahn and J. M. Leger, *Journal of Electroanalytical Chemistry*, 2005, **577**, 223-234.
72. J. R. Fish, E. Kubaszewski, A. Peat, T. Malinski, J. Kaczor, P. Kus and L. Czuchajowski, *Chemistry of Materials*, 1992, **4**, 795-803.
73. E. do Nascimento, G. D. Silva, F. A. Caetano, M. A. M. Fernandez, D. C. da Silva, M. de Carvalho, J. M. Pernaut, J. S. Reboucas and Y. M. Idemori, *Journal of Inorganic Biochemistry*, 2005, **99**, 1193-1204.
74. M. Kumar, P. Neta, T. P. G. Sutter and P. Hambright, *The Journal of Physical Chemistry*, 1992, **96**, 9571-9575.
75. R. Fukui, Y. Katayama and T. Miura, *Electrochimica Acta*, 2011, **56**, 1190-1196.
76. Y. Katayama, R. Fukui and T. Miura, *Journal of the Electrochemical Society*, 2007, **154**, D534-D537.
77. J. D. Holbrey, W. M. Reichert, M. Nieuwenhuyzen, O. Sheppard, C. Hardacre and R. D. Rogers, *Chemical Communications*, 2003, 476-477.

78. C. G. Hanke, A. Johansson, J. B. Harper and R. M. Lynden-Bell, *Chemical Physics Letters*, 2003, **374**, 85-90.
79. K. Seo, A. V. Konchenko, J. Lee, G. S. Bang and H. Lee, *Journal of the American Chemical Society*, 2008, **130**, 2553-2559.
80. G. E. Poirier and M. J. Tarlov, *Langmuir*, 1994, **10**, 2853-2856.

**University of Liverpool**

**Department of Chemistry**


# Contact and Medium Effects on Molecular Electronics

## Volume 2

Thesis submitted in accordance with the requirements of the University of Liverpool for the degree of Doctor of Philosophy

By

Samantha Catarelli

# Contents

# Chapter 5:

# Co

# Deposition

# from Ionic

# Liquids

# Introduction

Molecular spintronics is an exciting field still in its infancy. Unfortunately the ferromagnetic metals used in spintronics, Co, Ni and Fe, are quickly oxidized in ambient conditions. For progress to be made in the field of molecular spintronics a means of forming the oxide free metallic contacts, allowing measurements in standard laboratory conditions must be established. A one pot STM method would allow formation of these contacts without exposure to ambient conditions, while still allowing molecular conductance measurements to be performed. In this, the metal of interest is plated onto the STM substrate and tip from a solution containing both the metal ion and the molecule of interest. **Figure 1** depicts a schematic of such a setup**.** Performance of the deposition in the STM, severely limits the electrolyte solvents because of the need to be a low vapour pressure solvent so as not to destroy the STM electronics. An exciting environment which can be used is ionic liquids. Room temperature ionic liquids are of relatively high conductivity,[1-5] but unlike organic electrolytes, they have low vapour pressure.[3-6] Furthermore, ionic liquids present their own advantages for metal deposition.

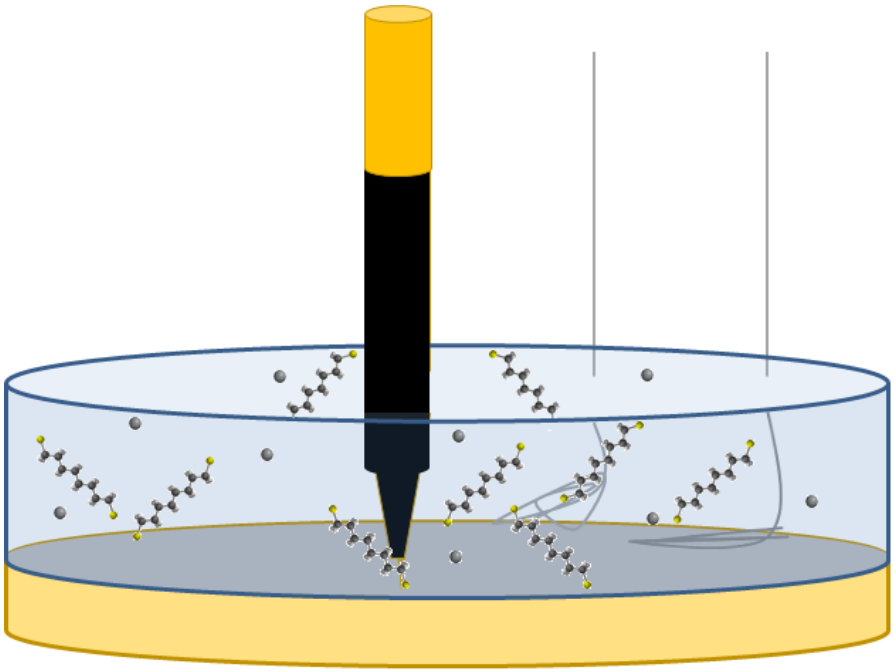

*Figure 1: The prospect of a one-pot technique to measure single molecule spintronics in the STM was investigated. To perform a one-pot spintronics experiment an ionic liquid environment would be used with both the metal complex and the molecular wire of interest present. This setup would allow for the in-situ electrodeposition of the metal followed by molecular conductance measurements. Prior to starting these investigations the ex-situ electrodeposition of Co was first investigated.*

Ionic Liquids for Electrodeposition

Many of the characteristics making ionic liquids advantageous in electrodeposition are the same as those which give rise to their benefits in electrochemistry. Aside from their high intrinsic conductivity,[2, 5, 7, 8] ionic liquids also have a large electrochemical window.[1-4, 7, 9-12] The wide electrochemical window arises in part because of the lack of hydrogen evolution, making ionic liquids advantageous for electrodeposition.[1-4, 7, 9-12] Hydrogen evolution can cause the incorporation of hydrogen into the metal deposit causing hydrogen embrittlement and therefore it is beneficial to avoid. Moreover, ionic liquids display a higher thermal stability than the traditional electrodeposition electrolytes, which allows higher

temperature deposition to improve the diffusion of the ions to the surface causing high quality deposits.[1, 2, 6, 10, 11] Finally, in aqueous plating baths the electrolytes often contain toxic ions such as cyanide. Ionic liquids remove the need for such toxic ions, resulting in more user friendly plating baths. It should be noted, however, that full toxicity and life cycle analyses have not been performed on most ionic liquids.[8]

Co Deposition from Aqueous Electrolyte

The electrodeposition of Co from aqueous electrolyte is a well-established process of particular interest. Through selection of the electrolyte, Co concentration, pH, and overpotential the structure of the Co deposit can be controlled. Previous studies performed on Au are of particular interest. When working with aqueous electrolytes hydrogen evolution must be accounted for. Cyclic voltammetry has shown the onset potential of bulk deposition with respect to hydrogen evolution is dependent on the electrolyte used.[13] Furthermore cyclic voltammetry demonstrates that Co bulk electrodeposition on gold occurs concomitantly with hydrogen evolution. Co UPD can also occur on gold.[14] Potentiostatic investigations of electrochemical deposition of Co onto Au, have been used in tandem with cyclic voltammetry. By fitting the resulting current transients the nucleation and growth mechanism of Co deposition is shown to be dependent on the identity of the substrate.[14, 15, 17-19] In the case of Au, at least, the substrate crystallinity does not affect the nucleation mechanism.[19] When fitting the current transients, it is often the two basic "opposing" nucleation models, instantaneous and progressive nucleation, which are explored. However, these "extremes" do not always adequately describe the system. Indeed, for a series of Co electrodeposition on Au experiments, Mendoza-Huizar *et al.*[15] saw a description incorporating contributions from both nucleation types, could better describe Co deposition from an aqueous $CoCl_2/NH_4Cl$ electrolyte. The use of electrochemical

analysis to investigate the processes occurring during electrodeposition is an invaluable stepping stone for more in depth studies on the deposition process.

Co Deposition from Ionic Liquids

The deposition of Co from aqueous electrolytes is limited by hydrogen evolution which can lead to poor quality deposits. The use of ionic liquids, however, can eliminate the deleterious effects of hydrogen evolution, and as such are an active area of research. A handful of published investigations on the electrodeposition of Co from ionic liquid electrolytes exist. Investigations of Co deposition, using ionic liquids, began in the 1980s with the use of first generation chloroaluminate ionic liquids. Although voltammetry and EC-STM show that Co deposition in ionic liquids occurs in a similar manner as from aqueous electrolyte, the $AlCl_3$ species of these molten salts causes problems. If the deposition potential or the ratio of Co species is not carefully chosen, then co-deposition of Al with Co occurs.[20, 21] This is also an issue when $ZnCl_2$ molten salts are used.[6] In these investigations the quality of the resulting deposit was dependent on the system potential, with better, silver coloured deposits formed at more negative deposition potentials.[6] While this gives a good finish, the improved crystallinity is due to increased Zn content, which is undesirable if pure Co deposits are the target. These metal chloride molten salts can also be formulated such that the Co species for deposition is present on the inorganic ion of the salt. When a $CoCl_2$-N-(n-butyl)pyridinium chloride ($CoCl_2$-BPC) solution was used, it was found that controlling the ratio of the Co:BPC controls the Co complex species.[22] Increasing the BPC content relative to the Co content decreases the Co:Cl ratio. This changes the Co ligation from $CoCl_3^-$ to the electroinactive $CoCl_4$, changing the deposit quality. In this case, a bright deposit is achieved if a molten salt of 1:1 Co:BPC composition is used.[20] Although first generation ionic liquids have successfully been used for Co

deposition, these molten salts are very difficult to work with. Unlike the current generation of ionic liquids, the chloroaluminates are extremely hydrophilic, with their advantageous qualities easily ruined by ambient conditions.[8] Furthermore, the alloy deposits which can result in deposits from these solutions is often not desirable. Nowadays, the non-chloroaluminate ionic liquids are most often used.

Starting in the mid to late 2000s, modern non-chloroaluminate ionic liquids have been investigated for use in Co deposition. Although the cation of choice tends to be the 1-butyl-3-methylimidazolium ion,[2, 4, 5, 7] the 1-butyl-1-methylpyrrolidinium ion is also used.[1, 3, 10] These cations have been employed in conjunction with the $TFSA^-$, $OTf^-$, $BF_4^-$, and $PF_6^-$ anions, with varying degrees of success. Using XPS or XRD the deposits formed from Co baths of BMP-TFSA and BMIM-Cl were seen to contain metallic Co.[1, 3] Purely metallic Co does not necessarily signal a high quality deposit. For instance, the deposit from BMP-TFSA is purely metallic Co, but appears shiny and grey.[3] There are only two reports of mirror-like Co deposits from non-haloaluminate ionic liquids. These mirror-like deposits were formed from a $Co(BF_4)_2$ in BMIM-$BF_4$ bath at 60 °C,[2] and a Co(TFSA) in BMP-TFSA bath at 200 °C.[1]

Based on the literature, a few trends are readily apparent in using ionic liquids to deposit Co. The cation should be either $BMP^+$ or $BMIM^+$. $BMIM^+$ is used as these ionic liquids are amongst the least hydrophilic. $BMP^+$ is used because of its high stability against cathodic breakdown.[23] The commercially available $CoCl_2$ complex, which is widely deployed in aqueous electrodeposition, is often used. The initial Co species is very important as this affects the resulting coordination environment, and therefore, the ability for electrodeposition, particularly as some are not electrochemically active.[22] Due to the inactivity of some Co species, the voltammetry of the system should be investigated before deposition is attempted. Finally, it has

been seen that the temperature of the plating bath is imperative. Lower temperatures can cause poor or even non-existent electrodeposits. When the temperature is elevated, as high as 200 °C, higher quality deposits can be achieved. These trends are accounted for in the current investigation of Co deposition from ionic liquid, with the most promising parameters used.

## Aim

The electrodeposition of Co was investigated with the ultimate aim of forming a one-pot molecular spintronic measurement technique. As Co is an easily oxidisable metal, ionic liquids, which can protect the Co from oxidation and which do not exhibit hydrogen evolution, are investigated as potential electrolytes for deposition. Before one-pot molecular spintronics measurements can be implemented, the ability to electrodeposit Co from an ionic liquid must be assessed. This work was performed with the aforementioned aim, with the ability of BMIM-TFSA, BMIM-OTf, and BMIM-$PF_6$ to act as switchable electrolytes assessed.

## Methods

### Cyclic Voltammetry of Co Plating

Cyclic voltammetry was performed using an Autolab PGSTAT30 computer controlled potentiostat. A small capacity 3 electrode cell composed of an Arrandee$^{TM}$ Au(111) slide working electrode and a Pt wire quasi-reference and counter electrode, was used for all voltammetry, unless otherwise stated. The systems were all referenced with respect to the $Fc/Fc^+$ couple. Electrolytes consisting of 0.23 M $CoCl_2$ in BMIM-TFSA, BMIM-OTf, and BMIM-$PF_6$ were prepared in a nitrogen atmosphere glovebox. $CoCl_2$ was first dissolved in a minimal amount of methanol, and added to the ionic liquid of choice. Originally the BMIM-TFSA was used as received from

Iolitec and the whole solution dried for a minimum of 2 hours at ~100 °C with nitrogen bubbling directly in to solution.[24] The eventual method used was to prepare the solution from ionic liquids, which had been dried for 18 hours under vacuum with heating at 120 °C. This was followed with further drying of the resulting solutions for 30 minutes after any colour change.

Electroplating of Co

Co electroplating was achieved using an Autolab PGSTAT30 computer controlled potentiostat with GPES software. Plating was carried out at 90 °C between -0.75 and -0.95 V and stopped at a charge of 60 mC. A sealed three electrode cell, which was setup within the nitrogen atmosphere glovebox, was used. For all temperatures, Pt wire quasi-reference and counter electrodes, were used. For all but the high temperature experiments, (≥ 150°C) a Au Arrandee$^{TM}$ slide, prepared by cleaning with piranha solution, followed by flame annealing, was used. The surface area of the exposed Au was 0.38 cm$^2$. The high temperature experiments used a Au wire, and terminated at a charge of 19 mC. The temperature of the experiment was controlled by placing the base of the sealed cell in an oil bath.

## Models of *i-t* Characteristics

Metal nucleation can occur in an instantaneous manner following a potential step, in which all the nuclei are formed at the same time, or a progressive manner, with the nuclei forming throughout the process. The growth of the metal centres may occur in a 2D or a 3D manner. The overall nucleation process can be determined by fitting the normalized current transient. For 2D growth, the current transient is plotted as $(i/i_m)$ as a function of $(t/t_m)$, where $i_m$ and $t_m$ are the maximum current and the time at which this occurs. This is then fitted with the following equations:[14]

$$\frac{i}{i_m} = \left(\frac{t}{t_m}\right) \exp\left[-\frac{1}{2}\left\{\frac{t^2 - t_m^2}{t_m^2}\right\}\right] \quad \textit{(Eq. 1)}$$

For the 2D instantaneous nucleation.

$$\frac{i}{i_m} = \left(\frac{t}{t_m}\right)^2 \exp\left[-\frac{2}{3}\left\{\frac{t^3 - t_m^3}{t_m^3}\right\}\right] \textit{(Eq. 2)}$$

For 2D progressive nucleation.

When investigating 3D growth mechanisms $(i/i_m)^2$ is plotted as function of $(t/t_m)$. This can then be fitted using the instantaneous and progressive nucleation equations.[15] 3D instantaneous nucleation is given by:

$$\left(\frac{i}{i_m}\right)^2 = \frac{1.9542}{\left(\frac{t}{t_m}\right)}\left\{1 - \exp\left[-1.2564\left(\frac{t}{t_m}\right)\right]\right\}^2 \quad \textit{(Eq. 3)}$$

Whereas 3D progressive nucleation is given by:

$$\left(\frac{i}{i_m}\right)^2 = \frac{1.2254}{\left(\frac{t}{t_m}\right)}\left\{1 - \exp\left[-2.3367\left(\frac{t}{t_m}\right)^2\right]\right\}^2 \textit{(Eq. 4)}$$

Using these four equations, and appropriate plots the nucleation mechanism of the system can be determined.

## Results and Discussion

The deposition of Co from ionic liquid was pursued from $CoCl_2$ in BMIM-TFSA, BMIM-OTf, and BMIM-$PF_6$ (see molecular structures presented **Figure 2**) with the aim of achieving thick mirror-like deposits of Co on Au(111). The $BMIM^+$ cation is common to all 3 ionic liquids and was chosen specifically for the hydrophilic nature of the ionic liquids. Varying the anion not only affects the solubility of the $CoCl_2$ in the ionic liquid, but also influences the conductivity and viscosity of the ionic

liquid as well.[25] When used at elevated temperature, these ionic liquids worked with varying success, although none repeatedly achieving high quality Co deposits.

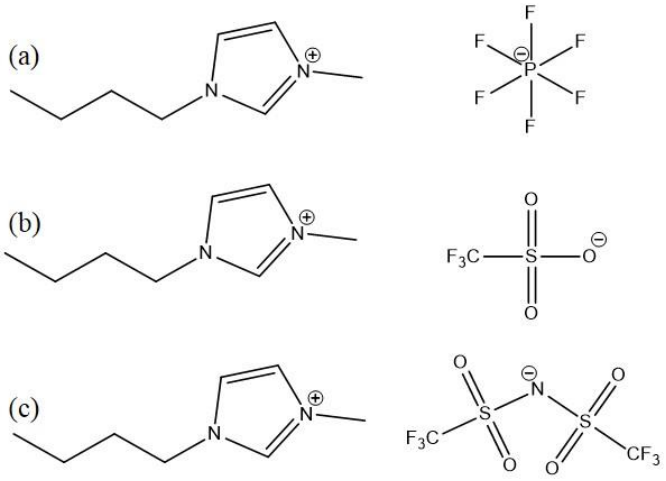


*Figure 2: Three ionic liquids were investigated as electrolytes in Co electrodeposition. These are (a) BMIM-$PF_6$, (b) BMIM-OTf, and (c) BMIM-TFSA.*

<u>BMIM-TFSA</u>

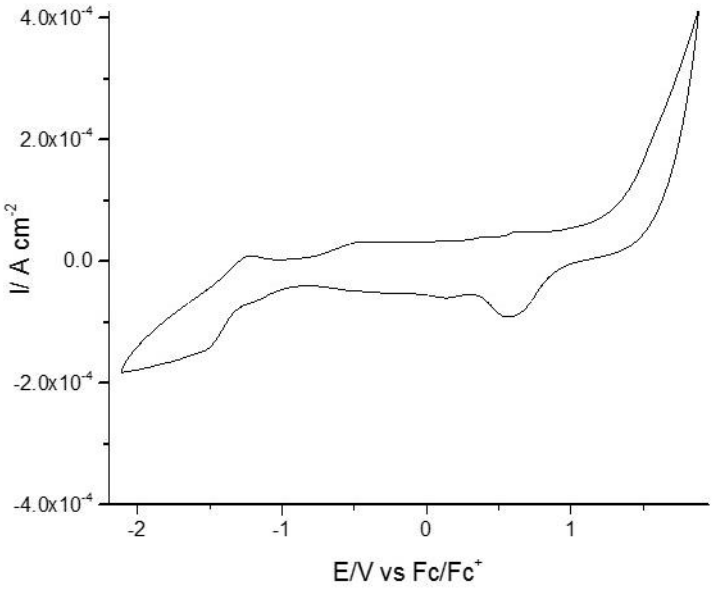


*Figure 3: The electrochemistry of BMIM-TFSA was investigated at a Au(111) Arrandee™ working electrode. The reference and counter electrodes were both Pt wire, with potential referenced to the $Fc/Fc^+$ couple. The scan rate was 0.1 V $s^{-1}$.*

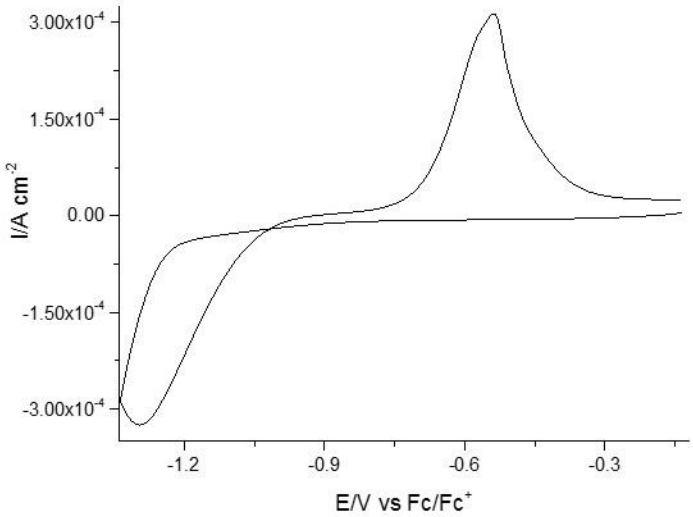


*Figure 4: The electrochemistry of 0.23 M $CoCl_2$ in BMIM-TFSA was investigated at a Au(111) Arrandee™ electrode, at a scan rate of 0.1 V $s^{-1}$. The counter and reference electrodes were both Pt wire. The stripping peak shows a coverage of 0.85 ML.*

BMIM-TFSA was the primary ionic liquid used for the deposition of Co from a 0.23 M $CoCl_2$ solution. **Figure 3** shows the voltammetry of neat BMIM-TFSA. The voltammetry demonstrates an electrochemical window of at least 3 V for BMIM-TFSA, in agreement with the literature.[25, 26] Before any deposition experiments were undertaken, the voltammetry of the $CoCl_2$ in BMIM-TFSA was investigated to determine if deposition could occur under the conditions used. These experiments were initially carried out with a Pt or Co quasi-reference electrode and a Co counter electrode. The resulting voltammogram is shown in **Figure 4**. In these initial experiments, a Co counter electrode was used to counteract the counter electrode dissolution which can occur in deposition experiments. This counter electrode dissolution is exacerbated by the use of ionic liquids which can remove passivating layers.[27] It is also possible that there is some dissolution of quasi-reference electrode, and indeed it was difficult to maintain the stability of the Co reference. In the Co deposition voltammetry the bulk deposition and stripping peaks occur at -1.30 and -0.54 V vs $Fc/Fc^+$, respectively. Integration of the stripping peak shows that 0.85

monolayers are deposited. A nucleation loop, indicative of the nucleation of Co on the Au surface was also seen.[28]

Ionic Liquid Drying Technique

Initial investigations of the deposition of Co from BMIM-TFSA, were performed after the ionic liquid was dried with the sweeping technique developed by Ren *et al.*,[24] which is reportedly as efficient at reducing the water and solvent content as the traditional vacuum drying technique, with the benefit of a much reduced time of 2 hours. In this technique, nitrogen is bubbled into the ionic liquid bringing the solvent molecules to the surface to evaporate off, this leads to the much faster drying time. It should be noted that this drying technique was employed after the $CoCl_2$ and the methanol were added to the ionic liquid. While the initial solution was a clear, deep blue, after 2 hours of drying the solution was an opaque and light blue colour. The subsequently electrodeposited cobalt exhibited a poor surface finish. As this drying technique never resulted in a high quality Co deposit, the conventional vacuum drying technique was used, in which the ionic liquid is dried under vacuum for 18 hours at 120 °C. The BMIM-TFSA was initially dried over 3 Å molecular sieves, although this step was omitted at a later stage. The methanol used as a carrier solvent was also distilled, and the $CoCl_2$, though anhydrous and stored in the glovebox, was further dried overnight at 120 °C and under nitrogen. Although methanol aids the solubility of the $CoCl_2$ in BMIM-TFSA, its presence can lead to a reduced potential window of the ionic liquid and ultimate hydrogen embrittlement. Since the ionic liquid is used to avoid hydrogen embrittlement, the methanol must be evaporated off, which was done with the sweeping method. This time, the solution was dried for 30 minutes past the time when the solution goes from deep blue to powder blue. By changing the drying method, high quality mirror-like Co deposits were achieved twice using an

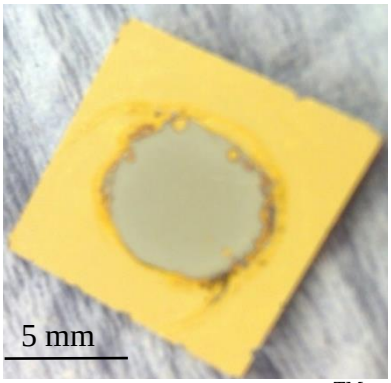


*Figure 5: Mirror-like deposits on Au(111) Arrandee™ slides were achieved twice from a 0.23 M $CoCl_2$ in BMIM-TFSA solution. An overpotential of -0.93 V vs. $Fc/Fc^+$ was applied until a 60 mC charge was reached. The RE and CE were Pt wire.*

overpotential of -0.93 V vs. $Fc/Fc^+$. The resulting deposit can be seen in **Figure 5**. Chronoamperometry was used to follow the electrodeposition processes, **Figure 6**. The first current transient shows two maxima and a single minimum in between. The current transient can be fitted to the theoretical nucleation and growth equations. The data clearly does not fit either progressive or instantaneous 2D growth models. The 3D models are a closer fit to the *i-t* transient although it is clear that no perfect fit is achieved. The presence of two maxima is key to assigning the growth mechanism to a 3D progressive growth. Previous modelling has shown progressive nucleation, with hemispherical geometry, occurs with two maxima and a single minimum.[29] This shape is due to the combination of the growth mechanism and the geometry of the nuclei. Either variable can be changed in such a way that the second maximum disappears. The second current transient (b in Figure 6) shows many more oscillations, though they are superimposed over two main maxima. Fitting of the normalized transients shows the 3D progressive growth fits reasonably well, although it seems likely this electrodeposition follows the same underlying mechanism as the former. Unfortunately, further attempts at Co electrodeposition resulted in visually poor deposits. As a quasi-reference electrode was used, the potential of the system may shift

for each new experiment. For this reason, electrodeposition was attempted at a few different potentials between -0.935 and -0.945 V vs $Fc/Fc^+$, with a noticeable change in *i-t* behaviour. As an illustration of the change in *i-t* behaviour, the transient resulting at -0.945 V vs. $Fc/Fc^+$ is shown in **Figure 7**. Analysis of this transient shows that 3D

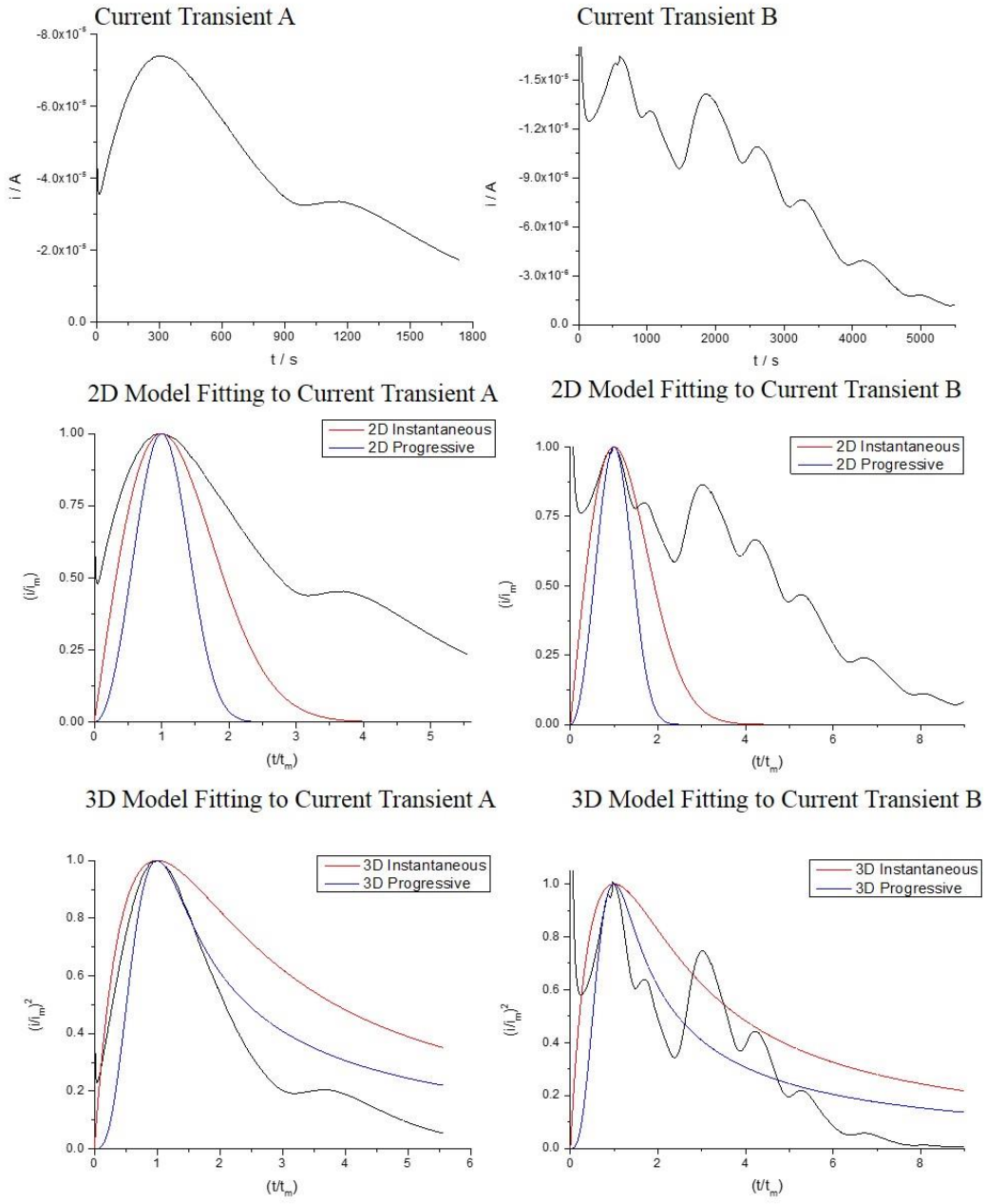


*Figure 6: The* i-t *characteristics of the Co deposition from 0.23 $CoCl_2$ in BMIM-TFSA at -0.925 V vs. $Fc/Fc^+$ are shown. These two transients are the results of electrodeposition processes of mirror-like Co. In both cases 3D progressive nucleation achieves the better fit.*

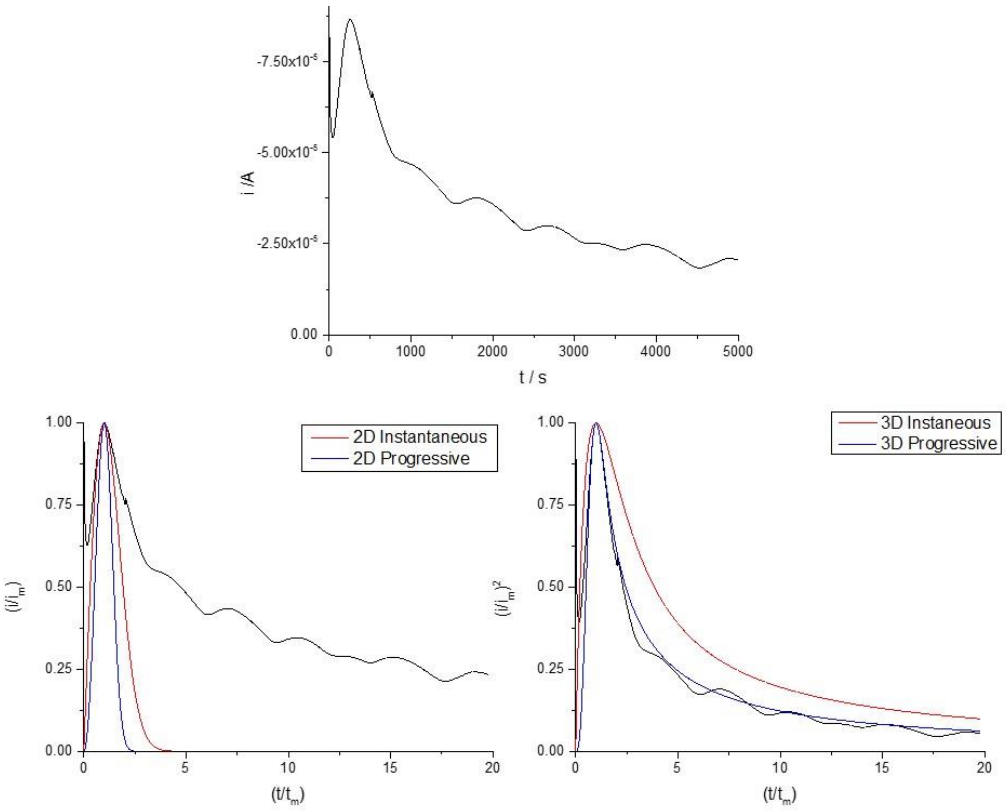


*Figure 7: After the two successful depositions, the deposits became poor, showing a change in* i-t *characteristics. An example measured at -0.945 V vs. Fc/Fc*$^{+}$ *is shown. This was performed at a Au(111) Arrandee*$^{TM}$ *slide, with Pt wire reference and counter electrodes. This transient is best fit by a 3D progressive growth mechanism.*

progressive growth is the dominant mechanism, although in this case there is a change in geometry of the nucleation sites as the number of maxima and minima has changed. The oscillations in this transient can be explained by new nucleation stages, which occur after a complete layer has grown and nucleation occurs on top of underlying layers.[30] The amplitude of these oscillations is a reflection of the heights of the electrodeposited clusters on the surface.[30]

The Use of Molecular Sieves

To dry the ionic liquids 3 Å molecular sieves were used to increase their useful operational lifetime after drying. Unfortunately, molecular sieves can introduce

impurities to the system. The presence of a noticeable amount of dust in the ionic liquid sometimes occurred when the molecular sieves were used. The high viscosity of the ionic liquid slows the time it takes for any contaminants from the sieves to settle out of solution. To try to remove some of the contaminants from the sieves they were rinsed in ethyl acetate prior to their activation. Ethyl acetate was chosen because of its low boiling point, making it easy to remove during activation of the sieves. Even after rinsing the sieves the resulting deposits were still not of mirror-like quality. As the molecular sieves are used to extend the operational lifetime of the ionic liquids, it was deemed that the problems caused by the contaminants introduced far outweighed this benefit. Therefore, it was decided molecular sieves would no longer be used. Following this decision the ionic liquid was freshly dried before its use in all subsequent studies.

Methanol Use

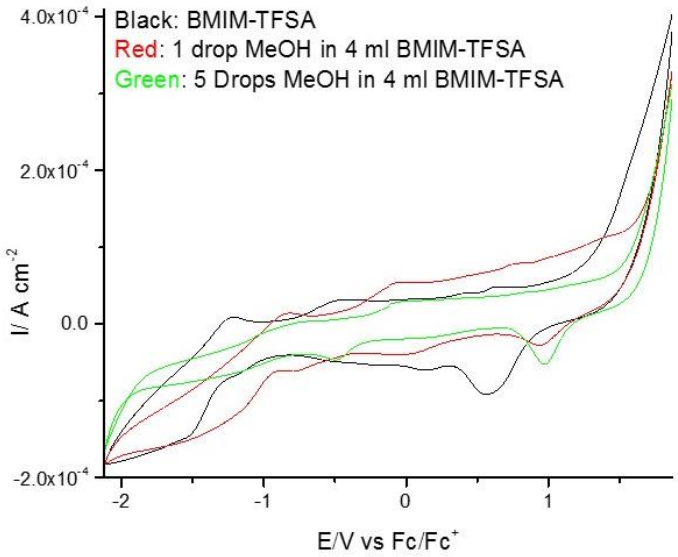


*Figure 8: CVs of BMIM-TFSA were recorded with addition of methanol at a Au(111) Arrandee™ slide. The CE and RE were Pt wire, and the system was referenced to the $Fc/Fc^+$ redox couple. All scans were performed at 0.1 V $s^{-1}$. Comparison to the pure, dry, ionic liquid shows methanol shrinks its potential window.*

The effect of the methanol content of the plating solution on the resulting deposit was investigated to determine its effect on the quality of the deposit. The presence of methanol which was used to dissolve the $CoCl_2$ in ionic liquid could give rise to hydrogen evolution, causing poor Co deposits. To determine if methanol leads to the poor Co deposits, it was not used as a carrier solvent. The $CoCl_2$ was added to the ionic liquid and heated until mostly in solution. When deposition was performed from the methanol free solution, no deposit was observed, because $CoCl_2$ precipitated out to cake the surface of the Au(111) slide. Based on these experiments, it was determined that methanol was necessary to keep the Co complex in solution. As methanol is obviously necessary for electrodeposition to occur, experiments to determine the effect of adding methanol to the plating solution, were carried out.

Before deposition experiments were undertaken, the effect of adding just methanol to the BMIM-TFSA was evaluated. The resulting voltammograms are seen in **Figure 8**. From these voltammograms, it can be concluded that increasing the methanol content of BMIM-TFSA reduces the electrochemical potential window. When these ratios of BMIM-TFSA: methanol were used as the supporting electrolyte for the deposition of Co, it was seen that the increasing methanol content aided deposition. For 1-2 drops of methanol in 4 mL of BMIM-TFSA, the system behaved in a similar manner to the methanol-free solution. When the amount of methanol in solution was increased to 3 drops in 4 mL, deposition occurred, resulting in visually poor quality grey deposits with black spots. Investigation of the current transient shows an inconsistent growth mechanism. One of the two *i-t* transients displayed in **Figure 9** is best fitted by 3D instantaneous growth, and the other by 2D progressive growth. Along with helping to solvate the $CoCl_2$, methanol acts as a diluent which is known to aid metal electrodeposition from ionic liquids. The use of diluents aids metal

deposition because they decrease viscosity, which facilitates better diffusion of the metal complex and increases the ionic liquid conductivity, while also reducing the surface tension of the ionic liquid.[25] All of these factors lead to improved electrodeposition from ionic liquids.

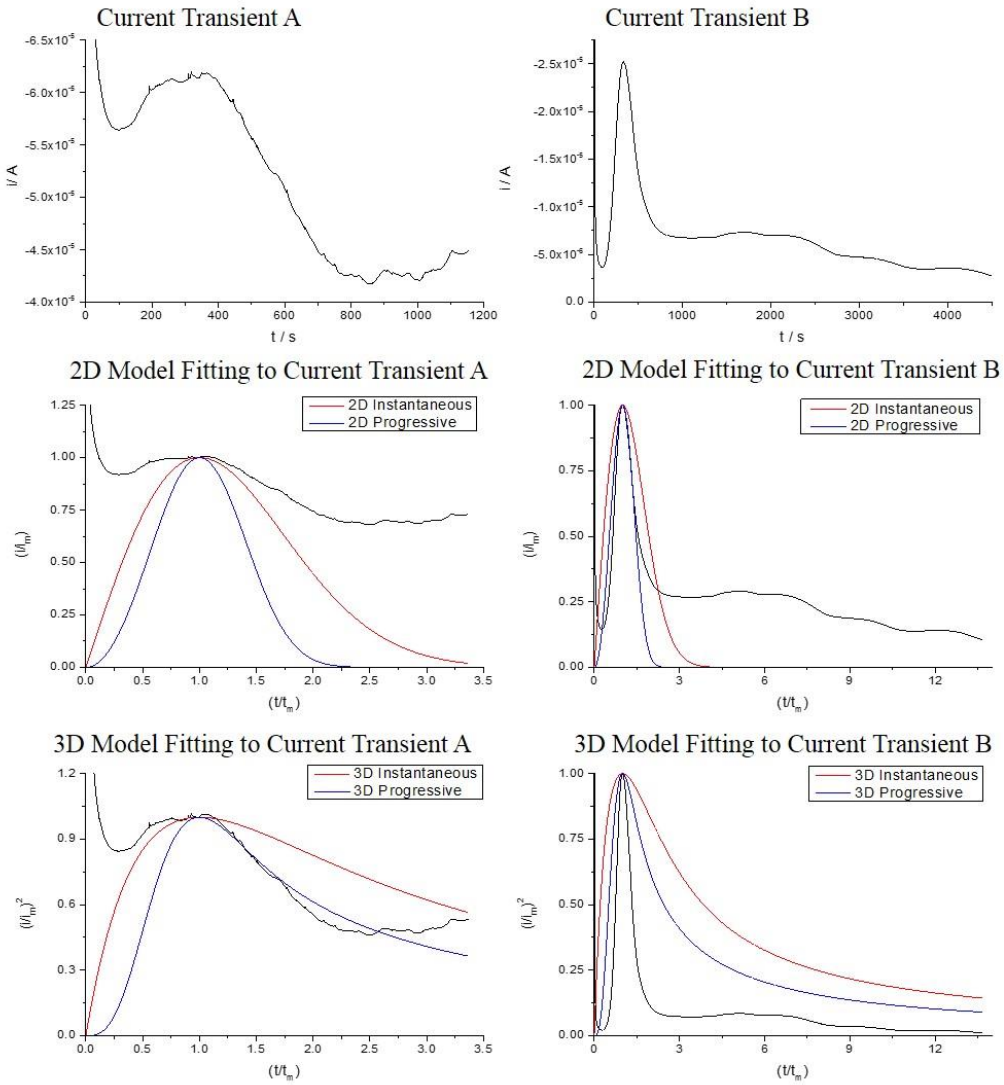


*Figure 9: Co deposition occurred using 3-4 drops of methanol in 4 ml of BMIM-TFSA. The working electrode was a Au(111) Arrandee™ slide, and the counter and reference electrodes were Pt wire. Deposition occurred at a potential of -0.925 V vs $Fc/Fc^{+}$. The resulting current transients show (A) 3D instantaneous growth, and (B) 2D progressive growth.*

BMIM-OTf

Before deposition from BMIM-OTf was attempted, the electrochemical window was first investigated using cyclic voltammetry, **Figure 10**. From this voltammetry, it can be seen that the electrochemical range is at least 3 V. Although the workable potential limit is less than that of BMIM-TFSA, the positive region appears to be extended.

After determining the useable electrochemical range of the BMIM-OTf, the voltammetry of the $CoCl_2$ in BMIM-OTf was investigated. Although prepared in the same manner as the BMIM-TFSA solution, no colour change occurs, instead the solution remains transparent and dark blue. The voltammetry resulting from this system is seen in **Figure 11**. Bulk deposition and stripping peaks can be seen at -1.07 and -0.28 V vs. Fc/Fc+, respectively. The change in the stripping and deposition potentials in this system is a result of a change in the structure of metal complex in the

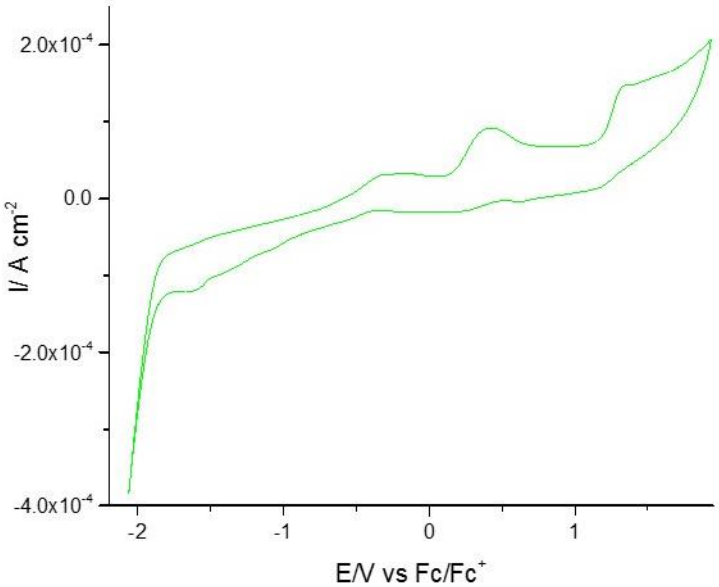


*Figure 10: The electrochemistry of BMIM-OTf, dried for 18 hours at 120 °C under vacuum, was measured at a Au(111) Arrandee™ electrode. The counter and reference electrodes were Pt wire, with the system referenced to the Fc/Fc⁺ couple. A scan rate of 0.1 V s⁻¹ was used.*

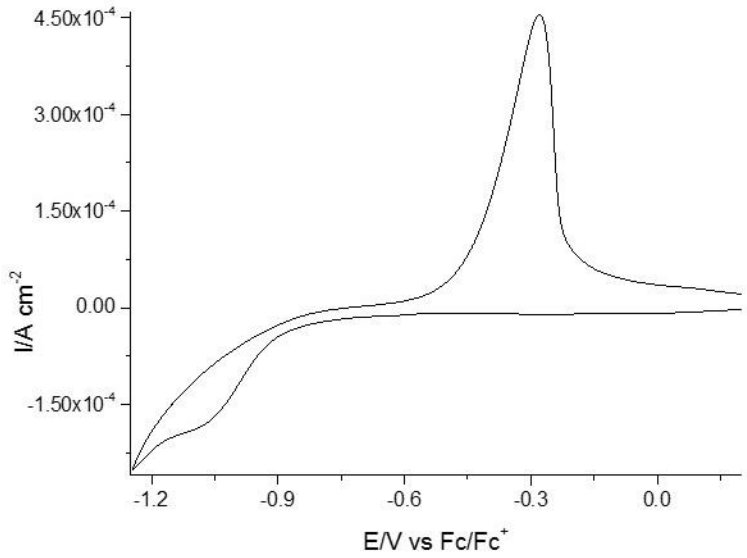


*Figure 11: The electrochemistry of 0.23 M $CoCl_2$ in BMIM-OTf, at a Au(111) Arrandee™ slide, was studied. Deposition and stripping peaks are seen, showing a coverage of 1.14 ML. The system was measured at a scan rate of 0.1 V $s^{-1}$ using a Pt counter and reference electrode.*

BMIM-OTf. The change in metal complex is evidenced by the change in colour from pale to dark blue, on changing from BMIM-TFSA to BMIM-OTf. By integrating the stripping peak, it can be estimated that 1.14 monolayers are deposited. Unlike in BMIM-TFSA, a nucleation loop is not apparent. This is likely to result from the hindered diffusion of the metal ion in BMIM-OTf.[31-33] This voltammetry shows deposition and stripping peaks at -1.06 and -0.29 V vs $Fc/Fc^+$.

**Figure 12** shows current transients for Co electrodeposition onto Au. Analysis of the current transient shows slow nucleation times and in one case the current maximum expected is never attained. In both cases when the transients are fitted to the model equations the growth mechanism is best described by 2D instantaneous growth. The oscillations seen can explained by the 3D growth followed by many subsequent 2D growth events,[34] **Figure 12b**.

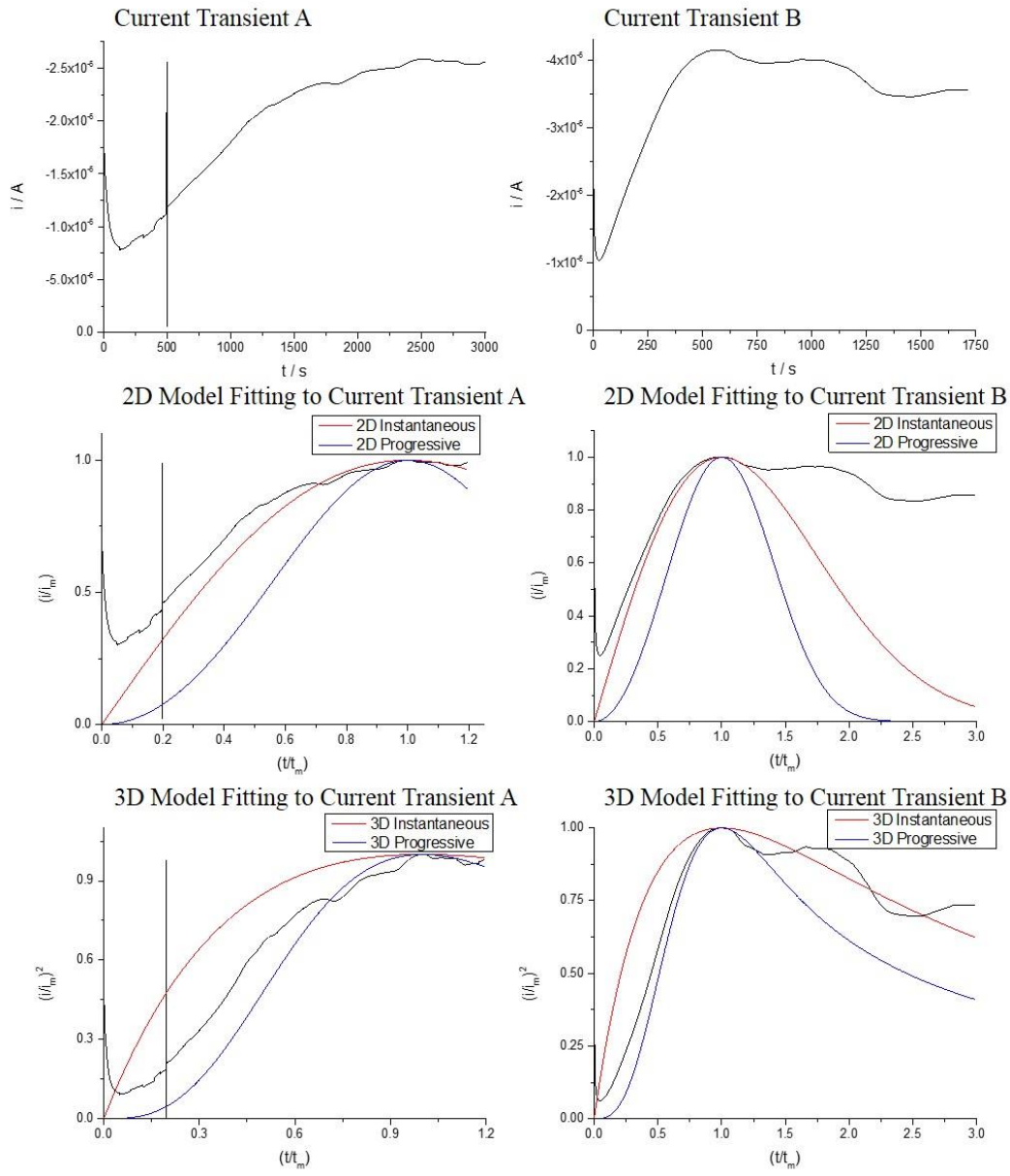


*Figure 12: Co electrodeposition transient was measured from a 0.23 M $CoCl_2$ in BMIM-OTf solution. Deposition was performed on an Arrandee™ Au(111) slide, with Pt wire counter and reference electrodes. The deposition in (A) was performed at -0.891 V vs. $Fc/Fc^+$. Fitting of the current transient shows a 2D instantaneous growth mechanism. Using the same deposition potential the transient in (B) was produced. From the fitting equations this deposition may have proceeded by 2D instantaneous, or 3D progressive nucleation and growth mechanisms.*

Double Potential Step Deposition

Double potential step deposition was tried to form mirror-like Co deposits from ionic liquids. In this technique, a high overpotential is briefly applied, aiming to instantaneously produce the nucleation sites, this is followed by a second, lower overpotential growth phase which aims to sustain the growth of the nuclei.[35, 36] Care when choosing the potentials used is necessary. The first pulse must be large enough to result in nucleation, and long enough to allow them to reach their critical size, while the second potential must be just large enough to sustain growth while not forming new nuclei.[36] Unfortunately, the idea behind the application of the double potential step method oversimplifies the deposition process by assuming nucleation is instantaneous.[36] However, when applied with care, it is a useful protocol for achieving electrodeposition. This technique was used with $CoCl_2$ in BMIM-OTf, with three different procedures: 1) -1.15 V for 5 s followed by completion at -0.97 V, 2) -1.27 for 5-6 s followed by completion at -0.97 V, and finally 3) -1.25 V for 5 s followed by plating at -0.97 V (all potentials are quoted against $Fc/Fc^+$). The current transient from method 1 is presented in **Figure 13**. This transient shows a rise to the maximum, although the expected decay from this point is not seen in the timescale of this experiment. Oscillations in the transient occur, implying new nucleation sites form on top of pre-existing sites. The use of a double potential step technique was unsuccessful in achieving visually high quality deposits. The double potential step depositions resulted in deposits which while shiny in areas, overall were dark and not uniform. With refinement, this technique may have proven successful, but unfortunately, this would have had to have been achieved through a time consuming trial and error process.

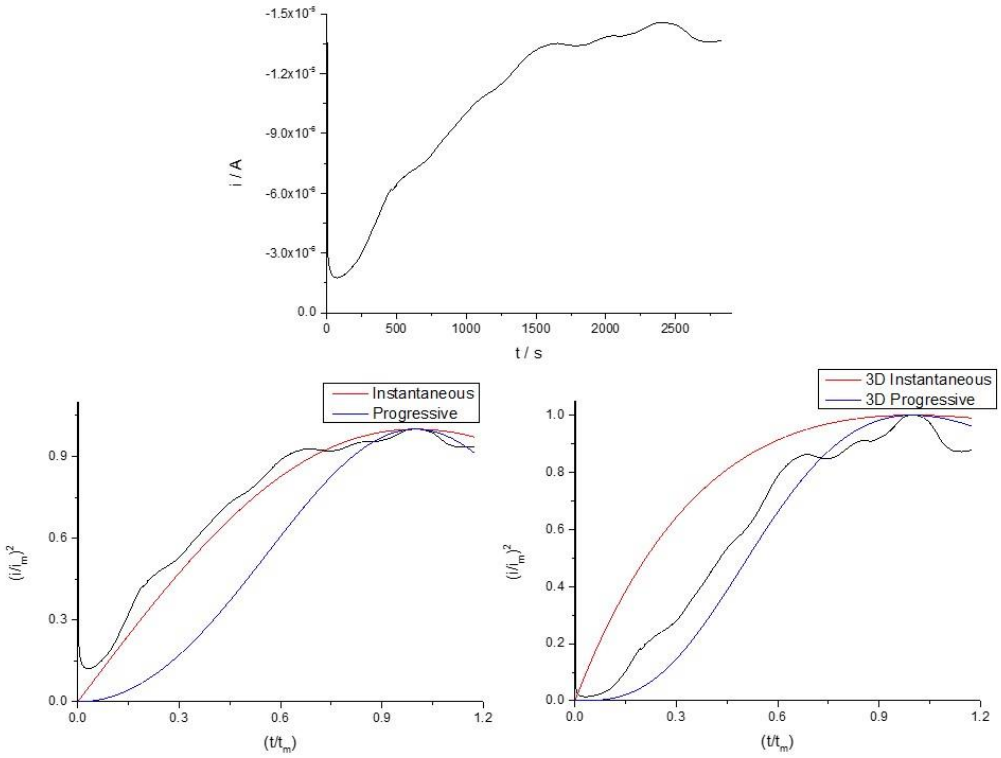


*Figure 13: A double potential step procedure was used with the first potential of -1.15 V vs. Fc/Fc$^+$ for 5 s, followed by -0.97 V vs. Fc/Fc$^+$ for the remaining duration. Co deposition was achieved from 0.23 M $CoCl_2$ in BMIM-OTf. The counter and reference electrodes were Pt wire. Fitting of the resulting transients is best for a 2D instantaneous nucleation and growth mechanism.*

BMIM-$PF_6$

The electrochemical window of dried BMIM-$PF_6$ is shown in **Figure 14**, demonstrating a window of at least 3 V, similar to BMIM-TFSA. After determining an adequate electrochemical window, the voltammetry of the $CoCl_2$ containing solution was investigated, **Figure 15**. Unlike in the other two ionic liquids, in BMIM-$PF_6$, the electrochemistry of $CoCl_2$ shows only the stripping peak at -0.46 V vs. Fc/Fc$^+$, which indicates a coverage of 1.04 ML.

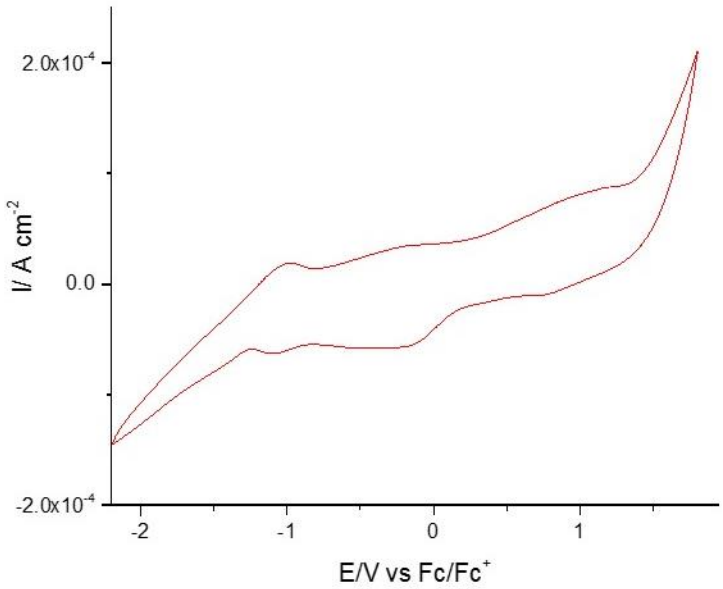


*Figure 14: The electrochemistry of neat BMIM-$PF_6$ was measured at a Au(111) Arrandee™ slide, using Pt wire counter and reference electrodes. The system was referenced to the $Fc/Fc^+$ redox couple. A scan rate of 0.1 V $s^{-1}$ was used.*

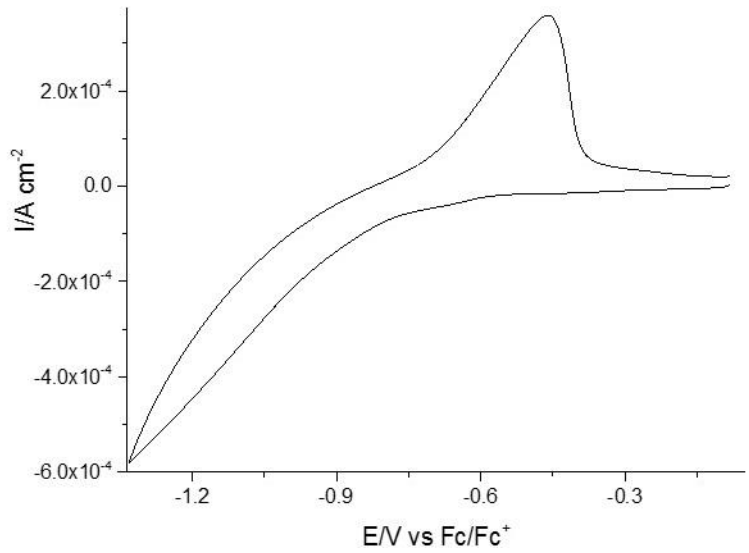


*Figure 15: The electrochemistry of 0.23 M $CoCl_2$ in BMIM-$PF_6$ was measured at an Arrandee™ Au(111) slide using Pt wire counter and reference electrodes. The system was referenced to the $Fc/Fc^+$ couple. A scan rate of 0.1 V $s^{-1}$ was used. A stripping peak is seen which relates to a coverage of 1.04 ML.*

High Temperature Deposition

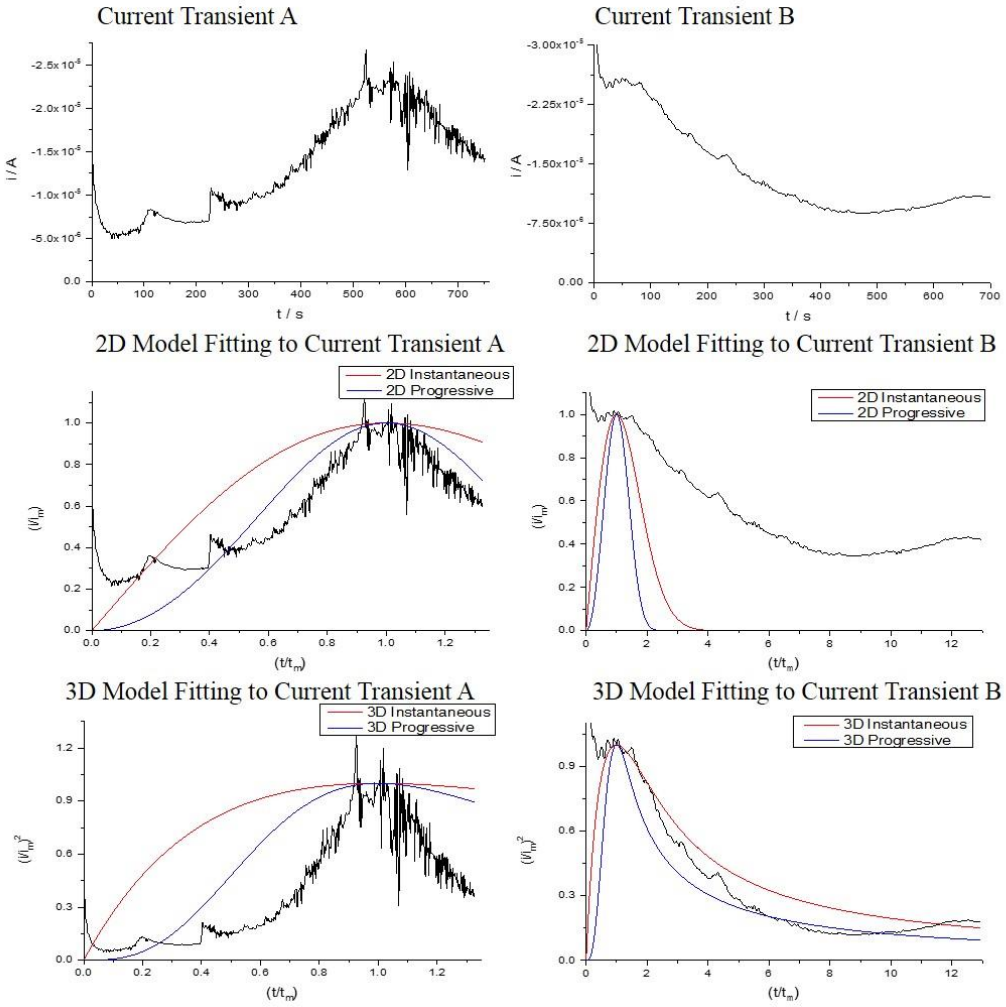


*Figure 16: Co deposition on a 0.25 mm Au wire was performed at a potential of -0.925 V vs. Fc/Fc$^+$, and a temperature of 200 °C. This was performed in 0.23 M $CoCl_2$ in BMIM-TFSA. Fitting of the* i-t *characteristics of (A) did not provide any information on the nucleation and growth mechanism. Transient (B) fits best to a 3D instantaneous nucleation and growth mechanism.*

One of the advantages of using ionic liquids is their stability at high temperatures. Unfortunately, because this work was performed for eventual use in an STM cell, this could not be fully taken advantage of. Working with the Au Arrandee$^{TM}$ slides means the temperature of deposition is limited to under 100 °C, as above this the slide cracks. As a final attempt to achieve a shiny mirror-like deposit, deposition

was performed on a Au wire allowing use of an elevated temperature of 200 °C. When deposition was performed in this manner, the majority of deposits were shiny and grey. Current transients from these depositions are shown in **Figure 16**. While in the initial case the normalized transient cannot be fitted, in the second case 3D instantaneous nucleation provides the best fit.

Overall outcome

Although ionic liquids are a viable deposition solvent for many metals and have in the past produced shiny mirror-like Co, in this investigation a high quality plate could not be achieved. Even though on a handful of occasions the Co deposit was of high quality and mirror-like, overall the best repeatable outcome was a shiny and grey deposit. Of the 88 experiments performed, shiny and bright deposits were only achieved 3.4 % of the time, whereas nearly half of the deposits had no lustre at all. The overall outcomes of these experiments are shown in **Figure 17** and the various methods and their outcomes are summarized in **Table 1**. **Figure 18** shows photos of some of the resulting deposits.

After reviewing the data, two general conclusions for achieving mirror-like deposits can be made. The first is that 3D progressive nucleation is necessary to achieve a shiny deposit. The second is that full coverage of the surface with nuclei should occur between 10 and 20 % of the time required for completion of the deposit. A possible explanation for the initial two successful deposits is that impurities were deposition in the recesses of the surface.[37, 38] Brighteners promote the formation of crystallite deposits smaller than the wavelengths of visible light.[37] Unfortunately, without knowledge of the identity of the impurities, it is difficult to determine the mechanism through which the inadvertent additive is operating. It is unlikely that the

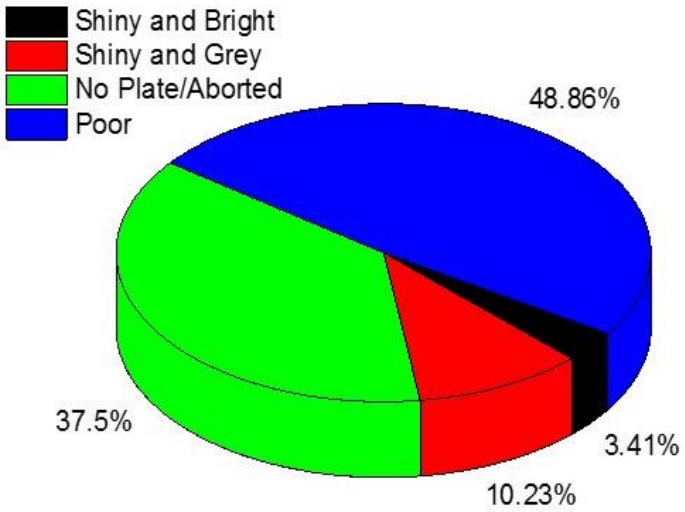


*Figure 17: Co plating from ionic liquid solutions was performed a total of 88 times. By altering the experimental setup, i.e. temperature, ionic liquid, etc., four different classes of plates were achieved. A poor deposit was defined as one which was black, coloured, grey and dull, or spotted. The desired mirror-like finish was achieved just over 3% of the time.*

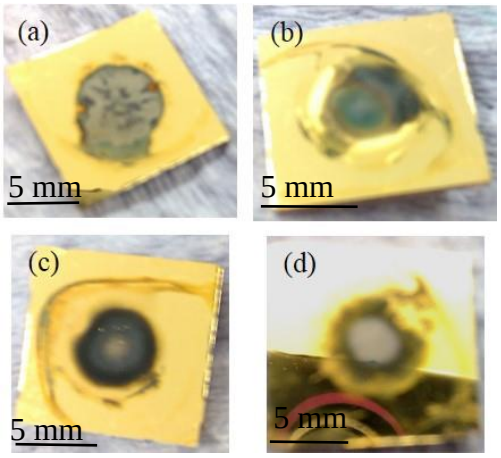


*Figure 18: A selection of the deposits achieved throughout this investigation are shown. All deposits are on a Au(111) Arrandee™ slide, and were formed using Pt wire counter and reference electrodes. All deposits shown were plated from a 0.23 M $CoCl_2$ in BMIM-TFSA solution. The potentials of deposition were (a) and (b) -0.9175, (c)-0.9165 and (d) -0.916 V vs. $Fc/Fc^+$.*

*Table 1: The plating procedures tried and the deposits resulting are summarized.*

| Procedure | Result |
|---|---|
| 0.3 M $CoCl_2$ in BMIM-TFSA plating solution, dried for 2 hours at 100 °C with $N_2$ bubbling through. Pt QRE, Co CE. Overpotential of -0.95 to -0.75 V. | Poor black deposits. Improved with sonicating and oven drying of cell |
| All components were dried. Methanol was distilled over molecular sieves. BMIM-TFSA dried over sieves, under vacuum at 120 °C for 18 hours. $CoCl_2$ dried overnight at 120 °C under $N_2$. | Shiny deposit briefly achieved, at an overpotential of -0.81 V. Other overpotentials tried. |
| Molecular sieves used for ionic liquid which were rinsed with ethyl acetate before use to remove dust. | Shiny deposit not achieved. Dust may still have been present. |
| Ionic liquid dried **without** sieves at 120 °C under vacuum for 18 hours. | Shiny deposit not achieved. |
| New Pt QRE, Co CE, and Au ring for contact with Au WE used. | Shiny deposit not achieved. Not very mirror like. |
| Small changes in overpotentials from -0.81 V to -0.80 V were carried out. | Shiny deposit not achieved. -0.801 V and higher, seem to be too positive for anything. |
| Minimum of 2.5 ml plating solution used to fill reservoir. | Shiny deposit not achieved, but any less than this and plating was very slow. |
| Au cleaned twice in boiling piranha. | Shiny deposit not achieved. |
| Pt QRE and CE used. | Shiny deposit not achieved, however, only Pt electrodes used from this point |
| Plating solution made without methanol by heating of ionic liquid until $CoCl_2$ mostly dissolved. Overpotential varied. (NB last use of Co CE) | Deposit not achieved. $CoCl_2$ settled out of solution and caked surface. |
| 1-3 drops methanol added to plating solution with aim of increasing $CoCl_2$ solubility and allowing for plating. | Deposit not achieved for 1-2 drops. Grey deposit with black spots achieved for 3+ drops. |
| BMIM-$PF_6$ used instead of BMIM-TFSA. | CV shows deposition and stripping peaks. Deposit not achieved. |
| BMIM-OTf used instead of BMIM-TFSA. | No apparent colour change in plating solution during drying. CV shows deposition and stripping peaks in similar locations to other ionic liquids. Deposit achieved at -0.825 V, dark grey but shiny |
| Double potential step deposition from BMIM-OTf solution. | Various potential steps attempted. Results seemed shiny in places, but were dark grey, and not uniform. |
| 200 °C deposition on Au wire. | Shiny deposit initially achieved, but could not be repeated. |

impurity acts as a complexing agent, as there is no visible change in the plating solution and it is unlikely to be at high enough concentration to fully complex the metal ions. It should be noted, that the additive effect may not be on the deposition itself, but on secondary reactions, like hydrogen evolution.[39] It is entirely possible, therefore, that the impurities present in these solutions supressed any residual hydrogen evolution, which may, in turn, eliminate hydrogen embrittlement.

As has been seen previously in the literature, the deployment of ionic liquids for the electrodeposition of Co is more often than not unsuccessful. Although in the

past, and indeed in this investigation, bright mirror-like deposits have been achieved, there are a number of possible explanations for the poor deposits achieved. 1) Although the cation chosen may be ideal for one-pot investigations of molecular spintronics, it may not be the best choice for Co deposition. It has been seen in the past that different ionic liquids interact with the Au surface to different degrees, with the cations and anions adsorbing on the Au surface.[26, 40, 41] While in $BMP^+$ ionic liquids the cation acts as a brightener, improving the deposits, this may not be the case for the $BMIM^+$ ionic liquids.[26] Furthermore, the opposite may even be true with the cation hindering the steps necessary for electrodeposition, such as charge transfer, nucleation, and surface diffusion.[1, 3] 2) The viscosity of the ionic liquid could cause difficulties with the electrodeposition because of the reduced diffusion rate of the metal complex to the electrode surface. The effect of viscosity was probed in these investigations by altering the cation, although other factors may have been affected by this change as well.[25] 3) The potential at the Pt QRE may have shifted during the deposition, altering the potential of deposition.[42, 43] 4) Based on anecdotal evidence, the ionic liquid over long periods may dissolve the Co deposit, hindering the nucleation and growth process.

## Conclusion

After extensive studies into the deposition of Co onto Au substrates from various $BMIM^+$ containing ionic liquids, it was determined this was not a viable method to reproducibly form high quality Co deposits. Collation and analysis of all the experimental data shows that the vast majority of the time, no deposit, or a deposit lacking any lustre, was achieved. In the end the best repeatable outcome was the deposition of shiny, dark grey, deposits. Since bright, flat and oxide free deposits are desired this makes a truly one pot method for molecular spintronics measurements

unachievable at this time. Regardless of this, ionic liquids still hold promise in the field of molecular spintronics as a medium for these investigations to be performed.

## References


1. Y. Katayama, R. Fukui and T. Miura, *Journal of the Electrochemical Society*, 2007, **154**, D534-D537.
2. C. Su, M. An, P. Yang, H. Gu and X. Guo, *Applied Surface Science*, 2010, **256**, 4888-4893.
3. R. Fukui, Y. Katayama and T. Miura, *Electrochimica Acta*, 2011, **56**, 1190-1196.
4. L. G. Lin, J. W. Yan, Y. Wang, Y. C. Fu and B. W. Mao, *Journal of Experimental Nanoscience*, 2006, **1**, 269-278.
5. Z. Zhou, D. L. He, Z. D. Cui, J. F. Zhong and G. X. Li, *Journal of Central South University of Technology*, 2008, **15**, 617-621.
6. J. Moreland and J. W. Ekin, *Journal of Applied Physics*, 1985, **58**, 3888-3895.
7. S. Schaltin, P. Nockemann, B. Thijs, K. Binnemans and J. Fransaer, *Electrochemical and Solid State Letters*, 2007, **10**, D104-D107.
8. T. Beyersdorff, T. Schubert, U. Welz-Biermann, W. Pitner, A. P. Abbott, K. J. McKenzie and K. S. Ryder, in *Electrodeposition from Ionic Liquids*, eds. F. Endres, D. R. MacFarlane and A. P. Abbott, Wiley-VCH, Editon edn., 2008, pp. 15-46.
9. W. Freyland, C. A. Zell, S. Z. E. Abedin and F. Endres, *Electrochimica Acta*, 2003, **48**, 3053-3061.
10. A. Ispas, M. Buschbeck, S. Pitula, A. Mudring, M. Uhlemann, A. Bund and F. Endres, *ECS Trans.*, 2009, **16**, 119-127.
11. A. Ispas, M. Bushbeck, M. Uhlemann, A. Bund, S. Pitula, A. Mudring and F. Endres, *ECS Trans.*, 2008, **13**, 113-119.
12. C. A. Zell and W. Freyland, *Langmuir*, 2003, **19**, 7445-7450.
13. L. Cagnon, A. Gundel, T. Devolder, A. Morrone, C. Chappert, J. E. Schmidt and P. Allongue, *Applied Surface Science*, 2000, **164**, 22-28.
14. L. H. Mendoza-Huizar, J. Robles and M. Palomar-Pardavé, *Journal of Electroanalytical Chemistry*, 2002, **521**, 95-106.
15. L. H. Mendoza-Huizar, J. Robles and M. Palomar-Pardavé, *Journal of Electroanalytical Chemistry*, 2003, **545**, 39-45.
16. J. M. van Ruitenbeek, A. Alvarez, I. Piñeyro, C. Grahmann, P. Joyez, M. H. Devoret, D. Esteve and C. Urbina, *Review of Scientific Instruments*, 1996, **67**, 108-111.
17. A. B. Soto, E. M. Arce, M. Palomar-Pardavé and I. González, *Electrochimica Acta*, 1996, **41**, 2647-2655.
18. M. Palomar-Pardavé, B. R. Scharifker, E. M. Arce and M. Romero-Romo, *Electrochimica Acta*, 2005, **50**, 4736-4745.
19. L. H. Mendoza-Huizar, J. Robles and M. Palomar-Pardave, *Journal of the Electrochemical Society*, 2005, **152**, c265-c271.
20. J. Reichert, R. Ochs, D. Beckmann, H. B. Weber, M. Mayor and H. von Lohneysen, *Physical Review Letters*, 2002, **88**, 4.

21. W. Chen, J. R. Widawsky, H. Vázquez, S. T. Schneebeli, M. S. Hybertsen, R. Breslow and L. Venkataraman, *Journal of the American Chemical Society*, 2011, **133**, 17160-17163.
22. J. Lee, H. Chang, S. Kim, G. S. Bang and H. Lee, *Angewandte Chemie*, 2009, **121**, 8653-8656.
23. F. Endres and S. Z. El Abedin, in *Electrodeposition from Ionic Liquids*, eds. F. Endres, D. R. MacFarlane and A. P. Abbott, Wiley-VCH, Editon edn., 2008, pp. 239-257.
24. S. Ren, Y. Hou, W. Wu and W. Liu, *Journal of Chemical & Engineering Data*, 2010, **55**, 5074-5077.
25. A. P. Abbott and K. J. McKenzie, *Physical Chemistry Chemical Physics*, 2006, **8**, 4265-4279.
26. R. Atkin, S. Z. E. Abedin, R. Hayes, L. H. S. Gasparotto, N. Borisenko and F. Endres, *The Journal of Physical Chemistry C*, 2009, **113**, 13266-13272.
27. D. S. Silvester, E. I. Rogers, R. G. Compton, K. J. McKenzie, K. S. Ryder, F. Endres, D. R. MacFarlane and A. P. Abbott, in *Electrodeposition from Ionic Liquids*, eds. F. Endres, D. R. MacFarlane and A. P. Abbott, Wiley-VCH, Editon edn., 2008, pp. 287-351.
28. S. Park, G. Wang, B. Cho, Y. Kim, S. Song, Y. Ji, M.-H. Yoon and T. Lee, *Nature Nanotechnology*, 2012, **7**, 438-442.
29. E. Bosco and S. K. Rangarajan, *Journal of Electroanalytical Chemistry and Interfacial Electrochemistry*, 1982, **134**, 213-224.
30. G. H. Gilmer, *Faraday Symposia of the Chemical Society*, 1977, **12**, 59-69.
31. A. V. Rudnev, E. B. Molodkina, A. I. Danilov and Y. M. Polukarov, *Russ J Electrochem*, 2006, **42**, 689-698.
32. S. Daniele, M. A. Baldo, M. Corbetta and G. A. Mazzocchin, *Journal of Electroanalytical Chemistry*, 1994, **379**, 261-270.
33. M. Platt, R. A. W. Dryfe and E. P. L. Roberts, *Electrochimica Acta*, 2004, **49**, 3937-3945.
34. M. Palomar-Pardavé, I. González, A. B. Soto and E. M. Arce, *Journal of Electroanalytical Chemistry*, 1998, **443**, 125-136.
35. M. E. Hyde and R. G. Compton, *Journal of Electroanalytical Chemistry*, 2003, **549**, 1-12.
36. G. Gunawardena, G. Hills, I. Montenegro and B. Scharifker, *Journal of Electroanalytical Chemistry and Interfacial Electrochemistry*, 1982, **138**, 255-271.
37. L. Oniciu and L. Mureşan, *J Appl Electrochem*, 1991, **21**, 565-574.
38. M. Datta and D. Landolt, *Electrochimica Acta*, 2000, **45**, 2535-2558.
39. T. C. Franklin, *Surface and Coatings Technology*, 1987, **30**, 415-428.
40. T. Waldmann, H.-H. Huang, H. E. Hoster, O. Höfft, F. Endres and R. J. Behm, *ChemPhysChem*, 2011, **12**, 2565-2567.
41. B. Uhl, F. Buchner, D. Alwast, N. Wagner and R. J. Behm, *Beilstein Journal of Nanotechnology*, 2013, **4**, 903-918.
42. J. Ghilane, P. Hapiot and A. J. Bard, *Analytical Chemistry*, 2006, **78**, 6868-6872.
43. K. K. Kasem and S. Jones, *Platinum Metals Review*, 2008, **52**, 100-106.

# Chapter 6:

# Molecular Electronics Investigations on Co

# Introduction

Since the publication of Tao's[1] and Haiss'[2] methods for measuring single molecule conductance there has been a wealth of research investigating the applications of single molecules in molecular electronics. By far the contact of choice for break junction and *I*(*s*) measurements has been gold. While the ease of preparation of an oxide free surface, under ambient conditions, makes gold useful, it is limited to the field of molecular electronics. To access the field of molecular spintronics one of the elemental ferromagnetic metals, Fe, Ni or Co, should be used. Based on the citations of the Tao and Haiss papers this has rarely been done. The dependence of everyday life on products dependent on solid state spintronic devices has, however, caused increased interest in molecular spintronics. The value of spintronics in everyday life was made evident in 2007 with the award of the Nobel Prize in Physics to Albert Fert and Peter Grünberg who simultaneously discovered Giant Magnetoresistance, the basis for modern spin memory.[3] Of particular interest for molecular spintronics is Co, referenced in the 2007 Nobel Prize press release as a ferromagnetic element already proving itself in traditional solid state spintronic devices.[4] Fully inorganic spintronic devices have clearly found important technological implementation and the investigation of complementary organic devices, such as ferromagnetic/organic/ferromagnetic spin valves, is a natural progression.

Investigations into the role of Co in organic and molecular spintronic devices have already begun. In recent years Co has acted as the top contact in a molecular ensemble of a $La_{2/3}Sr_{1/3}MnO_3$/dodecylphosphonic acid SAM/Co tunnel junction. These devices give TMR values similar to those of fully inorganic tunnel junctions.[5] Co has even been used in single molecule spintronics in investigations on GMR

through a phthalocyanine molecule contacted on both ends by Co. Under UHV at 4 K a GMR of 60 % was measured for this system.[6] Such fundamental investigations are necessary for understanding spin transport through molecules. These fundamental investigations act to inspire the future use of Co and other ferromagnetic metals as contacts for molecular electronic and spintronic devices. For progress to be made on metals other than Au a simple means of preparing and measuring single molecule junctions using standard laboratory conditions must be achieved.

Metal contacts other than gold have been investigated in the past. The study of the interaction between the metal contact and molecular anchor is important. As Au is relatively easy to use, there have been many investigations of the molecular anchor group to determine the metal-molecule interaction and its effect on molecular conductance.[7-13] Recently limited investigations at more demanding metal substrates have been performed to elucidate the role of the metal contact in molecular conductance. Pt was an obvious choice, after Au, for these investigations as it too can be prepared simply by flame annealing. In 2007-2008 Kiguchi *et al* used the STM break junction technique to investigate a series of 1,4-disubstituted benzene molecules which had, thiol,[14] isocyanide,[14] and amine end groups at Pt.[15] The relative conductances of these systems were compared to their Au counterparts and related to the interaction between the metal and molecule. Continuing from here Pd, which is in the same group as Pt, but with a work function similar to Au, was investigated, showing that in these instances the character of the metal contributes strongly to the conductance of the system. In 2008 Mao's group pioneered the jump-to-contact STM break junction technique, which allows measurement at easily oxidisable metals by continuously plating them onto the STM tip.[16] Using this method the molecular conductance of succinic acid was measured at Cu and Ag and compared to Au.[17] The

increased metal-molecule bonding interaction at Cu and Ag led to markedly higher conductance. For *I*(*s*) conductance measurements to be performed with Co contacts a means of tethering the molecule of interest to the Co surface, while keeping the Co oxide free had to be devised. Both of these goals could be easily achieved by the formation of a passivating self-assembled monolayer, which could also act as the source of the desired molecular wire.

Due to the simplicity of alkanedithiols and their affinity for gold, the conductance of alkanedithiols in gold-molecule-gold junctions has been very well studied, both experimentally[18-24] and theoretically.[25-27] This detailed background knowledge of the experimental properties alkanedithiols makes them an ideal choice to investigate on Co. The technological importance of easily oxidisable ferromagnetic surfaces, like Co, has meant their passivation with alkanethiol monolayers have been well studied. The Mekhalif group has done a substantial amount of investigation into the formation of alkanethiol monolayers on Fe,[28] Ni,[29-31] and Co,[32] predominantly using XPS. Their work has shown that for all the ferromagnetic metal surfaces studied first reducing the metal oxide was key to forming good alkanethiol monolayers through standard self-assembly techniques. Though the oxide may not be fully reduced electrochemically the surface could oxidise the thiol, giving a pure metal contact. The resulting thiolate could then be desorbed allowing fresh thiol to adsorb resulting in a good oxide free monolayer.[28, 33] Alkanethiol monolayers on Co have also been investigated by Hoertz *et al.*,[8] who examined the quality of these monolayers formed on Co from ambient self-assembly, self-assembly in an inert atmosphere and assembly under potential control using XPS, CV and IRRAS. They observed that although both the electroreduced and glovebox prepared Co show low levels of oxide on the surface initially, the electroreduction procedure is superior as the oxide is slower to return

upon exposure of the alkanethiol coated surface to air. However, while the oxide of the Co is reduced through electrode potential controlled assembly careful control of this step is necessary so as not to etch the surface. To avoid the difficulties previously seen in preparing alkanethiol monolayers on Co, particularly hydrogen evolution, ionic liquids were investigated. Ionic liquids have been used to form alkanethiol monolayers on Co because they allow for *in-situ* reduction of the Co surface, without exposure to the atmosphere during preparation. Furthermore ionic liquids promote the formation of more ordered self-assembled monolayers than traditional solvents because their bulky size and high viscosity makes it more difficult for their charged groups to intercalate into the monolayer than traditional solvents.[34]

In this work BMIM-OTf has been used for electrode potential controlled assembly of well-ordered alkanethiol monolayers on electrodeposited Co. Through electrochemical techniques these monolayers have been shown to electrochemically passivate the Co surface. Furthermore, the monolayers have an ordering similar to that of the same monolayers on Au. Building on this means of surface passivation single molecule conductance measurements could be performed on a novel Co contact system using methods available in a standard laboratory set up for the first time. Utilizing the *I*(*s*) technique the conductance of Co-octanedithiol-Co junctions were measured and compared to the analogous Au junction.

## Aim

The use of ferromagnetic contacts in molecular electronics studies has been extremely limited, due in no small part to their rapid oxidation on exposure to ambient conditions. While there have been measurements on Co performed under UHV,[6] measurements which could be performed under standard laboratory conditions have

not been seen in the literature. By utilizing ionic liquids this work aims to form and examine alkanethiol monolayers. Once satisfactory alkanethiol monolayers are formed on Co the same technique can be extended to form analogous alkanedithiol monolayers, which can act as both the molecular wire and a means of passivating the Co to facilitate the first single molecule conductance measurements on Co.

## Methods

### Co Aqueous Plating

Co was plated onto a Au(111) Arrandee™ slide from a pH 4.5, 0.2 M $CoSO_4$/0.5 M $B(OH)_3$ aqueous solution. Before plating the Au slide was rinsed with ethanol and Milli-Q® water, then flame annealed. Any previous Co plate was stripped off by cleaning in fresh piranha solution (3:1 reagent grade $H_2SO_4$: 30 wt. % $H_2O_2$) for 30 seconds. **WARNING: Preparation of piranha solution results in an exothermic reaction which can be dangerous. This reaction can become violent when organic compounds are added. Care should be taken with $H_2O_2$ added to $H_2SO_4$.** A flattened crocodile clip was used to contact one corner of the Au slide, and wrapped with PTFE tape to keep the plating solution from seeping up. A Pt mesh counter electrode and a SCE reference electrode were used. Plating was carried out on an Autolab PGSTAT30 computer controlled potentiostat, at a potential of -0.9 V to a cut off charge of 300 mC. Upon completion of the plating the slide was rinsed with Milli-Q® water only and dried immediately with nitrogen.

Cyclic voltammetry of the 0.2 M $CoSO_4$/0.5 M $B(OH)_3$ was performed in a 3-compartment, 3-electrode cell composed of a Au(111) bead working electrode with hanging meniscus, a Pt mesh counter electrode, and a SCE reference electrode connected to the working electrode via a Luggin capillary. The system was bubbled

with oxygen free nitrogen for 20 minutes prior to experiments. The system was kept under a nitrogen flow throughout the measurements. To counter act the iR-drop an iR-compensation of 1999.5 Ω was used.

Monolayer Formation

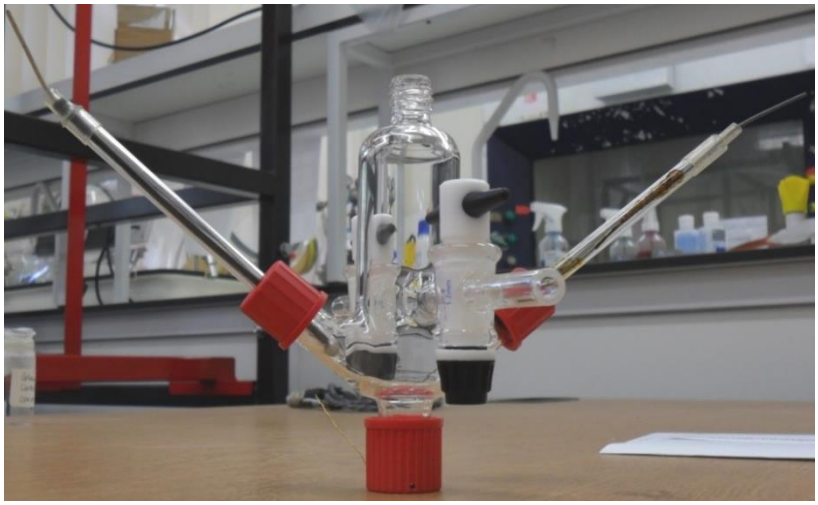

*Figure 1: The 1-1.5 mL cell pictured that has been used for all electrochemical measurements performed. The screw fittings of the electrodes, and the taps ensure that the cell can be sealed to contain a nitrogen atmosphere.*

Octanethiol, octanedithiol and mercaptooctanoic acid monolayers were formed on the electroplated Co from 10 mM BMIM-OTf solutions. Prior to use the ionic liquid was dried for 18 hours under vacuum at 120 °C. Karl-Fischer Titration showed a water content of ~100 ppm. A 1 mL capacity 3-electrode cell **(Figure 1)** with 0.5 mm Pt wire counter and quasi-reference electrodes was prepared and filled in an oxygen free nitrogen filled glovebox, before sealing and removing from the glovebox. The Co surface oxide was removed by cycling between -1.28 and -2.28 V vs. $Fc/Fc^+$. The system was held negative of the oxide reduction potential, -2.03 V vs. $Fc/Fc^+$, for 1 hour. The Co was removed from the ionic liquid solution, rinsed for 1.5 minutes with ethanol, 30 seconds with Milli-Q® water and dried with nitrogen.

PM-IRRAS Studies

PM-IRRAS studies were performed on freshly prepared octanethiol monolayers on Co using the PMA 37 module of a Bruker IFS 66v/S spectrophotometer controlled by OPUS software. Before intercepting the Co sample at near-grazing incidence the IR beam is modulated by a Hinds Instruments PEM-90 photoelastic modulator. A liquid nitrogen cooled, mercury cadmium telluride infrared detector from Infrared Associates was used. A background slide of BMIM-OTf on Co, prepared in the manner outlined but with neat ionic liquid, and was used to correct the final spectra. The resulting spectra was analysed using the OPUS software.

Electrochemical Studies

Cyclic voltammetry of the resulting monolayers was carried out on an Autolab PGSTAT30 computer controlled instrument running GPES. All experiments were run in a sealed 3-electrode cell prepared in a $N_2$ atmosphere glovebox. The working electrode was the electrodeposited Co, and 0.5 mm Pt wire quasi-reference and counter electrodes were used. The $Fc/Fc^+$ internal reference was measured after the experiment. BMIM-OTf was dried for 18 hours under vacuum and heated to 120 °C, and stored within the glovebox. A 7.5 mM paraquat in BMIM-OTf solution was made by first dissolving the paraquat in methanol, before adding BMIM-OTf to this and heating the methanol off with OFN bubbling directly in to the solution for 1 hour. A 5 mM Fc in BMIM-OTf solution was made by dissolving the Fc with gentle heating. Surface oxidation hysteresis studies were performed using neat BMIM-OTf. This study allowed the effectiveness of the surface passivation by the molecular monolayer could be gauged. Hydrogen evolution studies were performed in a 3-electrode cell with the bare and modified Co used as the working electrode, a Pt wire counter electrode and a SCE reference electrode. The Co electrode was cycled from -0.75 to

-2 V in aqueous 0.05 M $Na_2SO_4$ (pH < 3) electrolyte, as hydrogen evolution will not occur in well dried ionic liquids. Hydrogen evolution was used to judge the effectiveness of the monolayer to passivate the surface from electrochemical processes.

Electrochemical impedance spectroscopy was performed on an Autolab PGSTAT20 computer controlled potentiostat running FRA. Measurements were carried out in a 3-electrode sealed cell composed of the plated Co, or Au(111) Arrandee™ slide, working electrode, and a 0.5 mm Pt wire quasi-reference and counter electrode. The Co samples were prepared as previously outlined. To prepare the Au samples the Arrandee™ slide was rinsed in ethanol and Milli-Q® water before being dried under nitrogen and flame annealed. The octanethiol monolayer was formed by adsorption from a 10 mM octanethiol in ethanol solution for 1 hour followed by rinsing with ethanol and Milli-Q® water and drying in nitrogen. The cell was set up with a 5 mM Fc in BMIM-OTf solution and sealed within a nitrogen filled glovebox, for both the Au and Co systems. The Au system was also tested against an aqueous 1 mM $K_3[Fe(CN)_6]$/0.5 M KCl solution. Impedance spectra were taken at the equilibrium potential of the Fc or $K_3[Fe(CN)_6]$ redox probe. The impedance spectra was run between 0.1 and 10000 Hz, however, because deviations at the lower frequencies can occur spectra from 0.79 Hz and higher are shown.

*I*(*s*) Measurements

Co samples modified with octanedithiol were used with the Teflon STM fluid cell, cleaned in acid prior to use. The cell was filled with vacuum dried BMIM-OTf, and placed under a nitrogen atmosphere for 1 hour prior to, and throughout measurements. Measurements were taken with 3 types of tips, Au, Co, and oxide free Co. The Co samples were prepared using the method outlined, and the Au samples

were prepared as outlined for electrochemical impedance spectroscopy. Au tips were prepared by cutting 0.25 mm Au wire and coating with Apiezon wax. All Co tips were prepared by electrochemical etching followed by coating in Apiezon wax. The etching method was described by Albonetti *et. al.*[35, 36] Co tips are made from 0.25 mm Co wire etched in a 1 M KCl solution with 3 V applied between the Co anode and a 15 mm diameter Pt ring cathode. When a long Co wire is used a 1 g ball of clay can be attached to the bottom of the wire which splits the wire when etching is complete, forming two usable tips. To remove the surface oxide from the Co tip it is cycled *in-situ* in the STM between -1 V and -2 V versus the Pt quasi-reference electrode. A Pt wire counter electrode is also used. Au-octanedithiol-Au measurements were also performed, using Au tips prepared as already outlined. The Au substrate was prepared by rinsing in ethanol, and Milli-Q® water, followed by drying in nitrogen, and flame annealing. The monolayer was prepared from a 10 mM octanedithiol in ethanol solution with 1 hour adsorption.

Spartan® Calculations

Spartan® '08 v.1.2.0 was used to model the IR frequencies of octanethiol chemisorbed to Au and Co, as well as the frontier orbitals, and their energies, for octanedithiol chemisorbed at both ends to Co and/or Au. Calculations were performed for the equilibrium geometry in a vacuum using Density Functional Theory, at the B3LYP 6-31G* level. In order to model the system the Au, and Co atoms are treated as pseudopotentials.

## Results and Discussion

BMIM-OTf was used as a medium for potential assisted adsorption of octanethiol to form monolayers on Co, shown through PM-IRRAS, cyclic

voltammetry, and electrochemical impedance spectroscopy to be well ordered and compact. Cyclic voltammetry also showed 1,8-octanedithiol and 8-mercaptooctanoic acid were viable target molecules for assembly in this manner. The formation of 1,8-octanedithiol monolayers on Co allowed the single molecule conductance of these molecules on Co to be measured and compared to measurements for the analogous Au contacted junction. This formation and testing process can be broken down in to Co plating and reduction of the surface oxide, monolayer formation, and characterization.

Co Plating

Co was electroplated onto Arrandee$^{TM}$ slides from an aqueous electrolyte giving mirror-like surfaces, as in **Figure 2**. The plating was stopped at a charge proportional to 500 monolayers of Co on Au, if 100 % faradaic efficiency is assumed ("cut off charge"). The quality of the deposit is determined through visual examination of the resulting plate. The process is followed throughout by chronoamperometry, and cyclic voltammetry is used for further analysis of the deposition.

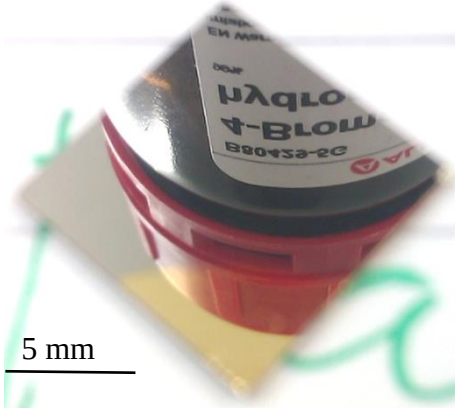


*Figure 2: Electrodeposition of Co onto Au(111) Arrandee$^{TM}$ slide from aqueous 0.2 M $CoSO_4$ /0.5 M $B(OH)_3$ pH 4.5 is seen to result in a mirror-like finish.*

The plating bath used in Co deposition is aqueous pH 4.5 0.2 M $CoSO_4$/ 0.5 M $B(OH)_3$. The high $Co^{2+}$ concentration used avoided the poor plates and low current efficiencies which occur when the concentration is too low.[37] The high pH counteracts

the hydrogen evolution which can occur when the concentration of the metal ion at the surface is too low for bulk plating to effectively occur.[37] The boric acid acts as a buffer to counteract any pH changes, while not affecting the deposition rate or efficiency in the process.[38] The pH of the plating bath is important in aqueous deposition as it affects the reactions occurring during the deposition, particularly hydrogen evolution. At lower pH values Co deposition occurs with hydrogen evolution through the following reactions:[37]

1) $Co^{2+} + OH^- \rightarrow CoOH^+$ *(Eq. 1)*

2) $H^+ + e^- \rightarrow H_{ads}$ *(Eq. 2)*

3) $CoOH^+ + H_{ads} + 2e^- \rightarrow Co + OH^- + H_{ads}$ *(Eq. 3)*

Though metallic Co is formed the intermediate $CoOH^+$ can be incorporated into the plate, causing a poor deposit.[38] Furthermore at the more acidic pH values $H_{ads}$ exists in both the physisorbed and chemisorbed forms, with chemisorption occurring through the reaction:[39]

$H^+ + Co + e^- \rightarrow Co\text{-}H$ *(Eq. 4)*

It is important to note the chemisorbed Co-H state occurs for more acidic pH values causing the chemisorbed state to have a stronger influence than the physisorbed state.[39] At higher pH hydrogen evolution has less impact on the plating, because deposition occurs through the following:[37]

1) $Co^{2+} + 2OH^- \rightarrow Co(OH)_2$ *(Eq. 5)*

2) $Co(OH)_2 + e^- \rightarrow Co(OH)_{ads} + OH^-$ *(Eq. 6)*

3) $Co(OH)_{ads} + e^- \rightarrow Co + OH^-$ *(Eq. 7)*

In contrast to the acidic reactions $H_2$ evolution does not occur, though $OH^-$ is generated causing a localized increase in the pH at the electrode surface. The localized pH rise

should be counteracted by the boric acid in the plating solution. This too can cause problems for the deposit, as the $Co(OH)_{ads}$ intermediate can be incorporated into the bulk, rather than forming the metallic Co. Although higher pH is better for the deposition process there is an optimum point, when the pH is too high the solution resistance increases to the point where the resulting iR drop can no longer be ignored.[38] It was found that pH 4.5 was the optimum for a mirror like finish in this plating bath.

Following the current vs. time characteristics of the Co deposition facilitates characterization of the metal deposition and growth. In all transients a rapid decrease in current in the initial seconds of the experiment followed by its exponential rise was witnessed. The initial sharp decrease in current is due to the double layer charging current.[40] The final behaviour of this *i-t* transient was explained by Soto *et. al.*[41] as resulting from 3 steps.

1) The current rises as a result of the rising number of nuclei sites and/or the formation of a new growth phase.
2) Overlapping diffusion zones cause the current to peak.
3) The current drops due to planar diffusion across the electrode surface.

Co deposition can occur by either progressive or instantaneous nucleation**.** In progressive nucleation the new nucleation sites appear throughout the deposition, while in instantaneous nucleation all of the nucleation sites are present from the start, without the appearance of new ones during the deposition.[42] The *i-t* transients of the Co deposition can be compared to model equations to allow further insight into the type of growth mechanism the deposition proceeds by. For both growth mechanisms there is both a two dimensional and three dimensional equation which can be used to fit the current transient. The 2D growth equations are given as:[43]

$$\frac{i}{i_m} = \left(\frac{t}{t_m}\right) exp\left[-\frac{1}{2}\left\{\frac{t^2-t_m^2}{t_m^2}\right\}\right] \quad (Eq.8)$$

For 2D instantaneous nucleation

$$\frac{i}{i_m} = \left(\frac{t}{t_m}\right)^2 \exp\left[-\frac{2}{3}\left\{\frac{t^3-t_m^3}{t_m^3}\right\}\right] \quad (Eq.\ 9)$$

For 2D progressive nucleation

In these equations *i* and *t* are time and current, and $i_m$ and $t_m$ are the maximum current and the time at which this occurs. As seen in **Figure 3**, these fits do not show a dominant growth mechanism for the Co deposition, therefore the 3D growth equations are used. 3D instantaneous nucleation can be explained by the equation:[41, 44]

$$\left(\frac{i}{i_m}\right)^2 = \frac{1.9542}{\left(\frac{t}{t_m}\right)}\left\{1 - \exp\left[-1.2564\left(\frac{t}{t_m}\right)\right]\right\}^2 \quad (Eq.\ 10)$$

Whereas the progressive nucleation is fit by:

$$\left(\frac{i}{i_m}\right)^2 = \frac{1.2254}{\left(\frac{t}{t_m}\right)}\left\{1 - \exp\left[-2.3367\left(\frac{t}{t_m}\right)^2\right]\right\}^2 \qquad (Eq.\ 11)$$

The variables in these equations have the same meanings as for the 2D nucleation equations. When this fitting procedure is used, as presented in **Figure 3b**, and the rising nucleation portion of the transient is focused on, the Co deposition is best described by a 3D instantaneous growth mechanism. This growth mechanism has been previously observed for Co deposition on Au from an aqueous $CoCl_2/NH_4Cl$

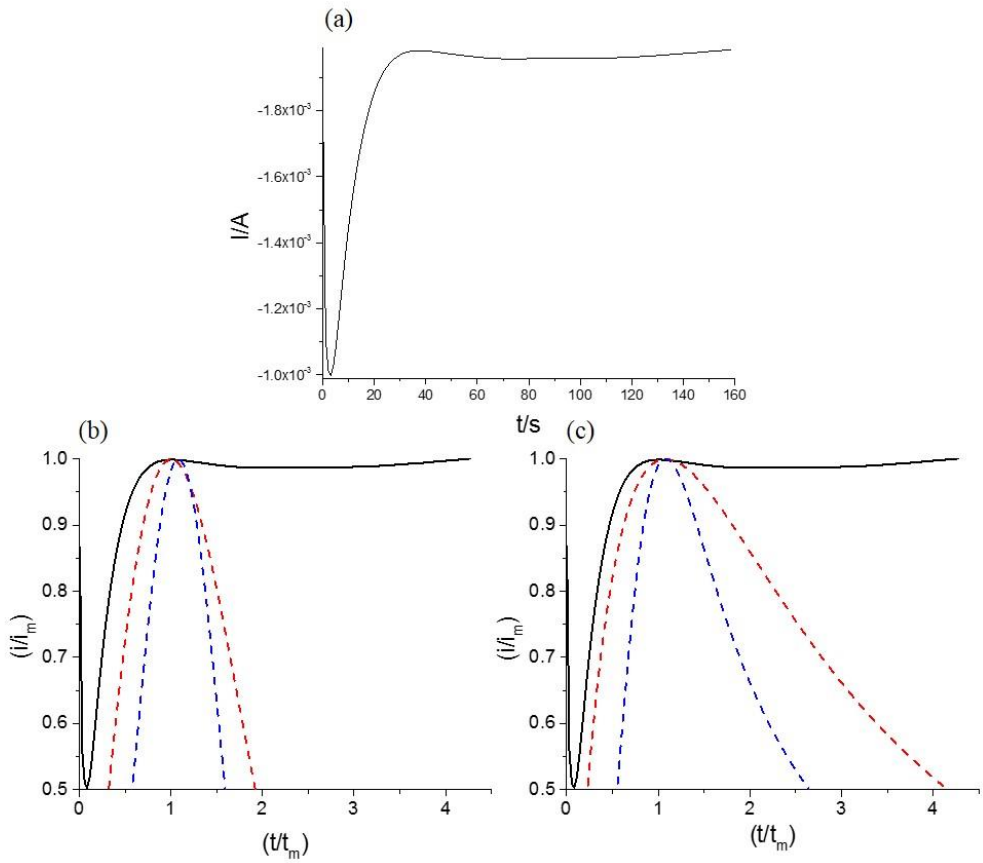


*Figure 3: A typical current transient for the deposition of Co onto the Au(111) Arrandee™ slide is shown in (a). By plotting* $i/i_m$ *as a function of* $t/t_m$ *the deposition can be compared to the ideal depositions for the 2D and 3D instantaneous and progressive nucleations. Transient (b) plots the 2D progressive (blue) and instantaneous (red) nucleation transients, while (c) plots the 3D progressive (blue) and instantaneous (red) nucleation transients.*

solution.[44] From **Figure 3b**, it is obvious the theoretical instantaneous growth mechanism, only fits the nucleation portion of the *i-t* plots. The steady state current after the current maximum, has previously been modelled by accounting for 3D instantaneous nucleation and hemispherical growth.[45] This plateau may also arise from hydrogen evolution. Grujicic *et. al*.[46] have also seen similar steady state currents for aqueous Co deposition. They propose that this steady state region is a direct result of hydrogen evolution during the deposition, which has a larger contribution as the Co

plating forms a full monolayer. The larger surface area of Co later in the plating causes higher current because it helps catalyse the hydrogen evolution reaction. This is not necessarily detrimental to the deposition because the hydrogen evolution can force the growth of Co nuclei at new sites, either by blocking a pre-existing site or by *"pushing…or providing buoyancy to a nucleus"* to aid in its diffusion across the surface.[46] This in turn causes a transition to progressive nucleation and may explain the observed deviation from the fit to instantaneous nucleation. A complimentary technique to measuring the *i-t* characteristics is cyclic voltammetry which allows further qualitative and quantitative analysis to aid in the formation of a full picture of the deposition process.

Cyclic voltammetry is useful in the investigation of metal deposition allowing the deposition to be qualitatively and quantitatively characterised. Initial voltammetric investigations of Co deposition were performed without any attempt to compensate for iR (ohmic) drop, a phenomenon related to the resistance of the electrolyte, which causes a difference in measured and expected potential.[47-49] iR drop is defined as the potential resulting from the product of the current flowing multiplied by the uncompensated resistance, i.e. that caused by the electrolyte itself, represented mathematically as $\Delta E = iR_u$.[49] iR drop results in cathodic potential less negative than expected, and anodic potential more negative than expected. The iR drop is not, however, an overpotential, as it is involved in driving the current in solution, not in the electrode reaction.[50] Unfortunately iR drop is virtually unavoidable when measuring electrode potential versus the non-polarizable reference, though in most cases the result is ignored as it is less than a few millivolts.[51] There are times, however, when iR drop cannot be ignored, these are a result of a number of factors including electrolyte conductivity, the relative positions of the working and reference electrodes,

and the magnitude of the current flowing.[49, 52] If the experiment allows there are ways to mitigate iR drop before countering this phenomena through the utilization of the potentiostat's iR compensation function. Because solution resistance is a root cause of iR drop, using an electrolyte of high salt concentration is crucial, as this increases the conductivity of the solution. iR drop is expected when a low conductance solution, like a blank solvent,[51] is used therefore the high concentration of Co salt in the plating solution should play a role in avoiding iR drop. iR drop is directly proportional to the current flowing through the system, therefore anything which reduces the current will reduce the iR drop. To this end a small area Au(111) bead was used, along with a slow scan rate of 0.05 V $s^{-1}$. Finally the impact of the resistance is reduced by limiting the distance the ionic current travels between the working and reference electrode. Physical restraints may limit the placement of the reference as close to the working electrode. This can be counteracted by connecting the reference electrode compartment and working electrode compartment via a Luggin capillary. As the Luggin capillary is insulating and has a small area bore the electric field gradient of the iR drop does not extend through to the working electrode.[48] In the black curve of **Figure 4**, iR drop is obvious from the identical slope in the deposition and striping regions. There are two ways to account for this using the GPES software controlling the potentiostat. 1) iR drop correction, as shown in the red curve in **Figure 4**, or 2) iR-compensation during the experiment, as shown in **Figure 5**. For both of these methods the solution resistance needed to first be determined through electrochemical impedance spectroscopy. The iR drop correction function of the GPES software uses the equation $E_{corrected} = E_{applied} - iR_u$.When the value of $R_u$ is inserted the potential of each point, based on the current flowing at the time, can be reassessed and plotted.[46] Looking at **Fig 4b** the most obvious change is the slope of the deposition

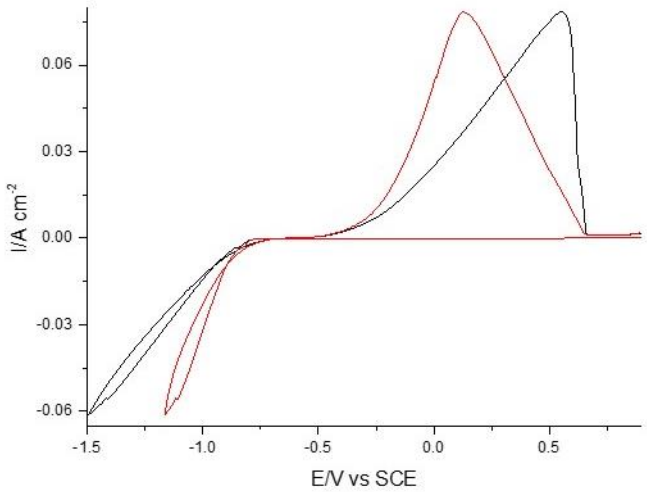


*Figure 4: Cyclic voltammetry of Au(111) bead working electrode in 0.2 M $CoSO_4$/0.5 M $B(OH)_3$ at 0.05 V $s^{-1}$ . The black curve arises from physical methods to reduce iR drop, while the red curve occurs from iR drop correction applied using the GPES software. A coverage of 664 ML is determined by integrating the charge under the stripping peak in the black curve.*

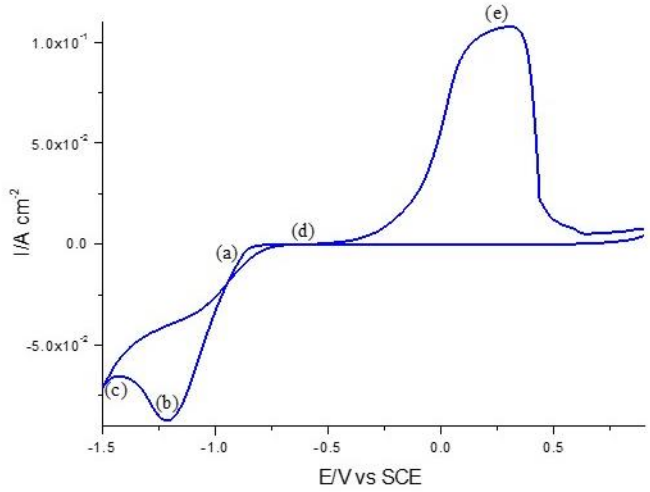


*Figure 5: Cyclic voltammetry of a Au(111) bead working electrode in 0.2 M $CoSO_4$/0.5M $B(OH)_3$ at 0.05 V $s^{-1}$ was measured using the iR compensation function of the GPES software. (a) is the nucleation potential, (b) is the potential of bulk deposition, (c) arises from hydrogen evolution, (d) the crossover potential, and (e) is the anodic stripping peak. Integration of the stripping peak shows a coverage of ~1590 ML.*

and stripping processes, while the effect of the change in potential with correction by $R_u$ is best illustrated by the shift in the vertex of the stripping peak. Before correction, the potential of this peak is 0.55 V vs SCE, after correction it shifts by 0.42 V vs SCE to 0.13 V vs SCE. Regardless of these facts, however, the resulting voltammogram is distorted, and iR drop is still obvious upon comparison of the slopes of the deposition and stripping processes, indicating this method is too simplistic. To rectify the iR drop seen in these experiments the measurement was repeated, using the iR-compensation control built into the potentiostat. In these sorts of measurements the $R_u$ value is entered into the manual control which allows for the resulting iR drop compensation through a DAC working on a positive feedback system which continually monitors and compares the $E_{applied}$ to the $E_{measured}$, the potential at the counter electrode is corrected to remove the error between the two values.[51, 53] Utilizing this method the voltammogram shown in **Figure 5** was produced. It is this voltammogram which has been used to characterize the Co deposition process.

The cyclic voltammogram of the deposition of Co onto the Au(111) surface shown in **Figure 5** can be broken down into 5 key parts labelled (a)-(e). The scan was run between 0.9 and -1.5 V vs SCE at a scan rate of 0.05 V $s^{-1}$. (a) The most negative crossover point is the nucleation potential, $E_n$, this is the point at which the nucleation of a new phase occurs.[41, 43, 54, 55] The peak current of the overpotential deposition is seen at (b), which occurs around -1.2 V vs SCE.[44, 56] Scanning to more negative potentials the current decreases due to diffusion control of the bulk deposition and then starts to increase at point (c). Point (c) arises from the hydrogen evolution reaction. Moving on from (c) the nucleation loop closes as it passes back through (a). The current seen for the reverse process is higher than that seen for the for forward process until it passes through (d), the crossover potential, $E_c$.[41] The behaviour of the

current between the potentials of (a) and (d) indicates it is energetically more favourable for the Co to deposit onto itself, than onto the bare Au surface as it has to do during initial nucleation.[41, 55, 57] The final point of interest is (e), the anodic stripping peak, due to the removal and dissolution of the Co deposit. As long as the sweep potential is far enough positive of the stripping potential then full stripping of the Co from the Au surface can occur. The large, sharp shape of this peak arises because unlike in solution electrochemistry all of the electroactive species are at the surface so diffusion need not occur.[48] In order to determine the Co coverage it must be assumed that the only reaction contributing to this peak is $Co \rightarrow Co^{2+} + 2e^-$.[58] When this is assumed and the charge of a monolayer is taken as 590 $\mu C\ cm^{-2}$ [43] the total number of monolayers of Co can be found by using the measured total charge of the stripping peak. In the voltammogram shown the charge of the stripping was 0.94 C $cm^{-2}$, therefore the total coverage of Co is ~1590 ML. Based on the peak potentials of the OPD and stripping peak the redox potential of the $Co^{2+} + 2e^- \rightarrow Co$ process is estimated as -0.45 V.

Oxide Removal

Ferromagnetic metals are often overlooked in molecular electronics and spintronics studies because they rapidly form oxide layers,[59, 60] which passivate the surface, and cause trouble for monolayer formation, particularly as on metals like Fe the oxide layer is thermodynamically stable.[28] Monolayer formation on readily oxidisable surfaces is well known, and has been attempted on all 3 ferromagnetic elements,[8, 28-32] as well as Zn[61] and Cu.[33] In most cases when the surface is used

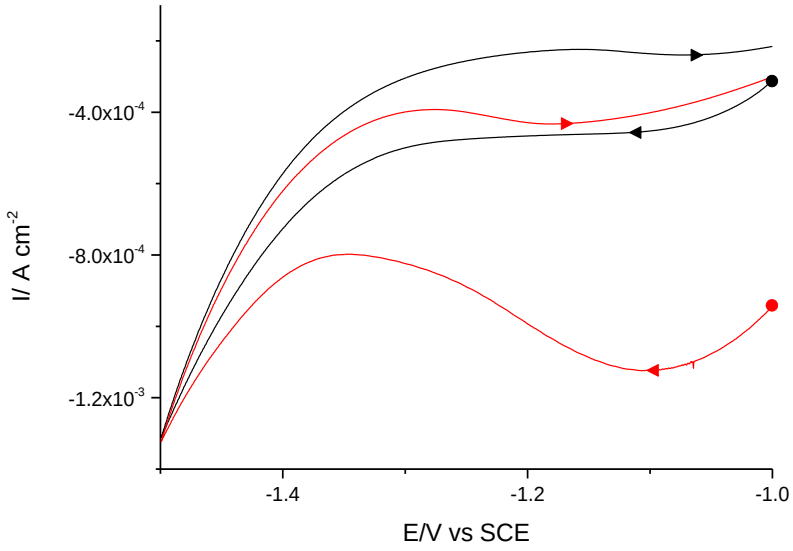


*Figure 6: Attempts to remove the Co surface oxide by cycling in 0.05 M $Na_2SO_4$ results in the electrochemistry shown. The peak in the red curve is due to hydrogen evolution, rather than oxide reduction.*

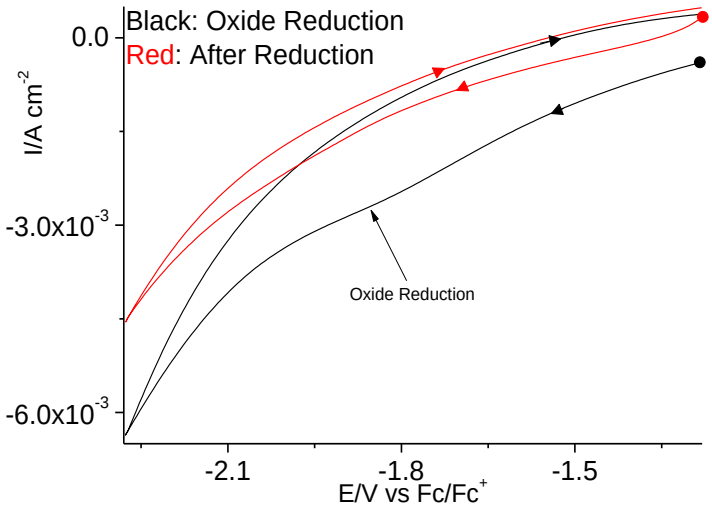


*Figure 7: Before monolayer formation the electroplated Co is reduced in-situ, in the $10^{-2}$ M organothiol in BMIM-OTf, to remove the oxide layer. By running voltammetry between -1.28 and -2.28 V vs $Fc/Fc^+$ the oxide layer can be reduced as seen in the initial scan (black). On the second scan (red) the oxide is not seen to return.*

without reduction of the oxide the resulting self-assembled monolayer is poor. XPS studies have shown that on these surfaces high coverage monolayers mainly include physisorbed S anchors, which cause poor, low stability monolayers.[61] The poor quality of the monolayer also results from the oxide surface oxidising the S end group to sulfonate, and sulfonite.[31, 33] On the other hand when the metal surface is first electrochemically reduced the monolayers are of good quality. XPS measurements have shown the monolayers formed on the resulting oxide free surfaces to be of mostly chemisorbed S end groups, with alkane chains in the *trans* orientation.[31] Furthermore, as the thiol end group is known to reduce the metal oxide if any is present then a sacrificial thiol will first be oxidised, reducing the surface and desorbing to reveal a pure metallic site.[29, 30] The resulting monolayers have been shown to be stable through contact angle measurements, and cyclic voltammetry.[31] Although working with ferromagnetic metals presents problems not encountered for gold, through the right electrochemical preparation high quality organic monolayers can be formed.

The aim of this work is to form well-ordered thiol monolayers on Co, with the oxide layer being removed electrochemically prior to any monolayer formation. This oxide removal was initially investigated in 0.05 M $Na_2SO_4$ aqueous electrolyte, **Figure 6**. When the surface is cycled from -1 to -1.4 V vs SCE a broad peak around -1.1 V vs SCE with a current density of 1480 μC $cm^{-2}$ is evident. The large current density of this peak, as well as its location after the onset of hydrogen evolution,[62] implies it is due to hydrogen evolution. This conclusion is upheld by the fact that Co reduction has been seen to occur in other studies alongside $H_2$ evolution.[63] To avoid hydrogen evolution occurring concurrently with the removal of the Co surface oxide BMIM-OTf, which rules out hydrogen evolution as a possible side reaction, is used. The first and second cycles of voltammetry of surface oxide removal in BMIM-OTf

is shown in **Figure 7**. The first cycle, depicted in black, shows the reduction of the oxide at ~-1.8 V vs. $Fc/Fc^+$, followed by a rapid increase in current. The final rapid increase in current is likely a result of the limit of the usable potential range of the ionic liquid being reached, this ionic liquid has a negative limit of -2 V vs $Fc/Fc^+$ for Au working electrode before the onset of large cathodic currents. It can be seen from the second cycle (in red) that following the first reduction in ionic liquid the oxide reduction peak does not return. This is in agreement with studies on iron oxide NPs which show the reduction of the oxide is an irreversible process.[64] With it established that a Co electrodeposit can be formed and its oxide reduced the passivation of the surface using an alkanethiol monolayer can be investigated.

Thiol Deposition

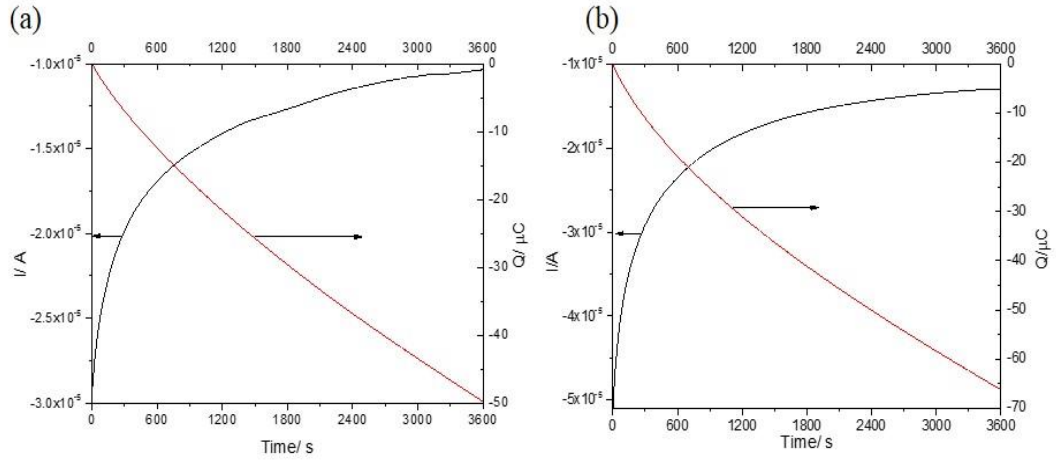


*Figure 8: Typical current versus time, and charge versus time transients are shown for octanethiol (a) and octanedithiol (b) after 1 hour of adsorption from a $10^{-2}$ M alkanethiol in BMIM-OTf solution at a potential of -1.85 V vs. $Fc/Fc^+$.*

Following reduction of the Co oxide the alkanethiol monolayers are formed on the surface with potential control at -1.85 V vs. $Fc/Fc^+$ for 1 hour. This process is followed through chronoamperometry, **Figure 8**. These figures show an exponential decay in the current density due to the two-step formation of the organothiol

monolayers. The initial sharp decrease in current density arises from the rapid adsorption of the organothiol on to the Co surface (a),[65-68] leading to 70-80 % of the total monolayer coverage.[67] In the following step, seen as a slow tailing off and plateau of current, the remainder of the monolayer coverage occurs through reorganization and ordering of the monolayer to give a compact well order structure (b).[65-68] Although the current density is greatly reduced it is a non-zero value for all 3 types of monolayer. Such behaviour has been observed before, for similar monolayers formed from an aqueous electrolyte on Ni[69] and Au.[66, 67, 70] This non-zero current may be due to tunnelling through the monolayer,[71] the presence of small defect sites in the monolayer which do not affect the long range ordering,[33, 65] the oxidation of the sulphur end groups to disulphides which then desorb[67] and/or multilayer formation.[67] The non-zero current may even be intrinsic to the use of the ionic liquid. $BMIM^+$ can intercalate into the monolayer through its alkyl chains,[72-75] allowing electron tunnelling through the alkanethiol to the $BMIM^+$ group. This can manifest itself in the electrochemistry of redox active molecules through weak redox waves.[73] It should be noted that usually the potential controlled assembly of the monolayer occurs not far from the OCP of the system,[66] while the potential used in these experiments is particularly negative of the OCP of this system. The potential used can be problematic for monolayer adsorption when it is too negative, as then the thiols are prone to rapid desorption, which manifests itself in the current transient as a sharp, intense peak.[70] None of the current transients in these experiments show the sharp peaks expected for rapid desorption, therefore this potential is acceptable. This negative potential is also likely beneficial to the formation process. As the surface is held negative of the reduction potential it should be in a pure metallic state, and should not oxidise the thiol allowing the thiolate to chemisorb to the surface without the need for the sacrificial thiol step. While it is

insightful to follow the monolayer formation process through *i-t* transients, these experiments on their own do not present a full description of the resulting monolayer

Monolayer Characterisation

PM-IRRAS

An octanethiol monolayer on Co was formed from BMIM-OTf and investigated *ex-situ* by PM-IRRAS, as is seen in **Figure 9**. The peak positions are shown in **Table 1**. PM-IRRAS is a useful surface science technique which confirms the presence of the monolayer, and facilitates a qualitative assessment of the monolayer ordering. PM-IRRAS and related techniques only allow for an average of the monolayer ordering to be determined, therefore while a monolayer may be assessed by PM-IRRAS as high quality there may be defect sites present.[70] Therefore, as was the case with this investigation, PM-IRRAS should be used in conjunction with other techniques.

In the original spectra obtained from the octanedithiol monolayer the expected alkanethiol peaks at 2850-3000 $cm^{-1}$ are seen,[76] as well as a sharp, intense peak at 1189 $cm^{-1}$ due to the presence of F in the monolayer, arising from the asymmetric C-F

*Table 1: The peak positions and assignments of octanethiol on Co are shown.*

| Peak Position ($cm^{-1}$) | Assignment |
|---|---|
| 2962 | $\nu_{as}(CH_3)$ |
| 2923 | $\nu_{as}(CH_2)$ |
| 2873 | $\nu_{s}(CH_3)$ |
| 2856 | $\nu_{s}(CH_2)$ |
| 1730, 1459, 1263 | $CH_2$ Backbone |
| 1189, 1101 | $\nu_{as}$(C-F) |

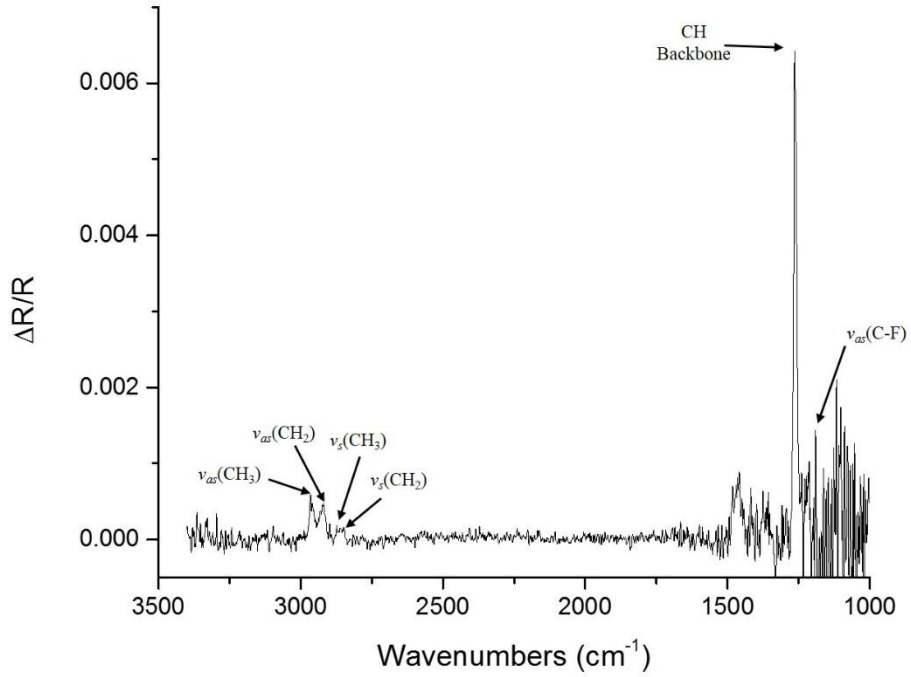


*Figure 9: PM-IRRAS spectra of an octanethiol monolayer formed on Co from potential control in BMIM-OTf. Spectroscopy was optimized at wavelength of 2850 $cm^{-1}$ and corrected to a spline background and a background of BMIM-OTf on Co was subtracted from the corrected spectra.*

stretch ($\nu_{as}$(C-F)).[77] The presence of this peak implies that even with substantial rinsing in ethanol and water at least the anion of the ionic liquid cannot be washed away. The presence of the cation is difficult to determine from this spectra because these peaks occur in the same location as the alkanethiol peaks. It has been proposed that the cation of the ionic liquid, particularly ones like $BMIM^+$, can intercalate into the alkanethiol monolayers via their alkyl chains.[72-74] It is also known that in ionic liquid droplets charge alternation occurs so that ions of one charge are surrounded by ions of another charge.[78] It is likely, therefore, that the strong $\nu_{as}$(C-F) peak is seen because the $OTf^-$ anion remains at the surface due to its strong interaction with the intercalated $BMIM^+$ cation, and as a means of achieving charge neutrality in the interface. Because of the

persistence of the BMIM-OTf on the monolayer its manifestation in the spectra was removed subsequent through the subtraction of a background spectra. To do this neat BMIM-OTf was used to prepare a BMIM-OTf coated slide in exactly the same manner as before. After both spectra were corrected against their respective spline backgrounds the BMIM-OTf/Co spectra was subtracted from the BMIM-OTf/octanethiol/Co spectra. As can be seen from **Figure 9** this results in a clean spectra with only a very small peak due to $\nu_{as}$(C-F). The contribution from the ionic liquid likely remains because the ionic liquid is in different orientations on the bare and thiol coated surfaces. The peaks seen and their magnitudes are dependent on the surface selection rule, which dictates that only those dipole changes which are parallel to the surface are measured. This occurs because charge is free to move in a metal, therefore when a dipole change occurs at the metal surface an equal but opposite change occurs in the metal.[79] This is the image dipole. When the dipole change is parallel to the surface the change is cancelled by its image dipole, whereas when the change is perpendicular to the surface, it is enhanced by its image dipole. As a result different molecular orientations give different intensity peaks, and therefore unless exactly the same orientation and coverage of BMIM-OTf on the bare and alkanethiol coated Co occurs the spectral contribution from BMIM-OTf is reduced but not fully removed. By subtracting, or at least reducing, the contribution from BMIM-OTf the contribution from the octanethiol can be more easily focused on.

When investigating alkanethiol monolayers through PM-IRRAS the $CH_2$ and $CH_3$ stretching region, from 2850-3000 $cm^{-1}$ are of particular interest for a qualitative indication of the ordering of the monolayer, particularly when compared to model systems. In the spectra from the monolayer formed from BMIM-OTf four peaks can be seen at 2962, 2923, 2873, and 2856 $cm^{-1}$ due to $\nu_{as}(CH_3)$, $\nu_{as}(CH_2)$, $\nu_s(CH_3)$, and

$\nu_s(CH_2)$, respectively. The exact position and bandwidth of these peaks was determined through Lorentzian fittings. This has been confirmed by comparison to the literature,[80-84] and Spartan® calculations. The monolayer can be assessed by using the rule of thumb that all-*trans* configurations of the alkanethiol produce $\nu_{as}(CH_2)$ frequencies lower than 2920 $cm^{-1}$, and $\nu_s(CH_2)$ frequencies less than 2850 $cm^{-1}$. [69, 85] Based on this alone it can be inferred that the monolayers are well-ordered. Further evidence for this is obtained by direct comparison of the spectrum to that of an octanethiol monolayer on Au(111), an extensively characterized well-ordered monolayer film. There are two factors which can be assessed in order to comparatively determine monolayer ordering, the wavenumber and the bandwidth of the $CH_2$ stretches. As already discussed larger wavenumbers indicate a comparatively more disordered monolayer, with more *gauche* defects in the chains.[86] Larger bandwidths also indicate more *gauche* defects, as there are more varieties of molecular orientation contributing to the peak seen.[86] When these are directly compared for the octanethiol monolayer formed through potential control in BMIM-OTf on Co, and that formed through standard self-assembly on Au, **Figure 10,** the bandwidth and the wavenumber of these peaks is seen to be similar for both implying a similar degree of ordering. This allows the conclusion that, at least as an average over the whole monolayer, on Co a high quality compact monolayer has been achieved. This premise has been further investigated by electrochemistry and will be returned to in the coming sections.

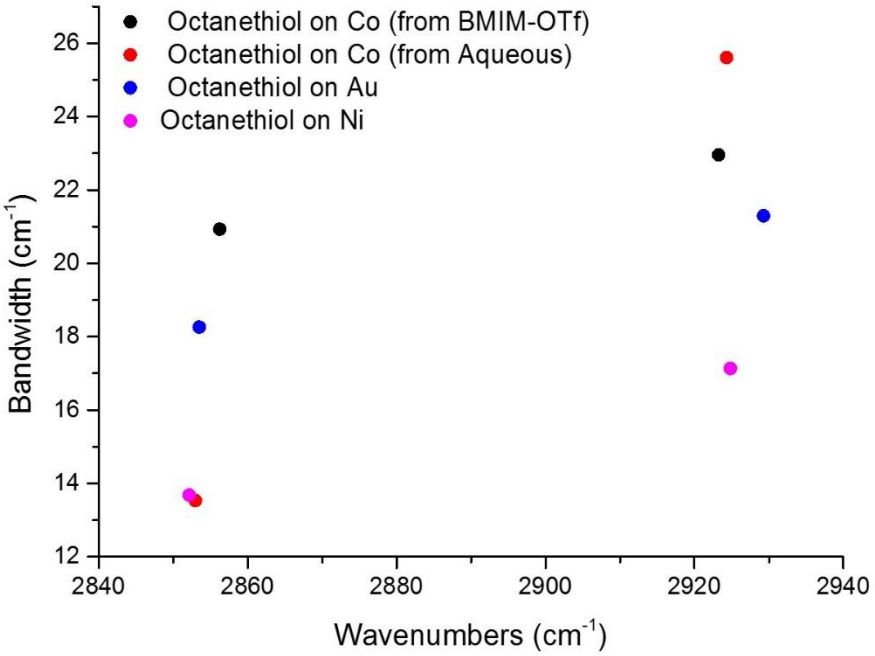


*Figure 10: The quality of the ordering of octanethiol on Co from BMIM-OTf can be compared to that of the same monolayer on other metals, as well as the same monolayer on Co formed by aqueous electroreduction. The monolayer on Au was formed by self-assembly in ethanol. For the aqueous examples the monolayers on Ni and Co were formed with potential control in aqueous 0.05 M pH < 3 $Na_2SO_4$.*

The use of PM-IRRAS has also allowed for a comparison of different methods of forming the octanethiol monolayer on Co. The monolayer formed from 0.05 M $Na_2SO_4$ (pH < 3) electrolyte with potential controlled deposition was also investigated. These are the same conditions as have been previously used for the formation of the same monolayer on Ni.[69] The comparison of the CH stretching region of the two methods of forming the octanethiol monolayer on Co is shown in **Figure 10**. This figure shows similar wavenumbers for the $CH_2$ stretching peaks of the monolayer formed from aqueous electrolyte. At the same time there is a noticeable variation in bandwidth. As has been previously stated the bandwidth can be a poor assessor of the

monolayer ordering due to the error involved in its measurement. In these spectra the CH region can be noisy, and the CH peaks overlap. These characteristics mean the bandwidth can be difficult to quantify, causing error in their comparison. Based on the relative peak positions, therefore, a similar degree of ordering between the monolayer on Co formed from aqueous and ionic liquid sources. It should be noted the spectrum from the aqueous deposition solution is more pronounced than that from the ionic liquid solution. When the monolayer is formed from the aqueous electrolyte there is sustained $H_2$ evolution which likely causes the Co surface to roughen. This damage is apparent from the pink hued spots which appeared on the Co surface. Discolouration of reactive metal surfaces with thiol adsorption has been noted before, and is associated with poor monolayers and pitting of the metal surface.[8, 87] This surface roughening allows for an inadvertent enhancement of the monolayer spectrum. Similar effects have been seen in *SEIRAS* investigations on electrodeposited Ag.[88] In this work the even with a surface roughening of Ag less than the wavelength of light an enhancement of the IR signal was measured. Although the quality of the monolayer from aqueous electrolyte is similar to that from ionic liquid, the roughening of the Co substrate rules this technique out. As the Co surface remains of apparent high quality, and the octanethiol monolayer formed from BMIM-OTf is of similar quality to the Au standard, this technique is investigated further. Electrochemistry, including cyclic voltammetry and electrochemical impedance spectroscopy, was performed to gain further insights into the monolayer properties and quality.

Cyclic Voltammetry

Having established high quality monolayers of octanethiol can be formed by potential controlled assembly in ionic liquid, electrochemistry can be used to further assess the monolayer quality. Cyclic voltammetry was performed using two very

different solution redox probes, paraquat and ferrocene. Changes in the voltammetric response in the Co oxidation region, and the $H_2$ evolution were also examined. There are three possible scenarios for the monolayer formed, which will manifest themselves differently in the CVs of the redox probes 1) The monolayer is of low quality, or non-existent, causing large areas of exposed Co surface, giving reduced electrochemistry 2) The most desirable result. The monolayer is highly ordered causing passivation,

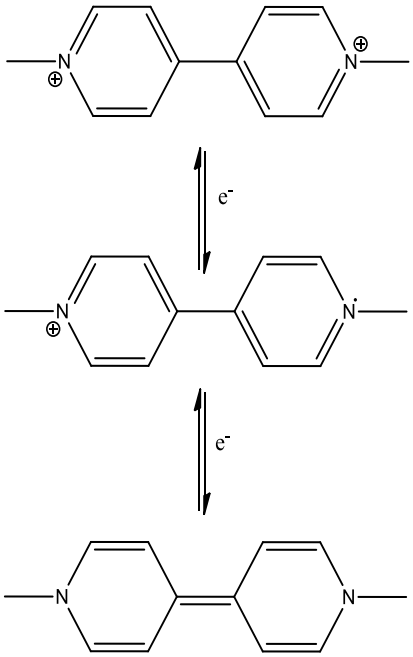


*Figure 11: Paraquat undergoes 2 electron transfers from $V^{2+}$ to $V^{+}$, and $V^{+}$ to $V^{0}$.*

and complete blocking of the electron transfer. No redox peaks appear in the CV. 3) The monolayer is fairly ordered with numerous defect sites throughout. These defect sites act as microelectrodes to give a sigmoidal response in the CV. The formation of monolayers like this is in fact a well-documented procedure for forming micro electrode arrays.[89]

Paraquat can undergo two reductions as shown in **Figure 11**. In aqueous electrolyte the second reduction occurs in conjunction with or close to the hydrogen evolution reaction, prompting the use of water-free ionic liquids for its study. The negligible water content of BMIM-OTf means hydrogen evolution does not occur,

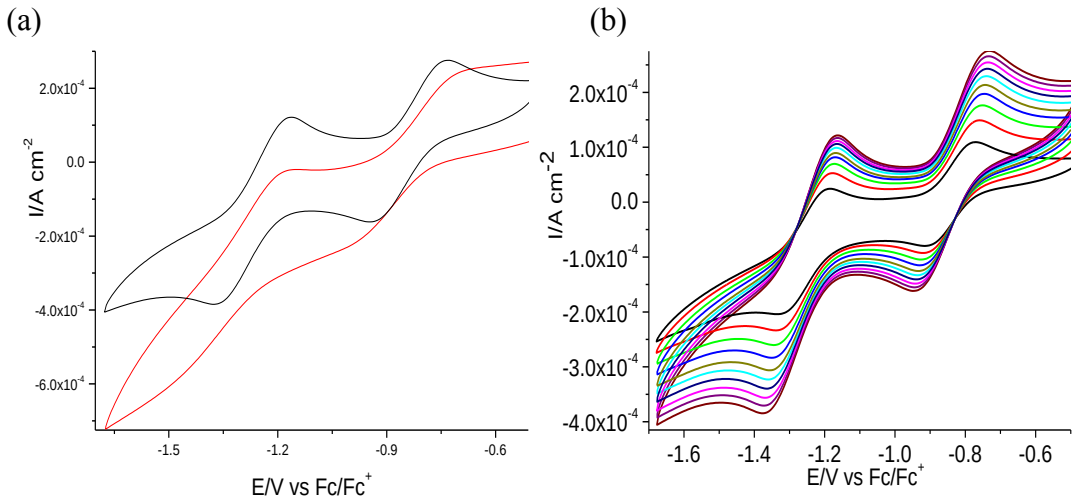


*Figure 12: A 7.5 mM paraquat in BMIM-OTf solution was used to investigate the ability of the octanethiol monolayer to passivate the Co surface. (a) compares the response after oxide reduction* in-situ, *whereas (b) shows the response of the bare Co surface without prior oxide removal. (a) compares the response of the second redox wave of the oxide-free, bare Co (black), to the monolayer passivated Co surface (red) at a scan rate of 0.5 V* $s^{-1}$*. In (b) going from navy to burgundy the scan rate changes from 0.1 to 1.0 V* $s^{-1}$.

allowing both electron transfers to be probed without its interference. Paraquat was chosen because when measurements were attempted on the electrodeposited Co in aqueous electrolyte against $Ru(NH)_6^{2+/3+}$ couple the Co layer was stripped off. As the ruthenium hexamine couple has a redox potential in the positive potential region a well-studied redox probe undergoing electron transfer relatively negative should avoid this problem. It must be noted that before measuring the redox activity of paraquat, reduction of the Co oxide was necessary. Before reduction of this oxide the electrochemical response of paraquat is apparent as poorly formed redox waves, as shown in the red curve in **Figure 12a**. Upon reduction of the oxide the peaks intensify to what is seen in the black curve in **Figure 12a**. Measurement of the two paraquat electron transfers at a variety of scan rates, **Figure 12b**, allowed determination of the

diffusion coefficient and rate constant of electron transfer of paraquat at a Co electrode. The diffusion coefficient was found using the Randles-Ševčik equation:[48]

$$i_p = 2.69 \times 10^5 n^{3/2} A D^{1/2} c^* v^{1/2} \quad \textit{(Eq. 12)}$$

Where $i_p$ is the peak height in Amps, $A$ is the electrode area in $cm^2$, $D$ is the diffusion coefficient in $cm^2\ s^{-1}$, $c^*$ the bulk concentration in mol $cm^{-3}$, and $v$ the scan rate in $V\ s^{-1}$. Using this equation a straight line graph can be achieved by plotting $i_p$ as a function of $v^{1/2}$, allowing $D$ to be found from the slope. By measuring paraquat at the oxide free Co electrode at a number of scan rates the diffusion coefficients were found to be 1.92 x $10^{-9}$, 2.45 x $10^{-9}$, 1.74 x $10^{-9}$, and 1.58 x $10^{-9}$ $cm^2\ s^{-1}$, for the anodic ($D_a$) and cathodic ($D_c$) diffusion coefficients of the transition from $V^{2+}$ to $V^{+\cdot}$ and $V^{+\cdot}$ to $V^0$, respectively. These values are compared to the $D$ values found against Au in **Table 2**. Regardless of the working electrode the diffusion coefficient is similar, this is to be expected as the redox species and the ionic liquid environment have remained unchanged. Using the diffusion coefficients the rate constant of electron transfer can be found using the Nicholson analysis.[90]

$$\Psi = \frac{\gamma^{\alpha} k_s}{\sqrt{\pi a v D_a}} \quad \textit{(Eq. 13)}$$

*Table 2: Diffusion coefficients for paraquat at Au and Co.*

| Peak | Au | Co |
|---|---|---|
| 1a | 1.59x10$^{-9}$ cm$^2$ s$^{-1}$ | 1.92x10$^{-9}$ cm$^2$ s$^{-1}$ |
| 1c | 6.88x10$^{-9}$ cm$^2$ s$^{-1}$ | 2.45x10$^{-9}$ cm$^2$ s$^{-1}$ |
| 2a | 1.90x10$^{-9}$ cm$^2$ s$^{-1}$ | 1.74x10$^{-9}$ cm$^2$ s$^{-1}$ |
| 2c | 3.41x10$^{-9}$ cm$^2$ s$^{-1}$ | 1.58x10$^{-9}$ cm$^2$ s$^{-1}$ |

*Table 3: Rate constants of electron transfer for paraquat in BMIM-OTf.*

| Peak | Au | Co |
|---|---|---|
| 1 | $(1.7 \pm 0.2)\text{x}10^{-6}$ $s^{-1}$ | $(3.1 \pm 0.8)\text{x}10^{-7}$ $s^{-1}$ |
| 2 | $(1.0 \pm 0.4)\ \text{x}10^{-6}$ $s^{-1}$ | $(3.9 \pm 0.7)\text{x}10^{-7}$ $s^{-1}$ |

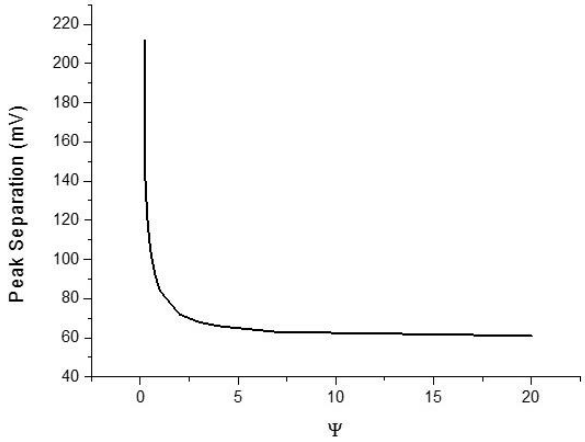


*Figure 13: Peak separation is plotted vs. Ψ values allowing for the Nicholson analysis.*

In this equation Ψ is the charge transfer parameter found from set values given by Nicholson,[91] γ is equivalent to√(D_a/D_c ), where Da and Dc are the anodic and cathodic diffusion coefficients, respectively, α is the charge transfer coefficient assumed to be 0.5, $k_s$ is the rate constant of electron transfer in $s^{-1}$, $a$ is given by $\frac{nF}{RT}$ which has its standard meanings, and $v$ is the scan rate in V $s^{-1}$. The difference in the anodic and cathodic peak potentials allow $\Psi$ to be determined from the key plot in **Figure 13**. This is used in the Nicholson equation, to find $k$. As a result of the shape of the plot to determine $\Psi$, the whole range of peak separations cannot be used, as outside of the curved section changes of just a few mV can have a dramatic influence on the determined $\Psi$. Therefore for these systems only $\Psi$ of between 0.23 and 1 is used. From this technique $k$ was determined to be $(3.1 \pm 0.8) \times 10^{-7}$ and $(3.9 \pm 0.7) \times 10^{-7}$ $s^{-1}$, respectively, for the first and second electron transfer between Co and paraquat, which is compared to the Au and paraquat system in **Table 3**. It can be seen that the rate constant of electron transfer is smaller when measured with a Co electrode than

when measured with a Au electrode. When altering the working electrode the rate constant of electron transfer can change based on primary or secondary effects. A primary effect is one in which the electrode has a direct influence on the reactant thereby affecting the rate, whereas a secondary effect is one in which the electrode effects the components of the system not involved in the reaction, like the solvent, which in turn influences the reactant.[92] Changes in the rate of electron transfer for Co and Au with paraquat can change with the density of states. The rate constant of a reduction, $k_{red}$ is related to the density of states by the following:[93]

$$k_{red} = A\rho(\epsilon)f(\epsilon)\exp\left(-\frac{(\lambda-\epsilon+e_0\eta)^2}{4\lambda kT}\right) \qquad (Eq.\ 14)$$

Where $A$ is the pre-exponential factor, $\rho(\epsilon)$ is the density of states of the electrode, $\lambda$ the reorganization energy, $\epsilon$ the dielectric constant, $e_0$ the unit charge, $\eta$ the overpotential, $k$ the Boltzman constant, and $T$ the temperature of the system. From this equation it is clear the metal with the larger DOS will have the faster rate of electron transfer, if all other factors are equal. In separate investigations of the DOS of Co and Au, the DOS at the Fermi level of Co was higher than that at the Fermi level of Au.[94, 95] Based on the relative DOS of Co and Au, therefore, the rate constant of electron transfer should be higher for Co, however in this system the lower rate constant is measured. It is possible that there is some residual oxide present on the Co surface, which causes a reduction in the DOS of Co giving rise to the reduced rate of electron transfer. There is, however, widespread belief that changing the metal does not have a primary effect on the rate of electron transfer, and therefore the reduced rate for Co can be more satisfactorily explained by secondary effects.[96-98] The most important secondary effect of the electrode is that on the electrochemical double layer. The double layer is composed of an inner region, the compact layer, composed of

localized charges, and an outer region, the diffuse layer, composed of the solvated electroactive and electroinactive ions.[92, 99] The plane between these two layers is the Outer Helmholtz Plane. The charge in the OHP is dependent on the effective charge at the electrode, which is itself dependent on the work function.[97] A straightforward explanation for the effect of the electrode is that with a higher effective negative charge at the electrode, the surface concentration of the oppositely charged redox couple will be greater, causing a higher rate of electron transfer.[97] A further secondary effect which may cause the reduction in rate of electron transfer for Co is the effect of the metal on the solvation shell of paraquat. It is possible the Au and Co surfaces interact with the ionic liquid solvation shell of paraquat in different ways giving rise to a change in the system entropy, in turn affecting the rate constant.[97] Finally it should be noted that the presence of adsorbates on the Co, could cause the lower rate constant of electron transfer by increasing the distance between the electrode and the electroactive species, and force electron tunnelling to occur over longer distances.[100] While it is possible that the lack of a flame annealing process for Co, unlike for Au, allows for the presence of environmental contamination, it is expected that any adsorbates would be removed by the very negative potentials in the reduction of the Co oxide layer. It is difficult to determine the precise cause for changes in rate constants for the different metal electrodes, however this change is most likely due to the associated change in the electrochemical double layer.

When investigating the ability of the octanethiol layer to protect the Co surface just the most negative of the two redox peaks of paraquat was focused on. **Figure 14** compares the bare and octanethiol coated Co substrate. The bare Co clearly shows a 1 electron transfer which is obviously blocked for the octanethiol coated surface. While paraquat has allowed insight into the blocking ability of the monolayer as a bulky

charged molecule it is not necessarily the best choice for this determination. While charged molecules can always be repelled from a monolayer because of electrostatic repulsion this can be particularly exacerbated in ionic liquids. For example when $Fc^+$ was investigated in ionic liquid the solvation shell was composed solely of the anion. The surrounding anion shell hinders the ability of $Fc^+$ to fully approach the monolayer because of unfavourable interaction with the cation intercalated monolayer. This in turn causes the electron transfer to be blocked, even when it may occur for the reduced form (Fc).[101] As aromatic molecules are known to be well solvated by ionic liquids in clathrate cages it is highly likely a similar effect occurs with paraquat.[102] Therefore, while the paraquat probe molecule provides insight into the monolayer packing it cannot standalone as a judge of monolayer quality. In order to get a fuller picture of the monolayer the ferrocene redox couple was investigated.

Small, neutral molecules, like Fc are better probes of monolayer packing than bulky charged molecules because at the defect sites investigated the electron transfer kinetics are slower for bulky molecules particularly when they must enter the monolayer defect sites.[75, 103] This problem is confounded when the molecule is charged, as it cannot approach the oppositely charged electrode surface as closely as a neutral molecule, therefore the electronic overlap with the surface is reduced.[103] Finally the hydrophobic nature of Fc makes it better at penetrating the SAM defect sites.[75] As with paraquat a good redox response occurs for ferrocene when the oxide layer is first reduced, leading to intense peaks. In **Figure 15** the bare and octanethiol coated Co are compared. Again it is seen that while the redox properties are clear for the bare surface, they are blocked for the monolayer coated surface. By exploiting the electrochemistry of Fc the stability of the octanethiol monolayers on Co upon 1 hour exposure to ambient atmosphere could be assessed. From **Figure 16** it is apparent the

redox waves of $Fc/Fc^+$ have not returned, meaning the monolayer is stable to ambient conditions. Ferrocene was used to investigate octanedithiol and mercaptooctanoic acid monolayers on Co. The results for octanedithiol are shown in **Figure 17**. As with the octanethiol monolayer, such comparisons show octanedithiol and mercaptooctanoic acid monolayers block the electron transfer between Co and Fc.

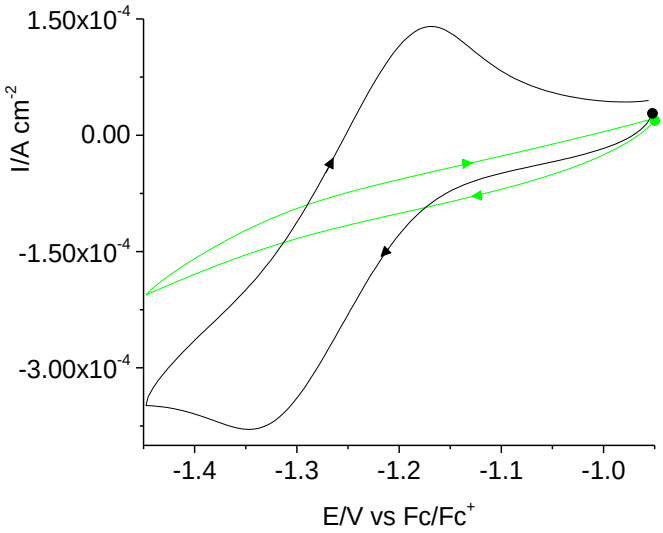


*Figure 14: Bare (black) and octanethiol (green) monolayer passivated Co were investigated in 7.5 mM paraquat in BMIM-OTf. By looking at the second redox process the octanethiol monolayer is seen to passivate the Co surface against electron transfer with paraquat.*

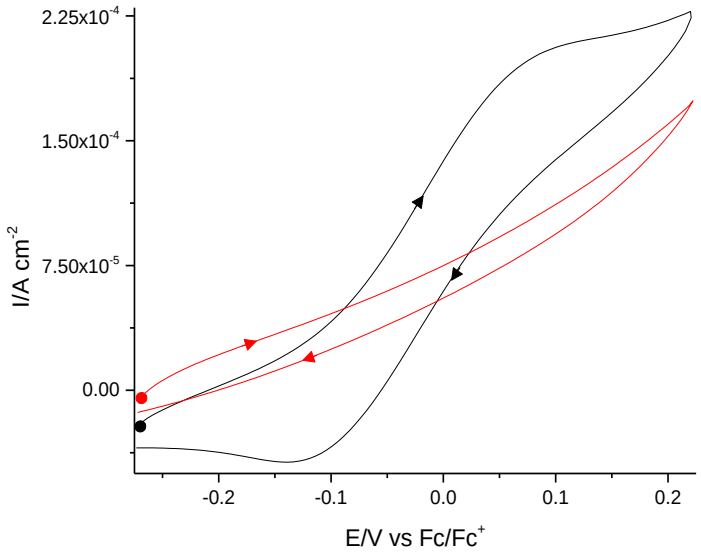


*Figure 15: The response of the bare oxide free Co (black) and the octanethiol monolayer passivated Co (red) are investigated in in 5 mM Fc in BMIM-OTf. A scan rate of 0.5 V $s^{-1}$.*

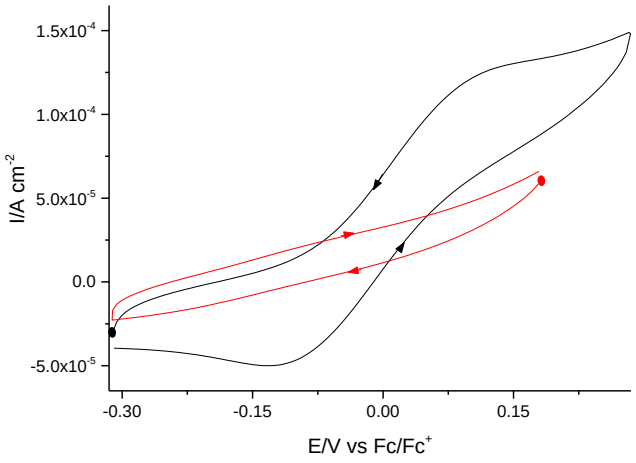


*Figure 16: The stability of the octanethiol monolayer in ambient conditions was investigated by comparison of the response of bare oxide free Co in 5 mM Fc in BMIM-OTf (black) to that of the octanethiol monolayer protected Co after 1 hour exposure to ambient conditions (red). The scan rate used was 0.5 V $s^{-1}$.*

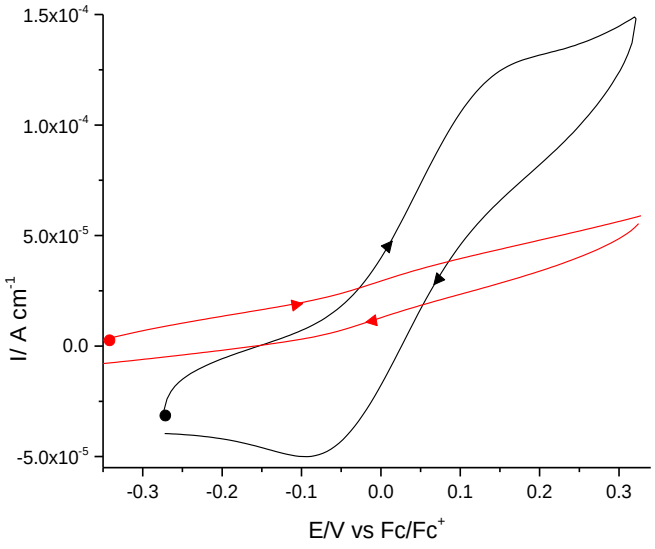


*Figure 17: The ability of the octanedithiol monolayer to passivate the Co surface was investigated using 5 mM Fc in BMIM-OTf. Comparison of the bare (black) and octanedithiol monolayer coated Co (red) shows the surface is passivated. Scans were run at 0.5 V $s^{-1}$.*

When investigating the presence of simple organothiol molecules on Au surfaces standard practice is to look at the reductive desorption of the monolayer. The reductive desorption of the monolayer occurs based on the following electrochemical reaction:

$$RS - M + e^- \rightarrow M + RS^- \quad \textit{(Eq. 15)}$$

When investigating the reductive desorption of organothiol monolayers from Au the process is easy to follow and quantify using cyclic voltammetry. By investigating the reductive desorption the coverage of the monolayer on the gold surface as well as its relative binding energy on the surface can be determined based on the charge and potential of the reductive desorption respectively. It is expected that when reductive desorption is investigated for the octanethiol monolayer on Co it will occur at more

negative potentials than the same monolayer on Au, because of the more covalent bonding nature of the Co-S bond.[104] When these measurements were performed, however, the reductive desorption was not apparent in cyclic voltammetry even on bringing the potential to -2.74 V vs $Fc/Fc^+$. When performed with paraquat in solution, however, the redox properties of the probe return, indicating the removal of the organic monolayer.

Aside from the investigation of the change in the measured electron transfer between the electrode surface and a redox probe in the presence of an octanethiol monolayer, the change in the hysteresis pattern of the cyclic voltammetric curves for the Co surface has also been investigated. This change in hysteresis has been examined for the octanethiol (OT) and octanedithiol (ODT) monolayers on Co, and is shown in **Figure 18**. The anodic limit in ionic liquids at the gold electrode arises from the breakdown of the ionic liquid. The hysteresis looked at here, occurs at a much less positive potential than that seen for gold in the same ionic liquid, and therefore is unlikely due to the ionic liquid. The hysteresis appears to result from surface oxidation of the Co surface, which has been seen to occur at values of -0.76 V vs $Fc/Fc^+$ or higher, although this can change based on the electrolyte.[105, 106] The bare Co electrode undergoes a rapid exponential rise in current at around -0.4 V vs $Fc/Fc^+$, while for both the OT and ODT monolayer coated electrodes this is pushed to outside the limits of these experiments. This is a further simple proof that potential control in BMIM-OTf allows for formation of organothiol monolayers on Co which passivate the surface.

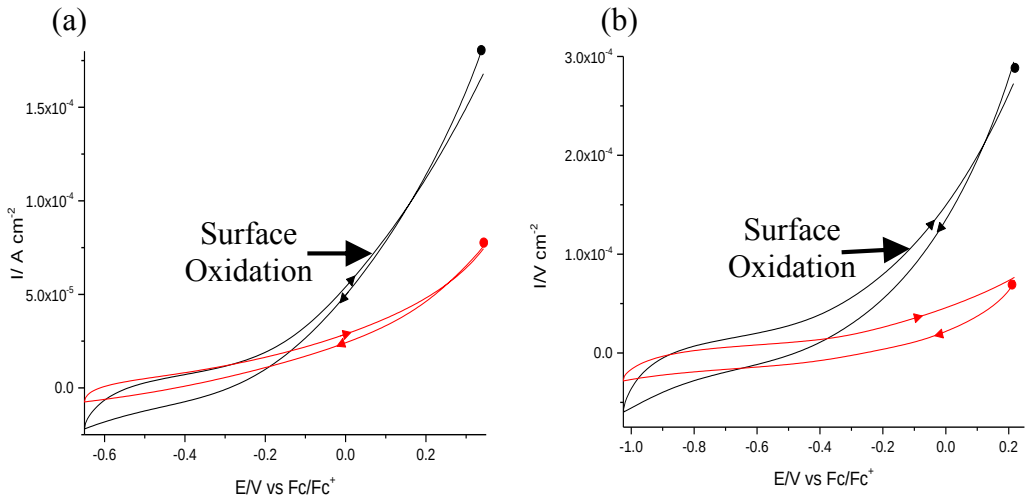


*Figure 18: The hysteresis in the surface oxidation voltammograms of (a) bare oxide free Co (black) and octanethiol monolayer passivated Co (red) and (b) bare oxide free Co (black) and octanedithiol monolayer passivated Co (red) in neat BMIM-OTf is shown. The scans pictured were run at a rate of 0.5 V $s^{-1}$.*

The stability of the octanethiol monolayer in aqueous electrolyte can easily be investigated by exploring the hydrogen evolution reaction (HER). When working in aqueous electrolytes hydrogen evolution causes a sharp increase in current at the negative vertex. This sharp increase in current changes upon modification of the electrode surface by an organic monolayer. Depending on the metal surface measured an increase or decrease in the hydrogen evolution current can occur.[69] The bare electrodeposited Co, and the octanethiol monolayer coated Co were investigated in aqueous 0.05 M NaOH (pH < 3) to determine the influence of the octanethiol monolayer on Co on the HER. In these investigations the octanethiol monolayer on Co led to an inhibition of hydrogen evolution.

It is actually fortuitous that the electrochemical measurements in BMIM-OTf have given such positive results. Self-assembled monolayers of organothiols have been measured in various aqueous and non-aqueous electrolytes. In aqueous

electrolytes the alkanethiol monolayers remain compact and well ordered, the ordering can even be considered to increase in the aqueous electrolyte with the end groups attracting each other to repel the water.[71] The high ordering of the alkanethiol monolayers in aqueous electrolyte means the monolayers effectively impede electron transfer between redox probe and electrode as the probe cannot penetrate the monolayer. In certain non-aqueous electrolytes, like acetonitrile and propylene carbonate, monolayers previously characterized as well-ordered do not block the electron transfer between the electrode and the redox probe.[71] This tends to occur for solvents without long range ordering, which have the ability to solvate the end of the alkanethiol, and force the monolayer to disorder, allowing the redox probe to come within close proximity of the electrode surface.[71] Since the impact of the solvent on the adsorbed monolayer is difficult to predict a positive outcome with ionic liquids was not necessarily guaranteed. BMIM-OTf, however, shows long range ordering promoted by the fact that it is composed solely of ions. Ionic liquids have been shown through theoretical investigation to have a strong charge ordering with the anions and cations alternating throughout the solution.[107] The cyclic voltammetry experiments carried out here have not only shown BMIM-OTf to be a viable test environment for monolayer stability, but has shown qualitatively that the monolayers formed are well-ordered.

Electrochemical Impedance Spectroscopy

Electrochemical impedance spectra of the octanethiol monolayer formed on Co in BMIM-OTf were measured and compared to the analogous SAM on gold; these results are shown in **Figure 19**. The octanethiol monolayer on gold was measured in both, aqueous 1 mM $K_3[Fe(CN)_6]$/0.5 M KCl, and a solution of 5 mM Fc in BMIM-OTf, while the same monolayer on Co was measured only in 5 mM Fc in BMIM-OTf.

All three systems were fitted to a Randles equivalent circuit, the diagram of which is shown in **Figure 20**. In this circuit $R_\Omega$ is the solution resistance, $R_{CT}$ the charge transfer resistance, and CPE the constant phase element. While the Randles circuit would traditionally use an ideal capacitor, electrochemical systems are far from ideal, this is corrected with a CPE which allows for analysis of the system using commercial software.[108] This is the case since unlike a pure capacitor the CPE accounts for inhomogeniety in the non-ideal system,[108-110] arising from surface roughness, varying composition and thickness of the deposit. To determine the $R_\Omega$, $R_{CT}$, and CPE values a simple semi-circle fitting was performed using the FRA software.[109] For all three systems the black curve is the bare metal electrode, whereas the red curve is the monolayer protected system. For all of these systems the straight line portion of the curve dominates the spectra when the electrode is bare, whereas in the presence of a monolayer the semi-circle dominates. These different dominating factors indicate two different equivalent circuits, and differing interplay between different factors controlling electron transfer. The near perfect semi-circle for the monolayer spectra would seem to indicate that the mechanism of electron transfer involves a single

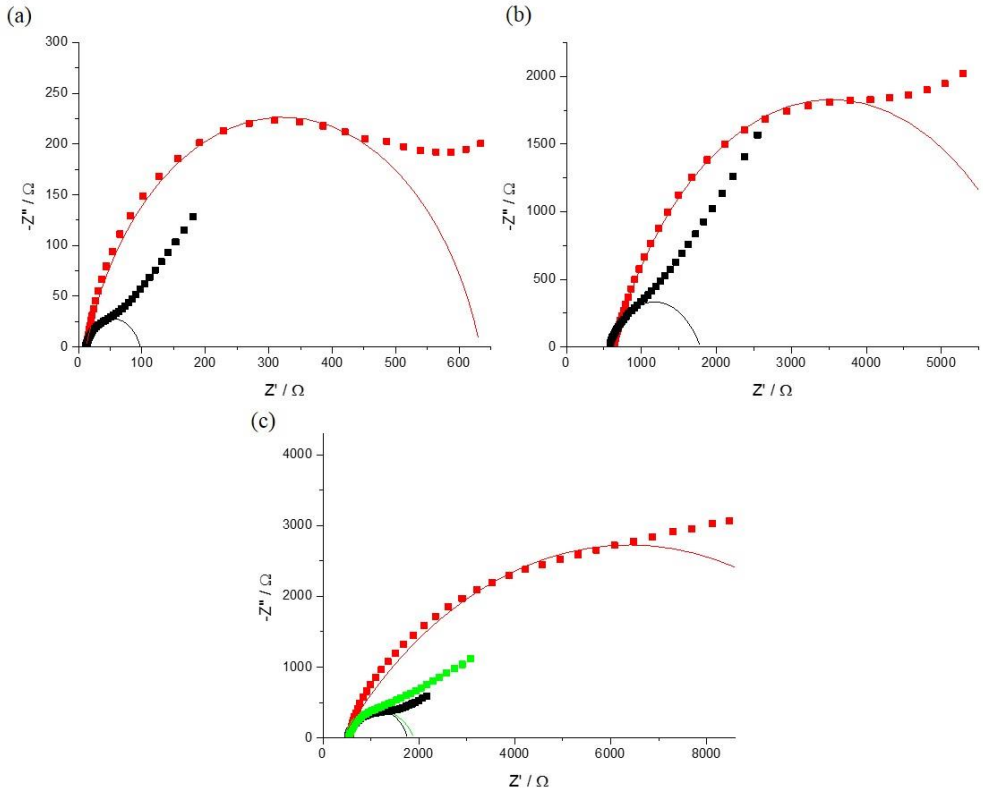


| System | $R_{CT}$ Bare (Monolayer Removed)/ Ω | $R_{CT}$ Monolayer/ Ω | $R_{\Omega}$ Bare (Monolayer Removed)/ Ω | $R_{\Omega}$ Monolayer/ Ω | Coverage |
|---|---|---|---|---|---|
| (a) Au-ODT Aqueous | 86.5 | 621.0 | 11.1 | 12.0 | 86% |
| (b)Au-ODT BMIM-OTf | 1220.9 | 5803.1 | 564.4 | 629.6 | 79% |
| (c) Co-ODT BMIM-OTf | 1224.8 (1383.8) | 11947.8 | 540.1 (515.7) | 410.2 | 90% |

*Figure 19: Electrochemical impedance spectra for octanethiol on gold and cobalt systems are shown. (a) Depicts the spectra of bare (black) and octanethiol monolayer coated Au (red) in aqueous 1 mM $K_3[Fe(CN)_6]$/0.5 M KCl. (b) Shows the spectra of bare (black) and octanethiol monolayer coated Au in 5 mM Fc in BMIM-OTf. Finally (c) depicts the spectra of the bare (black) and octanethiol monolayer coated Co (red), as well as the Co surface after the octanethiol has been reductively desorbed (green). All spectra have been fit to a semi-circle. By comparing the charge transfer resistance of the bare and monolayer coated surfaces the relative coverage of the monolayer can be determined.*

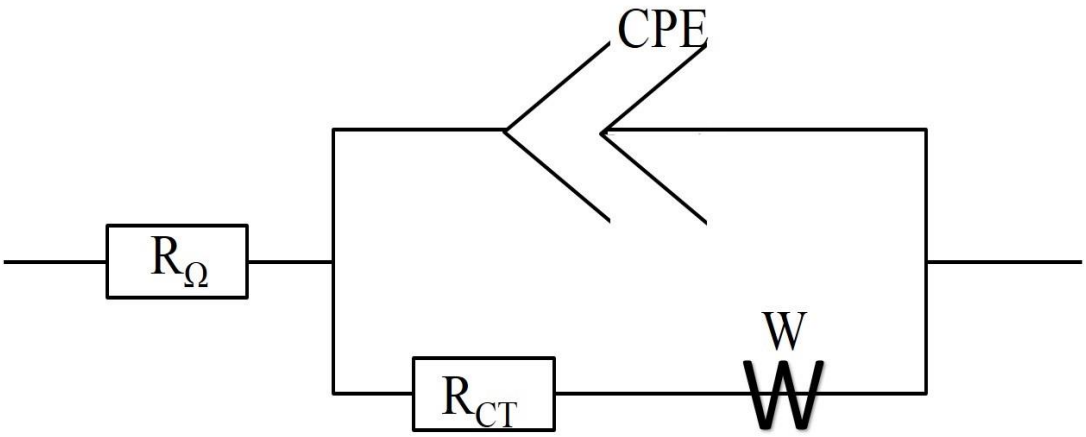


*Figure 20: The Randles Equivalent Circuit used for fitting all EIS data*

Activation energy process, which is controlled solely by charge transfer resistance and double layer capacitance.[111] This type of electron transfer, in which the charge transfer resistance is large can be considered to be kinetically slow,[112] as would be expected for an electron transfer blocked by a passivating layer. On looking at the bare surfaces the semi-circle is poorly defined, indicating a low contribution from the charge transfer resistance.[47] Instead in the bare surface spectra the Warburg impedance dominates the plot. The bare metal curves in **Figure 19**, show a straight line portion with a slope of 45 ° indicative of the dominance of the Warburg impedance (W), meaning the Warburg impedance must be accounted for in the equivalent circuit diagram. The clarity of the straight line portion of the spectra is furthermore indicative of a change in the controlling factor of the electron transfer; unlike for the monolayer passivated surface the electron transfer to the bare surface is dominated by mass transfer,[47] as expected.

By measuring the gold system in both aqueous and ionic liquid environments the effect of the ionic liquid on the spectra can be assessed, allowing better assessment

of the response of the Co system. Looking at the spectra it is obvious that upon going from aqueous to ionic liquid environments the origin of the spectra shifts, resulting from a change in solution resistance, $R_\Omega$. It can also be seen that the Z values are an order of magnitude larger than in the aqueous system, which is related to the $R_\Omega$ and $R_{CT}$ values being an order of magnitude larger in the ionic liquid than in the aqueous electrolyte. The $R_\Omega$ value is due to the solution resistance, large values of which are usually indicative of uncompensated solution resistance, i.e. iR drop. If these values were caused by iR drop the same or even a magnified effect would be expected for the measurements in the aqueous electrolyte. iR drop is exacerbated by a poorly conducting solution, this is unlikely to be the case for the BMIM-OTf electrolyte in either the Au or Co setup, as ionic liquids are highly conductive, more so than aqueous electrolytes. The conductance of BMIM-OTf is quoted in the literature as 9.8 S $cm^{-1}$,[113] compared to a value of 1.3 x $10^{-2}$ S $cm^{-1}$ for 0.1 M KCl.[114] Another cause of iR drop is poor positioning of the reference electrode with respect to the working electrode, these electrodes should be as close as possible. Because of the small volume of the cell used in these measurements the reference electrode is always close to the surface, so iR drop is unlikely, and has not been witnessed in other investigations performed in ionic liquids throughout this work. To avoid problems which may have arisen because of the reference electrode the same setup was used for both the BMIM-OTf and aqueous measurements, including the small volume cell and the Pt wire QRE. Therefore, if iR drop were to arise as a result of the reference electrode positioning it should carry through to the aqueous setup as well. Therefore, at this time, the reason underlying the measured higher apparent solution resistance ($R_\Omega$) for BMIM-OTf is not known.

As it has already been seen that different solvents affect the monolayers differently it is also useful to assess the relative electron transfer properties of the bare and monolayer protected Au surfaces. This can be done by using the following equation:[115, 116]

$$\text{Relative Passivation} = 1 - (R_{CT}\ bare/R_{CT}\ protected) \quad (Eq.\ 16)$$

This in effect assesses the "blocking ability" of the monolayer. Through this simple assessment it can be seen that high blocking and presumably high coverages of the three different systems are achieved. The values obtained from the above equation for the octanethiol protected Au are 86 % and 84 % in the aqueous and ionic liquid solvents, respectively. It should be noted that the different redox probes used may show apparent discrepancies between these values, particularly because ferrocene as a small neutral molecule may be able to get closer to the electrode surface than the charged ferricyanide used in the aqueous measurements. Regardless, however, first comparing the aqueous and ionic liquid behaviour of the octanethiol monolayer allows a better understanding of the behaviour of the octanethiol monolayer on Co in BMIM-OTf.

On investigating the octanethiol monolayer on Co it is apparent that the system behaves in a similar manner as on gold, that is there are relatively large $R_\Omega$ and Z values. Since this has already been seen for the gold system it is obvious this trait is due to the ionic liquid not the Co. In contrast to the Au system there is the possibility that when the bare Co surface is used oxidation of the surface may occur during measurement, which would have a large effect on the EIS. Given this possibility the Co surface is measured in three different states. 1) "Bare," with the surface electrochemically reduced first, 2) coated with the octanethiol monolayer and 3)

directly after reductive desorption of the octanethiol monolayer, these are shown in **Figure 19c** as the black, red, and green curves, respectively. The black and green curves are fairly similar, whereas the red curve is obviously different. This helps strengthen the conclusion that the monolayer can be formed and then removed through reductive desorption. As with the gold systems the reduction in electron transfer rates on going from the bare to the monolayer protected Co surface can be assessed, showing a 91% reduction when the initial bare electrode is used, or a 90% reduction when the bare electrode after reductive desorption is used. These EIS measurements have shown the monolayers formed on Co with potential control in BMIM-OTf are of at least a similar quality as those formed on Au through standard self-assembly methods as they give rise to a better passivating layer than for the Au system.

Single Molecule Conductance Measurements

*I*(*s*) measurements were performed on octanedithiol monolayers on Au and Co which were formed through standard self-assembly and potential controlled assembly respectively. Although *I*(*s*) measurements are usually performed using submonolayer coverage full monolayers were used in this investigation to protect the Co surface from oxidation long enough for the STM to be set up. Measurements were performed in BMIM-OTf in a nitrogen atmosphere of low moisture content to further protect the Co surface. As the *I*(*s*) measurements are carried out the constant contact with, and burrowing into the surface by the STM tip means the monolayer is destroyed in places[117] opening the Co up to degradation if the experiments were performed under ambient conditions. To allow for a like for like comparison the octanedithiol on Au experiments were performed in the same manner, with full monolayer coverage and in BMIM-OTf. For the best understanding of the conductance of octanedithiol between two Co contacts four systems were examined: (a) octanedithiol on a gold

substrate with a cut and Apiezon-wax coated gold tip, (b) octanedithiol on a Co substrate with a cut and Apiezon-wax coated gold tip, (c) electrochemically etched and Apiezon-wax coated Co (CoO) tip and (d) electrochemically etched and Apiezon-wax coated Co reduced *in-situ* to give an oxide free surface (Co) tip.

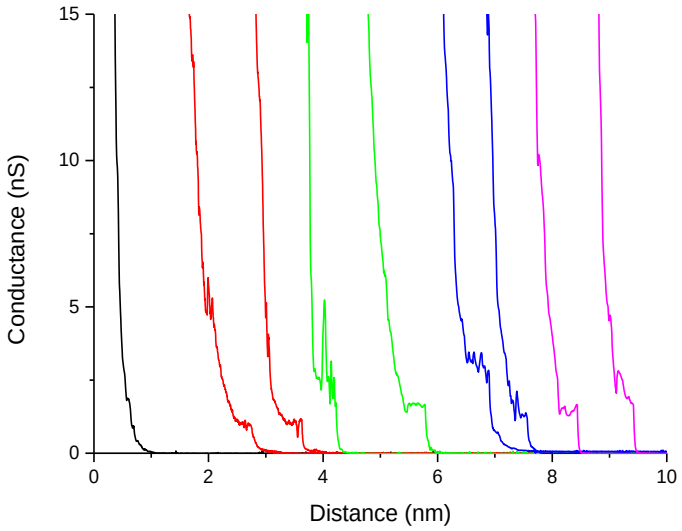


*Figure 21: Example* I(s) *curves for (black) a junction in which no molecule spans the gap, and (coloured) junctions in which octanedithiol spans the gap. Red: Au/ODT/Au, Green: Co/ODT/Au, Blue: Co/ODT/CoO, Magenta: Co/ODT/Co.*

When performing $I(s)$ measurements one of two types of decay curves is seen. The majority of the time there are no molecules present in the junction causing the pure exponential decay, in the black curve in **Figure 21**. When a molecule spans the gap, as is the case for coloured curves in **Figure 21**, a plateau is seen. These curves behave in a similar manner for all 4 systems. While curves with plateaus occur relatively infrequently, by collecting enough of these curves a statistically significant value for the conductance can be obtained from the histogram. The distances shown in these curves are relative values, although they can be defined with respect to the absolute distance of the tip from the surface by calibrating back to the $G_0$ distance, $s_0$,

which can be added to the experimental distance values. The value of $s_0$ can be found using the equation:[117, 118]

$$s_0 = \frac{\ln\left({}^{G_0 V_t}/_{I_0}\right)}{{}^{d\ln(I)}/_{d\,s}} \qquad (Eq.\ 17)$$

In this equation $G_0$ is the quantum point contact conductance, known to be 77.4 μS from the equation $G_0 = 2e^2/h$, $V_t$ is the tip bias, $I_0$ is the set point current, and $d\ln(I)/ds$ is the slope of the ln($I$)-$s$ plot of the exponential curve with no molecule present. The $s_0$ values of the 4 systems were similar with values of 1.5, 1.3, 1.1, and 1.2 nm for the Au-ODT-Au, Co-ODT-Au, Co-ODT-CoO, and Co-ODT-CoO systems, respectively.

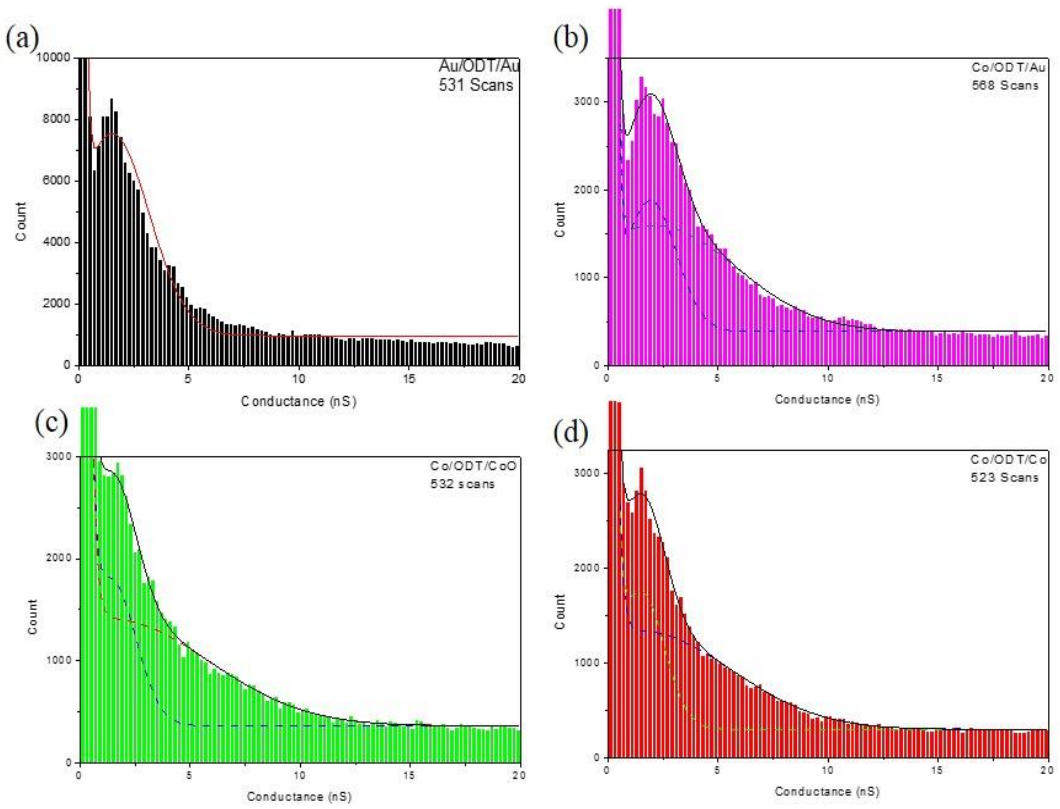


*Figure 22: Histograms used to determine the conductance of the (a) Au/ODT/Au, (b) Co/ODT/Au, (c) Co/ODT/CoO, and (d) Co/ODT/Co junction. All histograms were formed from more than 500 scans. To determine the conductance Gaussians were fitted.*

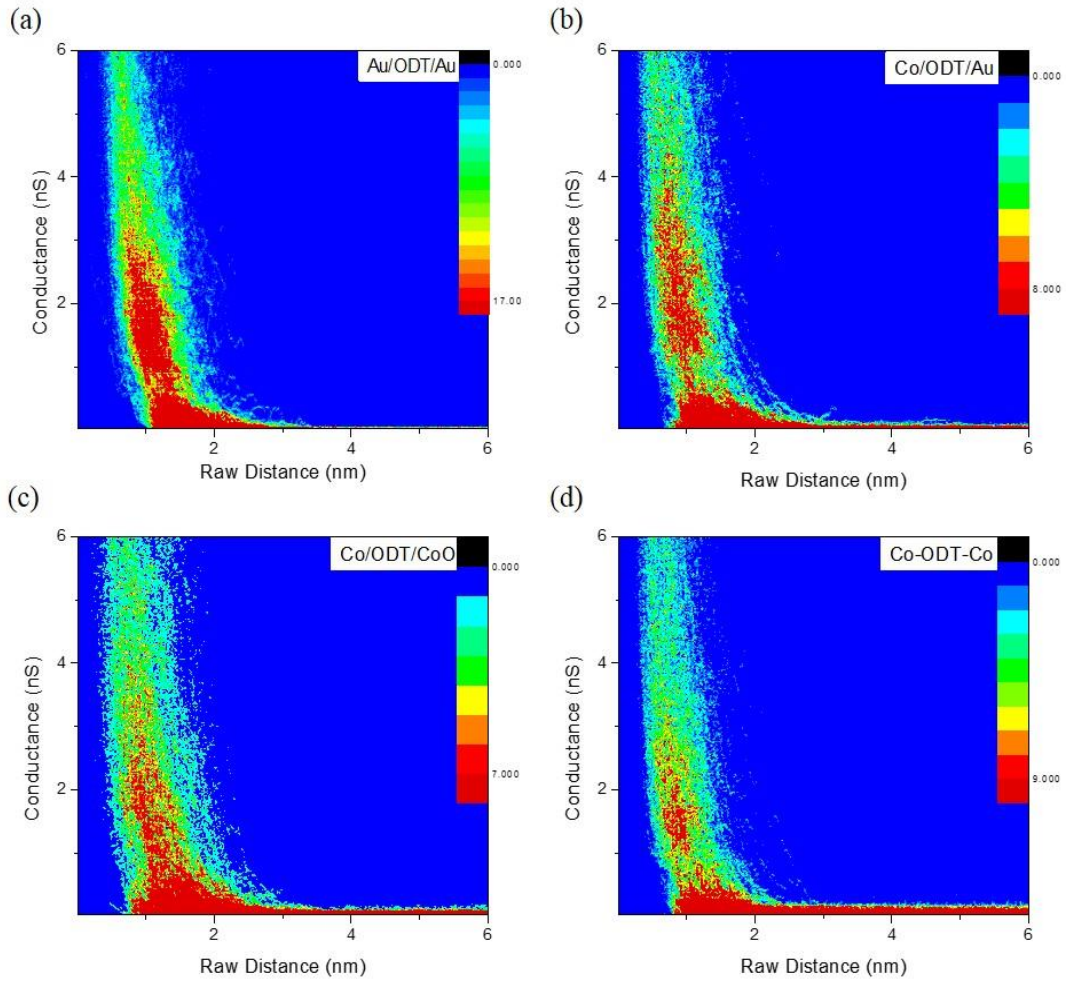


*Figure 23: 2D histograms of the conductance of the (a) Au/ODT/Au, (b) Co/ODT/Au, (c) Co/ODT/CoO, and (d) Co/ODT/Co junction.*

Octanedithiol on gold, at submonolayer coverages is a well-studied system known to give conductance values of 0.9 to 1.2 nS regardless of the environment.[21, 23, 119-121] To ensure a rigorous comparison the only difference between the Au octanedithiol system and the Co octanedithiol system was the metal contact, meaning measurement on monolayer covered Au was necessary. A histogram of the conductance of the Au-ODT-Au system in BMIM-OTf, system was produced from 531 *I*(*s*) scans, all with apparent plateaus, **Figure 22a**. From the histogram the conductance of the Au-ODT-Au is 1.5 nS which agree, within error, with literature values.[23, 119]

Unlike Au cobalt is an easily oxidisable metal. Oxide surfaces add increased complexity to any measurements performed on the Co-ODT system. To get a better idea as to how well the Co-ODT system will work for conductance measurements the *I*(*s*) measurements were performed using three different tips. These were cut and coated gold (Au), electrochemically etched and coated Co (CoO), and electrochemically etched and coated Co, which was reduced *in-situ* to give an oxide free surface (Co). The results of the measurements using these three types of tip are shown in **Figure 22b-d**. Looking at these three systems the conductance show reasonable agreement at 1.9, 1.4, and 1.5 nS for Co-ODT-Au, Co-ODT-CoO, and Co-ODT-Co, respectively. The most obvious difference between the three tip types is the degree of peak clarity in the histogram, which increases in the order Co-ODT-CoO < Co-ODT-Co < Co-ODT-Au. This change is likely a result of the junction stability, as more stable junctions allow longer plateaus, increasing in the number of data points for that conductance. When a metal surface is oxidised the bond between the metal and the thiol has been seen by XPS to be more likely to be a weaker chemisorbed or even physisorbed bond,[61] causing a shorter break off distance than the stronger chemisorbed bond, giving rise to the lower clarity peak for the CoO tip than the Co tip. While the Co-S bond is of more covalent character than the Au-S bond the thiol end group is known to pull out the Au atoms when adsorbed on the surface.[122] As the Au junctions can stretch further than either of the Co junctions the number of data points per plateau should be greatest for the Au junctions giving rise to the higher clarity peak. Further evidence of the different stretching of the junctions can be seen from the 2D histograms of the different junctions in **Figure 23**.

When the conductance value of the Co-ODT-Co system is compared to that of the Au-ODT-Au system it can be seen that the conductance values are almost

concurrent. The resulting tunnelling current of an STM may be given by the equation:[123]

$$I = \left(\frac{e^2}{\hbar}\right)\left(\frac{\kappa_0}{4\pi^2 s}\right) V e^{(-2\kappa_0\, s)} \quad \textit{(Eq. 18)}$$

The variables in the above equation can be defined as *s*, the effective tunnel distance in Å, $\kappa_0$, the inverse decay length of the wave function density outside the surface in Å, *V*, the applied voltage in volts, and $\left(\frac{e^2}{\hbar}\right) = 2.44 \times 10^{-4}$ in $\Omega^{-1}$. $\kappa_0$ can be found using the expression $2\kappa_0 = 1.025\sqrt{Ø}$ where Ø is the effective barrier height in eV. When using this equation it is usual to assume that Ø is equivalent to the average work function of the electrodes, ϕ, in eV.[123] On the basis of this assumption it can be seen that current is exponentially related to work function by the following:

$$I \propto V e^{-2s\sqrt{2\phi}} \textit{ (Eq. 19)}$$

On changing the metal contacts involved in the measurements the only variable affected in this simple equation is the work function of the metal. The effects of changes in metal work function have previously been investigated by conductive AFM of dithiol monolayers on various metals by the Frisbie group.[124] They found that by changing the metal contacts, to change the work function, the resistance measured for the system increased with decreasing work function. The theory behind this is that in the alkanedithiol system the conductance mechanism is hole transport, and therefore through the HOMO of the molecule. By raising the work function the barrier to hole transport, and therefore resistance to transport, decreases. It should be noted though that because there is a density of states across the system, i.e. related to the molecule as well, changing the metal does not have as drastic of an effect as it would do for more localized systems. Unlike more localized systems, in this work it is expected that

the delocalization occurs with a pinning of the Fermi level of the electrode with respect to the HOMO* and LUMO* positions, so the energy offset of the two is independent of the metal.[124] On going from Au to Co the work function changes from 5.4 eV for Au,[125, 126] to 5.0 eV for Co.[127] It is known however, that the stronger the interaction between the metal surface and the alkanethiol, the higher the conductance. Because Co has a stronger, more covalent bonding character with the thiol end group than Au does, it would be predicted based on this that the Co-ODT system would have the higher conductance. This increased bonding character may therefore counteract the increase in conductance expected for the Au based on work function alone.

Spartan® calculations were performed to further understand the conductances of the Co and Au systems, these are found in **Figure 24-27**. The values of the HOMO-LUMO gap of the system were first assessed, as the smaller this value is, the higher the conductance is predicted to be.[128, 129] The HOMO-LUMO gap was found to be 2.77 eV, 1.51 eV, and 1.51 eV for the Au-ODT-Au, Co-ODT-Au, and Co-ODT-Co systems, respectively. While it is obvious the HOMO-LUMO gap calculation is dependent on the alkane backbone of the molecular bridge, the metal contacts are also important. For similar calculations performed on Au-alkanedithiol systems the presence of the S-Au bonding and antibonding orbitals between the HOMO-LUMO gap of the alkanethiolate bridge led the HOMO-LUMO gap decreasing due to an increase in HOMO energy.[130] The stronger S-Co bonding interaction, compared to S-Au, may cause the greater decrease in HOMO-LUMO gap for the Co bonded systems. Given that these calculations account for the interaction of the discrete molecular orbitals with the metal DOS,[130] it is unsurprising that different metal contacts see a change in the electronic structures of the system. Considering the differences in conductance values of the three systems are statistically insignificant, this cannot be

used to justify the measured values. Molecular conductance of the alkanethiol occurs through orbitals which are delocalized across the molecule. These "spanning" orbitals can be termed "frontier orbitals", while those orbitals localized on the metal-thiol bonds are known as "gateway orbitals". [131, 132] The size of the energy gap between the gateway orbital and the metal work function is a good indication of molecular conductance. The metal work functions for the systems are 5.4 eV for the symmetric Au system,[125, 126] 5.0eV for the symmetric Co system,[127] and for the asymmetric Au-Co system the average is used.[123] Based on these work functions the energy gap is 2.77 eV, 2.63 eV, and 2.54 eV for the Au-ODT-Au, Co-ODT-Co, and Co-ODT-Au junctions respectively. The small difference calculated for each energy gap here likely causes the negligible difference in conductance measured experimentally.

Comparison of the Co-ODT-Co and Au-ODT-Au conductance values shows a negligible change on changing the metal. Au is an incredibly well-studied and easy to use contact system. Though Au is limited in its functionalities and future prospects in CMOS devices, these characteristics have meant research has shied away from the use of other metals. Although the method outlined here for Co-molecule-Co junctions is less straightforward than for preparing Au-molecule-Au junctions, it can still be carried out with standard laboratory conditions and techniques. By sacrificing some ease of use, however, more interesting, and technologically applicable contacts, like Co can be used.

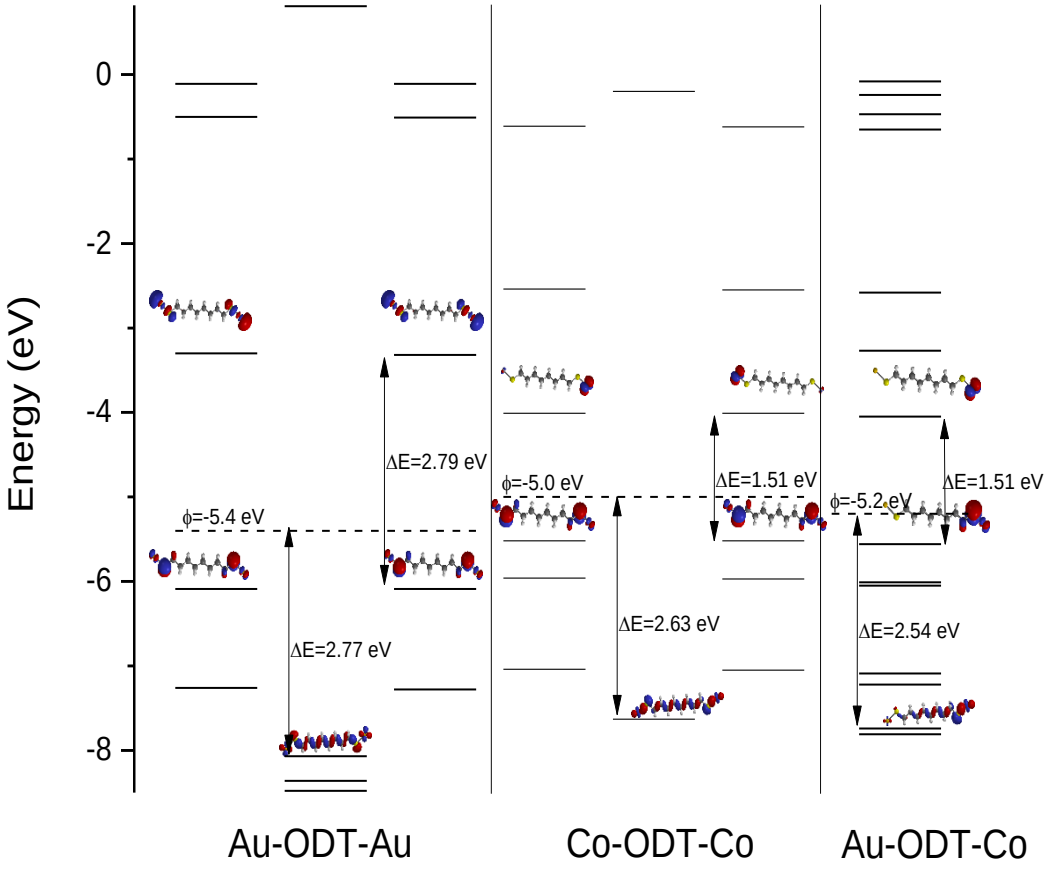


*Figure 24: The frontier orbital energy levels found through Spartan® calculations of octanedithiolate chemisorbed to a metal atom at both $S^-$ ends are shown. Three columns exist for the Au-ODT-Au and Co-ODT-Co systems to account for molecular orbitals with the same energy. The work functions of Au-ODT-Au, Co-ODT-Co, and Au-ODT-Co, the size of the HOMO-LUMO gap and the energy difference between the work function and fully delocalized HOMO are shown.*

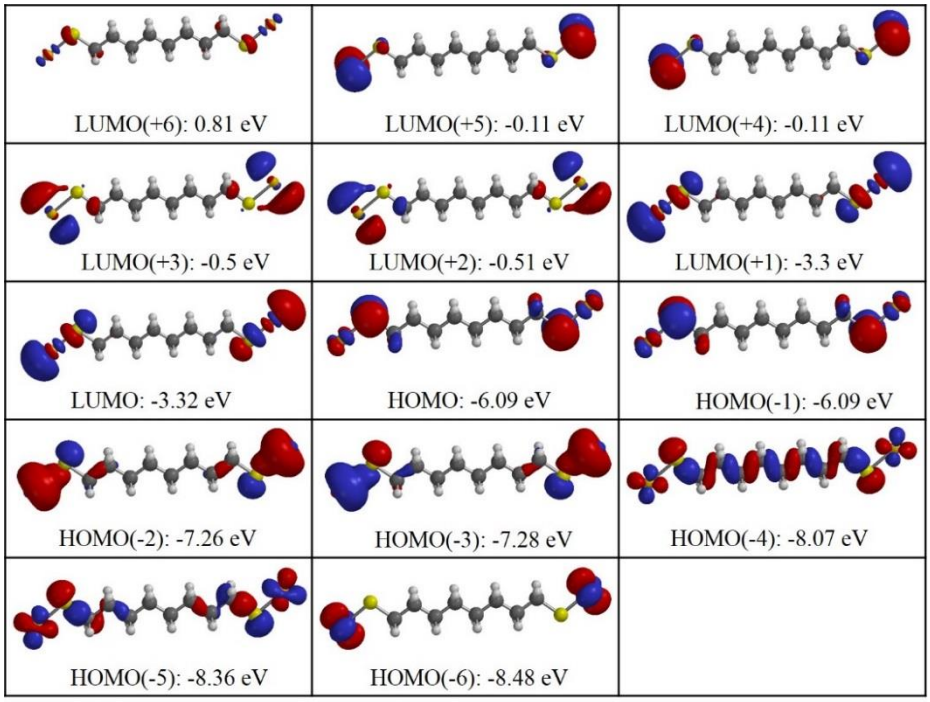


*Figure 25: The frontier orbitals of Au-ODT-Au were modelled with Spartan® using density functional theory at the B3LYP 6-31G* level of theory. From these it is seen that the H OMO (-4) orbital is the most important for the conductance of the system.*

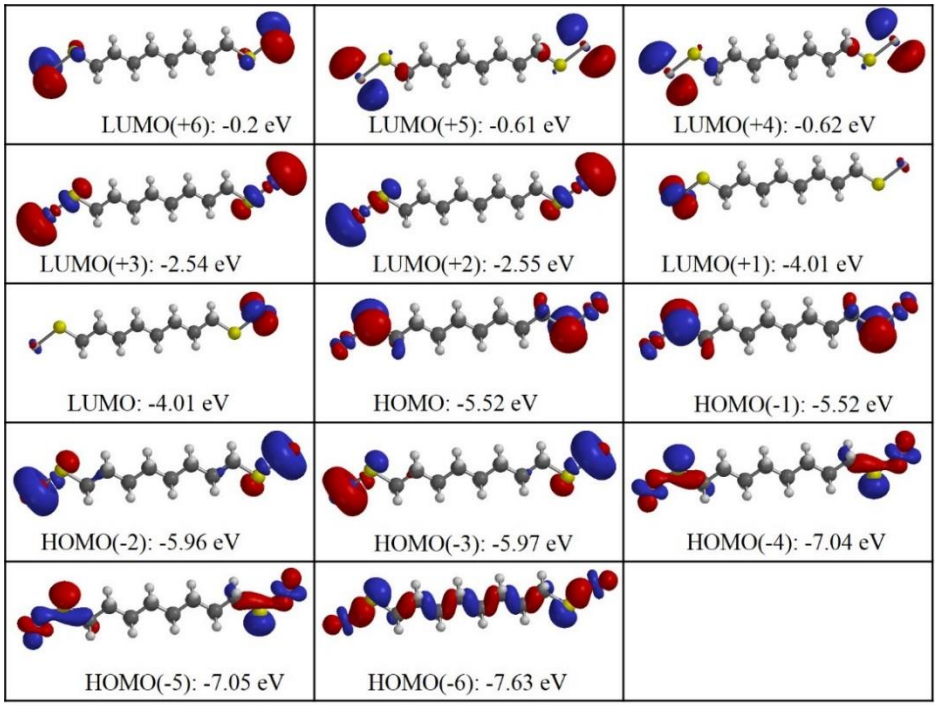


*Figure 26: The frontier orbitals of Co-ODT-Co were modelled using Spartan® using density functional theory at the B3LYP 6-31G* level of theory. From these it is seen that the HOMO (-6) orbital is the most important for the conductance of the system.*

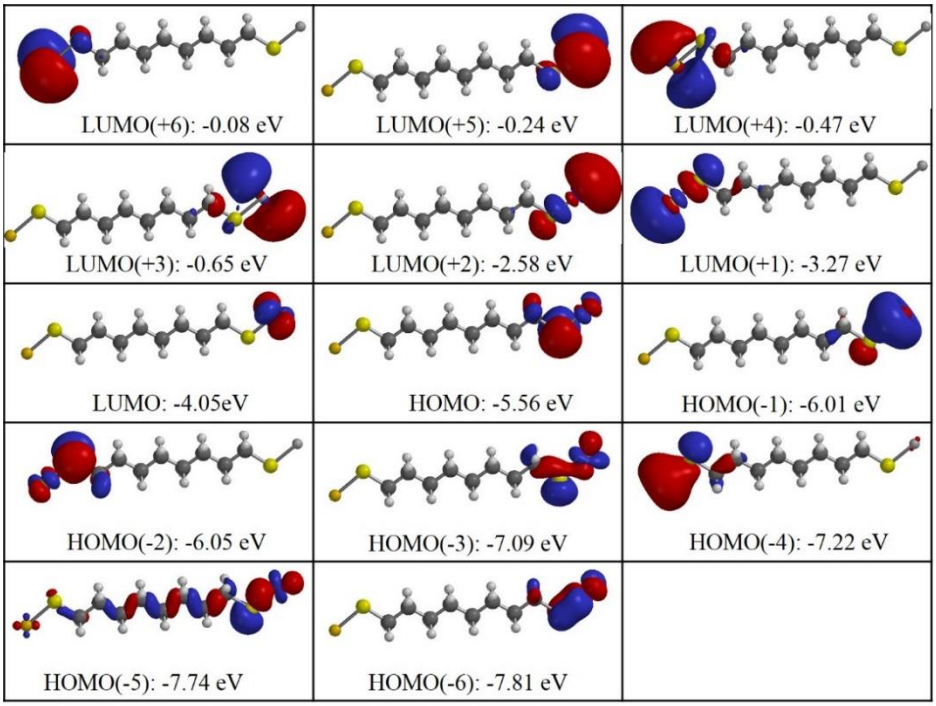


*Figure 27: The frontier orbitals of Au-ODT-Co were modelled using Spartan® using density functional theory at the B3LYP 6-31G* level of theory. From these it is seen that the frontier orbitals are a mixture of the Au-ODT-Au, and Co-ODT-Co orbitals. The HOMO (-5) orbital is the most important for the conductance of the system.*

## Conclusions

Although it has been well studied and is generally well behaved, gold is not necessarily the best contact metal for molecular electronics devices. Gold, as a non-magnetic metal, cannot be applied in molecular spintronics and for future application it should be appreciated that it is not CMOS compatible. The wide use of gold in fundamental studies has been driven by its ease of use in standard laboratory conditions. In order to move on to ferromagnetic metals for spintronics measurements, such as Co, a method to repeatedly prepare an oxide free metal-molecule system had to be found. By utilizing potential controlled molecular assembly in BMIM-OTf well-ordered, passivating monolayers of octanethiol, octanedithiol, and mercaptooctanoic acid were formed. Exploiting this fabrication method single molecule conductance

studies of a completely symmetric Co-ODT-Co system were carried out. This showed a similar conductance to that determined in the analogous Au-ODT-Au system. This result means that using a slightly more complicated setup a method to form a system with a metal contact other than gold has been found. This facilitates an increase in the contact functionality without a large loss in performance compared to gold. The overall outcome is that by using a somewhat more involved procedure, metal contacts other than gold, but which are prone to oxidation in air, can be used. Utilizing this experimental setup it should be possible in the future to measure the magnetoresistance of octanedithiol between two Co contacts. It is foreseeable that a similar method with minor adjustments would allow for other metal contacts, like Ni and Fe, to be studied.

## Declaration

*Karl Fischer titrations were carried out with the help and guidance of Iain Aldous at the University of Liverpool.*

## References


1. B. Xu and N. J. Tao, *Science*, 2003, **301**, 1221-1223.
2. W. Haiss, H. van Zalinge, S. J. Higgins, D. Bethell, H. Höbenreich, D. J. Schiffrin and R. J. Nichols, *Journal of the American Chemical Society*, 2003, **125**, 15294-15295.
3. www.nobelprize.org/nobel_prizes/physics/laureates/2007/, *The Nobel Prize in Physics 2007*, Accessed 30 March, 2014.
4. www.nobelprize.org/nobel_prizes/physics/laureates/2007/advanced.html, *The Nobel Prize in Physics 2007 - Advanced Information*, Accessed 30 March, 2014.
5. M. Galbiati, C. Barraud, S. Tatay, K. Bouzehouane, C. Deranlot, E. Jacquet, A. Fert, P. Seneor, R. Mattana and F. Petroff, *Advanced Materials*, 2012, **24**, 6429-6432.
6. S. Schmaus, A. Bagrets, Y. Nahas, T. K. Yamada, A. Bork, M. Bowen, E. Beaurepaire, F. Evers and W. Wulfhekel, *Nature Nanotechnology*, 2011, **6**, 185-189.
7. G. Pera, S. Martín, L. M. Ballesteros, A. J. Hope, P. J. Low, R. J. Nichols and P. Cea, *Chemistry – A European Journal*, 2010, **16**, 13398-13405.
8. P. G. Hoertz, J. R. Niskala, P. Dai, H. T. Black and W. You, *Journal of the American Chemical Society*, 2008, **130**, 9763-9772.

9. M. Kiguchi, S. Miura, K. Hara, M. Sawamura and K. Murakoshi, *Applied Physics Letters*, 2006, **89**, 213104.
10. F. Chen, X. Li, J. Hihath, Z. Huang and N. Tao, *Journal of the American Chemical Society*, 2006, **128**, 15874-15881.
11. L. Venkataraman, J. E. Klare, I. W. Tam, C. Nuckolls, M. S. Hybertsen and M. L. Steigerwald, *Nano Letters*, 2006, **6**, 458-462.
12. Y. Feng, S. Chen, J. You and W. Guo, *Electrochimica Acta*, 2007, **53**, 1743-1753.
13. P. Moreno-García, M. Gulcur, D. Z. Manrique, T. Pope, W. Hong, V. Kaliginedi, C. Huang, A. S. Batsanov, M. R. Bryce, C. Lambert and T. Wandlowski, *Journal of the American Chemical Society*, 2013, **135**, 12228-12240.
14. M. Kiguchi, S. Miura, K. Hara, M. Sawamura and K. Murakoshi, *Applied Physics Letters*, 2007, **91**, -.
15. M. Kiguchi, S. Miura, T. Takahashi, K. Hara, M. Sawamura and K. Murakoshi, *The Journal of Physical Chemistry C*, 2008, **112**, 13349-13352.
16. X.-S. Zhou, Y.-M. Wei, L. Liu, Z.-B. Chen, J. Tang and B.-W. Mao, *Journal of the American Chemical Society*, 2008, **130**, 13228-13230.
17. X.-S. Zhou, J.-H. Liang, Z.-B. Chen and B.-W. Mao, *Electrochemistry Communications*, 2011, **13**, 407-410.
18. E. Pires, J. E. Macdonald and M. Elliott, *Nanoscale*, 2013, **5**, 9397-9403.
19. Z. Jianfeng, G. Cunlan and X. Bingqian, *Journal of Physics: Condensed Matter*, 2012, **24**, 164209.
20. E. Wierzbinski and K. Slowinski, *Langmuir*, 2006, **22**, 5205-5208.
21. W. Haiss, S. Martin, L. E. Scullion, L. Bouffier, S. J. Higgins and R. J. Nichols, *Physical Chemistry Chemical Physics*, 2009, **11**, 10831-10838.
22. M. Taniguchi, M. Tsutsui, K. Yokota and T. Kawai, *Chemical Science*, 2010, **1**, 247-253.
23. N. J. Kay, R. J. Nichols, S. J. Higgins, W. Haiss, G. Sedghi, W. Schwarzacher and B.-W. Mao, *The Journal of Physical Chemistry C*, 2011, **115**, 21402-21408.
24. X. D. Cui, A. Primak, X. Zarate, J. Tomfohr, O. F. Sankey, A. L. Moore, T. A. Moore, D. Gust, L. A. Nagahara and S. M. Lindsay, *The Journal of Physical Chemistry B*, 2002, **106**, 8609-8614.
25. S. A. Paz, M. E. Zoloff Michoff, C. F. A. Negre, J. A. Olmos-Asar, M. M. Mariscal, C. G. Sánchez and E. P. M. Leiva, *Journal of Chemical Theory and Computation*, 2012, **8**, 4539-4545.
26. A. Sen and C.-C. Kaun, *ACS Nano*, 2010, **4**, 6404-6408.
27. K. H. Müller, *Physical Review B*, 2006, **73**, 045403.
28. C. Pirlot, J. Delhalle, J. J. Pireaux and Z. Mekhalif, *Surface and Coatings Technology*, 2001, **138**, 166-172.
29. L. Tortech, Z. Mekhalif, J. Delhalle, F. Guittard and S. Géribaldi, *Thin Solid Films*, 2005, **491**, 253-259.
30. Z. Mekhalif, A. Lazarescu, L. Hevesi, J. j. Pireaux and J. Delhalle, *Journal of Materials Chemistry*, 1998, **8**, 545-551.
31. Z. Mekhalif, J. Riga, J. J. Pireaux and J. Delhalle, *Langmuir*, 1997, **13**, 2285-2290.
32. S. Devillers, A. Hennart, J. Delhalle and Z. Mekhalif, *Langmuir*, 2011, **27**, 14849-14860.

33. Z. Mekhalif, G. Fonder, D. Auguste, F. Laffineur and J. Delhalle, *Journal of Electroanalytical Chemistry*, 2008, **618**, 24-32.
34. J. Dai, J. Cheng, J. Jin, Z. Li, J. Kong and S. Bi, *Electrochemistry Communications*, 2008, **10**, 587-591.
35. C. Albonetti, M. Cavallini, M. Massi, J. F. Moulin and F. Biscarini, *Journal of Vacuum Science & Technology B*, 2005, **23**, 2564-2566.
36. C. Albonetti, I. Bergenti, M. Cavallini, V. Dediu, M. Massi, J.-F. Moulin and F. Biscarini, *Review of Scientific Instruments*, 2002, **73**, 4254-4256.
37. N. Pradhan, T. Subbaiah, S. C. Das and U. N. Dash, *J Appl Electrochem*, 1997, **27**, 713-719.
38. M. I. Jeffrey, W. L. Choo and P. L. Breuer, *Minerals Engineering*, 2000, **13**, 1231-1241.
39. D. R. Gabe, *J Appl Electrochem*, 1997, **27**, 908-915.
40. *Instrumental Methods in Electrochemistry / Southampton Electrochemistry*, Horwood Publishing, Chichester, 2001.
41. A. B. Soto, E. M. Arce, M. Palomar-Pardavé and I. González, *Electrochimica Acta*, 1996, **41**, 2647-2655.
42. E. Herrero, L. J. Buller, J. Li, A. C. Finnefrock, A. B. Salomón, C. Alonso, J. D. Brock and H. D. Abruña, *Electrochimica Acta*, 1998, **44**, 983-992.
43. L. H. Mendoza-Huizar, J. Robles and M. Palomar-Pardavé, *Journal of Electroanalytical Chemistry*, 2002, **521**, 95-106.
44. L. H. Mendoza-Huizar, J. Robles and M. Palomar-Pardavé, *Journal of Electroanalytical Chemistry*, 2003, **545**, 39-45.
45. E. Bosco and S. K. Rangarajan, *Journal of Electroanalytical Chemistry and Interfacial Electrochemistry*, 1982, **134**, 213-224.
46. D. Grujicic and B. Pesic, *Electrochimica Acta*, 2004, **49**, 4719-4732.
47. A. J. Bard and L. R. Faulkner, *Electrochemical Methods: Fundamentals and Applications*, 2nd edn., John Wiley & Sons Inc, New York, 2001.
48. D. T. Sawyer, A. Sobkowiak and J. L. Roberts Jr., *Electrochemistry for Chemists*, 2nd edn., John Wiley & Sons Inc, New York, 1995.
49. http://www.ecochemie.nl/download/Applicationnotes/Autolab_Application_Note_EC03.pdf, *Autolab Application Note EC03: Ohmic Drop Part 1 - Basic Principles*, Accessed 2/4/14, 2014.
50. A. J. Bard and L. R. Faulkner, in *Electrochemical Methods: Fundamentals and Applications*, John Wiley & Sons Inc, New York, Editon edn., 2001, pp. 1-43.
51. http://www.gamry.com/application-notes/understanding-ir-compensation/, *Gamry Instruments: Understanding iR Compensation*, Accessed 2/4/14, 2014.
52. C. Lefrou, P. Fabry and J.-C. Poignet, in *Electrochemistry*, Springer Berlin Heidelberg, Editon edn., 2012, pp. 51-118.
53. http://www.ecochemie.nl/download/NovaTutorials/iR_compensation_tutorial.pdf, *Metrohm: NOVA iR Compensation Tutorial*, Accessed 3/4/2014, 2014.
54. L. H. Mendoza-Huizar, C. H. R. Reyes, M. Rivera and C. A. Galán-Vidal, *ADVANCES IN TECHNOLOGY OF MATERIALS AND MATERIALS PROCESSING JOURNAL*, 2007, **8**, 152-159.
55. J. T. Matsushima, F. Trivinho-Strixino and E. C. Pereira, *Electrochimica Acta*, 2006, **51**, 1960-1966.
56. L. H. Mendoza-Huizar, J. Robles and M. Palomar-Pardave, *Journal of the Electrochemical Society*, 2005, **152**, c265-c271.
57. M. Palomar-Pardavé, B. R. Scharifker, E. M. Arce and M. Romero-Romo, *Electrochimica Acta*, 2005, **50**, 4736-4745.

58. L. Cagnon, A. Gundel, T. Devolder, A. Morrone, C. Chappert, J. E. Schmidt and P. Allongue, *Applied Surface Science*, 2000, **164**, 22-28.
59. B. Rellinghaus, S. Fernandez DeAvila, G. Armelles, R. Beyers, A. Kellock and D. Weller, *Magnetics, IEEE Transactions on*, 1997, **33**, 3238-3240.
60. D. S. Hall, C. Bock and B. R. MacDougall, *Journal of the Electrochemical Society*, 2013, **160**, F235-F243.
61. F. Sinapi, T. Issakova, J. Delhalle and Z. Mekhalif, *Thin Solid Films*, 2007, **515**, 6833-6843.
62. M. Grdeń and J. Jagiełło, *Journal of Solid State Electrochemistry*, 2013, **17**, 145-156.
63. R. P. Šimpraga, *Journal of Electroanalytical Chemistry*, 1993, **355**, 79-96.
64. E. Dubois and J. Chevalet, *Langmuir*, 2003, **19**, 10892-10900.
65. S. Rifai, G. P. Lopinski, T. Ward, D. D. M. Wayner and M. Morin, *Langmuir*, 2003, **19**, 8916-8921.
66. F. Ma and R. B. Lennox, *Langmuir*, 2000, **16**, 6188-6190.
67. Ž. Petrović, M. Metikoš-Huković and R. Babić, *Journal of Electroanalytical Chemistry*, 2008, **623**, 54-60.
68. T. Sumi, H. Wano and K. Uosaki, *Journal of Electroanalytical Chemistry*, 2003, **550–551**, 321-325.
69. J. E. Sadler, D. S. Szumski, A. Kierzkowska, S. R. Catarelli, K. Stella, R. J. Nichols, M. H. Fonticelli, G. Benitez, B. Blum, R. C. Salvarezza and W. Schwarzacher, *Physical Chemistry Chemical Physics*, 2011, **13**, 17987-17993.
70. P. Diao, Q. Hou, M. Guo, M. Xiang and Q. Zhang, *Journal of Electroanalytical Chemistry*, 2006, **597**, 103-110.
71. U. K. Sur and V. Lakshminarayanan, *Journal of Electroanalytical Chemistry*, 2001, **516**, 31-38.
72. D. E. Khoshtariya, T. D. Dolidze and R. van Eldik, *Physical Review E*, 2009, **80**, 065101.
73. D. E. Khoshtariya, T. D. Dolidze and R. van Eldik, *Chemistry – A European Journal*, 2009, **15**, 5254-5262.
74. A. D. Le and L. Yu, *Journal of the Electrochemical Society*, 2011, **158**, F10-F14.
75. T. D. Dolidze, D. E. Khoshtariya, P. Illner and R. v. Eldik, *Chemical Communications*, 2008, 2112-2114.
76. Y. T. Tao, *Journal of the American Chemical Society*, 1993, **115**, 4350-4358.
77. K. B. Myli and V. H. Grassian, *The Journal of Physical Chemistry*, 1995, **99**, 5581-5587.
78. A. M. Cione, O. A. Mazyar, B. D. Booth, C. McCabe and G. K. Jennings, *The Journal of Physical Chemistry C*, 2009, **113**, 2384-2392.
79. H. A. Pearce and N. Sheppard, *Surface Science*, 1976, **59**, 205-217.
80. S. Subramanian and S. Sampath, *Anal Bioanal Chem*, 2007, **388**, 135-145.
81. S. Subramanian and S. Sampath, *Pramana - J. Phys.*, 2005, **65**, 753-761.
82. Z. Li, S.-C. Chang and R. S. Williams, *Langmuir*, 2003, **19**, 6744-6749.
83. M. D. Porter, T. B. Bright, D. L. Allara and C. E. D. Chidsey, *Journal of the American Chemical Society*, 1987, **109**, 3559-3568.
84. R. G. Nuzzo, E. M. Korenic and L. H. Dubois, *The Journal of Chemical Physics*, 1990, **93**, 767-773.
85. G. Fonder, F. Cecchet, A. Peremans, P. A. Thiry, J. Delhalle and Z. Mekhalif, *Surface Science*, 2009, **603**, 2276-2282.
86. C. Nogues and P. Lang, *Langmuir*, 2007, **23**, 8385-8391.

87. P. E. Laibinis, G. M. Whitesides, D. L. Allara, Y. T. Tao, A. N. Parikh and R. G. Nuzzo, *Journal of the American Chemical Society*, 1991, **113**, 7152-7167.
88. H. D. Wanzenbock, B. Mizaikoff, N. Weissenbacher and R. Kellner, *Fresenius' Journal of Analytical Chemistry*, 1998, **362**, 15-20.
89. G. Che, Z. Li, H. Zhang and C. R. Cabrera, *Journal of Electroanalytical Chemistry*, 1998, **453**, 9-17.
90. B. Zumbrägel, *Electrochemistry: A workbook for 910 PSTAT mini*, Switzerland, 2013.
91. R. S. Nicholson, *Analytical Chemistry*, 1965, **37**, 1351-1355.
92. R. Parsons, *Surface Science*, 1964, **2**, 418-435.
93. W. Schmickler, *Interfacial Electrochemistry*, Oxford University Press, New York, 1996.
94. R. A. Ballinger and C. A. W. Marshall, *Journal of Physics F: Metal Physics*, 1973, **3**, 735.
95. N. E. Christensen and B. O. Seraphin, *Physical Review B*, 1971, **4**, 3321-3344.
96. J. O. Bockris, apos, M, R. J. Mannan and A. Damjanovic, *The Journal of Chemical Physics*, 1968, **48**, 1898-1904.
97. D. Galizzioli and S. Trasatti, *Journal of Electroanalytical Chemistry and Interfacial Electrochemistry*, 1973, **44**, 367-388.
98. M. Hromadová and W. R. Fawcett, *The Journal of Physical Chemistry A*, 2000, **104**, 4356-4363.
99. Y. Xiaoling and Z. Guigen, *Nanotechnology*, 2008, **19**, 465504.
100. C. Miller, P. Cuendet and M. Graetzel, *The Journal of Physical Chemistry*, 1991, **95**, 877-886.
101. Y. Yang and L. Yu, *Physical Chemistry Chemical Physics*, 2013, **15**, 2669-2683.
102. J. D. Holbrey, W. M. Reichert, M. Nieuwenhuyzen, O. Sheppard, C. Hardacre and R. D. Rogers, *Chemical Communications*, 2003, 476-477.
103. K. A. Groat and S. E. Creager, *Langmuir*, 1993, **9**, 3668-3675.
104. A. N. Caruso, L. G. Wang, S. S. Jaswal, E. Y. Tsymbal and P. A. Dowben, *J Mater Sci*, 2006, **41**, 6198-6206.
105. R. D. Cowling and A. C. Riddiford, *Electrochimica Acta*, 1969, **14**, 981-989.
106. S. Ando, T. Suzuki and K. Itaya, *Journal of Electroanalytical Chemistry*, 1997, **431**, 277-284.
107. C. Hardacre, J. D. Holbrey, M. Nieuwenhuyzen and T. G. A. Youngs, *Accounts of Chemical Research*, 2007, **40**, 1146-1155.
108. V. D. Jovic http://www.gamry.com/assets/Application-Notes/Determination-of-Double-Layer-Capacitance-from-a-CPE.pdf, *Determination of the correct value of Cdl from the impedance results fitted by the commercially available software*, Accessed 6/4/2014, 2014.
109. X. Z. Yuan, C. J. Song, H. J. Wang and J. J. Zhang, *EIS Equivalent Circuits*, Springer, New York, 2010.
110. http://www.metrohm-autolab.co.uk/Downloads/Appl013.pdf, *Autolab Application Note: Electrochemical Impedance Spectroscopy (EIS): 3. Data Analysis (EIS): 3. Data Analysis*, Accessed 6/4/14, 2014.
111. M. E. Orazem and B. Tribollet, in *Electrochemical Impedance Spectroscopy*, John Wiley & Sons, Inc., Editon edn., 2008, pp. 307-331.
112. X.-Z. Yuan, C. Song, H. Wang and J. Zhang, *Impedance and its Corresponding Electrochemical Processes*, 2010.

113. H. Tokuda, K. Hayamizu, K. Ishii, M. A. B. H. Susan and M. Watanabe, *The Journal of Physical Chemistry B*, 2004, **108**, 16593-16600.
114. Y. C. Wu, W. F. Koch and K. W. Pratt, *J. Res. Natl. Inst. Stand. Technol.*, 1991, **96**, 191-201.
115. K. Bandyopadhyay and K. Vijayamohanan, *Langmuir*, 1998, **14**, 625-629.
116. K. Nakano, T. Sato, M. Tazaki and M. Takagi, *Langmuir*, 2000, **16**, 2225-2229.
117. L. M. Ballesteros, S. Martín, G. Pera, P. A. Schauer, N. J. Kay, M. a. C. López, P. J. Low, R. J. Nichols and P. Cea, *Langmuir*, 2011, **27**, 3600-3610.
118. S. Martín, W. Haiss, S. Higgins, P. Cea, M. C. López and R. J. Nichols, *The Journal of Physical Chemistry C*, 2008, **112**, 3941-3948.
119. N. J. Kay, PhD Thesis, University of Liverpool, 2012.
120. W. Haiss, R. J. Nichols, H. van Zalinge, S. J. Higgins, D. Bethell and D. J. Schiffrin, *Physical Chemistry Chemical Physics*, 2004, **6**, 4330-4337.
121. C. M. Kim and J. Bechhoefer, *The Journal of Chemical Physics*, 2013, **138**, -.
122. N. A. Kautz and S. A. Kandel, *Journal of the American Chemical Society*, 2008, **130**, 6908-6909.
123. G. Binnig and H. Rohrer, *IBM Journal of Research and Development*, 2000, **44**, 279-293.
124. V. B. Engelkes, J. M. Beebe and C. D. Frisbie, *Journal of the American Chemical Society*, 2004, **126**, 14287-14296.
125. S. Saito, T. Maeda, T. Soumura and K. Takeda, *Applied Surface Science*, 1988, **33–34**, 1088-1093.
126. M. Uda, A. Nakamura, T. Yamamoto and Y. Fujimoto, *Journal of Electron Spectroscopy and Related Phenomena*, 1998, **88–91**, 643-648.
127. D. E. Eastman, *Physical Review B*, 1970, **2**, 1-2.
128. X. Xiao, L. A. Nagahara, A. M. Rawlett and N. Tao, *Journal of the American Chemical Society*, 2005, **127**, 9235-9240.
129. S. M. Wu, M. T. Gonzalez, R. Huber, S. Grunder, M. Mayor, C. Schonenberger and M. Calame, *Nature Nanotechnology*, 2008, **3**, 569-574.
130. J. M. Seminario and L. Yan, *International Journal of Quantum Chemistry*, 2005, **102**, 711-723.
131. C. Joachim and M. A. Ratner, *Proceedings of the National Academy of Sciences of the United States of America*, 2005, **102**, 8801-8808.
132. A. Troisi and M. A. Ratner, *Physical Review B*, 2005, **72**, 033408.

# Chapter 7:

# EC-STM in

# Ionic Liquids

# Introduction

The richness of possibilities allowed by organic and inorganic chemistries, allows molecular electronics to use molecules as common place electronic components such as wire, diodes and switches.[1-3] Over the past decades, it has become apparent that the range of functionalities afforded by utilizing molecules is more diverse than those which researchers originally set out to investigate. These functionalities include molecular redox activity, their optoelectronic and spintronic properties and more. A recent consensus of the community[5] has indicated investigations into these more novel functionalities should be pursued with vigour, as the technological applicability of molecular electronics may arise from such research.

Under standard laboratory conditions redox active molecules can allow for conductance switching. This property is readily controlled by performing the conductance measurements in an electrochemical STM environment. In the EC-STM a 4-electrode configuration, in which both the tip and substrate are working electrodes, and a reference electrode and counter electrode are present, is used. In this configuration, the short Debye screening length of the electrolyte facilitates short charge screening length, even if the reference and counter electrodes must be placed physically far away.[7] This setup mimics semiconductor devices, **Figure 1**. The tip and substrate are considered the source and the drain, and the reference electrode the gate electrode which controls the tunnelling between the two.[10, 11] The ultimate aim of using the STM in this manner is to increase molecular conductance by tuning the molecular orbitals and Fermi energies into resonance.[4, 7, 10] The ability to tune the Fermi and molecular levels with respect to each other makes EC-STM a powerful technique for the investigation of the conductance of redox active molecules.

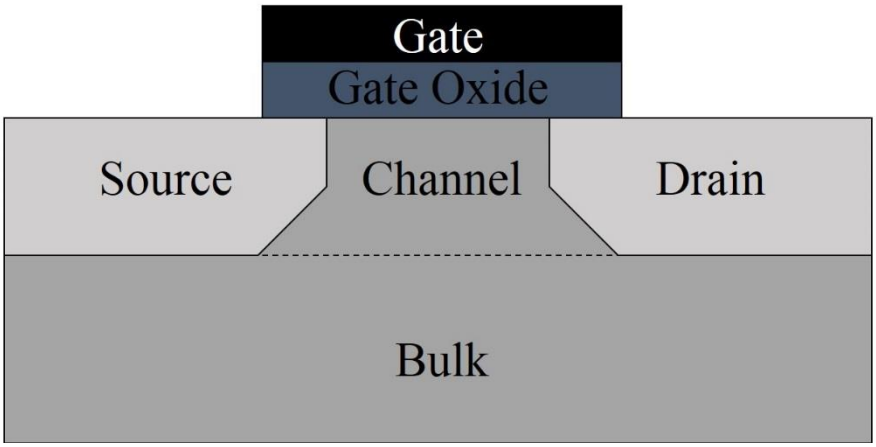


*Figure 1: The four-electrode setup of an EC-STM cell in molecular electronics investigations mimics semiconductor MOSFET devices. These devices are composed of a source and drain electrode. The potential of the channel between the source and drain is controlled by the gate electrode.*[9]

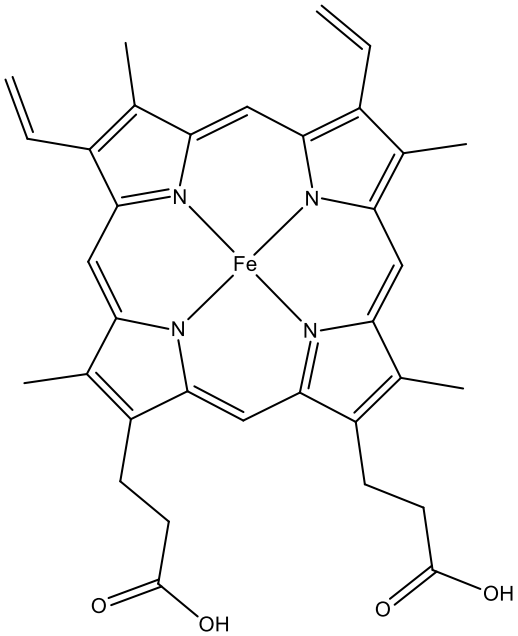


*Figure 2: In 1996 the first molecular electronics measurements in which the conductance of the molecule was controlled by the molecule's redox properties were performed. In these investigations Tao et al.*[4] *measured Fe(III)-protoporphyrin IX. These systems allowed the effect of the redox potential on molecular conductance to be determined by measuring the apparent height change of the protoporphyrin with changing potential.*

Attempts to control molecular conductance through the redox properties of molecular wires were first made by Tao[4] on Fe(III)-protoporphyrin IX, **Figure 2**. In this pioneering work, the apparent height of the protoporphyrin molecule was measured as the substrate potential and molecular redox potential were brought into resonance, in turn causing the molecular LUMO and the substrate Fermi level to align. The alignment of these two levels caused an increase in the apparent height of the protoporphyrin by 2.2 Å, equivalent to nearly an order of magnitude increase in tunnelling conductance. Investigations of the effect of gate voltage on molecular conductance continued on from this work with fervour, particularly as techniques to directly contact both ends of the molecular wire were developed. The first redox active molecule measured by directly tethering the molecule between the STM tip and substrate was 6-[1'-(6-mercapto-hexyl)-[4,4']bipyridinium]-hexane-1-thiol (6V6).[12] An off-on switching with changing potential was measured, by the *I*(*s*) technique, for the 6V6 molecule. The on state showed a 6-fold increase in conductance over the off state. Work in the area of electrochemically gated molecular conductance remained active and in 2006 Albrecht *et al*[13] investigated for the first time an ionic liquid as the gating electrolyte. The modulation of conductance of an Os bisterpyridine with changing potential was investigated using scanning tunnelling spectroscopy (STS). In BMIM-$PF_6$, the Os complex shows off-on-off switching with a 50 fold increase in the on state conductance. The measured increase in conductance is, however, dependent on the number of molecules in the junction. As ionic liquids presented a viable electrolyte for gating, their use for conductance switching, using the *I*(*s*) technique, was explored for 6pTTF6, **Figure 3**.[7] In BMIM-OTf, the second electron transfer to 6pTTF6 could also be studied. 6pTTF6 exhibited an off-on-off-on-off switching, with a 4-fold increase in the molecular conductance in the on state. By exploiting the redox

properties of molecular wires significant increases in the conductance can be attained due to the alignment of the molecular orbitals and the contact Fermi levels. The use of ionic liquids as the gate electrode provides an interesting opportunity to measure molecular wires whose redox states are inaccessible in the more commonly used aqueous electrolytes. The extremely limited number of molecules measured in ionic liquids means their full capabilities have not yet been assessed, for this reason it is important to further develop their use as a test bed for molecular electronics.

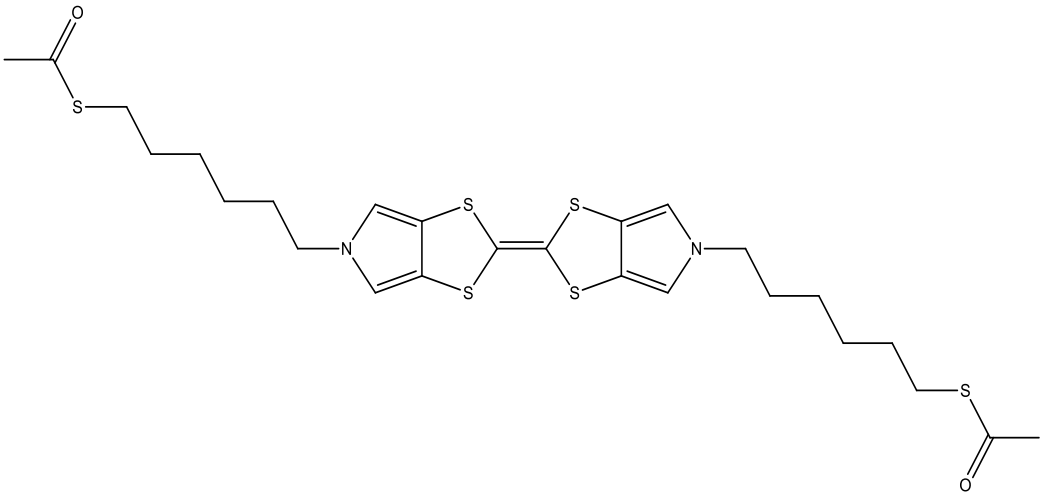


*Figure 3: In 2012 6pTTF6 was investigated in BMIM-OTf using the I(s) technique. By investigating the change in conductance of pTTF6 with changing system potential the molecular switching abilities were determined. In BMIM-OTf it was possible to measure both redox transitions of 6pTTF6. This molecule showed off-on-off-on-off switching.*[7]

The abilities of a viologen and a Ru containing molecule as redox active molecular wires were investigated in this work. These molecules were examined using the *I*(*s*) technique under electrochemical control to determine the effect of changing the gate voltage on the molecular conductance. In these investigations, ionic liquids were the environment for both the initial electrochemical assessment of the potential wires, as well as the conductance measurements of those determined to be suited for these measurements. Ionic liquids are used because they are a good environment for

molecular conductance studies, and have a wide electrochemical window, which allows redox processes less accessible in aqueous electrolytes to be studied, a particular advantage for the viologen containing molecule.

## Aim

With the advent of single molecule methods in the last decade great impetus has been given to the study of the electrochemical properties of "functional" molecules. The use of redox active molecules which can act as switches is a particularly promising area of molecular electronics which is comparatively easy to study. A selection of redox active molecules were assessed for their potential as molecular bridges in metal/molecule/metal junctions, and the conductance of those most promising molecules was investigated under electrochemical potential control. To allow for as full of a range of electron transfer processes as possible, ionic liquids were used.

## Methods

### Electrochemistry

All electrochemistry was performed in a low volume three-electrode sealed electrochemical cell. The cell was prepared and sealed in a nitrogen atmosphere glovebox to allow investigation of the electrochemistry. The working electrode was a Au(111) bead electrode with a hanging meniscus, the counter and reference electrode were both 0.5 mm Pt wire electrodes. The Au electrode was rinsed in ethanol and Milli-Q® water and flame annealed until just glowing. Flame annealing was repeated multiple times allowing the Au bead to cool each time. The Pt electrodes were also prepared by flame annealing. An Autolab PGSTAT30 computer controlled

potentiostat running GPES was used. Analysis of the electrochemistry was performed using GPES and/or Origin 9.

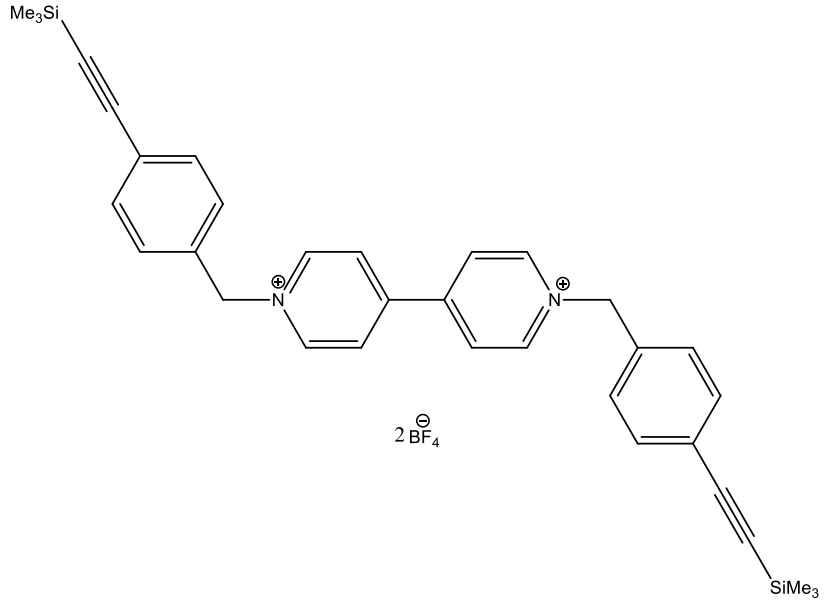


*Figure 4: TMS-V-TMS redox active molecular wire prepared by Dr. Josef Gluyas.*

The TMS-V-TMS molecule in **Figure 4** was synthesized and characterized by Dr. Josef Gluyas of Prof. Paul Low's group in Durham University. Electrochemistry of this molecule was performed by Dr. Gluyas in a 3-electrode cell with a Pt working electrode and Pt wire counter and reference electrodes. Electrochemistry was performed in 0.1 M tetrabutyl ammonium hexafluorophosphate in acetonitrile. Solution electrochemistry was performed at Liverpool in a 7.5 mM TMS-V-TMS in BMIM-OTf solution. To prepare this solution the TMS-V-TMS was dissolved in a minimum volume of methanol before BMIM-OTf was added. The methanol was heated off with nitrogen bubbling.

A series of 4 Ru molecules (**Figure 5: 2-5**) were provided by Santiago Marquez-Gonzalez of Paul Low's group of the University of Durham, with differing end groups, all 4 molecules were measured in BMIM-OTf and BMIM-TFSA. Electrochemistry of Ru-$NH_2$/-COOMe, and Ru-$NH_2$/-$NH_2$ in 0.1 M

tertrabutylammonium tetrafluoroborate in DCM, was performed and provided, by Santiago Marquez-Gonzalez. This electrochemistry is referenced to decamethyl ferrocene. Because a limited quantity was available, and in some cases the molecules are only sparingly soluble, 0.44 mM solutions were used. To improve the solubility of these molecules they were dissolved first in the smallest possible amount of DCM, which was heated off with nitrogen bubbling for 1 hour. The low concentration and solubility of the Ru compounds led to weak intensity redox peaks in the cyclic voltammograms, these were better resolved using differential pulse voltammetry (DPV). To further improve the resolution of the redox peaks solid state electrochemistry was performed.[14] In this technique a fine powder of the chemical of interest is pressed onto the electrode surface using a cotton bud. Care is taken to insert the electrode into the cell without disturbing the surface. Due to the sparing solubility of the Ru molecules of interest the formation of a hanging meniscus with the electrode is possible without fear of loss of the molecular layer.

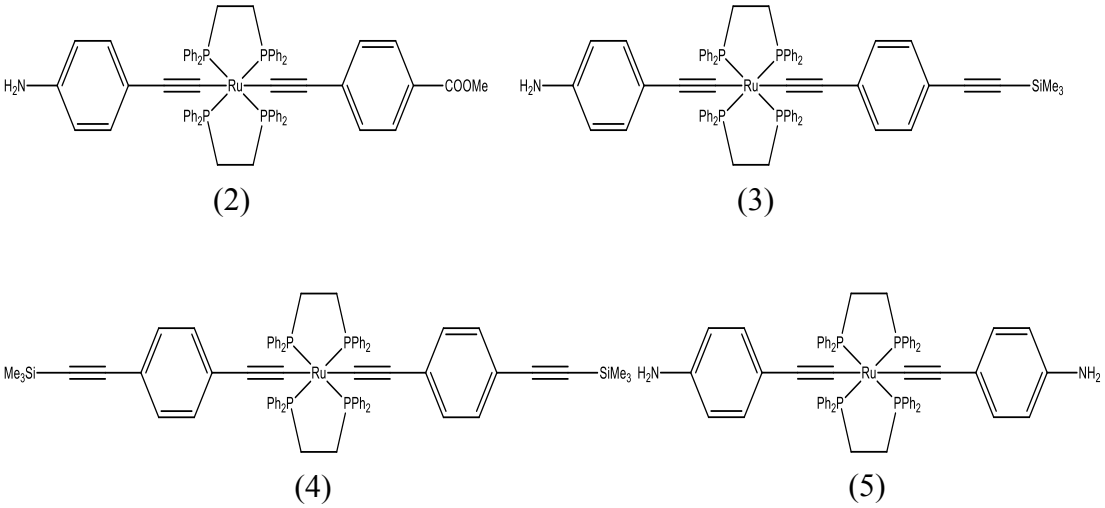


*Figure 5: Ru redox active molecular wires prepared by Santi Marquez-Gonzalez*

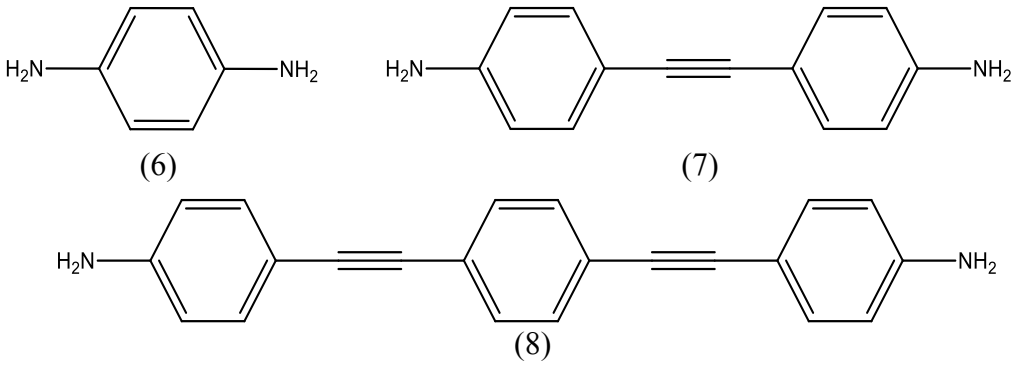


*Figure 6: Amine terminated OPE type molecules prepared by Dr. Ross Davidson.*

A series of 3 OPE molecules, synthesized by Dr. Ross Davidson of Prof. Low's group (**Figure 6: 6-8**), was investigated in BMIM-OTf. Molecules 6 and 8 were measured in a 10 mM solution, whereas a 20 mM solution was used for molecule 7. The solution of molecule 6 was prepared by first dissolving in THF and heating off with nitrogen bubbling after addition of the ionic liquid. Molecule 8 dissolved in BMIM-OTf with gentle heating of the solution. Molecule 7 can exist as either a brown compound in which the amine is oxidized[15] or as an orange compound, the OPE structure of interest. Molecule 7, as it arrived, had degraded to the oxidized amine form and therefore it was converted back to the desired OPE structure by dissolving in diethyl ether to which a drop of $NH_4OH$ was added. The solvent was partially removed and the ionic liquid added. The remaining solvent was heated off with nitrogen bubbling. The oxidised amine form went into BMIM-OTf with just gentle heating.

STM Measurements

STM measurements were performed using an Agilent Technologies 2500 or 5500 controller. All measurements were performed in an environmental chamber with a nitrogen atmosphere, which was started at least 1 hour before the experiment and continued throughout. All experiments used a Teflon cell which was cleaned in acid

between systems to avoid contamination. Measurements were performed using the *I*(*s*) spectroscopy function of PicoScan 5.0. All measurements used a 10 nA/V scanner at a sample bias of 0.6 V and a set point current of 20 mV. Those spectra showing plateau were saved and analysed using an in-house Labview program which allowed collation of all points in the spectra, and exported to the Origin software for plotting the histogram. Unless stated, a minimum of 500 scans were included in each histogram.

All measurements were performed on Arrandee™ Au(111) slides. The slides were rinsed with ethanol followed by Milli-Q® water, then dried under nitrogen. This was followed by flame annealing for 5 second intervals over a 1-2 minute period. The Au(111) slide was allowed to cool before continuing.

The conductance of the molecular wire in the ionic liquid without electrochemical control was assessed prior to use of electrochemical control. This was done to ensure the system allowed for the formation of quality molecular junctions.

The TMS-V-TMS molecule was investigated in BMIM-OTf using the *I*(*s*) technique with and without electrochemical control. The TMS-V-TMS molecule was adsorbed on the surface for 10-15 minutes in a 7.5 mM methanol solution, followed by rinsing in ethanol or methanol and Milli-Q® water, and drying with nitrogen. A 1.5 mM TMS-V-TMS BMIM-OTf solution, prepared in the manner outlined for the electrochemical experiments, acted as the ionic liquid environment. For measurements under electrochemical control, a 0.25 mm Pt counter electrode and a 0.25 mm polypyrrole on Pt wire reference electrode were used. This electrode was prepared using a $10^{-2}$ M polypyrrole/ 0.1 M tetrabutylammonium triflate in acetonitrile solution, in a three electrode cell composed of the Pt wire to be plated as the working electrode, a Pt mesh counter electrode and a SCE reference electrode**.** The Pt wire was cycled 50

times between -0.6 and +1.1 V at 100 mV $s^{-1}$.[16] The growth of the polypyrrole was followed through the cyclic voltammetry, **Figure 7**.

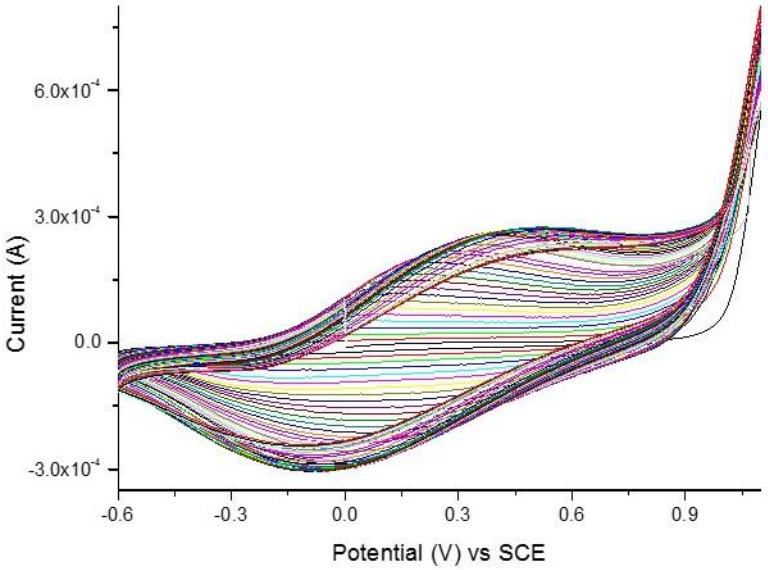


*Figure 7: Electrochemical growth of polypyrrole on Pt quasi-reference electrode. This was performed in a $10^{-2}$ M polypyrrole/0.1 M tetrabutylammonium triflate in acetonitrile solution, against an SCE reference and Pt mesh counter electrode. A scan rate of 100 mV $s^{-1}$ is used.*

The symmetric $NH_2$-Ru–$NH_2$ molecule (**5**) was investigated in BMIM-OTf using the *I*(*s*) technique both with and without electrochemical control. The Ru molecule was adsorbed on the Au for 10-15 minutes from a 0.1 mM THF solution, then rinsed with THF and Milli-Q® water, and dried with nitrogen. It was measured in a solution of 0.44 mM $NH_2$-Ru–$NH_2$ in BMIM-OTf, prepared in the manner outlined for the electrochemical measurements. For measurements under electrochemical control the reference and counter electrodes were both 0.25 mm Pt wire, prepared by flame annealing.

The conductance of the smallest OPE molecule (**6**) was investigated using the *I*(*s*) technique. The OPE was present on the Au surface and in solution. Molecule 6 was adsorbed on the surface from a 0.1 mM THF solution for 10-15 minutes followed

by rinsing with THF and Milli-Q water, then drying under nitrogen. A 0.44 mM BMIM-OTf solution was used.

## Electron Tunnelling Models

EC-STM can be used to induce conductance switching in redox active molecules. This occurs by changing the overpotential of the system to alter the local potential at the redox site.[17-19] Changing the potential at the redox site can move the redox levels of the molecule into range of the Fermi levels of the tip and substrate.[7, 20] The amplification of the current measured through redox active molecules depends on the electron transfer mechanism. The two main classes of electron transfer mechanism are the resonant tunnelling mechanism, as first outlined by Schmickler,[21] and the 2-step electron transfer mechanism, which is a hopping type mechanism.

### Resonant Tunnelling Model

A defining feature of the resonant tunnelling model, **Figure 8**, is that relaxation does not occur in the electron transfer process, as the electron transfers immediately after occupying the redox centre.[8] In this model, at resonance the energy levels of the tip, molecule and substrate are all aligned, which facilitates electron transfer through the bridge. Resonant electron transfer does not occur if the molecular energy level is substantially misaligned with the metal Fermi level.[22] Owing to the assumption made in this model, the relative densities of states of the tip, substrate and molecular orbitals are of great importance. The density of states of the molecular orbitals involved in the resonant electron transfer are broadened by the interaction with the metal and altered by their interaction with the surrounding solvent as is reflected by the reorganization energy.[23] Schmickler assumed the shape of the molecular density of states of the oxidised species, $D_{ox}$, to be Gaussian, based on the predictions by Gerischer:[21]

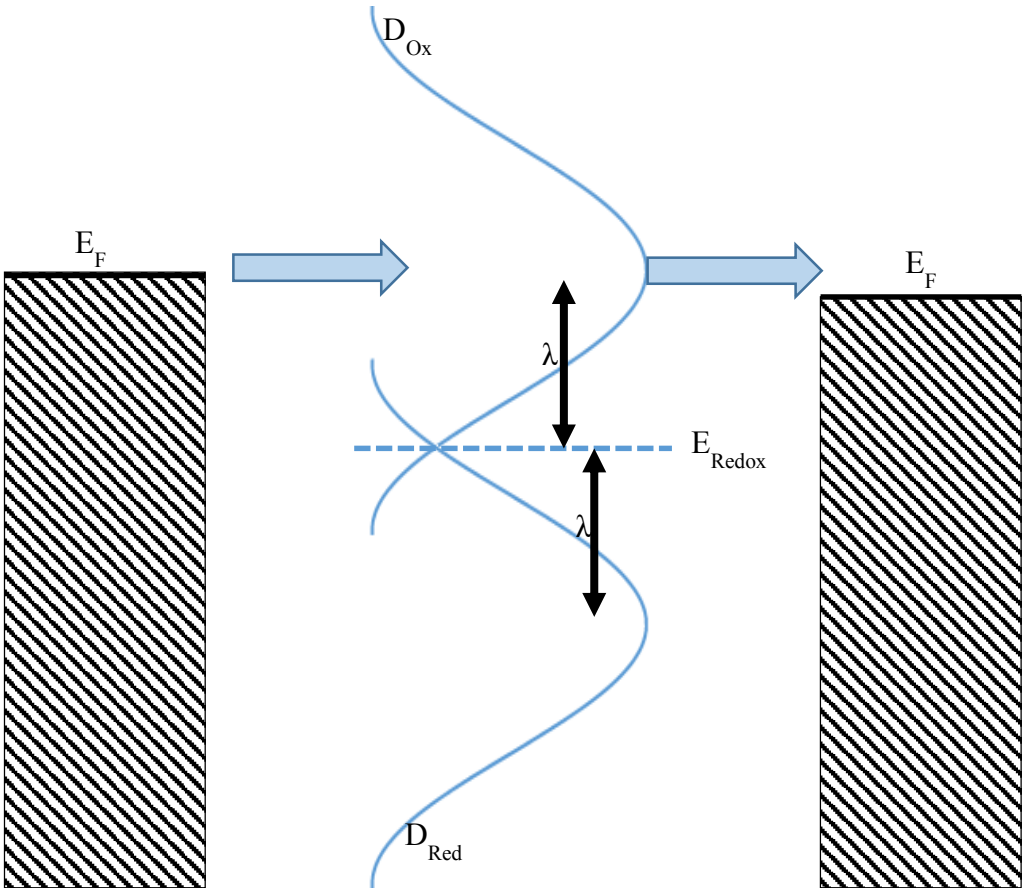


*Figure 8: In the resonant tunnelling model relaxation of the molecular states does not occur during electron transfer. In this situation the energy of the molecular orbitals are aligned with the metal Fermi level, and their interaction with each other causes broadening of the molecular orbitals. In this mechanism the redox level of the molecule is offset from the metal Fermi levels by the reorganization energy of the molecule. This reorganization energy is dependent on the interaction between the molecule and its surrounding solvent. Due to the nature of this mechanism the maximum in conductance of the system occurs offset from the redox potential of the molecule.*[6]

$$\lim_{\Delta \to 0} D_{ox}(\epsilon) = \sqrt{\frac{\pi}{kT\lambda}} \exp\left[-\frac{(\epsilon-\epsilon_r)^2}{4kT\lambda}\right] \quad (Eq.\ 1)$$

Where $\epsilon$ is energy, $k$ is the Boltzman constant, $T$ the absolute temperature, and $\epsilon_r$ the energy of the electronic state of the redox couple. This equation shows the density of states is highly dependent on the reorganization energy, with the resulting current dependent on the probability of finding a molecular state with energy in resonance with the tip and substrate, and the reorganization energy. As a result, when the molecular levels are in equilibrium with the tip and substrate Fermi levels, the energy of the redox state is offset from that of the metal by the reorganization energy,[23] causing the maximum in conductance to be offset from the redox potential of the molecule. This is a key feature of the resonant tunnelling model which distinguishes it from the 2-step electron transfer hopping model.

Hopping Model

In the 2-step electron transfer hopping model population and depopulation of the redox centre shuttles electrons between the STM tip and substrate, **Figure 9**.[20, 24] In the first step of this mechanism, an electron is transferred from substrate to the oxidized molecule, when in resonance with the tip Fermi level, reducing it in the process. In the second step, the molecular energy level begins to relax towards the substrate Fermi level, allowing an electron to transfer to the tip, and re-oxidise the molecular centre.[8, 18, 19, 22, 25] During this process there are two possible outcomes depending on the coupling of the molecule to the metal electrodes. When there is weak coupling, at the diabatic limit, electron transfer is slower than the relaxation of the redox levels.[8, 20, 22] In the diabatic limit the redox level relaxes below the Fermi level of the acceptor before the electron can transfer onto it and therefore electron transfer requires thermal excitation. Minimal enhancement in tunnel current is expected from

this sort of electron transfer because only one electron can transfer from tip to substrate during the relaxation process.[19] The opposite limit, the adiabatic limit, involves strong metal-molecule coupling. In this model the first electron transfer occurs in the same manner as before, with the difference arising from the second step. In the adiabatic limit, the electron transfers from the redox centre to the substrate Fermi level before the redox molecular level has fully relaxed, the molecular level then returns to the energy of the oxidised species allowing a second electron to move onto the site, and the cycle to repeat. [8, 10, 18-20, 22, 24, 26] The repetition of the 2-step electron transfers causes an increase in tunnelling current as many electrons can transfer in a single relaxation process. This can be explained by the Kuznetsov-Ulstrup model,[10] which unlike the resonant tunnelling model can be modelled numerically with the equation:[8]

$$I_{enh} = e\kappa\rho(eE_b)\frac{\omega}{2\pi}\left\{\begin{matrix}\exp\left[\frac{e}{4\lambda kT}(\lambda+\xi\eta+\gamma E_b)^2\right] \\ +\exp\left[\frac{e}{4\lambda kT}(\lambda+E_b-\xi\eta-\gamma E_b)^2\right]\end{matrix}\right\}^{-1} \qquad \textit{(Eq. 2)}$$

Where $e$ is the elementary charge, $\kappa$ is the electronic transmission coefficient, $\rho$ is the density of electronic states at the metal Fermi level, $E_b$ the bias voltage, $\omega$ the characteristic nuclear vibration frequency, $\eta$ the overpotential, $k$ is the Boltzman constant, $T$ the absolute temperature, $\xi$ is a modelling parameter between 0 and 1 related to the effective electrode potential at the redox centre with changing overpotential, and $\gamma$ a modelling parameter between 0 and 1 related to the effect of the bias voltage on the effective electrode potential of the redox centre. This equation shows the maximum tunnelling current occurs at the equilibrium redox potential of the molecule.[7, 25] This distinguishes this model from that of the resonant tunnelling molecule, in which the maximum tunnelling current is offset from that of the redox potential.

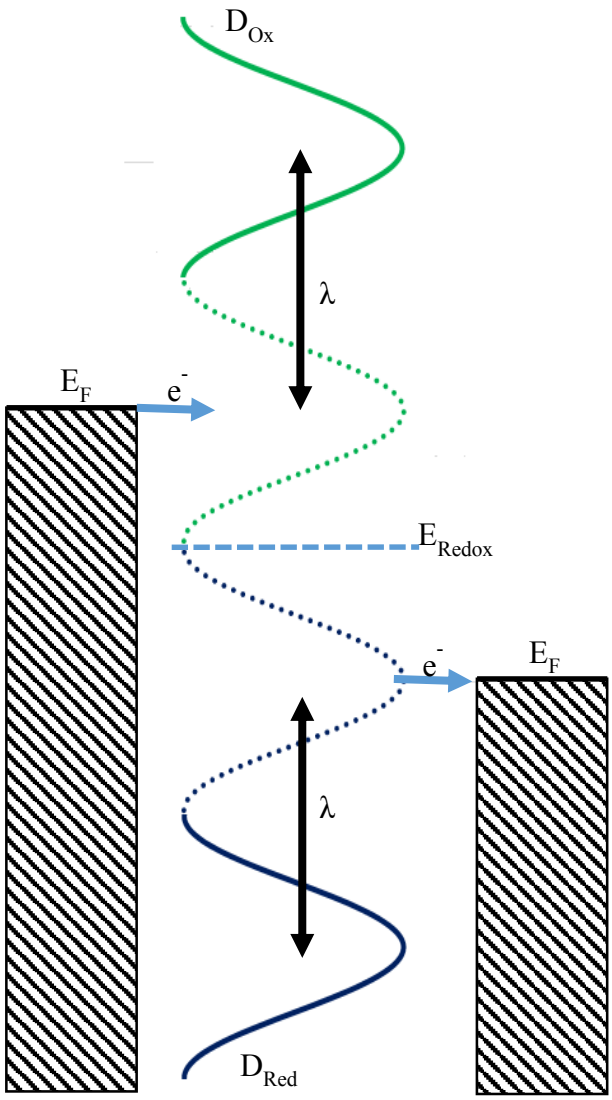


*Figure 9: The two step hopping mechanism occurs with population and depopulation of the redox centre. In this mechanism an electron is transferred from the tip to the oxidized molecule. This electron transfer causes the molecular state to relax towards the reduced energy state. If the relaxation occurs before the electron is transferred off of the molecule then a negligible conductance enhancement will be seen. If, however, the electron transfers before full energy relaxation then the energy state will return to the oxidized energy level, allowing for another electron to transfer. This cycle can repeat many times, resulting in a conductance enhancement at the redox potential of the molecule.*[8]

# Results and Discussion

## TMS-V-TMS

Both the TMS end group and the viologen redox centre are of interest in the TMS-V-TMS molecule. The TMS group is quickly proving itself as a viable molecular anchor. The TMS end group, when directly bonded to the electron withdrawing C≡C group, undergoes chemical bonding to the Au contact forming a pentacoordinate silyl group.[27, 28] With the bulkiness of the pentacoordinate Si, the adsorption sites available to the TMS group are limited providing a means of limiting the number of conductance groups seen, particularly compared to the thiol group.[29] The ability of this end group was recently demonstrated in measurements on an asymmetric TMS terminated OPE molecule.[29] A conductance with a similar order of magnitude to other studies was seen, therefore, the effectiveness of the anchor is not lost using the TMS group. The viologen centre is interesting in its own right. The electrochemistry of the viologen redox centre is well studied,[30-32] and known to be stable and reversible making it alluring for molecular electronics. The drive to study viologen molecules for molecular electronics has existed since before the development of Tao's break junction method and Haiss' $I(s)$ method.[33, 34] Viologens were the first molecules to be directly tethered as single molecules between Au contacts and electrochemical gate potential changed.[12] As the TMS-V-TMS molecule combines a historic, and stable, redox centre with a novel anchor group, it is an exciting molecule for investigation using the electrochemically controlled $I(s)$ method.

## Electrochemistry

Dr Gluyas performed the electrochemistry of the TMS-V-TMS in 0.1 M tetrabutylammonium hexafluorophosphate in acetonitrile in **Figure 10**. This electrochemistry has been referenced to a ferrocene internal reference, which is seen

at 0 V. The two redox waves of the viologen centre are at -0.74 and -1.14 V vs $Fc/Fc^{+}$. These potential values indicate investigation of the full electrochemistry of this viologen in aqueous electrolyte would be near impossible, because hydrogen evolution would occur concurrent with the second redox wave. Similar to the acetonitrile, ionic liquids, which lack hydrogen evolution, will allow the second redox wave of TMS-V-TMS to be visible. Unlike acetonitrile, ionic liquids have a low volatility, meaning they can be used in conjunction with the STM. The electrochemistry of 7.5 mM TMS-V-TMS in BMIM-OTf was therefore measured, **Figure 11**. The expected redox waves in this occur at -0.77 and -1.16 V vs $Fc/Fc^{+}$, unlike in the acetonitrile electrochemistry a third redox wave occurs at -1.29 V vs $Fc/Fc^{+}$. This third redox wave may be due to an insoluble film formation from the TMS-V-TMS on the Au(111) surface or as a result of reduction of dimers or other molecular adsorbates. Integration of the third peak demonstrates a coverage of (4.6 ± 0.3) mol $cm^{-2}$, an order of magnitude less than that seen for self-assembling monolayers of other viologen molecules on Au,[35-37] and therefore supports the assertion that this peak is due to an adsorbate. The electrochemistry of the TMS-V-TMS can be analysed to find the diffusion coefficient, and rate constant of electron transfer. The diffusion coefficient is 1.07 x $10^{-8}$, 1.70 x $10^{-8}$, 4.56 x $10^{-9}$, and 5.46 x $10^{-9}$ cm $s^{-1}$ for the anodic and cathodic $V^{2+}$ to $V^{+\cdot}$, and anodic and cathodic $V^{+\cdot}$ to $V^{0}$ transitions respectively. The rate constant is 3.88 x $10^{-6}$ and 2.86 x $10^{-6}$ $s^{-1}$ for the $V^{2+}$ to $V^{+\cdot}$, and $V^{+\cdot}$ to $V^{0}$ electron transfers respectively.

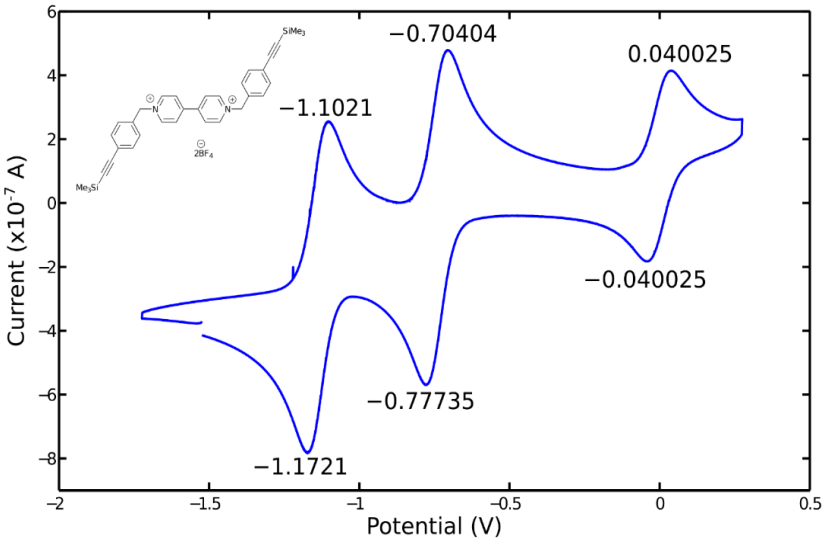


*Figure 10: Electrochemistry on TMS-V-TMS in 0.1 M tetrabutyl ammonium hexafluorophosphate in acetonitrile was performed by Dr. Josef Gluyas. A scan rate of 0.1 V s$^{-1}$ is used, the internal reference of Fc/Fc$^{+}$ is shown.*

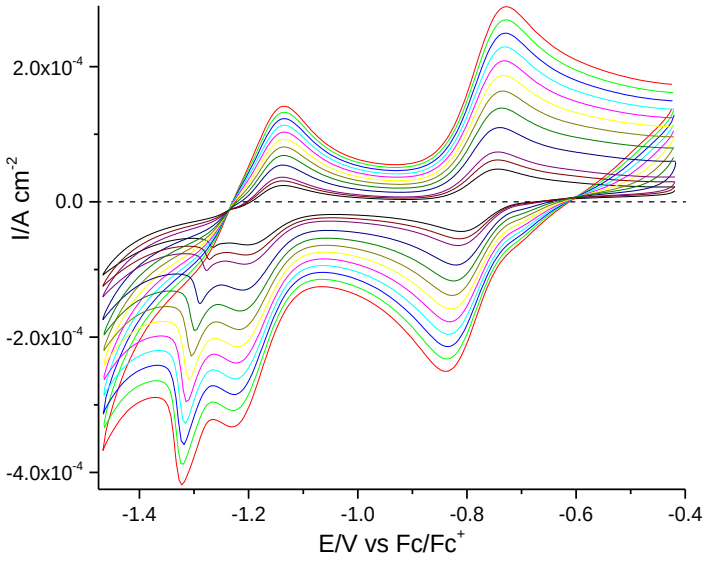


*Figure 11: 7.5 mM TMS-V-TMS in BMIM-OTf vs. Au(111) WE. On going from the red to the black curve the sweep rate follows the order 1.0, 0.9, 0.8, 0.6, 0.5, 0.4, 0.3, 0.2, 0.1, 0.075, and 0.05 V s$^{-1}$.*

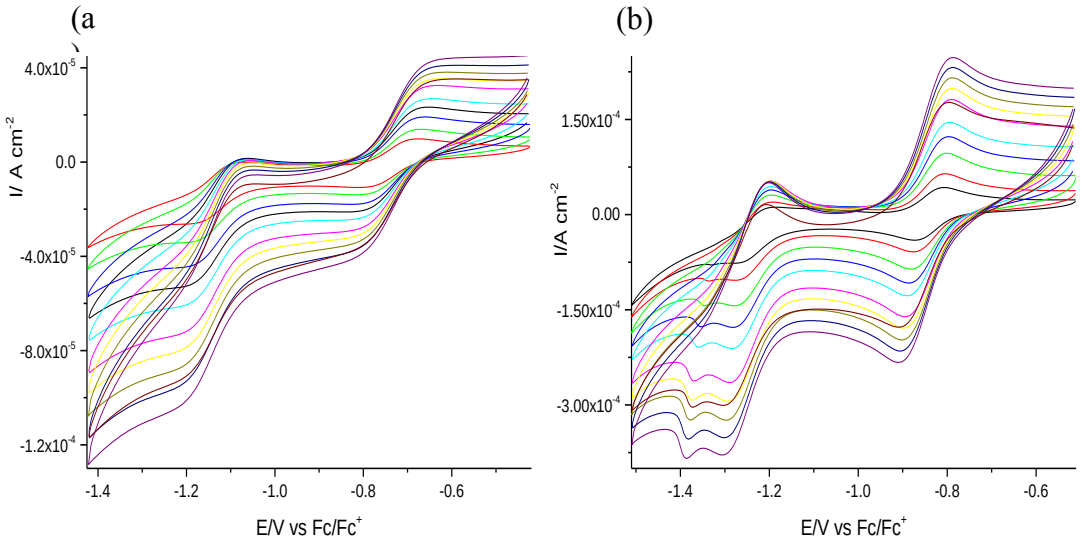


*Figure 12: Electrochemistry of 7.5 mM TMS-V-TMS in BMIM-OTf. Electrochemistry in (a) was performed against a AgCl quasi-reference electrode, whereas that in (b) was performed against a polypyrrole quasi-reference electrode.*

While Pt is an acceptable quasi-reference electrode for solution electrochemistry, its long term stability can be questionable. When EC-STM experiments were initially performed using the Pt QRE the potentials of the redox peaks shifted throughout the experiment, therefore, a different quasi-reference electrode was needed. A standard quasi-reference electrode in ionic liquid electrochemistry is the AgCl wire QRE. The resulting solution electrochemistry of 7.5 mM in BMIM-OTf is shown in **Figure 12a**. The voltammetry from this investigation shows the two TMS-V-TMS redox waves at similar potentials to those measured against Pt, -0.75 and -1.15 V vs $Fc/Fc^+$. However, when compared to the original investigation against Pt, the intensity of these peaks is clearly reduced and the 3$^{rd}$ redox peak is missing. This reduction may result from $Cl^-$ ion transfer into the BMIM-OTf, which then adsorbs on the Au surface to reduce the rate of electron transfer, and block the adsorption sites. On the other hand the electrochemistry of the viologens is also known to be sensitive to the anions due to their association with $V^{2+}$ and $V^{+\cdot}$.[36, 38-40]

Although the AgCl QRE has been successfully used in the past for investigations in ionic liquids, in this instance it is a poor choice of QRE.

Although not previously used in the literature as a reference electrode for ionic liquids, the polypyrrole QRE has been successfully used in our group. It acts to stabilize the reference potential of a QRE by avoiding problems like the surface contamination and oxidation possible with Pt QREs.[41] This electrode is formed by electrochemical polymerization of a polypyrrole layer on Pt wire. As the polypyrrole layer can incorporate the anion of the electrolyte during deposition,[16] OTf was used to match the ionic liquid. The voltammetry of 7.5 mM TMS-V-TMS in BMIM-OTf against the polypyrrole QRE is seen in **Figure 12b**. This voltammetry compares well with that taken against the Pt QRE. Not only are the main peaks as intense as in the Pt QRE investigations, but the 3$^{rd}$ peak, presumed to be from adsorption, also reappears. These peaks occur at -0.74, -1.14, and -1.30 V vs $Fc/Fc^{+}$. As the investigations against the polypyrrole reference electrode compare well to those against the Pt QRE, this electrode will be used as the reference in the EC-STM experiments.

Single Molecule Conductance Measurements

The single molecule conductance of TMS-V-TMS was investigated by the STM *I*(*s*) technique. As a TMS terminated molecule, the affinity of this end group is lower for gold than that of thiol, therefore it will have a low probability of forming a molecular junction during an *I*(s) measurement ("hit rate"). To ensure a hit rate high enough for a statistically significant data set, a 2-step approach was taken. The TMS-V-TMS molecule was adsorbed on the Au surface, and measurements were performed with the target molecule dissolved in BMIM-OTf ("doped ionic liquid"). Using adsorbed TMS-V-TMS together with doped ionic liquid ensures a high hit rate and a

substantial amount of electroactive species to allow for clear electrochemistry in the STM.

*Without Electrochemical Control*

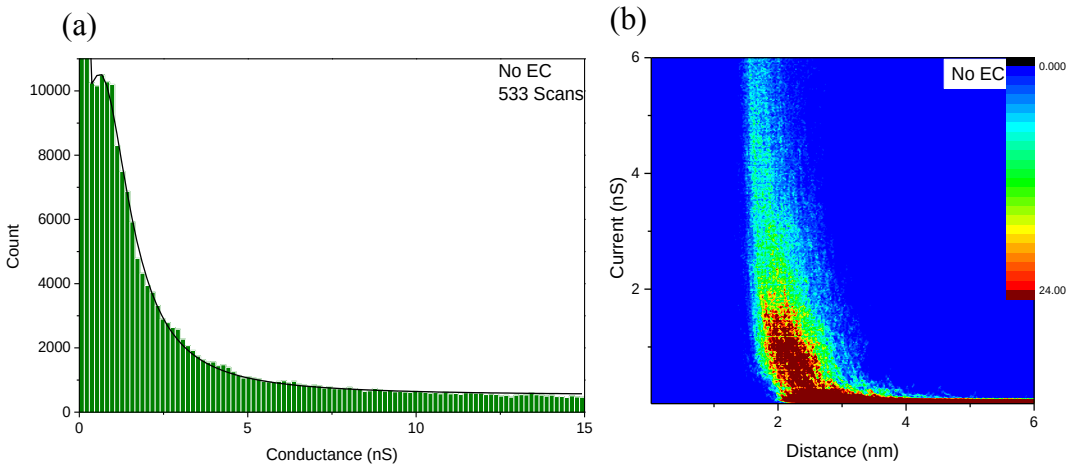


*Figure 13: Measurement of the TMS-V-TMS molecule by the* I(s) *technique showed a conductance of 0.61 nS. A set point of 20 nA, and bias voltage of -0.6 V were used. (a) 1D histogram of 533 plateau containing* I(s) *traces, these trace were also used to compose the 2D histogram (b).*

The conductance of TMS-V-TMS was first measured without electrochemical potential control. This measurement was performed to determine if the conductance of these molecules could be measured by the *I*(*s*) technique and to establish the conductance of the molecule under 2-terminal conditions. To measure TMS-V-TMS a 1.5 mM in BMIM-OTf solution was used, after first adsorbing the molecule on the Au(111) surface. The result of 533 scans is shown in the 1D and 2D histograms in **Figure 13**. Based on the 1D histogram the conductance of TMS-V-TMS is 0.61 nS, with a break off distance of (2.42 ± 0.57) nm, which is within error of the length of the TMS-V-TMS molecule measured in Spartan®. This conductance is about three times larger than that found in the literature for 6V6.[12] The difference in conductance is likely to be a result of the shorter length and higher degree of conjugation of this

molecule compared to 6V6, particularly as the ionic liquid has not noticeably altered the conductance of other molecules. These measurements, along with the electrochemistry, prove TMS-V-TMS is a viable target molecule for measurement in the EC-STM.

*With Electrochemical Potential Control*

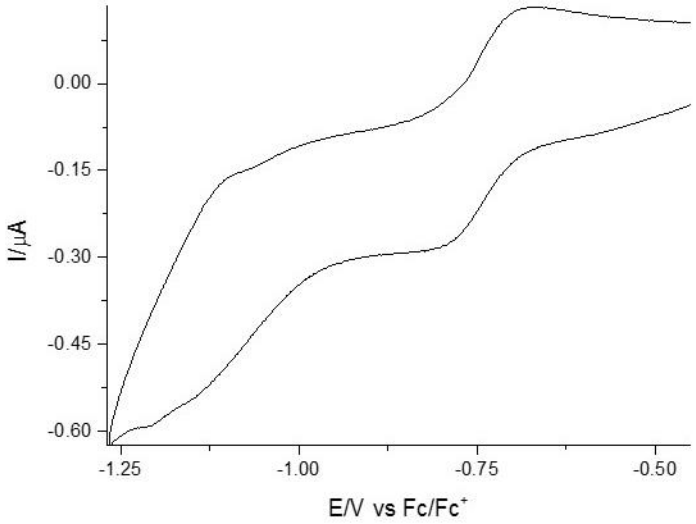


*Figure 14: By adsorbing TMS-V-TMS on the Au substrate, and doping the BMIM-OTf with it clear redox peaks could be seen in the STM electrochemistry. A scan rate of 0.1 V $s^{-1}$ was used.*

Single molecule conductance measurements were performed in the same manner as before, but with an EC-STM. In these experiments the potential was controlled against a polypyrrole QRE. Since BMIM-OTf is doped with TMS-V-TMS and the molecule is present on the surface, the electrochemistry is clearly seen in the STM cell, **Figure 14**. The electrochemistry measured in the STM matches well with that measured in the electrochemical cell, including the presence of the adsorbate peak. The improved electrochemistry and the quality of the conductance measurements show having the molecular wire present in solution and as an adsorbate is a viable method of improving the hit rate of the experiment. The doping of the ionic liquid has proven vital to the experiments as the improved electrochemistry possible has allowed

for the potential of the system to be accurately followed throughout. Furthermore, by having the TMS-V-TMS in solution it is possible to see the expected clear to blue colour change of the viologen occurring during reduction. This colouration was located nearest the reference and counter electrodes.

The potential range in which the measurements were performed was carefully chosen based on the resulting tip potential. As the tip potential became more negative the measurements became more difficult to perform. The cations of ionic liquids adsorb on the gold surface, and block adsorption site,[42] therefore it is likely a cation layer which stops the tip from contacting the molecule, causing a low hit rate formed. Due to the difficulties encountered when investigating more negative potentials only the first transition, from the dication to radical cation state, is measured. Though both electron transfers are of interest, the change in conductance with the first electron transfer is important in its own right. This change has been investigated before in aqueous electrolytes, with the first reported investigation by the Nichols' group.[10] In this work the conductance of 6V6 was investigated, with the *I*(*s*) technique, over a range of electrode potentials to bring it through the $V^{2+} \rightarrow V^{+\cdot}$ transition, its first electron transfer. The conductance increased 6-fold when the molecular orbitals were brought within resonance of the metal Fermi level, however, it never drops off as expected when the levels move out of resonance of one another. This change gives a sigmoidal, rather than the expected bell-shaped, conductance versus potential curve. Developing on these measurements, the Wandlowski group looked at the conductance change of 6V6 with changing potential in a similar manner.[37, 39, 40] They, too, saw a sigmoidal dependence for the 6V6 molecular conductance on electrode potential. However, in later experiments by the Wandlowski group, the conductance of 6V6H monolayers was examined by STS in an asymmetric molecular junction.[8, 39] These

measurements showed the conductance has a bell-shaped dependence on electrode potential, as expected when the molecular orbitals move in and out of line with the Fermi level of the Au contacts.[8] The reasons for the different current versus potential curves will be discussed later, however, it is apparent that it is difficult to predict how the conductance of viologen containing molecules will be affected by varying the electrode potential.

The single molecule conductance of TMS-V-TMS is measured in BMIM-OTf at 12 potentials between -0.593 and -0.870 V vs $Fc/Fc^{+}$. **Figure 15** displays the histograms formed from the collection of I(s) traces. The molecular conductance is found by fitting a Lorentzian line shape. This data was also plotted in 2D histograms, **Figure 16**, and the breakoff distances found, **Table 1**. The molecular distance of TMS-V-TMS as measured in Spartan® is 2.38 nm, with the assumption that Si covalently bonds to Au, the final break-off distance is 2.88 nm.[43, 44] This break-off distance value is within error of the experimental break-off distances measured. The discrepancies which may arise are due to the assumptions made, which include that the Si-Au bond is covalent, and that no stretching of the Au contact during *I*(s) measurement occurs.

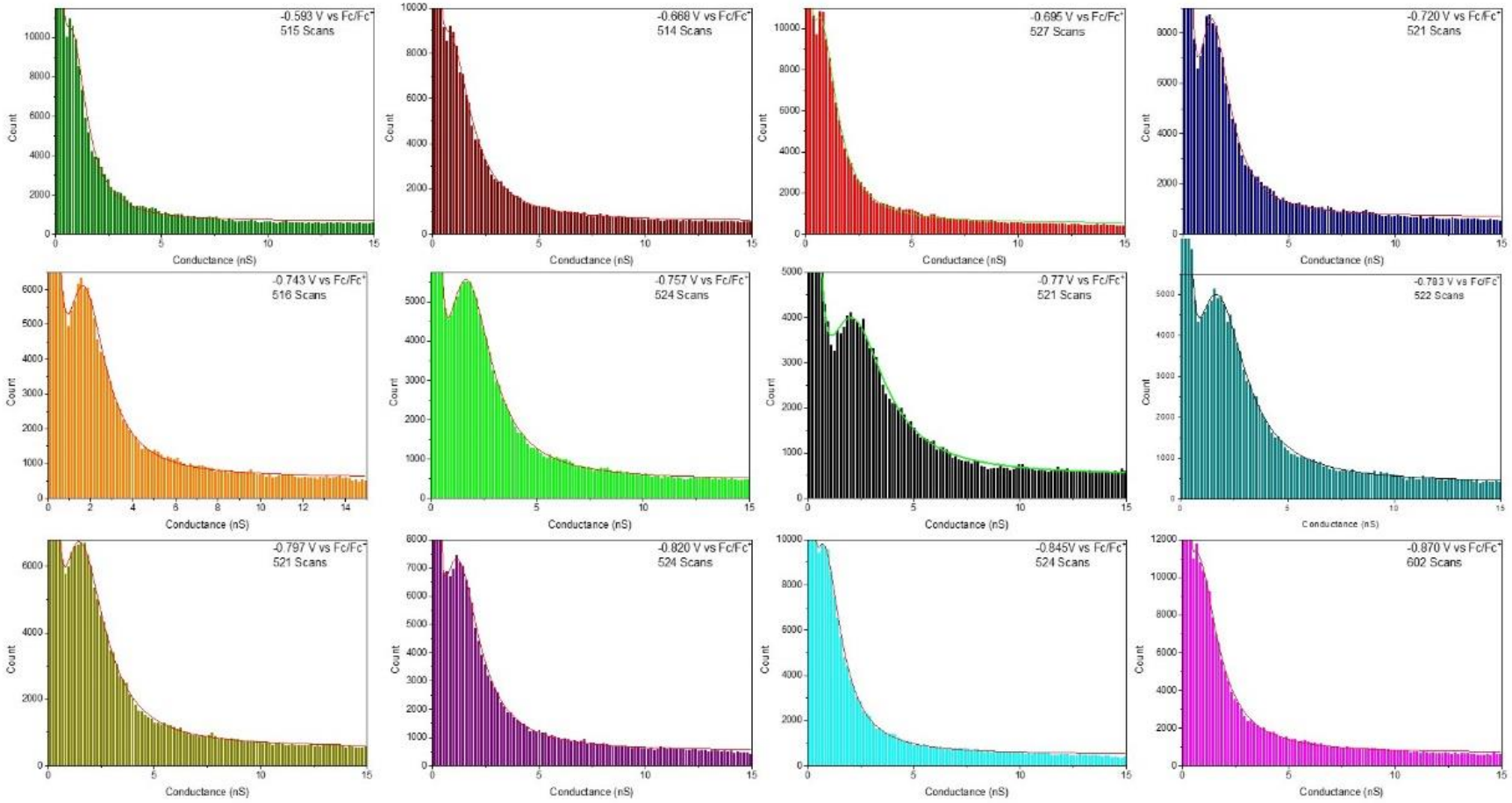


*Figure 15: TMS-V-TMS was measured at a variety of potential values allowing the first electron transfer of the redox molecule to be probed.*

*All histograms were formed from over 500* I(s) *traces each containing a conductance plateau.*

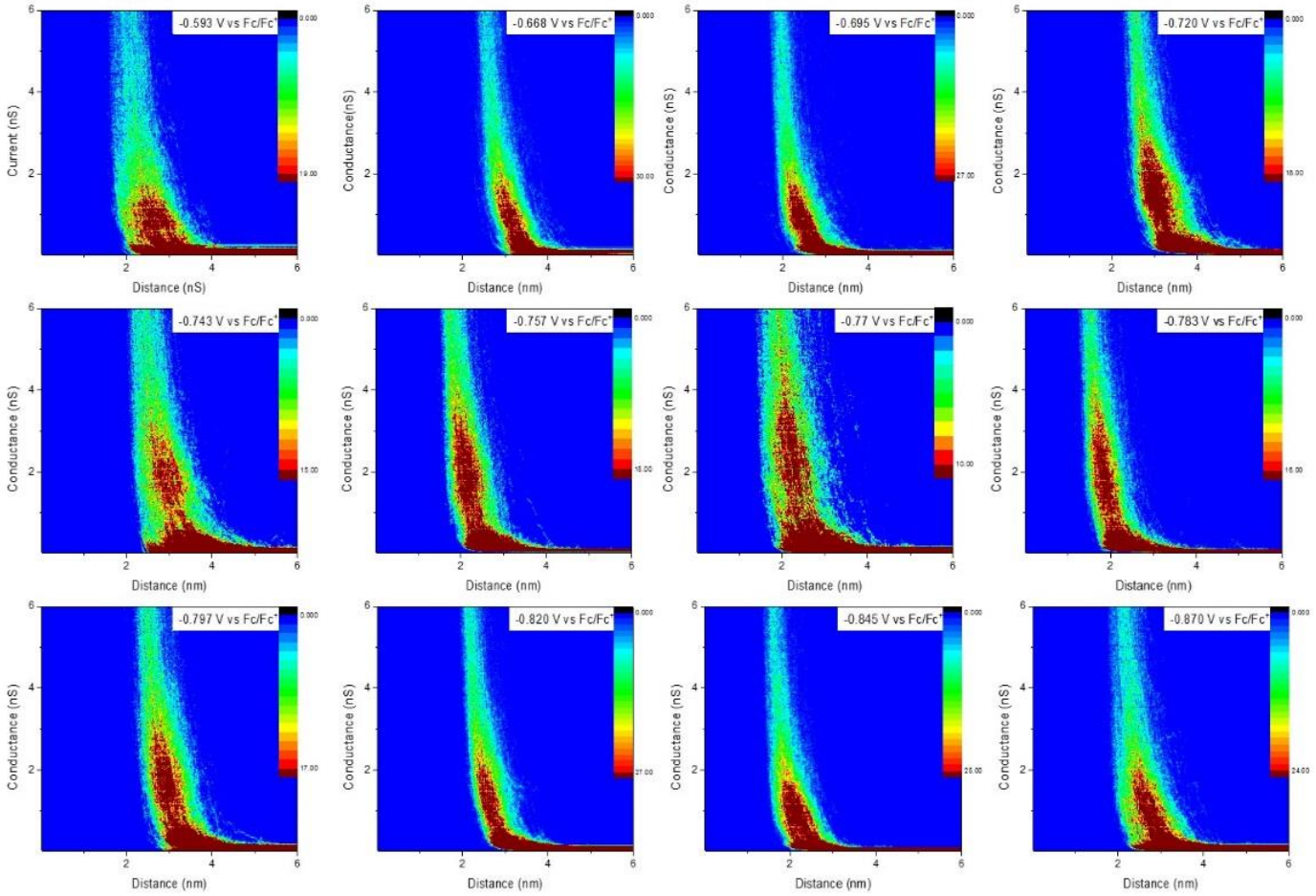


*Figure 16: The traces used to form the 1D histograms in Figure 15 can be compiled to allow the formation of 2D histograms. These 2D histograms allow the current-distance changes with potential to be seen.*

*Table 1: Conductance and break-off values of TMS-V-TMS in BMIM-OTf are shown.*

| Potential (V vs $Fc/Fc^+$) | Conductance (nS) | Break Off w/ $s_0$ (nm) | Break Off w/o $s_0$ (nm) |
|---|---|---|---|
| No EC | 0.61 | (2.42 ± 0.57) | (1.24 ± 0.29) |
| -0.87 | 0.66 | (2.82 ± 0.66) | (1.31 ± 0.36) |
| -0.845 | 0.72 | (2.29 ± 0.42) | (1.15 ± 0.26) |
| -0.82 | 1.1 | (2.83 ± 0.36) | (1.19 ± 0.23) |
| -0.797 | 1.5 | (3.17 ± 0.46) | (1.32 ± 0.29) |
| -0.783 | 1.7 | (2.07 ± 0.43) | (1.02 ± 0.25) |
| -0.77 | 2 | (2.39 ± 0.60) | (1.25 ± 0.36) |
| -0.757 | 1.7 | (2.37 ± 0.39) | (1.10 ± 0.27) |
| -0.743 | 1.6 | (3.02 ± 0.72) | (1.23 ± 0.41) |
| -0.72 | 1.4 | (3.28 ± 0.46) | (1.36 ± 0.29) |
| -0.695 | 0.67 | (2.62 ± 0.50) | (1.17 ± 0.26) |
| -0.668 | 0.75 | (3.27 ± 0.37) | (1.35 ± 0.29) |
| -0.593 | 0.73 | (2.70 ± 0.74) | (1.34 ± 0.43) |

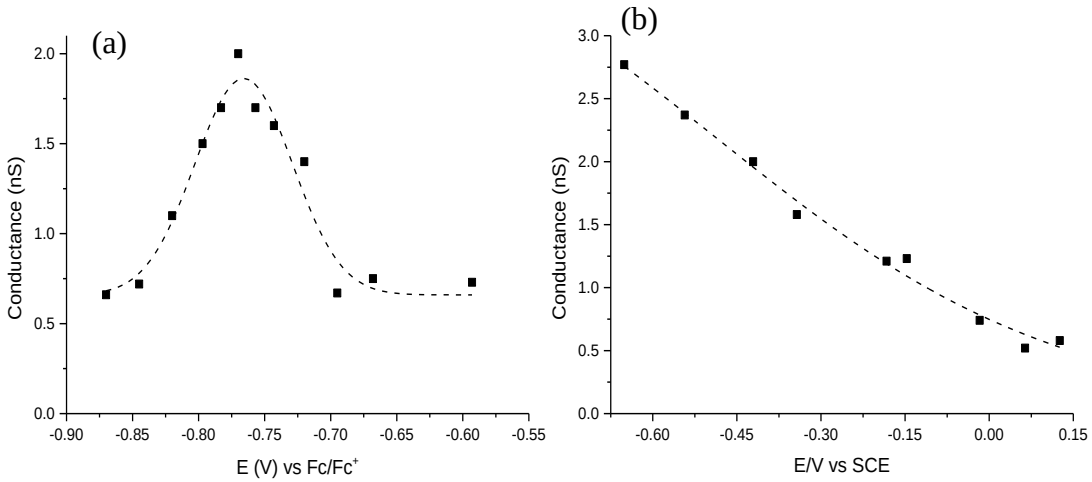


*Figure 17: (a) Conductance is plotted as a function of potential for TMS-V-TMS. A clear off-on-off switching, as TMS-V-TMS is brought through its first redox potential, is seen. (b) Conductance of 6V6, from the work of Haiss et al.[10] is plotted as a function of potential. A sigmoidal off-on switching is seen.*

The change in molecular conductance with electrode potential is shown in **Figure 17**, the Gaussian is fitted to aid the eye. This plot shows off-on-off switching, with conductance increasing 3-fold from ~0.66 nS to ~2.0nS. The conductance maximum occurs at the redox potential of the viologen moiety, which is indicative of the Kuznetsov-Ulstrup mechanism. To better resolve the lowest conductance peaks, a

relatively large bias potential had to be used. Unfortunately, at this time the given form of the Kuznetsov-Ulstrup model cannot be used to model high bias voltage measurements, as this model assumes $V_{bias}$ is much smaller than the reorganization energy. The position of the conductance maximum at the equilibrium redox potential is a good indication the Kuznetsov-Ulstrup model is followed rather than resonant electron transfer. The noticeable change in conductance with potential change means the electron transfer occurs in the adiabatic region. The strong coupling between the molecule redox state and the electrodes allows an electron to transfer from the tip to the molecular redox level, and reduce the dication, as the tip Fermi level and viologen molecular energy level move into resonance. The molecular redox level then relaxes towards the Fermi level of the substrate, however, before this relaxation is complete the electron transfers from the molecule onto the substrate, causing the molecule to re-oxidize. The relaxation of the molecular energy level back up to the oxidised state allows another electron to transfer and the cycle to repeat. This cycle repeats many times in one process causing the increase in current seen. The present results in ionic liquid clearly differ from the sigmoidal behaviour measured for symmetric junctions in aqueous electrolyte by both Haiss *et al.* and the Wandlowski group.[10, 37, 39, 40] The conductance versus potential behaviour measured by Haiss *et al.* is shown in **Figure 17** to allow comparison with this work. Haiss *et al.* further investigated the electron transport process in 2007.[10] Although a large increase in conductance was seen for 6V6 in a symmetric setup, no maximum was recorded, ruling out a direct application of the 2-step electron transfer model. The electron transfer was determined to occur through molecular levels which are off-resonance with respect to the metal Fermi levels, causing the absence of a conductance maximum. This off-resonance nature arises because of the conformational gating of the $V^{2+}$ and $V^{+\cdot}$ states. The $V^{+\cdot}$ has a

different conformation to the $V^{2+}$ state, and is a higher energy state because of conformational and electrochemical properties. In this experiment the electron tunnelling occurs predominantly through the $V^{2+}$ state, because of the increased energy barrier to the $V^{+\cdot}$ state, due to the change in conformation. As the substrate potential is swept it never becomes large enough to fully overcome the energy barrier due to conformation to populate the off-resonance redox states. The continued rise of conductance with potential indicated the redox levels eventually begin to approach alignment with the metal Fermi levels. The electrochemical gating effect can be explained within a superexchange model. Superexchange arises when a non-resonant energy is sufficiently low-lying to act as a dominant molecular level in electron transport. This would be the oxidised level ($V^{2+}$) here. As a "less rigid" molecule than others measured, 6V6 is susceptible to conformational changes, causing the large gap in the oxidised and reduced levels. Here "less rigid" refers to conformation mobility around the C-C bond connecting the two rings in $V^{2+}$. In the $V^{2+}$ state the pyridyl rings are connected by a C-C bond and can therefore freely rotate, while in the $V^{+\cdot}$ state the rings are locked in conformation by a C=C bond.[45] This led to the concept of "soft gating" in which conformational effects help to control the position of the energy level and reorganization dynamics. Wandlowski *et al.* propose a superexchange model arising as a result of the increased conjugation and electron density in the cation radical than the dication state.[37] In our present work we propose the pyridyl rings are conformationally locked in the dication with respect to the cation radical state, this causes the off-on-off conductance for TMS-V-TMS. This proposal holds merit from the monolayer measurements of the 6V6H conductance by the Wandlowski group which also saw off-on-off switching.[8, 39] This is attributed to conformational locking of the molecules in a condensed monolayer. It is highly probable that changing from

an aqueous electrolyte to BMIM-OTf the conformation of the pyridyl rings is locked by the interaction of the viologen moiety with BMIM-OTf.

Ionic liquids are viscous, highly ordered environments, dominated by the cation-anion interactions. Aromatic molecules have a strong interaction with ionic liquids. When an aromatic molecule is dissolved in an ionic liquid ordered clatherate cages can be built by the ionic liquid cation and anion. In such structures the associative interactions of the cation-anion pair force their separation into a cage-like structure surrounding the aromatic molecule.[46, 47] As a consequence of the clathrate cage formation around the aromatic molecule the solute can be considered as an isolated and encapsulated molecule which is forced into the most desirable state for interaction with the cage.[46] While the formation of the clathrate cage around benzene allows for its rotation about the $C_6$ axis it does not allow the molecule to tumble within solution.[48] TMS-V-TMS is highly aromatic, containing both the viologen centre and phenyl rings on the arms anchoring it to the Au surface. This high aromaticity means it is extremely likely some degree of clathrate cage forms. Similar to the inhibition of the tumbling of benzene, the formation of clathrate cages likely locks the pyridyl units of the viologen with respect to one another. By locking the orientation of the pyridyl rings, the effect of changing only the redox state rather than the combined effect of a change in redox state and ring orientation is seen. Unfortunately though, it is unlikely that the description of the ionic liquid surrounding the TMS-V-TMS molecule is this simple, as the viologen moiety is switched between charged states which themselves differ in terms of solvation by the ionic liquid. Computational studies on ferrocene in ionic liquid demonstrated the change from a charged to a neutral molecule occurs with a change in the ionic solvation layer, which because of the strong cation-anion ordering in ionic liquids is not limited to the first solvation shell. When ferrocene is in

the neutral state the ionic liquid solvation shell is made up of cations and anions. Upon oxidation to $Fc^+$, the solvation shell is only the anion, an effect seen throughout the layers of the ionic liquid.[49] If TMS-V-TMS were to exhibit comparable behaviour, then it is likely that at least the viologen core is surrounded solely by the $OTf^-$ anion in the initial dication state. Upon reduction to the radical cation, the solvation layer may then change, although the extent to which the $BMIM^+$ cation can infiltrate the shell is unknown. The resulting degree of clathrate cage formation around the charged viologen centre requires further theoretical or experimental investigations. Nevertheless it is expected the solvation shell around the viologen would be influenced by the propensity to build a clathrate cage around an aromatic moiety, while retaining the strong cation-anion interactions of the ionic liquid. The resulting solvation shell will strongly affect the orientation and conformation mobility of the TMS-V-TMS viologen core and thereby influence the resulting conductance behaviour. It is hypothesized that the resulting solvation shell locks the pyridyl rings in a coplanar manner. By locking the orientation of the viologen, the dominant influences on the conductance of the molecule are the electrode potential dependent alignment of the molecular orbitals with respect to the Fermi levels of the gold surface, reorganizational energies, and vibrational dynamics.

The long adsorption times and addition of the target molecule into the BMIM-OTf environment, may have inadvertently led to the formation of a full monolayer on the Au surface. This is entirely plausible as it is known that monolayers of alkanethiols can form on Au from ionic liquids, and furthermore, these monolayers are more ordered than those formed from the standard solvents.[50] If this occurs then a well ordered monolayer of TMS-V-TMS would give rise to a system with the anchoring arms and the long axis of the viologen centre tilted to the surface normal.[40] This high

degree of ordering would lock the viologen centre in place causing little to no change in the orientation of the pyridyl rings on going from the dication to the radical anion state. As with the proposed clathrate cage model the viologen pyridyls are locked in a specific orientation throughout the electron transfer. Note, however, that the bulky TMS groups may be expected to inhibit the formation of tightly packed SAMs of TMS-V-TMS, favouring the ionic liquid clathrate cage model.

Unfortunately, STM experiments themselves are not enough to validate the hypothesis that the ionic liquid environment locks the redox active centres in a coplanar orientation, allowing the facilitation of model Kuznetsov-Ulstrup behaviour. Experimentally, it could be possible to elucidate the structural effects of BMIM-OTf on TMS-V-TMS through the use of spectroelectrochemistry. Spectroelectrochemistry is a well-established field allowing the simultaneous measurement of the electrochemistry of a system while measuring its spectroscopy *in-situ*.[51] By combining these two fields, spectroelectrochemistry provides a powerful tool, which allows the relationship between a compound's electrochemistry and its structure to be elucidated. Examples of spectroelectrochemical measurements in ionic liquids in the literature are extremely limited. TMS-V-TMS in BMIM-OTf may act as a model system for spectroelectrochemical measurements in ionic liquids for a few reasons. Unlike some molecules, TMS-V-TMS is highly soluble in BMIM-OTf, the resulting electrochemistry is robust and repeatable and a high concentration of the TMS-V-TMS in BMIM-OTf is possible. Due to the ease of use of TMS-V-TMS in BMIM-OTf, and the possibility of proving that the ionic liquid locks the molecule into a planar confirmation, it is proposed that the next step would be to perform spectroelectrochemistry on the system.

Ruthenium Containing Redox Active Molecules

Santiago Marquez-Gonzalez of the Low group at the University of Durham provided the 4 Ru containing compounds in **Figure 5**. The end groups of the 4 molecules differ, causing variation in solubility and anchoring abilities. There are 2 asymmetric molecules terminated in $NH_2$/$SiMe_3$ and $NH_2$/COOMe, and 2 symmetric molecules, one with $SiMe_3$ end groups and another with $NH_2$ end groups. The Ru redox centre and OPE type backbone of these molecules are of interest. OPE molecules, in particular, cause a reduced $\beta$-value due to their relatively small HOMO-LUMO gap,[52] and the delocalization of electrons across the OPE backbone.[53] The $\beta$-value of OPE is further reduced in mixed OPE-Ru compounds. The low $\beta$-value of these compounds is reflected in the similar conductances of molecules composed of multiple Ru units. The low $\beta$-value implies that in these molecules the frontier orbitals have a similar energy to the Au Fermi level allowing for the improved conductance.[54] The low $\beta$-value achieved using the mixed OPE-Ru molecules is of interest because it indicates a high transmission efficiency over longer distances, and is a direct reflection of the electrical properties of the junction.[55] While relatively low $\beta$-values can be achieved using simple OPE molecules, the use of Ru containing molecules allows functionalities not possible with standard OPE molecules. By using Ru containing molecules the molecular redox state can be controlled, permitting the molecular redox switching to be investigated.[54] Aside from the control of redox state, Ru also presents opportunities for control of its spin state,[54] which opens up these molecules to spintronic investigations.

Electrochemistry of Ru Redox Active Compounds

*Ru-$NH_2$/-COOMe*

Ru-$NH_2$/-COOMe was the first molecule in this series investigated. Although the -COOMe group is a poor anchor group in single molecule conductance studies, it gives increased solubility compared to the other related compounds.

**Organic Electrolyte**

Ru-$NH_2$/-COOMe was investigated by Santiago Marquez-Gonzalez in 0.1 M tetrabutylammonium tetrafluoroborate and referenced to a $Me_{10}Fc$ internal reference. The resulting electrochemistry is shown in **Figure 18**. This molecule shows 2 redox processes at 0.34 and 0.75 V vs. $Me_{10}Fc/Me_{10}Fc^+$.

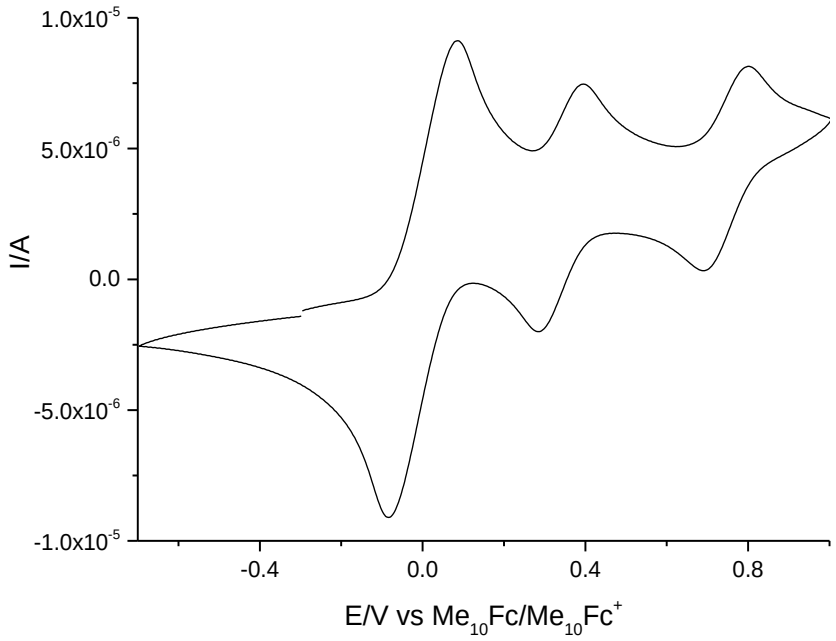


*Figure 18: Electrochemistry of Ru-$NH_2$/-COOMe in 0.1 M tertrabutylammonium tetrafluoroborate in DCM was performed by Santi Marquez-Gonzalez. A scan rate of 0.2 V $s^{-1}$ was used.*

**Ionic Liquid Electrolyte**

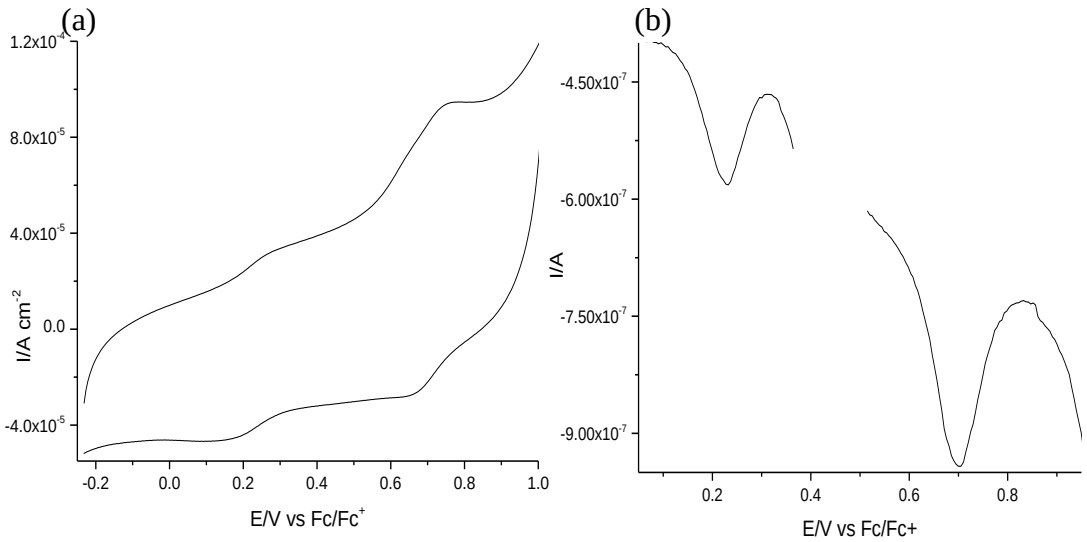


*Figure 19: Electrochemistry of 0.44 mM Ru-$NH_2$/-COOMe in BMIM-OTf. (a) Using a scan rate of 0.5 V $s^{-1}$ cyclic voltammetry was produced. (b) Differential pulse voltammetry was also used to investigate the Ru-$NH_2$/-COOMe molecule.*

The electrochemistry of Ru-$NH_2$/-COOMe was investigated in both BMIM-OTf and BMIM-TFSA. A concentration of only 0.44 mM was used because of the limited quantity of available compound. **Figure 19a** shows the electrochemistry of this molecule in BMIM-OTf. As expected two redox waves are seen, one from the Ru centre and the other from the aniline end group. These redox waves occur at 0.23 and 0.71 V vs. $Fc/Fc^+$ in BMIM-OTf, and 0.29 and 0.71 V vs $Fc/Fc^+$ in BMIM-TFSA. Based on literature results of similar Ru containing redox molecules, the first electron transfer is assigned to that of the Ru centre, and the second to the aniline group.[54, 56] To improve the clarity of these rather broad and shallow peaks, differential pulse voltammetry was used. In differential pulse voltammetry, the base potential is changed throughout the measurement in increments of 10-100 mV, with two current samples taken during each pulse, the difference between the two current measurements is plotted. As a difference plot, the background current is largely removed and peak

clarity is enhanced allowing for resolution of the electron transfer peaks of interest.[57] The results of these experiments are seen in **Figure 19b**. As with the cyclic voltammetry 2 redox waves from the 2 redox groups can be seen.

*Ru-$NH_2$/-$SiMe_3$*

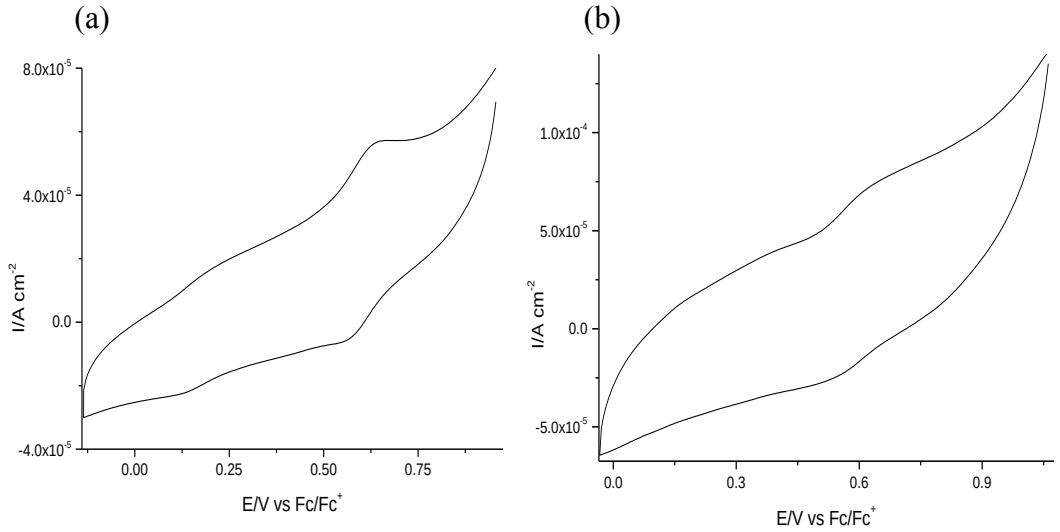


*Figure 20: Electrochemistry of 0.43 mM Ru-$NH_2$/-$SiMe_3$ in (a) BMIM-OTf, at a scan rate of 0.1 V $s^{-1}$, chosen as it shows the clearest electrochemistry. Electrochemistry in BMIM-TFSA is shown in (b) is measured at a scan rate of 0.5 V $s^{-1}$, this is the only clear voltammogram measured for this system.*

The second asymmetric Ru compound provided was terminated in $NH_2$ and $SiMe_3$. This was investigated in both BMIM-OTf and BMIM-TFSA, **Figure 20**. In BMIM-OTf, the two expected redox waves from the Ru centre and the aniline end group, respectively, are seen at 0.17 and 0.60 V vs. $Fc/Fc^+$, while in BMIM-TFSA only the second redox wave, at 0.59 V vs. $Fc/Fc^+$ is seen. Differential pulse measurements were also carried out. When performed on the system in BMIM-OTf two peaks are seen. The disappearance of the first peak in BMIM-TFSA is difficult to explain, because the weak electrochemistry cannot be quantitatively analysed. A smaller diffusion coefficient in this ionic liquid could cause the apparent loss of the

defined electrochemical response, although because the electrochemistry in both systems is poor the diffusion coefficients could not be found. An added degree of complexity for molecular electronics measurements arises from the asymmetry of the molecule, which means that while this compound may eventually prove an effective target for single molecule conductance measurements, it would be best to start the studies on these molecules with a symmetric analogue instead.

*Ru-SiMe$_3$/-SiMe$_3$*

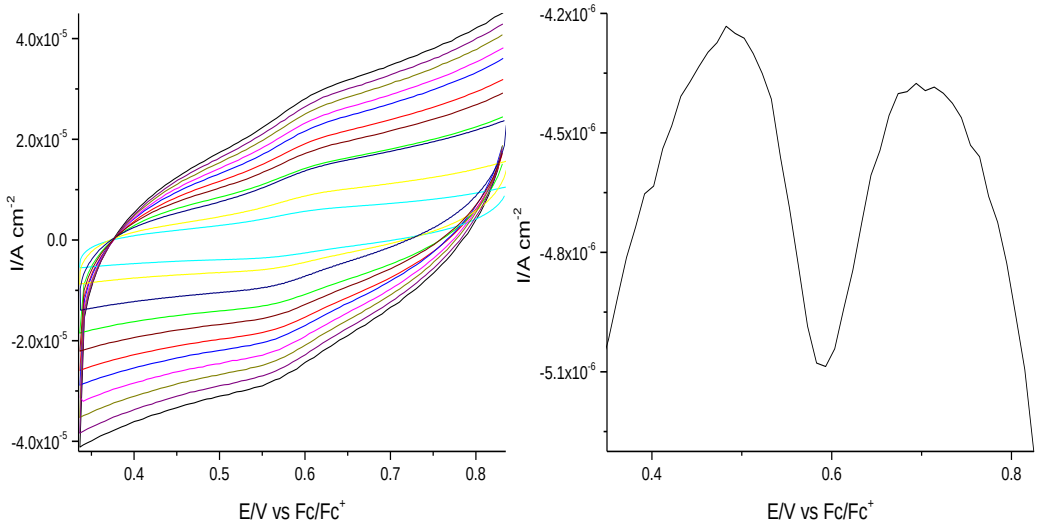


*Figure 21: 0.42 mM Ru-SiMe$_3$/-SiMe$_3$ in BMIM-TFSA showed a single electron transfer to the Ru centre. (a) Cyclic voltammetry over multiple scan rates, with no loss in activity seen. (b) Differential pulse voltammetry allowed the background current to be reduced.*

Unlike the two asymmetric molecules, this symmetric molecule was sparingly soluble in both ionic liquids. Nevertheless, electrochemistry was attempted in both BMIM-OTf and BMIM-TFSA. In BMIM-OTf the compound was determined to be redox inactive, this is likely due to its poor solubility. The electrochemistry in BMIM-TFSA is much clearer, showing a single redox wave at 0.58 V vs. Fc/Fc$^+$, **Figure 21a**. Although weak in the cyclic voltammetry, the use of differential pulse voltammetry to

distinguish the peak from the background current strengthens the response, with the electron transfer showing a sharp peak, at 0.59 V vs $Fc/Fc^+$, **Figure 21b**.

Although Ru-$SiMe_3$/-$SiMe_3$ is redox active in BMIM-TFSA its poor solubility rules it out as a possible candidate for straightforward molecule conductance measurements with the target dissolved in the ionic liquid.

*Ru-$NH_2$/-$NH_2$*

**Organic Electrolyte**

The final compound provided was a symmetric Ru-$NH_2$/-$NH_2$ complex investigated in 0.1 M tertrabutylammonium tetrafluoroborate in DCM, by Santiago Marquez-Gonzalez, producing the voltammetry shown in **Figure 22**. These measurements showed 3 redox waves occurring at 0.24, 0.63, and 0.99 V vs. $Me_{10}Fc/Me_{10}Fc^+$. These peaks arise from the Ru redox centre and the two aniline end groups, respectively.

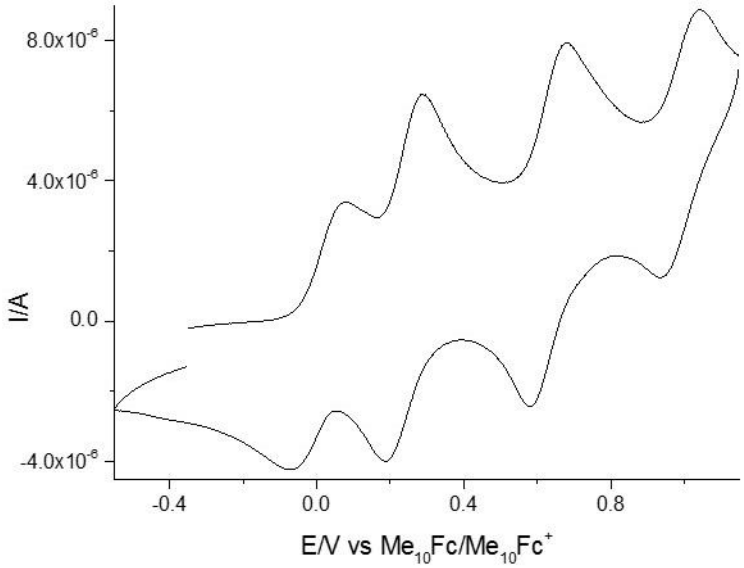


*Figure 22: Santi Marquez-Gonzalez performed cyclic voltammetry measurements on Ru-$NH_2$/-$NH_2$ in 0.1 M tertrabutylammonium tetrafluoroborate in DCM. A scan rate of 0.2 V $s^{-1}$ was used. All potentials are quoted to decamethyl ferrocene internal reference.*

**Ionic Liquid Electrolyte**

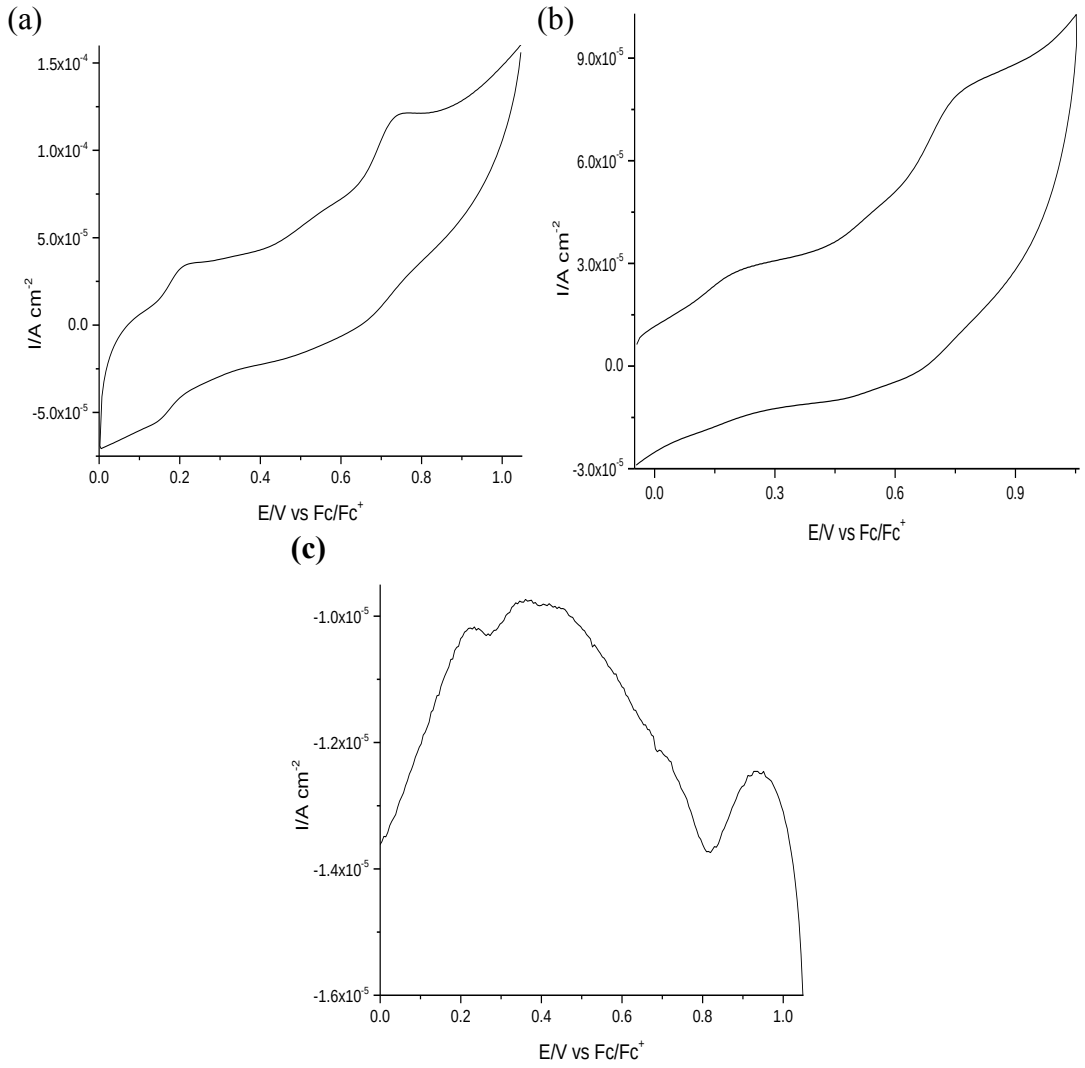


*Figure 23: 0.44 mM Ru-$NH_2$/-$NH_2$ in BMIM-OTf (a) and BMIM-TFSA (b) was measured by CV, and DPV in BMIM-OTf (c).*

Ru-$NH_2$/-$NH_2$ was measured in BMIM-OTf and BMIM-TFSA. The electrochemistry of this molecule is shown in **Figure 23a** and **b**. The redox potentials of this system are 0.27 and 0.68 V vs. $Fc/Fc^+$ in BMIM-OTf, and 0.16 and 0.70 V vs. $Fc/Fc^+$ in BMIM-TFSA. In both solutions the peaks decrease with time, in BMIM-OTf, however by shaking the cell and re-establishing the hanging meniscus, the electrochemical response reappears. Shaking the cell may help re-dissolve the redox

species. The attempt to reinvigorate the electrochemistry of the Ru-$NH_2$/-$NH_2$ molecule was not performed for BMIM-TFSA as the peaks started weaker than in BMIM-OTf, and therefore this solution was already ruled out as a system for EC-STM measurements. It was expected that the electrochemistry in the ionic liquids would match that in DCM, however there is one less peak seen, this may be a result of the low solubility of the Ru-$NH_2$/-$NH_2$ in the ionic liquid which leads to the depressed electrochemical response seen. The peaks seen are assigned to the Ru redox centre and the aniline end groups respectively. Due to the low concentration of these solutions, differential pulse voltammetry was also used for the BMIM-OTf solution. The results of this investigation is shown in **Figure 23c**, which exhibits two peaks in similar locations as seen for the cyclic voltammetry.

Based on the convincing electrochemistry of Ru-$NH_2$/-$NH_2$, and the presence of the well-known $NH_2$ anchor group, the single molecule conductance of this compound was measured by the *I*(*s*) technique.

Single molecule Conductance measurements of Ru-$NH_2$/-$NH_2$

*Without Electrochemical Potential Control*

The molecular conductance of the Ru-$NH_2$/-$NH_2$ complex was investigated by the *I*(*s*) technique, in BMIM-OTf. By first measuring the molecule in the ionic liquid without electrochemical control it could be determined if this molecule could be measured by the *I*(*s*) technique. An advantage of measuring the conductance in BMIM-OTf is that the hit rate for forming the molecule junction could be increased by doping the ionic liquid with the Ru complex, while also adsorbing the molecule on the Au substrate. This two-fold approach allowed 520 *I*(*s*) traces containing a plateau from molecular conductance to be collected, and plotted in the 1D and 2D histograms

shown in **Figure 24**. Analysis of this histogram shows the Ru-$NH_2$/-$NH_2$ complex has a conductance of (3.3 ± 1.1) nS, and a break-off distance of (2.29 ± 0.53) nm. This conductance is within error of that for the Ru-$SiMe_3$/-$SiMe_3$ complex.[58] The break-off distance is slightly larger than the 2.07 nm predicted by Spartan® calculations, though these calculations do fall within the error of the measurements. The slightly longer break-off distance measured here may be due to an over estimation of the $s_0$ value, due to an underestimation of the $d\ln I/ds$ values used in the distance calibration.

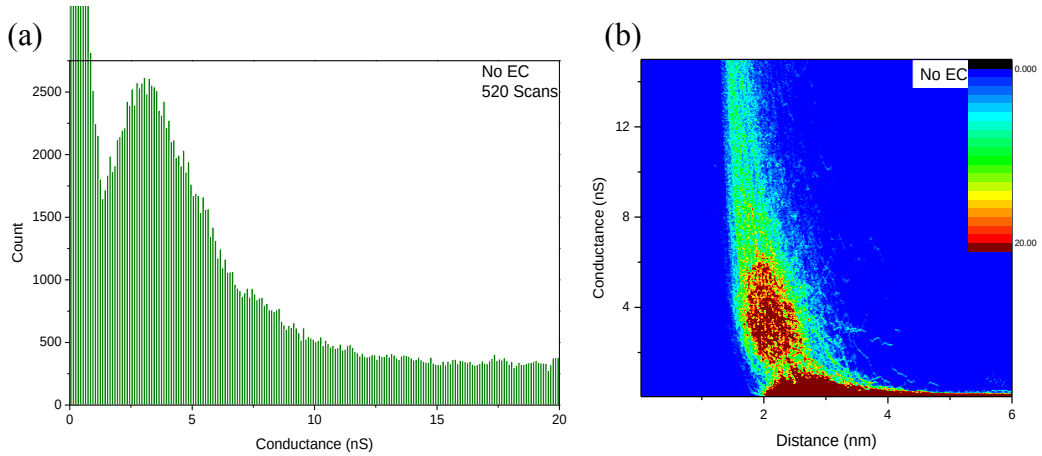


*Figure 24: Ru-$NH_2$/-$NH_2$ was investigated by the* I(s) *technique in BMIM-OTf. Using 520 plateau containing* I(s) *traces a 1D histogram (a) was produced. The same* I(s) *traces were used to produce the 2D histogram (b).*

*With Electrochemical Potential Control*

Ru-$NH_2$/-$NH_2$ was investigated by EC-STM in BMIM-OTf against a Pt QRE, at 6 potentials from 0.235 to 0.785 V vs $Fc/Fc^+$. The resulting 1D and 2D histograms of these measurements are shown in **Figure 25**, and **Figure 26**, respectively. **Table 2** summarizes the determined break-off distance and conductance values. For the potentials 0.235 to 0.535 V vs $Fc/Fc^+$ the histograms are composed of ~500 *I*(*s*) scans containing a plateau, whereas for the potential 0.785 V vs $Fc/Fc^+$, the histogram is composed of ~300 scans. The break-off distances seen here are all longer than those

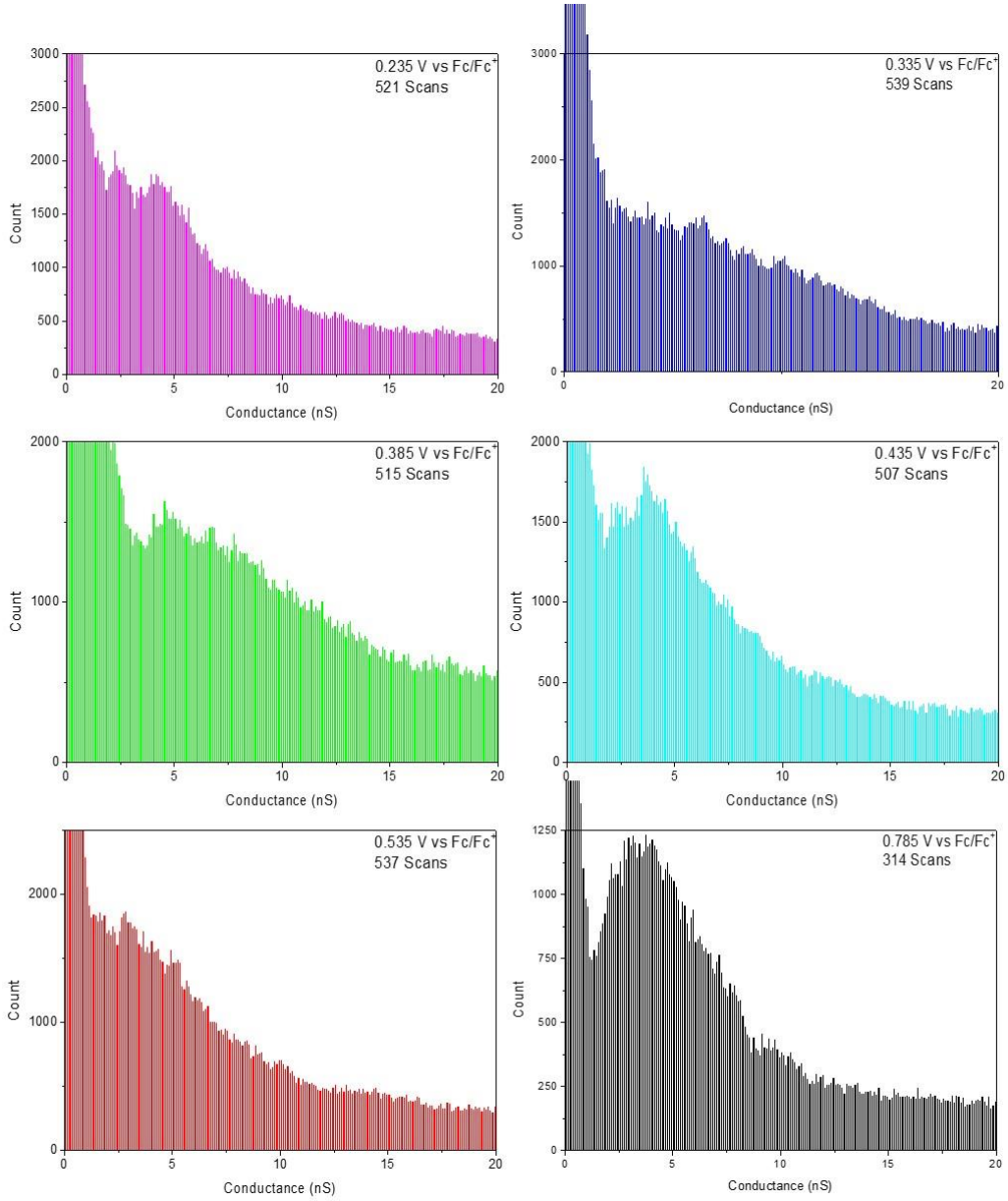


*Figure 25: Ru-$NH_2$/-$NH_2$ was measured by the* I(s) *technique at a variety of potentials. Collection of the plateau containing* I(s) *traces allowed the 1D histograms shown to be constructed and the conductance to be found.*

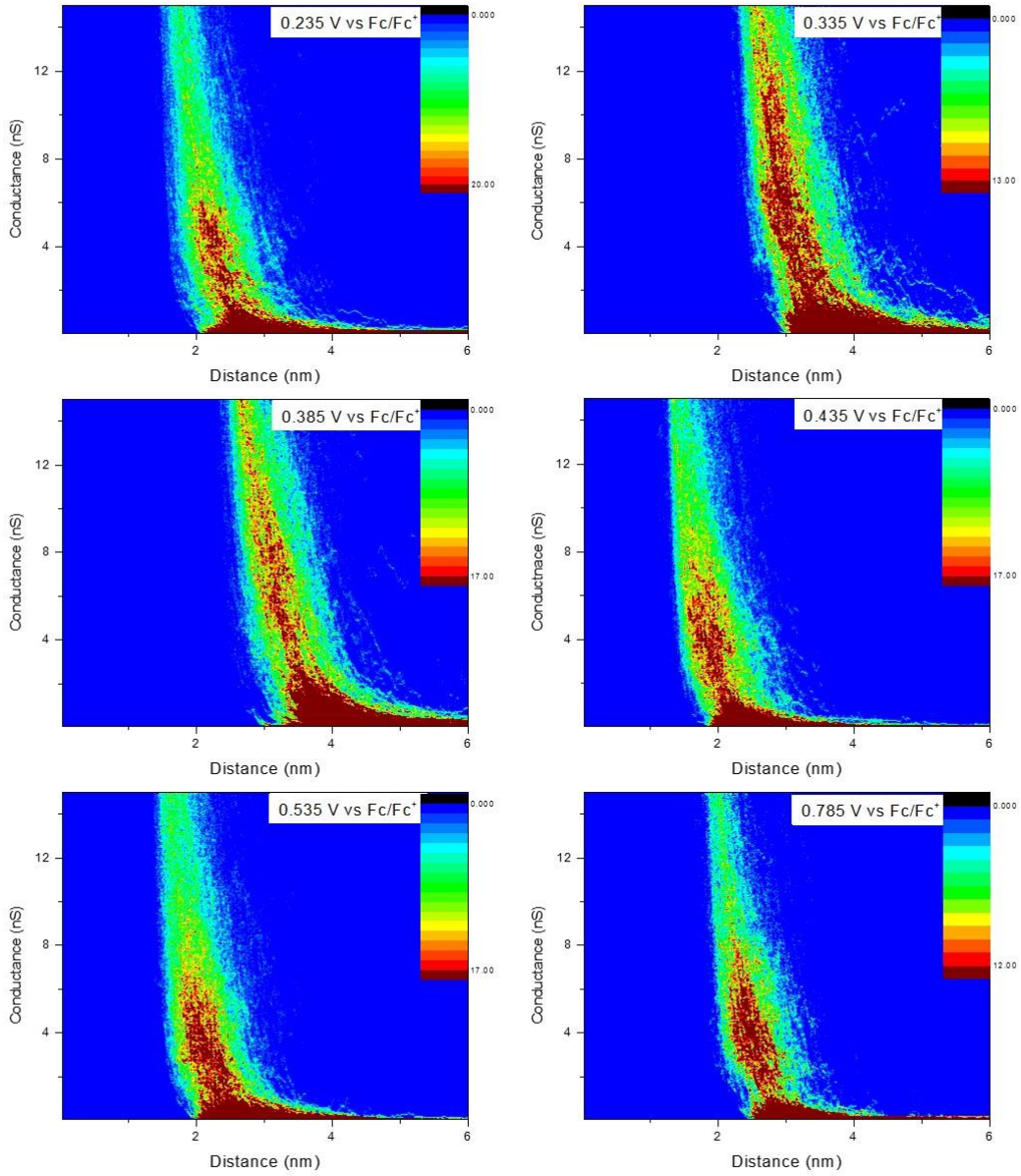


*Figure 26: Using the* I(s) *traces collected for the 1D histograms, 2D histograms showing the conductance of Ru-$NH_2$/-$NH_2$ as a function of the distance between tip and substrate could be constructed.*

*Table 2: Conductance and break off values of Ru-$NH_2$/-$NH_2$ are compared.*

| Potential (V vs $Fc/Fc^+$) | Conductance (nS) | Break Off w/ $s_0$ (nm) | Break Off w/o $s_0$ (nm) |
|---|---|---|---|
| No EC | (3.3 ± 1.1) | (2.29 ± 0.53) | (1.20 ± 0.33) |
| 0.235 | (3.8 ± 1.2) | (2.75 ± 0.92) | (1.14 ± 0.36) |
| 0.335 | * | (2.50 ± 0.73) | (1.17 ± 0.35) |
| 0.385 | (5.2 ± 1.3) | (3.45 ± 1.17) | (1.31 ± 0.34) |
| 0.435 | (3.6 ± 1.1) | (2.14 ± 0.46) | (1.06 ± 0.29) |
| 0.535 | (3.2 ± 1.2) | (2.32 ± 0.71) | (1.07 ± 0.30) |
| 0.785 | (3.9 ± 1.5) | (2.79 ± 0.45) | (1.16 ± 0.33) |

predicted by Spartan® calculations. While some are within error of the theoretical distance, this is not always the case. The long break-off distances seen here are likely to arise from an overestimation of $s_0$, this is due to shortcomings in this calibration under certain conditions as discussed in **Chapter 4: STM in Ionic Liquids.** At 0.27 and 0.68 V vs $Fc/Fc^+$, the redox state of Ru-$NH_2$/-$NH_2$ is in its on state implying a higher conductance should be seen. What occurs, however, is a statistically insignificant increase in conductance, and a broadening and eventual loss of the peak in the histogram. There are two possible causes for the weak change in conductance seen here. The first possibility is that a 2-step electron transfer, in the diabatic limit of the Kuznetsov-Ulstrup model, occurs. In this limit, the molecular state fully relaxes after the electron transfer to the redox centre, allowing a single electron transfer in a relaxation cycle, and no conductance enhancement is seen. The other possibility is that the anchor group does not behave in the expected manner. When attached to a phenyl ring the amine end group can instead be thought of as an aniline end group. Aniline is redox active and undergoes the electron transfer process depicted in **Figure 27**. It is possible the electrochemical response recorded for Ru-$NH_2$/-$NH_2$ in the region investigated is actually that of the aniline end group. This could either disrupt the binding ability of the end group, or change the electron transmission at the electrode/molecule contact. The impact of altering the amine end group through

external factors has been investigated in the past. Changes in pH have been seen to affect the anchoring ability of the amine.[59] By increasing the pH of the measurement environment, the amine end group was transformed from a poor anchor whose lone pair was tied up to form $–NH_3^+$, to the good anchor group $–NH_2$, which could bind to Au through its lone pair. The $–NH_3^+$ anchor group showed no clear peak in conductance histograms, while a conductance similar to a thiol terminated molecule is seen for the $–NH_2$ end group. A similar effect may occur with changes in electrode potential for this system. The oxidation undergone by the aniline end groups results in the formation of a double bond between the $–NH_2$ and the phenyl group, with the $–NH_2$ gaining a positive charge.[60] This is analogous to removing the lone pair functionality of the amine upon protonation, it is therefore unsurprising that it is no longer adequately performing. A means to investigate whether the amine end group should be treated instead as the redox active aniline group in terms of a molecular anchor is to look at the electrochemistry and conductance of a much simpler series of molecules in which the only redox active portion are aniline termini.

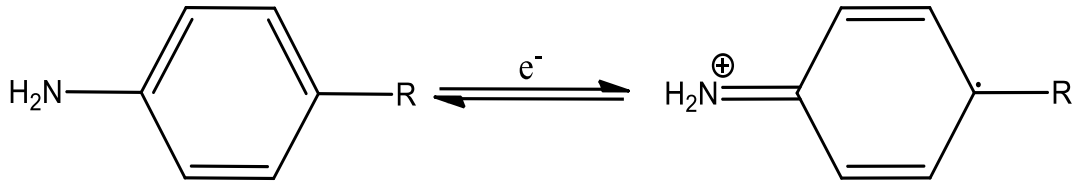


*Figure 27: The aniline end group undergoes the electrochemical process shown.*

OPE Compounds

To further investigate the behaviour of the aniline end group a series of three $–NH_2$ OPE type molecules were investigated. The three OPE molecules in **Figure 6** were provided by Dr. Ross Davidson of the Low group in Durham. The electrochemistry of all three were investigated in BMIM-OTf and conductance measurements were performed on OPE 1, to allow comparison to $H_2N$-Ru-$NH_2$

Electrochemistry

OPE 1 shows the clearest electrochemistry, exhibiting 2 redox waves at 0.58 and 0.05 V vs. $Fc/Fc^+$, as well as a shoulder at 0.51 V vs. $Fc/Fc^+$ at slower scan rates. **Figure 28a.** These values, including the shoulder, are in reasonable agreement with those seen in the literature.[61]

OPE 2 shows very complex electrochemistry. When in the structure shown OPE 2 exists as an orange compound, the molecule likely undergoes oxidation of the amine end group, which causes it to go brown. The original compound can be regenerated by dissolving the compound in diethyl ether, and adding a drop of ammonium hydroxide. The electrochemistry of both compounds was investigated, and was virtually identical, implying the compound had decomposed on dissolution. It is likely that in both cases the compound exists in both states, giving rise to the large number of peaks present.

Finally the electrochemistry of OPE 3 was measured, **Figure 28b**. The electrochemistry shows 2 weak peaks, even though a concentration of 10 mM in BMIM-OTf was used. These peaks occur around -0.06 and 0.61 V vs. $Fc/Fc^+$. As with the Ru complex, the electrochemical response of OPE 3 disappears during the experiments. In this case the electrochemistry of OPE 3 disappears after the second oxidation wave at 0.73 V vs. $Fc/Fc^+$, implying electron transfer followed by subsequent chemical reaction. This behaviour likely results from the polymerization of the OPE 3 molecule.[62, 63]

The electrochemistry of OPE 1 and Ru-$NH_2$/-$NH_2$ are compared in **Figure 28c**. The larger current density seen for OPE 1 relates to its higher solubility allowing use of a more concentrated solution. This comparison shows the electrode potential of

electron transfer is similar for both, implying the redox states probed in the EC-STM experiments are those of the aniline end group. Oxidation of the end group from $–NH_2$ to $=NH_2^+$ means the lone pair of the N is no longer available to attach the molecule to Au. In such a case the effect of changing the end group would be expected to dominate over the effect of the changing redox state of the Ru centre.

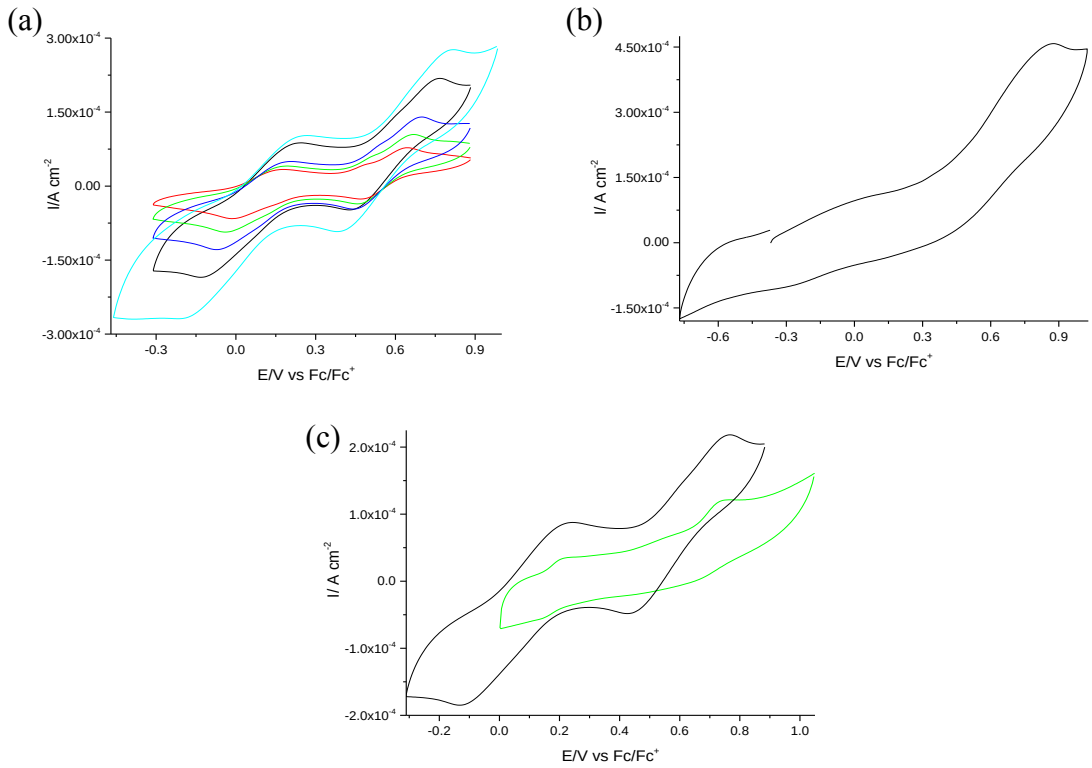


*Figure 28: (a) OPE 1 was investigated in BMIM-OTf. The cyclic voltammetry shows 2 separate electron transfer processes occur. (b) In BMIM-OTf OPE 3 shows 2 separate electron transfers, though these are not as strong as for OPE 1. (c) The electrochemistry of OPE 1, OPE 3 and Ru-$NH_2$/-$NH_2$ are compared showing similarities in the electrochemistry, which uphold the idea that in the EC-STM measurements the electrochemistry of the aniline end group rather than the Ru redox center are probed.*

Spartan®

To further investigate the influence of transforming the end group with changing potential Spartan® calculations were run on OPE 1 between two Au contacts

in its 3 redox states, **Figure 29**. These calculations show that in all cases charge transfer is through the HOMO states. In its neutral state the energy of the HOMO state is -6.14 eV, this increases to -8.55 eV for the anion state, and -14.72 eV for the final dianion state. Based on these calculations, as the aniline group undergoes electron transfer, the gap between the HOMO and the Fermi level of Au increases. This is expected to increase the tunnelling barrier and reduce molecular conductance.

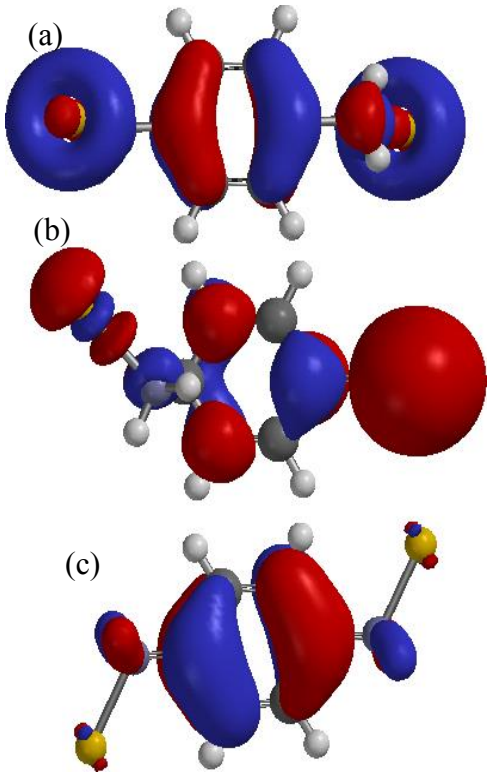


*Figure 29: Spartan® was used to investigate the effect of the electrochemical change in the amine end group. (a) Neutral molecule, (b) Cation radical, (c) Dication.*

OPE 1 Single Molecule Conductance Measurements

The conductance of OPE 1 was investigated in the same manner as the Ru molecule. Over 500 scans were collected into the histogram in **Figure 30**. The conductance measured for OPE 1 is 6.1 nS, with a break-off distance of (1.5 ± 0.2) nm. The break-off is larger than expected based on Spartan® calculations, though it is likely due to an overestimation in the $s_0$ value, as explained before. Although this

compound has been studied extensively in the literature, it has been investigated by the break junction technique,[64, 65] therefore this conductance value is not directly comparable. A series of phenyl group containing molecules with alkanethiol linkers at the 1,4-positions, has previously been measured.[66] The $\beta$-value of this series of compounds was experimentally determined to be 0.25 Å$^{-1}$. The conductance of OPE 1 fits well with this experimental trend. OPE 1 could be well suited for studies using the break junction technique, which would allow measurement of the high conductance groups. Providing the break junction investigations were successful without electrochemical control these molecules would be interesting targets for determination of the influence of electrochemical potential dependent changes in the

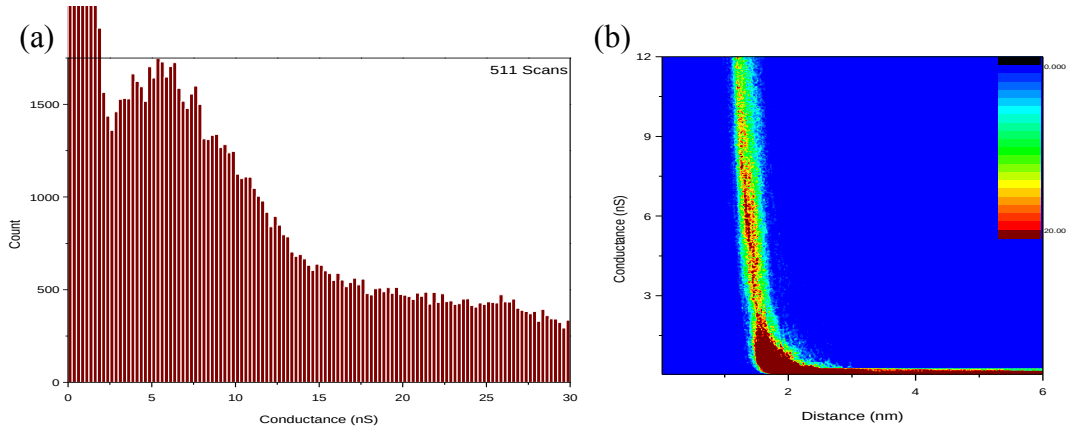


*Figure 30: The* I(s) *technique was used to investigate OPE 1. (a) 1D histograms were formed from 511* I(s) *traces containing plateau, these traces could then be used to prepare the 2D histograms (b).*

anchor group on the conductance.

## Conclusions

The use of redox active molecules in single molecule junctions provides an interesting avenue for molecular electronics investigations. When using redox active wires as archetypical molecular switches care is necessary as the success of such measurements is dependent on many factors. A viable electrochemical molecular

switch must have robust electrochemistry in solution before its conductance is even investigated. Even when the electrochemistry is robust, and the molecule is able to form metal/molecule/metal junctions, straightforward conductance switching may not occur. The $NH_2$-Ru-$NH_2$ analogue investigated here, for instance, showed detrimental effects from the redox activity of its anchor group on its ability to act as a straight forward redox switch. The solvent of the investigation is also important as witnessed when the TMS-V-TMS molecule was investigated in BMIM-OTf. The use of ionic liquids represents an important recent move away from the aqueous investigations of the viologen system of the past. When the system is carefully chosen, single molecule conductance switching can be reliably observed and significantly investigated. This is facilitating detailed study of charge transport across single molecules in various electrochemical environments. For TMS-V-TMS in BMIM-OTf a 3-fold conductance increase was seen upon electrochemical reduction at the reversible potential. With further developments in methodology it should be possible to measure the second electron transfer of the TMS-V-TMS.

## Declaration

*Measurements in this chapter were performed in collaboration with Prof. Paul Low's group, therefore, synthesis, and electrochemistry in organic electrolytes were not performed in Liverpool. The TMS-V-TMS molecule was synthesized by Dr. Josef Gluyas, who also provided the electrochemistry in organic electrolyte. The series of Ru containing compounds was synthesized and investigated in organic electrolyte by Santiago Marquez-Gonzalez. Dr. Ross Davidson synthesized the OPE molecules. All electrochemistry and STM measurements performed in ionic liquids were performed by myself in Liverpool.*

# References


1. N. Robertson and C. A. McGowan, *Chemical Society Reviews*, 2003, **32**, 96-103.
2. J. Y. Son and H. Song, *Current Applied Physics*, 2013, **13**, 1157-1171.
3. M. Tsutsui and M. Taniguchi, *Sensors*, 2012, **12**, 7259-7298.
4. N. J. Tao, *Physical Review Letters*, 1996, **76**, 4066-4069.
5. www.nobelprize.org/nobel_prizes/physics/laureates/2007/, *The Nobel Prize in Physics 2007*, Accessed 30 March, 2014.
6. S. J. Higgins and R. J. Nichols, in *Electrocatalysis: Theoretical Foundations and Model Experiments*, eds. R. C. Alkire, D. M. Kolb and J. Lipkowski, Wiley-VCH, Editon edn., 2014, vol. 14, pp. 99-136.
7. N. J. Kay, S. J. Higgins, J. O. Jeppesen, E. Leary, J. Lycoops, J. Ulstrup and R. J. Nichols, *Journal of the American Chemical Society*, 2012, **134**, 16817-16826.
8. I. V. Pobelov, Z. Li and T. Wandlowski, *Journal of the American Chemical Society*, 2008, **130**, 16045-16054.
9. M. Haselman and S. Hauck, *Proceedings of the IEEE*, 2010, **98**, 11-38.
10. W. Haiss, T. Albrecht, H. van Zalinge, S. J. Higgins, D. Bethell, H. Höbenreich, D. J. Schiffrin, R. J. Nichols, A. M. Kuznetsov, J. Zhang, Q. Chi and J. Ulstrup, *The Journal of Physical Chemistry B*, 2007, **111**, 6703-6712.
11. C. Li, A. Mishchenko and T. Wandlowski, in *Unimolecular and Supramolecular Electronics II*, ed. R. M. Metzger, Springer Berlin Heidelberg, Editon edn., 2012, vol. 313, pp. 121-188.
12. W. Haiss, H. van Zalinge, S. J. Higgins, D. Bethell, H. Höbenreich, D. J. Schiffrin and R. J. Nichols, *Journal of the American Chemical Society*, 2003, **125**, 15294-15295.
13. T. Albrecht, K. Moth-Poulsen, J. B. Christensen, J. Hjelm, T. Bjørnholm and J. Ulstrup, *Journal of the American Chemical Society*, 2006, **128**, 6574-6575.
14. J. Zhang and A. M. Bond, *Analytical Chemistry*, 2003, **75**, 2694-2702.
15. S. A. Paz, M. E. Zoloff Michoff, C. F. A. Negre, J. A. Olmos-Asar, M. M. Mariscal, C. G. Sánchez and E. P. M. Leiva, *Journal of Chemical Theory and Computation*, 2012, **8**, 4539-4545.
16. J. Ghilane, P. Hapiot and A. J. Bard, *Analytical Chemistry*, 2006, **78**, 6868-6872.
17. W. Schmickler and N. Tao, *Electrochimica Acta*, 1997, **42**, 2809-2815.
18. T. Albrecht, A. Guckian, A. M. Kuznetsov, J. G. Vos and J. Ulstrup, *Journal of the American Chemical Society*, 2006, **128**, 17132-17138.
19. S. J. Higgins and R. J. Nichols, in *Electrocatalysis: Theoretical Foundations and Model Experiments*, eds. R. C. Alkire, D. M. Kolb and J. Lipkowski, Wiley-VCH, Editon edn., 2013, vol. 14, pp. 99-136.
20. T. Albrecht, A. Guckian, J. Ulstrup and J. G. Vos, *Nano Letters*, 2005, **5**, 1451-1455.
21. W. Schmickler and C. Widrig, *Journal of Electroanalytical Chemistry*, 1992, **336**, 213-221.
22. A. Alessandrini, S. Corni and P. Facci, *Physical Chemistry Chemical Physics*, 2006, **8**, 4383-4397.
23. W. Schmickler, *Surface Science*, 1993, **295**, 43-56.

24. J. Zhang, A. M. Kuznetsov and J. Ulstrup, *Journal of Electroanalytical Chemistry*, 2003, **541**, 133-146.
25. J. Zhang, A. M. Kuznetsov, I. G. Medvedev, Q. Chi, T. Albrecht, P. S. Jensen and J. Ulstrup, *Chemical Reviews*, 2008, **108**, 2737-2791.
26. A. M. Kuznetsov, I. G. Medvedev and J. Ulstrup, *The Journal of Chemical Physics*, 2007, **127**, -.
27. N. Katsonis, A. Marchenko, S. Taillemite, D. Fichou, G. Chouraqui, C. Aubert and M. Malacria, *Chemistry – A European Journal*, 2003, **9**, 2574-2581.
28. A. Marchenko, N. Katsonis, D. Fichou, C. Aubert and M. Malacria, *Journal of the American Chemical Society*, 2002, **124**, 9998-9999.
29. G. Pera, S. Martín, L. M. Ballesteros, A. J. Hope, P. J. Low, R. J. Nichols and P. Cea, *Chemistry – A European Journal*, 2010, **16**, 13398-13405.
30. C. M. Gordon and A. J. McLean, *Chemical Communications*, 2000, 1395-1396.
31. S. R. Shin, C. K. Lee, S. I. Kim, I. So, G. M. Spinks, G. G. Wallace and S. J. Kim, *Langmuir*, 2008, **24**, 3562-3565.
32. C. Albonetti, M. Cavallini, M. Massi, J. F. Moulin and F. Biscarini, *Journal of Vacuum Science & Technology B*, 2005, **23**, 2564-2566.
33. D. I. Gittins, D. Bethell, R. J. Nichols and D. J. Schiffrin, *Journal of Materials Chemistry*, 2000, **10**, 79-83.
34. D. I. Gittins, D. Bethell, D. J. Schiffrin and R. J. Nichols, *Nature*, 2000, **408**, 67-69.
35. B. Liu, A. Blaszczyk, M. Mayor and T. Wandlowski, *ACS Nano*, 2011, **5**, 5662-5672.
36. H. C. De Long and D. A. Buttry, *Langmuir*, 1990, **6**, 1319-1322.
37. Z. H. Li, I. Pobelov, B. Han, T. Wandlowski, A. Blaszczyk and M. Mayor, *Nanotechnology*, 2007, **18**.
38. C. L. Bird and A. T. Kuhn, *Chemical Society Reviews*, 1981, **10**, 49-82.
39. Z. Li, B. Han, G. Meszaros, I. Pobelov, T. Wandlowski, A. Blaszczyk and M. Mayor, *Faraday Discussions*, 2006, **131**, 121-143.
40. B. Han, Z. Li, T. Wandlowski, A. Błaszczyk and M. Mayor, *The Journal of Physical Chemistry C*, 2007, **111**, 13855-13863.
41. K. K. Kasem and S. Jones, *Platinum Metals Review*, 2008, **52**, 100-106.
42. A. P. Abbott and K. J. McKenzie, *Physical Chemistry Chemical Physics*, 2006, **8**, 4265-4279.
43. J. Y. Lee and M. H. Kang, *Journal of the Korean Physical Society*, 2009, **55**, 2460-2464.
44. I. K. Robinson, P. A. Bennett and F. J. Himpsel, *Physical Review Letters*, 2002, **88**, 096104.
45. E. Leary, S. J. Higgins, H. van Zalinge, W. Haiss, R. J. Nichols, S. Nygaard, J. O. Jeppesen and J. Ulstrup, *Journal of the American Chemical Society*, 2008, **130**, 12204-12205.
46. J. D. Holbrey, W. M. Reichert, M. Nieuwenhuyzen, O. Sheppard, C. Hardacre and R. D. Rogers, *Chemical Communications*, 2003, 476-477.
47. J. K. D. Surette, L. Green and R. D. Singer, *Chemical Communications*, 1996, 2753-2754.
48. Y. Yoshiro, M. L. Klein, N. Masaru and M. Nobuyuki, *The Journal of Chemical Physics*, 2011, **134**, 191101.
49. Y. Yang and L. Yu, *Physical Chemistry Chemical Physics*, 2013, **15**, 2669-2683.

50. J. Dai, J. Cheng, J. Jin, Z. Li, J. Kong and S. Bi, *Electrochemistry Communications*, 2008, **10**, 587-591.
51. W. Kaim and J. Fiedler, *Chemical Society Reviews*, 2009, **38**, 3373-3382.
52. X. Xiao, L. A. Nagahara, A. M. Rawlett and N. Tao, *Journal of the American Chemical Society*, 2005, **127**, 9235-9240.
53. S. M. Wu, M. T. Gonzalez, R. Huber, S. Grunder, M. Mayor, C. Schonenberger and M. Calame, *Nature Nanotechnology*, 2008, **3**, 569-574.
54. Kim, J. M. Beebe, C. Olivier, S. Rigaut, D. Touchard, J. G. Kushmerick, X. Y. Zhu and C. D. Frisbie, *The Journal of Physical Chemistry C*, 2007, **111**, 7521-7526.
55. K. Liu, X. Wang and F. Wang, *ACS Nano*, 2008, **2**, 2315-2323.
56. L. Luo, A. Benameur, P. Brignou, S. H. Choi, S. Rigaut and C. D. Frisbie, *The Journal of Physical Chemistry C*, 2011, **115**, 19955-19961.
57. A. J. Bard and L. R. Faulkner, John Wiley & Sons Inc, New York, Editon edn., 2001, pp. 261-304.
58. C. Albonetti, I. Bergenti, M. Cavallini, V. Dediu, M. Massi, J.-F. Moulin and F. Biscarini, *Review of Scientific Instruments*, 2002, **73**, 4254-4256.
59. F. Chen, X. Li, J. Hihath, Z. Huang and N. Tao, *Journal of the American Chemical Society*, 2006, **128**, 15874-15881.
60. T. D. Selby, K.-Y. Kim and S. C. Blackstock, *Chemistry of Materials*, 2002, **14**, 1685-1690.
61. V. Dvořák, I. Němec and J. Zýka, *Microchemical Journal*, 1967, **12**, 324-349.
62. H. A. Abd El-Rahman and H. H. Rehan, *J Appl Electrochem*, 1993, **23**, 827-834.
63. H. A. A. El-Rahman, T. Ohsaka, F. Kitamura and K. Tokuda, *Journal of Electroanalytical Chemistry and Interfacial Electrochemistry*, 1991, **315**, 161-174.
64. S. Nakashima, Y. Takahashi and M. Kiguchi, *Beilstein Journal of Nanotechnology*, 2011, **2**, 755-759.
65. L. Venkataraman, Y. S. Park, A. C. Whalley, C. Nuckolls, M. S. Hybertsen and M. L. Steigerwald, *Nano Letters*, 2007, **7**, 502-506.
66. S. Subramanian and S. Sampath, *Pramana - J. Phys.*, 2005, **65**, 753-761.

# Chapter 8:

# Conclusions

Since the introduction of the integrated circuit the computational power of these devices has double every 1-2 years, in the manner predicted by Moore's Law. This growth has been driven by consumer demand which has acted to revolutionize everyday life. No longer are computers confined to research institutions, they can now instead be carried around in people's pockets. To continue to satisfy the ever growing desire for smaller and faster electronics, development of new techniques and devices is necessary. Though atomic level computational components are some way off, the limits of Moore's Law are within reach. Molecular electronics has the potential to satisfy the desire for improved electronics, though more work must be done to gain insight into these systems before they can enter the electronics industry.

This work has aimed to build the understanding of the whole molecular system. Often molecular electronics investigations focus on only the molecular back bone, here, however the effect of the environment and the contact have been examined. In these investigations both the environment and the contact affect the system. The effect of the environment has been investigated through measurements in ionic liquids, which is still a novel area for molecular electronics. The contact has been investigated by probing the effects of changing the metal contact, and the molecular anchor group.

The environment in which the molecular conductance studies are performed is incredibly important to the resulting investigation. In this work the influence of the environment has been witnessed in both electrochemistry and STM measurements performed in ionic liquid environments. In the **Electrochemistry in Ionic Liquids** series of experiments the electrochemistry of viologen containing compounds, and surface bound ferrocene species was measured. The measurements of viologen species in ionic liquids was an improvement over investigations in aqueous environments, as this allowed measurement of both the dication to radical cation, and the radical cation

to neutral species, redox transitions. When performed in solution the ionic liquid investigations resulted in lower diffusion coefficients and rate constant. The role of the environment was truly witnessed in the electrochemistry of the adsorbed 6V6, and ferrocene terminated species. For all measured surface bound species, the rate of electron transfer was slower in the BMIM-OTf than in the aqueous environment. This shows the important role the measurement environment plays. The difference in electron transfer in the two environments is a direct result of the different solvent interactions. Changing the electrolyte causes different solvations of the electroactive species, which can change the ability of the molecule to restructure to accommodate redox state changes. In ionic liquids it is more difficult for the molecule to restructure, causing a decrease in electron transfer in these environments. A more intrinsic proof of the importance of experiment environment occurred in the investigations of ferrocene moieties hydrogen bonded to monolayers on Au. Using BMIM-OTf it was possible to measure the rate constant of electron transfer through a series of ferrocene terminated monolayers, with a hydrogen bond. When similar experiments were performed in the past in organic electrolytes the hydrogen bond broke after the first measurement, making determination of the rate constant impossible. This shows that careful choice of the environment can allow investigations of molecular functionalities not possible otherwise. The importance of environment is also important in STM based molecular electronics investigations as seen in **STM in Ionic Liquids**. The investigation of bipyridine in both BMIM-OTf and BMIM-TFSA showed that while these ionic liquids do not noticeably affect the measured conductance, they do have an effect on the stability of the junction. Longer than expected break-off distances were measured in both systems, which are attributed to the pulling out of $BMIM^+$ ionic liquid stabilized Au nanowires. The use of the ionic liquid environment is

advantageous over ambient conditions for porphyrin measurements. In ambient conditions the molecules interact strongly with the Au surface, and can therefore only be measured with the addition of an axial ligand. Measurements in ionic liquids, however, were performed without the use of an axial ligand, because the ionic liquid cation interacts strongly with the Au surface, hindering its interaction with the porphyrin. The most dramatic effect of the environment was seen in **EC-STM in Ionic Liquids**, in which the change in single molecule conductance of TMS-V-TMS was measured with changing system potential. The analogous 6V6 measured previously using the *I*(*s*) technique, in aqueous electrolyte, showed an off-on conductance switching with changing potential, which was attributed to a change in conformation of the two pyridine rings. When TMS-V-TMS was measured in this work in BMIM-OTf the conductance undergoes an off-on-off transition, which is hypothesized to be a result of a locking of the ring conformation in the viologen centre. The ring locking is a direct result of the BMIM-OTf environment which can form a clathrate cage around the viologen centre and lock its structure. By looking at the electrochemistry and single molecule conductance of a series of molecules in ionic liquids the importance of the experimental environment has been seen. These investigations have shown that in future careful choice of the environment can allow for the investigation of specific functionalities. Through the use of ionic liquids it has been possible to measure redox states not possible in other environments, to measure intermolecular charge transfer, and to lock molecular conformation allowing the measurement of a single parameter at a time.

The role of the metal-molecule contact in molecular electronics has also been studied. This work has shown both the metal and the molecular end group should be carefully chosen for molecular electronics studies. While Au is by far the most popular

metal for molecular electronics, this popularity is due to its ease of use, rather than any intrinsic electronic ability. The use of ferromagnetic metals is of particular interest because of their potential use in molecular spintronics. In **PM-IRRAS** a variety of monolayers, formed through potential assisted assembly, were investigated on an electroplated Ni surface. The potential assisted assembly technique was refined using octanethiol monolayers formed on Ni. These monolayers showed a similar ordering of the analogous monolayers on Ni, implying that the use of Ni, to exploit its spintronic possibilities, will not diminish the quality of the resulting monolayers. To be of use in either molecular electronics or spintronics the Ni surface must be protected from oxidation, even with the addition of a molecular wire molecule, therefore, mixed monolayers on this surface were investigated. By using PM-IRRAS not only can the quality of a monolayer be assessed, but changes in composition can be as well. Using PM-IRRAS it was seen that well-ordered, molecular wire containing, monolayers of BDMT and HT, on Ni could be formed, with some degree of control over the monolayer composition. Expanding on the success of the measurements on the Ni contact, Co was also investigated. In **Co Deposition from Ionic Liquids** the possibility of using ionic liquid plating baths for Co was examined. Based on prior electroplating investigations, a $BMIM^+$ ionic liquid bath, with a $CoCl_2$ Co source, was used at elevated temperatures. Unfortunately though many permutations of the system were investigated, including different temperatures, potentials, and ionic liquids, mirror-like Co could not be repeatedly be achieved. While this ruled out the option of a one pot method for molecular electronics at a ferromagnetic contact, it did not rule out the use of Co in molecular electronics investigations. In **Molecular Electronics Investigations on Co** the use of octanethiol, and octanedithiol monolayers on Co were examined for molecular electronics applications. In this work Co was formed by

electrodeposition from an aqueous electrolyte, ensuring a fresh surface for each experiment. Much of the reason Co has been avoided in the past is because of its rapid oxidation on exposure to ambient conditions, this has been circumvented by *in-situ* reduction of the surface oxide. Reduction of the surface oxide is performed in an alkanethiol containing BMIM-OTf solution, allowing for subsequent potential controlled assembly of the thiol monolayer. The resulting octanethiol monolayer was assessed as high quality on Co, through the use of PM-IRRAS, electrochemistry, and electrochemical impedance spectroscopy. Using the same technique the molecular conductance of octanedithiol, in BMIM-OTf, in a Co-molecule-Co junction was measured. This experiment showed that changing the contact metal from Au to Co caused negligible change in the molecular conductance of octanedithiol, though the molecular junctions were less stable for Co than for Au. This result shows the spintronic functionalities of Co can be exploited, without any loss in conductivity. In molecular electronics it is not just the metal of the contact which is important, but also the molecular anchor group. In **STM in Ionic Liquids** the effect of the molecular end group on the molecular conductance was investigated by looking at the conductance of a pyridyl and a thiol terminated Zn porphyrin molecule. In this case both end groups strongly couple with the Au contact used, therefore little difference in the conductance was seen. A more dramatic effect of the molecular contact was seen in **EC-STM in Ionic Liquids**. In this chapter the molecular conductance of the Ru-$NH_2$/-$NH_2$ molecule between two Au contacts was measured in BMIM-OTf as a function of system potential. This experiment showed a broadening of the histogram peak with changing potential, and eventual loss of the peak, likely resulting from the $NH_2$ behaving as an aniline end group. When aniline undergoes its redox transitions the lone pair of the nitrogen is no longer free to bind to the Au contact, causing the loss of

conductance seen here. This experiment showed that the molecular anchor of the metal-molecule contact should be carefully chosen to suit the needs of the experiment. Through careful choice of both the metal and the molecular anchor group the best possible system for the molecular electronic purpose can be composed.

The work performed here can be built upon to gain a deeper understanding of molecular electronics systems. While there are general over-arching themes which could be insightful for many of the topics investigated, there are some areas which require more tailored attention.

Expanding on the technique presented in for alkanethiol monolayer formation on Co, it should be possible to investigate molecular conductance on a series a metal surfaces. Of particular interest would be investigations of monolayer formation, in this manner, on Ni and Fe. If a monolayer similar to that formed on Co could be made on these two metals a series of spintronic investigations could be carried out. The spintronic abilities of all three ferromagnetic elements could then be assessed and compared. Generally the use of different ionic liquids in the experiments performed throughout would be of great interest. While this would allow an expansion of the library of ionic liquids used in molecular electronics studies, it would also have more specific benefits for each series of experiments. For the experiments performed in STM in Ionic Liquids using an ionic liquid with a different anion could alter the interaction of the porphyrin molecular wires with the gold surface thereby changing the conductance characteristics. Furthermore the breakoff distances measured in this chapter could be investigated at more depth with different ionic liquids. It is expected that the Au chain which forms during the I(s) measurement would be affected differently by different ionic liquids. By replacing the BMIM cation the ability of the ionic liquid to stabilize the Au nanowire can be probed. It is likely cations with shorter

alkyl chains will not stabilize the nanowire showing a change in break-off distance. By investigating these systems with both the I(s) and break junction techniques an in-depth understanding of the effect of the ionic liquid on the molecular junction with regards to the metal contact could be developed. This could then be expanded to other metal contacts, like Ni and Co, to investigate the metal contact effect. Furthermore in the chapter EC-STM in ionic liquids it was seen that the ionic liquid environment can affect the molecular orientation. Therefore it is foreseeable that by changing the ionic liquid the molecular orientation may change, altering the current characteristics of the molecules. Finally, expanding the variety of ionic liquids used in this work could improve the deposition of Co as outlined in Co Deposition from Ionic Liquid. By utilizing ionic liquids with different cations improved deposition may occur through changes in Co diffusion, solvation, or even an additive effect. This may allow mirror-like Co plates to form, providing a route to a one-pot molecular spintronics method. Aside from allowing a traditional approach to a one-pot method this could also allow the jump-to-contact technique to be exploited for Co, and compared to a bulk Co contact.

The molecular spintronics work presented in the chapter Molecular Spintronics Investigations on Co, is an area of particular interest for further development. The ionic liquid mediated alkanethiol monolayer formation on Co can act as a starting point for performing further molecular spintronic investigations. With this technique more complex monolayers, like the BDMT mixed monolayer on Ni presented in PM-IRRAS, could be possible. This would allow for monolayers with more interesting functionalities to be investigated with contacts other than gold. This could include redox active molecules, molecules with spintronic possibilities, and more. The use of molecules with different anchor groups are also of great interest. By changing the

anchor group the orbital overlap between the metal contact and anchor group could increase, allowing for a higher conductance to be measured. Furthermore, thiols are known to give rise to multiple contact groups, and therefore multiple conductances. By changing to an anchor group such as –TMS the number of contact group can be reduced, resulting in a reduced spread in results. This monolayer formation technique could also be used with other technologically interesting contacts, such as Ni and Fe. The ultimate aim of further pursuing this work, however, should be to perform spintronic measurements. This technique has the ability to be adapted for single molecule measurements, or for molecular arrays. Therefore spintronic measurements could take a multi-faceted approach, with the effect of the application of a magnetic field investigated both by the I(s) technique, and through measurements of molecular array devices. These investigations would ideally be performed at a variety of temperatures.

The chapter EC-STM in Ionic Liquids provides many avenues for future work. The most interesting system to pursue further is the TMS-V-TMS molecular wire. To build on the second redox transition of this molecule should be measured, i.e. the $V^{+\cdot}$ to the V0 transition. Unfortunately to measure the second transition an improvement of the STM tip coating is necessary to reduce the leakage current. Further experiments are also necessary to elucidate the mechanism leading to the off-on-off conductance transition seen for the TMS-V-TMS molecule. Spectroelectrochemistry is of interest for TMS-V-TMS to determine the orientation of the pyridyl rings of the viologen core as the different redox states are probed. Computational analysis may also shed light on the interaction of the ionic liquid and the viologen core, though these measurements are likely to be computationally taxing. As the formation of a full monolayer can also lock the viologen core in a planar orientation the adsorption properties of the TMS-V-

TMS should also be examined. This would include formation of a TMS-V-TMS monolayer from BMIM-OTf, and methanol, followed by measurement of the surface electrochemistry and reductive desorption. While measurement of the redox transitions of the amine terminated Ru wire were possible this series of molecules warrants further investigation. Ru containing molecules like those presented here are of interest because of the increased functionalities, including the redox switching and potential as spintronic molecules. Given the success of the -TMS end group the Ru-TMS/-TMS molecule is the next molecule in this series which should be measured in ionic liquid both with and without electrochemical control. If electrochemical control is not used the Ru-NH2/-TMS molecule is also of interest to determine the effect of the molecular asymmetry on conductance. To finalize the measurements on the molecules presented in the chapter EC-STM in Ionic Liquids the OPE1 should be further examined. This molecule should be measured by the STM-BJ technique which is well suited to its highly conductive nature. Following measurements without electrochemical control the system should be measured in ionic liquid under electrochemical control. By performing measurements with electrochemical control the effect of the changing end group with changing potential can be assessed.

Investigations of the effect of the environment of the molecular electronics experiment and the metal-molecule contact have been performed. These examinations demonstrate the importance of controlling the whole system, not just the molecular back bone. By controlling the entire molecular system it is possible to exploit more than just the electronic functionalities of the system. For example control of the environment allows investigation of multiple redox states of a molecule allowing switching to be examined. Control of the contact on the other hand can allow for the exploitation of possible spintronic abilities of a molecular system. Through further in-

depth investigation of these properties it may be possible to form commercial molecular electronic devices with no analogous solid state system. These sorts of devices stand to revolutionize electronics.